ST. PETERSBURG STATE UNIVERSITY

Borisova Evgenia Borisovna

Staurolite: P-T-X conditions and patterns of formation (the Northern Ladoga region and other regions of the world)

Scientific specialty 1.6.4. Mineralogy, crystallography.
Geochemistry, geochemical methods of prospecting for mineral resources

DISSERTATION
submitted for the degree of the candidate
of geological and mineralogical sciences

Translation from Russian

Scientific advisor:
Doctor of Geological and Mineralogical Sciences,
Baltybaev Sh.K.

Saint Petersburg
2024

CONTENTS

INTRODUCTION

The relevance of the research

Staurolite ($Fe^{2+}Mg,Zn,Al^{3+})_2Al_2[(Si,Al)O_4]_4O_4[OH]_2$ is one of the common metamorphic "index minerals" with a limited P-T stability field, due to which it has become widely used in geological mapping of metamorphic complexes, with the identification of zones of different levels of metamorphism since the end of the 19th century (according Barrow, 1893). The regular appearance of staurolite in rocks of pelitic composition with an increase in the temperature of metamorphism to ~ 500°C and its disappearance at ~ 650°C allows us to distinguish a "staurolite zone", corresponding to the area of low-temperature amphibolite facies of metamorphism.

Although staurolite is typical of high-alumina metamorphic rocks, in particular metapelites, there are a number of finds of this mineral in mafic metamorphic rocks. Literary information about the conditions for the formation of staurolite indicates unusually wide P-T parameters for the formation of staurolite, depending on the substrate on which this mineral develops (Ríos et al., 2014, Purttscheller, Mogessie, 1984; Enami, Zang, 1988; Gil Ibarguchi et al., 1991; Tsujimori, Liou, 2004; Faryad, Hoinkes, 2006 and etc.). In this regard, it seems important to establish the patterns of staurolite formation not only in metapelites, but also in rocks of a composition atypical for its formation - metabasites. This work uses data on the composition of staurolite-bearing rocks from various regions, although the main focus is on staurolite-bearing rocks of the Northern Ladoga region.

The staurolite-containing rocks under study are widespread in the zonal metamorphic complex of the Northern Ladoga region (the southeastern end of the Svecofennian belt), where they represent part of the section of Early Proterozoic metamorphosed sediments (metaturbidites) of the Ladoga Group. The metamorphic zoning of the region can be traced from the northeast to the southwest from the biotite, garnet, staurolite zones through the sillimanite-muscovite and sillimanite-k-feldspar, to the high-temperature garnet-cordierite-k-feldspar zones (Baltybaev et al.., 2000 and etc.).

The identification of the staurolite facies of metamorphic rocks is determined by a set of critical mineral associations of the "staurolite" metamorphic zone, limited from adjacent zones by other "index minerals" or their parageneses. Each metamorphic facies is usually spatially correlated with a specific zone or zones within the metamorphic zonation. The position of staurolite-containing rocks in the scheme of metamorphic facies has been discussed for many decades (Ramberg, 1952; Francis, 1956; Hoschek, 1969; Facies of metamorphism..., 1970; Velikoslavinsky, 1972; Korikovsky, 1979; Likhanov et al., 2005, etc.). For the Northern Ladoga region, there are a number of metamorphic zoning schemes in which the low-temperature boundary of the staurolite zone (staurolite isograd) has different positions (Sudovikov, 1954; Predovsky, 1967; Nagaitsev, 1965, 1974; Kitsul, 1963; Geological structure..., 1989).

The ambiguous interpretation of the position of the staurolite isograd (and, accordingly, the zone of the same name) in the Northern Ladoga region can be explained by the peculiarity of the appearance

of staurolite: in addition to the necessary P-T-X conditions for its formation, a suitable chemical composition of the protolith is also required. In the absence of staurolite in the rock, it was classified as a zone of lower-temperature "pre-staurolite" metamorphism, considering that the temperatures here did not reach the level of staurolite appearance. However, without an analysis of the composition of the protolith, such a conclusion can often be erroneous.

This paper examines on a quantitative basis the influence of P-T-X parameters and protolith composition in relation to the author's collection of samples of Ladoga metapelites, as well as staurolite-bearing metapelites and metabasites from other regions of the world, the compositions of which are taken from literary sources. It is assumed that the widest coverage of possible compositions of protoliths and knowledge of the patterns of staurolite formation increases the reliability of determining the facies of rocks and helps to reasonably draw boundaries between zones with different levels of metamorphism when mapping metamorphic complexes.

Purpose and objectives of the study:

The purpose of the dissertation work is to establish the patterns of staurolite formation and reconstruct the evolution of staurolite mineral parageneses in metamorphic rocks of pelitic and basic compositions depending on changes in temperature, lithostatic pressure, chemical composition of the rock and the H_2O:CO_2 ratio in the metamorphic fluid. To achieve this goal, the following tasks were solved:

1. Petrographic-mineralogical, petrological and geochemical characteristics of staurolite-containing rocks of a wide composition;
2. Analysis of the composition of rock-forming minerals in staurolite-containing rocks;
3. Analysis of the composition of fluid inclusions in quartz from synmetamorphic veins of rocks of the staurolite zone;
4. Restoration of thermodynamic conditions of metamorphism of staurolite-containing rocks using thermo- and barometry methods;
5. Determination of the formation time of staurolite-containing mineral parageneses;
6. Computer modeling of the conditions for the occurrence of mineral parageneses with staurolite in metapelites and metabasites;
7. Identification of key factors determining the appearance of staurolite and development of petrochemical criteria that determine the critical conditions for its appearance in rocks of a wide range of compositions.

Factual material and research methods

The dissertation work is based on factual material collected by the author during field work in the Northern Ladoga region in the period from 2019-2021 (at the expense of the IPGG RAS), on the materials of previous field research by employees of IPGG RAS – Sh.K. Baltybaev (2000-2014) and

T.A. Myskova (2004), as well as on data from publications of researchers from the Northern Ladoga region and other regions of the world. The main objects of study are various schists and gneisses of the Ladoga series; in total, about 200 samples were used. For 25 samples, a chemical analysis of rocks was carried out for petrogenic oxides and for 15 for minor elements; more than 400 local chemical analyses of minerals were performed. Petrographic study of the samples was carried out using polarizing microscopes. The content of major elements in rocks was determined by the XRF method on a multichannel spectrometer ARL-9800 (Karpinsky Institute), trace and rare earth elements by the ICP-MS method on an ELAN-DRC-6100 device (Karpinsky Institute). The composition of mineral phases was determined by the EPMA method using a JEOL-JSM-6510 LA scanning electron microscope with a JED-2200 energy-dispersive spectrometer (JEOL) at the IPGG RAS. Fluid inclusions in quartz plates were studied using a Horiba Jobin-Yvon LabRam HR800 Raman spectrometer at the "Geomodel" Research Center of St. Petersburg State University. The analysis of the isotopic composition of monazite and other minerals was carried out on a TRITON TI multicollector mass spectrometer at the IPGG RAS.

Multi-equilibrium mineral geothermobarometry was carried out using winTWQ version 2.64 (Berman, 2007) using the JUN92.dat Dec06.dat databases. Thermodynamic modeling, including calculation of mineral stability fields, as well as additional P-T-X assessments of rock formation, were carried out in the PERPLE_X program v. 688 and 691 (Connolly, 2009-2019) with a database of solid solution models hp02ver and hp62ver (Holland, Powell, 1998, 2011).

Scientific novelty and practical significance of the work

A method has been developed for predicting the appearance of staurolite in metapelites and metabasites using calculated "petrochemical modules" in the form of ratios of the main rock-forming chemical components, the values of which are calibrated on natural objects and theoretical compositions of rocks possible in nature. A new methodological approach based on predicting the presence or absence of staurolite in rocks of a wide composition in a certain range of pressure and temperature is applicable in the compilation of maps and schemes of metamorphism.

Scope and structure of work

The dissertation consists of 5 chapters, introduction, conclusion, section "Factual material, methods and methodology", list of abbreviations, list of references and appendices. The first chapter provides a description and characteristics of the studied rocks and their constituent minerals. The second chapter presents the results of establishing P-T conditions and characteristics of the fluid regime of rock metamorphism. The third chapter presents the results of isotopic dating of the time of rock metamorphism. The fourth and fifth chapters present the petrochemical criteria and thermodynamic regime of staurolite formation in metapelites and metabasites, respectively.

The textual and illustrative material is presented on 133 pages and includes 53 figures, 13 tables in the form of appendices. The bibliography consists of 180 titles.

Approbation of work

The results of the study are presented in 14 publications, of which 5 articles are included in the Higher Attestation Commission, including 4 in scientific publications, refereed in the Scopus and Web of Science systems, intermediate results were presented at various geological conferences and published as 9 theses.

The author's personal contribution was participation in field work in 2019-2021, sampling, desk processing; petrographic study of the rocks under consider; preparation of samples for further geochemical and mineralogical studies; participation in carrying out part of the measurements to determine the chemical composition of mineral phases using the EPMA method and fluid inclusions on a Raman spectrometer; processing and interpretation of obtained geochemical and mineralogical data; in carrying out all calculations using the thermodynamic modeling method.

Acknowledgement

The author expresses deep gratitude and appreciation to his scientific supervisor Dr. Sh.K. Baltybaev, for trust, comprehensive assistance and support in the process of working on the dissertation. Thanks to the scientific supervisor, during the joint work the author acquired the most important theoretical knowledge and practical skills.

The author expresses sincere gratitude to his colleagues for their help, discussion of the results of the work, attention and interest in the research: P.Ya. Azimov, D.V. Dolivo-Dobrovolsky, I.I. Likhanov, A.I. Brusnitsyn, A.V. Yurchenko; for assistance in analytical studies to O.L. Galankina, V.N. Bocharov, N.G. Rizvanova, V.M. Savatenkov; for the provided material T.A. Myskovoy. The author also thanks all the professors of St. Petersburg State University who met the author during the 6-year path of study at the university.

The author expresses special gratitude to his colleagues in the laboratory of "Petro- and ore genesis" of the IPGG RAS E.S. Vivdich, R.L. Anisimov, P.A. Kirillova, M.E. Petrakova for assistance during field and laboratory work, for support and friendship.

The work was carried out within the framework of state assignments of the IPGG RAS №FMUW-2019-0013 (2019-2021) и № FMUW-2022-0002 (2022-2024).

Main scientific results

1. A comprehensive description of the staurolite-containing rocks of the Northern Ladoga region was obtained. Based on structural and material features, three blocks of development of rocks of the staurolite zone were identified for the first time (Borisova et al., 2024). Personal contribution is at least 80%.

2. For the first time, a method has been developed for identifying potentially staurolite-containing rocks using calculated "petrochemical modules" in the form of the ratio of the main rock-forming chemical components in metapelites (Borisova, Baltybaev, 2021) and metabasites (Borisova et

al., 2022). Personal contribution is at least 80%, all analytical and numerical calculations were performed personally by the author of the dissertation.

Propositions submitted for defense

1. Based on the characteristics of the chemical composition of the rocks, their constituent minerals and metamorphic fluid, the lateral heterogeneity of the staurolite zone of the Northern Ladoga region is recorded. The formation of staurolite-containing mineral parageneses in the metamorphic complex along the muscovite-chlorite association instead of chloritoid ones is determined by the geochemical features of the protolith, which were not favorable for the formation of chloritoid.

2. The formation of staurolite in medium-temperature metapelites is controlled by the chemical composition of the protolith; the quantitative parameters that make it possible to predict staurolite appearance are the ratios of petrogenic components: Al_2O_3/SiO_2 = 0.19–0.92, $CaO/(FeO_t+MgO)$ = 0.01–0.44, $K_2O/(FeO_t+MgO)$ = 0.07–0.83, $Na_2O/(FeO_t+MgO)$ = 0.02–0.34.

3. The stability of staurolite (configuration and number of P-T regions) in metabasites at moderate and high pressures is determined by the value of the iron-magnesium ratio ($FeO_t/MgO << 1$, $FeO_t/MgO \sim 1$, $FeO_t/MgO >> 1$) in protoliths, and the possibility the formation of staurolite in rocks is controlled by the ratios of petrogenic components MgO/CaO, $CaO/(FeO_t+MgO)$, $Al_2O_3/(FeO_t+MgO)$, determined for three groups of metabasites.

FACTUAL MATERIAL, METHODS AND METHODOLOGY

The research work is based on the study of a representative collection of samples of various schists and gneisses of the Ladoga series, selected by the author during summer field work as part of the group of the Laboratory of Petrogenesis and Ore Genesis of the IPGG RAS in 2019-2021 (at the expense of the IPGG RAS). Moreover, to complete the study, collections of samples and thin sections of Sh.K. Baltybaeva (2000-2014) and T.A. Myskova (2004) were used, data were also taken from publications of researchers from the Northern Ladoga region and other regions.

Field work was carried out in the Northern Ladoga region in South Karelia. Outcrops of Ladoga rocks were traced in the area of the Pitkyaranta region from the village Lyaskelya to the village Harlu and in the Sortavala region on the square framing the Kaalam intrusion, as well as through the village Ruskeala to the Finland border near the village Vyartsilya and along the northwestern coast of Lake Yanisjärvi. During the field work, the geological structure of the Ladoga series rocks was studied, rock varieties were identified and their relationships were examined. As a result, schematic drawings of bedrock outcrops were compiled, samples were taken, and the outcrops were described.

In total, about 200 samples of Ladoga rocks were used in the work. For 25 samples, a chemical analysis of rocks was made for major oxides and for 15 for minor elements, data on the chemical composition of rocks of the Ladoga series were also taken from the collective monograph (Ladozhskaya Proterozoic..., 2020), a total of 42 analyses. In addition, more than 400 local chemical analyses of minerals were performed.

To conduct a comprehensive study, it was necessary to carry out a number of analyses of rock and mineral samples using various *methods*:

For **petrographic analysis** of the rocks selected by the author during field research, transparent thin sections were prepared in the sample preparation laboratory (mineralogical group) of the IPGG RAS. Petrographic analysis of thin sections was carried out by the author using an Olympus BX 53 microscope for transmitted and reflected light with a digital camera for microphotography at the IPGG RAS.

The content of major oxides (wt. %) was determined by X-ray fluorescence analysis (XRF) on an ARL-9800 multichannel spectrometer, the content of minor elements using an ELAN-DRC-6100 inductively coupled plasma mass spectrometer (ICP-MS) in the central laboratory at the Karpinsky Institute (St. Petersburg).

The composition of mineral phases and microimages of rocks (BSE) were obtained by electron probe analysis (EPMA) using a JEOL JSM-6510LA scanning electron microscope (SEM) with a JED-2200 energy dispersive spectrometer at the IPGG RAS (analyst O.L. Galankina).

Fluid inclusions in quartz thin sections were studied using a Horiba Jobin-Yvon LabRam HR800 Raman spectrometer at the Geomodel Research Center of St. Petersburg State University (analyst V.N.

Bocharov). Raman spectroscopy (Raman et. Al, 1928) is a non-destructive technique that is excellent at analysing liquid and gaseous compounds, solids and solutes in liquid inclusions. One of the main advantages is the ability to determine the chemical and structural characteristics of samples down to 1 μm in diameter, a resolution not available with traditional petrography, microthermometry, and other spectroscopic techniques (e.g., infrared spectroscopy). It is assumed that fluid inclusions in synmetamorphic quartz veins from metapelites of the Ladoga series reflect the composition of metamorphic fluid of the progressive stage of Svecofennian metamorphism.

Multi-equilibrium mineral geothermobarometry was carried out in winTWQ version 2.64 (Berman, 2007) using the JUN92.dat and Dec06.dat databases based on the chemical composition of equilibrium minerals. Together with it, the TWQ_Comb auxiliary program (author D.V. Dolivo-Dobrovolsky http://www.dimadd.ru/) was used, designed to automatically generate all possible combinations from selected microprobe analyses of different minerals made in a local area of the sample, and their processing in the CMP.EXE and TWQ.EXE programs of the TWQ thermobarometric complex (Berman, 1991, 2007).

Thermodynamic modeling, including calculation of mineral stability fields, as well as additional P-T-X assessments of rock formation, were carried out in the PERPLE_X v program. 688 and 691 (Connolly, 2009-2019) with a database of solid solution models hp02ver and hp62ver (Holland, Powell, 1998, 2011). This program allows you to calculate the stable state of a natural mineral system depending on pressure, temperature and chemical potential of the components by minimizing the Gibbs free energy of chemical reactions. The program calculates and displays phase equilibrium diagrams and other thermodynamic diagrams.

Additional programs for material processing:

- The construction of classification and variation diagrams was carried out using the GCDkit program (Janoušek et al., 2000-2018). The GCDkit program allows you to work with a vast amount of data: group individual analyses into coherent groups, search according to various criteria. Data can be plotted on frequently used classification charts, as well as on various custom charts (binary and ternary, multiple charts, spider charts).
- The mineral formulas were calculated using the MINAL-2 and MINAL-3 programs (author D.V. Dolivo-Dobrovolsky http://www.dimadd.ru/). Calculation of mineral formulas was carried out based on the results of microprobe analysis (composition of minerals in mass percent of oxides and/or elements). The main emphasis in this program is on rapid primary processing of a large number of analyses, mainly for solving petrological problems.
- To create text and tables, programs from the Microsoft Office package were used.
- The creation of vector images (maps, diagrams, diagrams) was carried out in the CorelDRAW program.

For the main sections of the research work, a more detailed description of the *methods* is provided below (Borisova, Baltybaev, 2021; Borisova et al. 2023):

Thermodynamic modeling of mineral formation

To estimate the P-T-X conditions for the formation of mineral parageneses in metapelites, computer modeling based on Gibbs energy minimization was used. In our work, modeling of phase equilibria was performed using the PERPLE_X v program. 6.88 and v. 6.90-6.91 (Connolly, 1990, with updates until 2020) with a database of thermodynamic data of minerals and solid solutions of biotite, plagioclase, amphiboles, chlorites, garnet, spinel, orthopyroxene, light micas, chloritoid, staurolite, cordierite, ilmenite etc. from databases hp02ver and hp62ver (Holland, Powell, 1998, 2011). For the calculations, the model system MnNCKFMASH (MnO-Na_2O-CaO-K_2O-FeO-MgO-Al_2O_3-SiO_2-H_2O), and the T-P intervals were taken: 300–900 C° and 1–10 (for metapelite systems) and 1 –40 (for metabasic systems) kbar. The input data were the results of chemical analysis of metapelites of the Ladoga series, metapelites and metabasites from literature data (Tables 1, 2). For calculations based on Ladoga rocks, it was assumed that the studied system contains aqueous-carbon dioxide fluid, the mole fraction of carbon dioxide (X_{CO2}) in which was assumed to be 0.3 based on the study of fluid inclusions in quartz veins contained in metapelites (Baltybaev et al., 2000). For calculations with metabasites, a purely aqueous fluid was used.

The use of thermodynamic data, including the properties of minerals characteristic of metapelites, makes it possible to calculate the limits of stability of mineral associations in P-T space. Such calculations are usually performed in relatively simple chemical systems with a limited number of phases considered. The pseudosection method used in this work (Hensen, 1971; Powell et al., 1998) displays only the theoretically most stable mineral assemblage, regardless of its dispersion, for any given P-T condition for a given rock composition Previously, the KFMASH system KFMASH (Ka_2O, FeO, MgO, Al_2O_3, SiO_2, H_2O) was mainly used to model metapelites (for example, Thompson, 1976; Pattison, Tracy, 1991; Spear, 1993), which, to a first approximation, provides an understanding of the sequence of occurrence of various minerals associations under changing P-T conditions. However, a number of studies (Stowell et al., 2001; Vance and Mahar, 1998; Tinkham and Stowell, 2000, Tinkham et al., 2001) have shown that using the more complete MnNCKFMASH system most reliably reflects the actual compositions of metapelite mineral assemblages. Currently, the MnNCKFMASH is the minimum set of components required for the quantitative application of the pseudosection method to natural metapelites (Tinkham et al., 2001). It is worth noting that this system does not allow the modeling of phases such as carbonates, sulfides, graphite, COH fluid and phases with Ti and Fe^{3+}-containing end members, but despite this, all rock-forming metapelite minerals can be modelled.

When using the chemical compositions of metamorphic rocks for model constructions as compositions of protoliths, it is important to take into account the degree of their preservation during

superimposed metamorphism. For Ladoga rocks, methodological work was carried out to assess the influence of different levels of metamorphism on their initial (pre-metamorphic) chemical composition of the rocks (Lobach-Zhuchenko et al., 1972: Ronov et al., 1977). The authors carried out an area selection of material using a specific grid covering all metamorphic zones in the Northern Ladoga region, and found that the rocks of the Ladoga series (formations) in all metamorphic zones have practically identical compositions. The results are interpreted as reflecting the isochemical nature of the metamorphism with respect to petrogenic components.

Non-petrogenic elements in the composition of protoliths and their role in the composition and structure of staurolite were considered in a number of works. For example, it has been shown that Li content generally does not correlate with the modal amount of staurolite in the rock (Dutrov et al., 1986). In metapelites with a high boron content (with tourmaline), no noticeable changes were observed in the properties and P-T parameters of the staurolite parageneses that arise in them (Henry, 1985).

Also, the research work includes the author's methodology for **calculating the petrochemical modules** of staurolite formation in both metapelitic and metabasic rocks based on the thermodynamic modeling method (Borisova, Baltybaev, 2021; Borisova et al. 2023).

- *For metapelites*

In order to identify protolith compositions potentially favourable for the formation of staurolite, staurolite-containing rocks of the Northern Ladoga region were used, for which petrographic observations established a connection between the presence of staurolite and the characteristics of the chemical composition of the rock. In addition, nearby staurolite-free schists and gneisses were analysed to identify petro- and geochemical parameters that preclude the staurolite formation, despite the presence of metamorphic conditions favourable for its formation.

Based on the observed correspondence "rock composition – presence/absence of staurolite," computer modeling of mineral formation was carried out and a 100% correspondence of the presence of staurolite to natural observations was obtained, but in staurolite-free rocks it was not reproduced. This has made it possible for computer modeling to use a wide range of possible protolith compositions and predict the presence or absence of this mineral for various "theoretical" protolith compositions.

The work used 74 chemical compositions of staurolite-containing metapelites from different regions, 22 compositions of staurolite-free rocks surrounded by staurolite-containing ones, as well as 574 theoretical compositions of protoliths of or close to the metapelite composition. Of the 47 rocks of the Northern Ladoga region, 25 are with staurolite parageneses, 22 are without them. When selecting 27 compositions of staurolite rocks from 11 other regions, preference was given not to the number of samples from one region (they are usually of similar composition), but rather to regional diversity in order to cover as wide a range of rock compositions as possible. The theoretical compositions of the protoliths, for which modeling of mineral formation was carried out in order to determine the boundary

contents of major elements critical for the appearance of staurolite, were generated on the basis of the actual compositions of metapelites.

Staurolite parageneses from metabasic metamorphic complexes (usually high-calcium and high-magnesium rocks) and from high-pressure environments were not used. Accordingly, the range of applicability of petrochemical modules should be limited to metapelitic rocks of low- and moderate-pressure metamorphic complexes (for metabasites this is not the case, as will be discussed below).

- *For metabasites*

To identify the compositions of protoliths potentially favorable for the appearance of staurolite in metabasic rocks, real compositions of amphibolites in which staurolite was unambiguously diagnosed were used (Purtscheller, Mogessie, 1984; Enami, Zang, 1988; Gil Ibarguchi et al., 1991; Tsujimori, Liou, 2004; Faryad, Hoinkes, 2006) and about 150 theoretical compositions of metabasites, which represent a modification of the actual compositions of rocks (Table 7). Modified compositions make it possible to accurately establish threshold values for the contents of various petrogenic components critical for the formation of staurolite in the test rock.

Despite the fact that there are a larger number of publications where the presence of staurolite in metabasites is noted, the choice was limited to rocks that strictly correspond to the concept of "metabasite", i.e. the chemical composition must correspond to the composition of the main rocks, in which the SiO_2 content is < 52 wt. %, CaO > 5 wt. %. These compositions were accepted as "basic".

To establish the range of compositions of metabasic protoliths in which staurolite can form, the basic compositions we selected were modified by alternately increasing and decreasing the contents of rock-forming elements in them with variable steps up to a deviation of 20% from their initial values. For all basic and modified rock compositions, pseudo-sections were simulated in the area at T = 500–800°C, P = 1–38 kbar. Thermodynamic modeling of mineral formation using real and theoretical chemical compositions of samples made it possible to identify the limiting contents of petrogenic components that determine the formation of staurolite and staurolite-free mineral parageneses in a given P-T region.

For modeling phase mineral equilibria using the PERPLE_X program (Connolly, 1990), the input data were the results of chemical analyses of metabasites (Table 7). When solving a direct modeling problem, i.e. reproducing mineral parageneses observed in nature for a given rock composition and P-T parameters, it was assumed that the system contains both a purely aqueous fluid and a mixture of water and carbon dioxide. In the second case, control recalculations of phase diagrams were carried out with step-by-step (0.2) addition of CO_2 to the fluid up to a maximum mole fraction of carbon dioxide of 0.8. Above this value (X_{CO2} >0.8), staurolite ceases to form in rocks of the entire range of studied compositions.

Calculation of CO_2 density in fluid inclusions

Fluid inclusions are typically small, confined volumes (<50 μm in diameter) in which pressure and temperature are interdependent variables. Both parameters are related by the equation of state of a closed fluid, which leads to an almost linear relationship in P-T space (isochore). Therefore, a key requirement for the research and application of P-T metry is the ability to characterize fluid composition and density. Information on these properties is usually obtained through petrographic and microthermometric studies (Poty et al., 1976). But in recent years, the more convenient and faster method of Raman spectroscopy has begun to be used to study fluid inclusions (Raman, Krishnan, 1928). It is a non-destructive method that is excellent at analyzing liquid and gaseous compounds, solids and solutes in liquid inclusions. One of the main advantages is the ability to determine the chemical and structural characteristics of samples down to 1 μm in diameter, a resolution not available with traditional petrography, microthermometry, and other spectroscopic techniques (e.g., infrared spectroscopy).

Early work with fluid inclusions led to the recognition of H_2O, CO_2, CH_4 и N_2 as the main components of metamorphic fluid. Also in some inclusions H_2S, COS, SO_2, CO, H_2, NH_3 и O_2 were detected in noticeable quantities (Frezzotti et al., 2012).

From the CO_2 spectrum, the density of carbon dioxide in the inclusion can be determined. The Raman spectrum of molecular CO_2 shows two strong bands at 1285 and 1388 cm^{-1} and two symmetrical weak bands below 1285 and above 1388 cm-1, the so-called hot bands. Also, in the spectrum there is a small peak at 1370 cm^{-1}, attributed to $^{13}CO_2$. The two sharp bands appear due to the resonance effect proposed by Fermi in 1931 to explain the doublet structure in the region of the symmetrical stretching vibration of CO_2. The distance between the Fermi doublet (Δ, in cm^{-1}) is proportional to the density of the liquid. The density of CO_2 can be determined in the range from 0.1 to 1.24 g/cm^3 with an accuracy of about 5% (Frezzotti et al., 2012).

CHAPTER 1. STAUROLITE ZONE IN THE METAMORPHIC COMPLEX OF THE NORTHERN LADOGA REGION (POSITION, SUBSTANCE AND MINERAL COMPOSITION OF ROCKS)

This chapter provides general information about staurolite, a brief geological description of the metamorphic complex of the Northern Ladoga region, the position of staurolite-bearing rocks in it, a detailed petrographic description of the rocks, petrochemical features of the rocks and their classification. A description of rock-forming minerals with characteristics of their chemical composition is also provided.

1.1. General information about staurolite

Staurolite (from the ancient Greek σταυρός - cross and λίθος - stone) is an island silicate of predominantly aluminum and iron with additional anions. The most common are ferruginous staurolites, typical of medium-temperature metapelites, as well as magnesian staurolites, which are sometimes found in various metabasites and metasomatites. There are exotic varieties of staurolite, such as lyusakite (Co) (Skerl, Bannister, 1934), zincostaurolite (Juurinen, 1956), nordmarkite (Mn), xantholite (Ca), they are not considered within the scope of this work.

Ferrous staurolite is usually presented in the form of short-prismatic, well-faceted crystals, large porphyroblasts (up to 10 cm, rarely up to 70 cm along the long axis), often forming cruciform twins, as well as irregular elongated grains and granular aggregates (Fedkin, 1975). Staurolite crystals almost always have a spongy structure, due to the presence of numerous inclusions of quartz, sometimes garnet, carbonaceous matter; accessory ones often include ilmenite, rutile, monazite, etc. There are several types of staurolite twinning, the most common: in the form of direct intergrowth, when individuals are at a right angle to each other, and oblique at an angle of 60° (Fig. I-1-1); six-pointed intergrowths of three crystals are less common (Fedkin, 1975).

Figure I-1-1. Staurolite twins (photo taken from the electronic resource mindat.org).

The crystal chemical structure of staurolite has been the subject of debate for over a hundred years since the late 19th century. Due to the difficulty of selecting and analyzing pure staurolite due to the large number of microscopic inclusions (mainly quartz), empirical formulas varied greatly in the

ratio of atoms in the staurolite structure. The first structural study of staurolite was reported by Cardoso in 1928 (Cardoso, 1928), he proposed the orthorhombic type space group Ccmm for staurolite. In 1929, Náray-Szabó (1929), using the same space group, proposed the chemical formula of staurolite $Fe_4Al_{16}Si_8O_{48}H_8$. However, it was not until 1956 that a thorough morphological and x-ray study by Hurst (Hurst et al., 1956), confirming the C-centered lattice of staurolite, showed that the staurolite is not rhombic, but monoclinic with space group symmetry C2/m. The presence of a centre of symmetry was assumed due to the negative piezoelectric effect. At the same time, Juurinen (1956) based on high quality chemical analyses determined a new idealized formula $Fe_4Al_{18}Si_8O_{48}H_4$ with a charge of +2, which is electrostatically neutral only if half the iron is ferric. New data led to a revision of the Náray-Szabó staurolite structure (Náray-Szabó and Sasvari, 1958), showing that their initial definition of staurolite structure was basically correct, but the proposed orthirhombic symmetry group turned out to be a pseudo-symmetry. And that the correct symmetry group is monoclinic C2/m with $\beta \approx 90°$, later confirmed by Smith in 1968 and later studies. Smith (1968) proposed a more general approach to the formula: (7 octahedral positions, mainly Al)$_{\sim 18}$(1 tetrahedral position, mainly Fe)$_{4 \text{ или } <4}$(1 tetrahedral position, mainly Si)$_8O_{48}H_{\sim 4}$, but he was unable to determine the absolute distributions of anions over positions based on X-ray diffraction data, since some positions are only partially filled and the chemical elements included in the staurolite structure are numerous. Although the structure of staurolite was determined in principle, the question of the distribution of all anions included in the structure of staurolite among positions remained open. New research allowed by the 90s determine most of the positions and substitution patterns in staurolite (Hawthorne et al., 1993a, b, c; Holdaway et al., 1986, 1991, Lonker, 1983, etc.).

The structure of staurolite is described in the form of parallel alternating layers of kyanite (Al_2SiO_5) type and layers of iron-aluminum oxide-hydroxide $Al_{0.7}Fe_2O_3(OH)_2$, composed of [FeO_4]-tetrahedra и [AlO_6]-octahedra connected through the vertices (Perchuk et al., 2015). The unit cell contains 48 oxygen atoms, which form a cubic packing. In addition to the main components of staurolite – Si, Al, Fe, Mg, H, O, it constantly contains a certain amount of Ti, Mn, Fe^{3+}, etc. Also, the composition of staurolite is complicated by the presence of light elements such as Li, H, the content of which varies greatly in different staurolites. Another difficulty lies in the distribution of elements in different positions: Al, Mg, Fe^{2+} and Fe^{3+}, small elements Ti, Cr, Zn, with sometimes high contents of Zn, Co and Li.

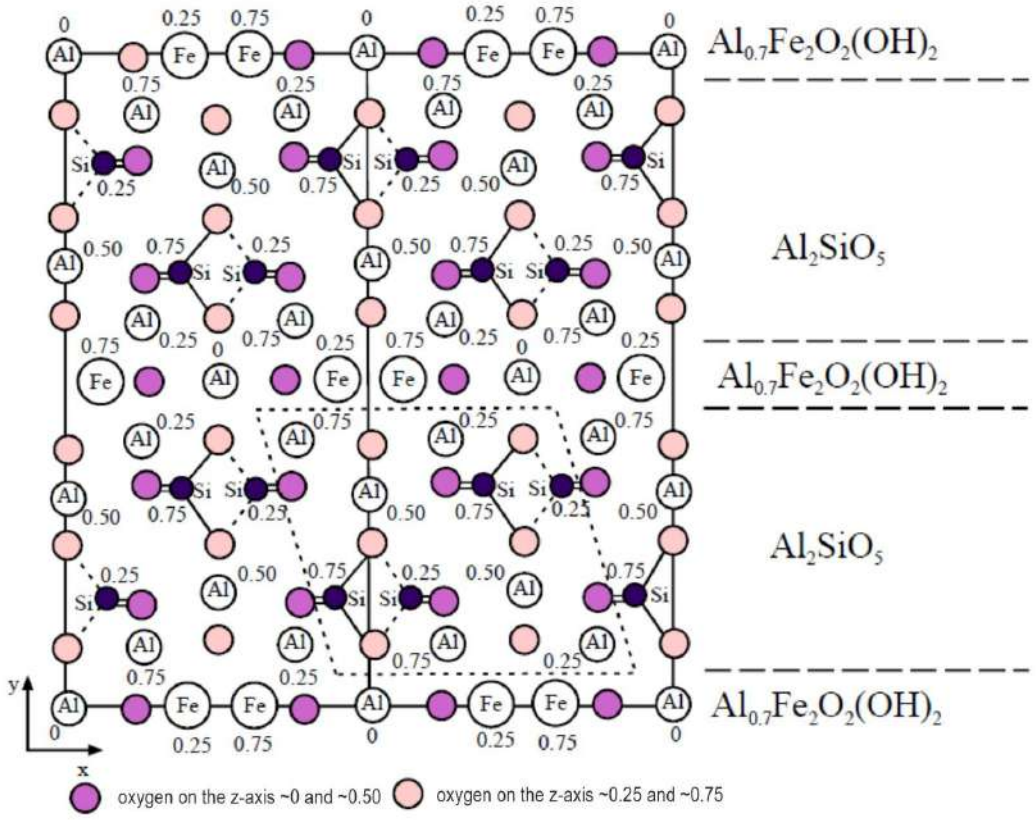

Figure I-1-2. Schematic representation of the structure of ferruginous staurolite (Perchuk et al. 2015).

Isomorphism in staurolite is highly diverse and complex. The divalent metal cations Zn^{2+}, Co^{2+}, Mg^{2+}, Ni^{2+}, Mn^{2+} which are close in ionic radius to Fe^{2+} ocupy tetrahedral Fe-vacancies, and Ca, Cr^{3+}, V, Ti, Fe^{3+} occupy larger octahedral positions. Also, Mg can be present at the aluminium position, which complicates the $Fe^{2+}\leftrightarrow Mg$ isomorphism typical of many silicates and, unlike rock-forming ferromagnesian amphiboles and pyroxenes, staurolite does not provide wide (absolute) ranges of chemical composition, i.e. it is not a continuous solid solution (Hawthorne et al., 1993a, b, c).

Most isomorphic substitutions in staurolite can be described by the general formula: $(Fe^{2+},Mg,\square)^{VI}_4(Fe^{2+},Mg,Ti^{4+},Zn,Mn)^{IV}_4(Fe^{3+},Cr,Al)^{VI}_{18}(Al,Mg,\square)^{VI}_4(Si,Al)^{IV}_8O_{48}(OH,F,O^{2-})_4$. Although chemistry, structure, and rough bond valence calculations support the substitutions presented, staurolite is a very complex mineral whose crystal chemistry is controlled more by local charge balance involving vacancies in the iron hydroxide layer than by formal substitutions. Thus, these substitutions should be considered as approximate mechanisms for achieving charge balance.

Ferrous staurolite is mainly found in high-alumina metapelites with low calcium content (Fedkin, 1975). In zoned-metamorphosed complexes, a staurolite (staurolite-andalusite) zone is distinguished, represented by the paragenesis Qtz + Bt + Pl + St + Ms ± Grt. The transition to the staurolite zone (the lower boundary of the zone is the staurolite isograd) is marked by the decomposition reaction of chloritoid, for example, Ctd + Qtz = St + Grt + H_2O; in the absence of chloritoid, staurolite is formed

due to the decomposition of the muscovite chlorite pair according to the following reaction: Ms + Chl ± Grt = St + Bt + Qtz + H_2O. The upper boundary of the staurolite zone in terms of temperature and pressure is determined by the appearance of aluminosilicate phases of sillimanite/kyanite, cordierite, for example, by the reaction St + Qtz = Crd/Grt + Al_2SiO_5 + H_2O (Perchuk et al., 2015). Staurolite often forms parallel intergrowths with kainite so that the (010) plane of staurolite is parallel to the (100) plane of kyanite (Fedkin, 1975).

The Fe-St + Qtz paragenesis has a rather narrow stability field at T ≈ 500-650°C, P ≈ 2-10 kbar, which is limited by several of the above mineral reactions (Fig. I-1-3). Due to its limited stability, mainly in temperature, Fe-staurolite has become widely used as an index mineral in geological mapping of metamorphic zoning since the end of the 19th century (according to Barrow, 1893). Recently, more and more finds of magnesian staurolite have appeared in high-pressure eclogite and granulite complexes (see Chapter 5). The P-T field of stability of magnesian staurolite, according to experimental data, is much wider than that of ferruginous staurolite, and is controlled by other reactions involving such aluminous phases as corundum, kyanite, chloritoid, diaspores, etc. (Perchuk et al., 2015) (Fig. I-1-3).

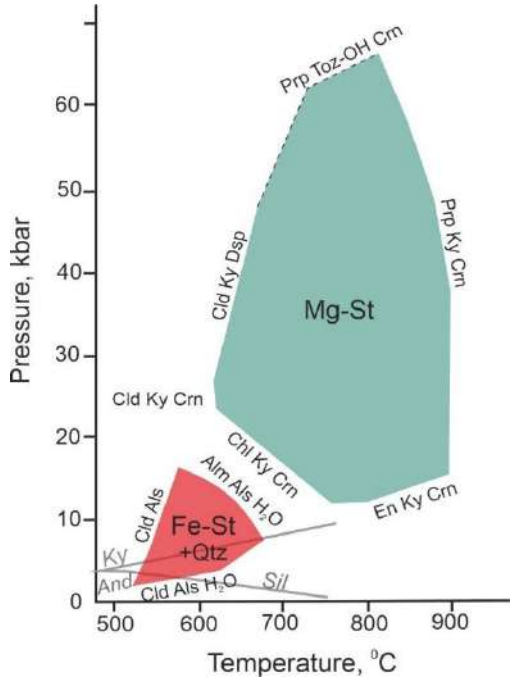

Figure I-1-3. Stability fields of Fe- and Mg-staurolite according to experimental data on the P-T diagram according to Yardley (1989) and Fockenberg (1998).

1.2. Geological position of staurolite-containing rocks

The territory of the Northern Ladoga region is the southeastern part of the Raahe-Ladoga tectonic zone of the Fennoscandian shield in the junction zone of the Epiarchean Karelian craton and the Paleoproterozoic Svecofennian mobile belt (Geological development..., 1970). At the foundation of the Raahe-Ladoga zone there is an Archean granite-gneiss basement, reworked together with the Paleoproterozoic volcanic-sedimentary cover during the Svecofennian orogeny (Fig. I-2-1) (Baltybaev et al., 2009).

The territory under consideration was studied by many researchers, who made important conclusions about the structure and evolution of endogenous processes in the Paleoproterozoic (Wegmann, 1928; Eskola, 1949; Sudovikov, 1954, 1970; Nagaytsev, 1965, 1974; Predovsky et al., 1967; Velikoslavinsky, 1971, 1972; Saranchina, 1976; Svetov, Sviridenko, 1992; Baltybaev et al., 2002, 2014, etc.

Within the Northern Ladoga region, there are Archean rocks of the Karelian craton and granite-gneiss domes of the foundation, Proterozoic metavolcanogenic-sedimentary and metaterrigenous complexes of the Sortavala, Ladoga and Lakhdenpokh series, as well as a large number of intrusions of various compositions and ages. Based on a complex of structural-material, tectonic and geophysical features, the Northern Ladoga region is divided into two large blocks - the Northern Domain (ND) and the Southern Domain (ND), which are articulated along a tectonic suture known as the Meyer thrust zone (Baltybaev et al., 1996).

Zonal high-gradient metamorphism of the andalusite-sillimanite type is manifested within the North domain, where the degree of metamorphism increases from northeast to southwest from greenschist facies to high-temperature amphibolite facies with the development of migmatites (Fig. I-2-1). The successive replacement of low-temperature parageneses by higher-temperature ones is clearly visible in the metapelites of the Ladoga series, which occupy most of the North domain territory (Sudovikov et al., 1970). The Ladoga series composes the interdome space, overlying the rocks of the Sortavala volcanogenic series, and is mainly represented by rhythmically layered metaterrigenous rocks (metaturbidites), considered as an analogue of the Kalevi terrigenous deposits of Finland (General Stratigraphic..., 2002). It is believed that the conditions under which sedimentation occurred can be equated to those of modern active margins (Huhma et al., 1991; Schuldiner et al., 1997).

As a result of a rather long history of studying the region, at the present time there are a number of different schemes of metamorphic zoning of the Northern Ladoga region (Sudovikov, 1954, 1970; Kitsul, 1963, Nagaitsev. 1965, 1974; Predovsky et al., 1967; Velikoslavinsky, 1972, etc.). The scheme of metamorphism includes biotite, garnet, staurolite (staurolite-andalusite), sillimanite-muscovite, sillimanite-K-feldspar, hypersthene zones according to the development of the corresponding critical mineral parageneses in the metapelites (Fig. I-2-1).

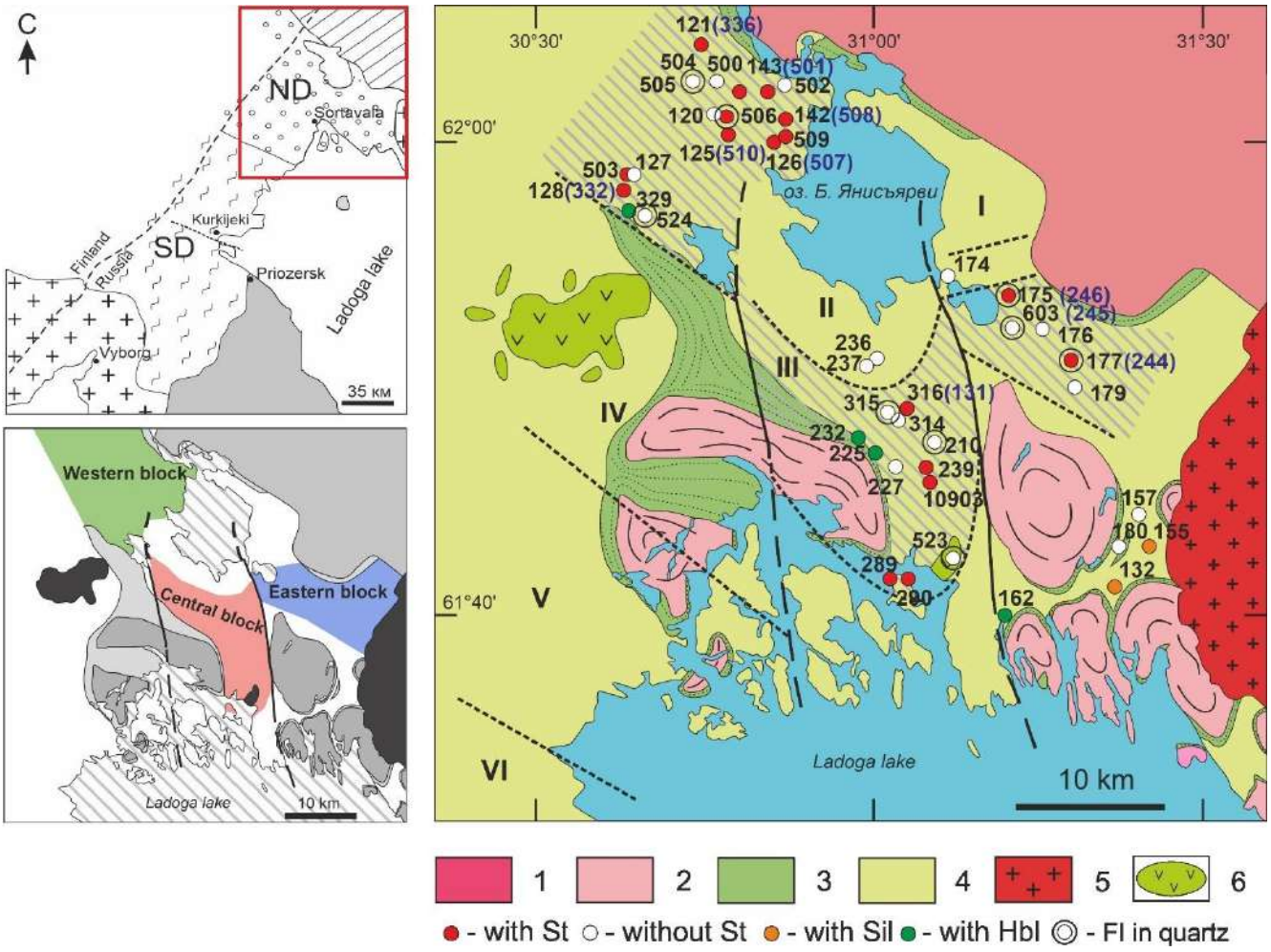

Figure I-2-1. Scheme of the geological structure of the Northern Ladoga region (according to "Ladoga Proterozoic..., 2020). 1, 2: Archean rocks (1 – Karelian craton, 2 – granite-gneiss domes); 3, 4: Paleoproterozoic supracrustal rocks (3 – volcanogenic-sedimentary Sortavala series, 4 – metaterrigenous Ladoga series); 5, 6: intrusions (5 – Mesoproterozoic Salma granite-rapakivi massif, 6 – Paleoproterozoic mafic-ultramafic Kalaam and Velimyak massifs). Dashed lines show isograds of index minerals (according to D.A. Velikoslavinsky, 1971 and Yu.V. Nagaitsev, 1965), Roman numerals indicate metamorphic zones: I – biotite, II – garnet, III – staurolite (shown by hatching), IV – sillimanite, V – hypersthenic. Sampling points are shown on the diagram. Inset: ND – Northern domain, SD – Southern domain (Baltybaev et al., 2000). FI – fluid inclusions.

The regular appearance and subsequent disappearance of staurolite with increasing temperature in zoned-metamorphosed complexes is used to identify the staurolite zone, which, along with other metamorphic zones, reflects the spatial distribution of temperature during the formation of metamorphic zoning. The identification of the staurolite facies of metamorphic rocks is determined by a set of critical mineral associations of the "staurolite" metamorphism zone, limited from adjacent zones by other "index minerals" or their parageneses. Each metamorphic facies can be spatially associated with a specific zone or zones within the metamorphic zonation. The metamorphic facies consists of several mineral subfacies; such a scheme was proposed at one time, in particular, by S.P. Korikovsky (1979), who at the same time identified the staurolite facies of metamorphism as an independent rank. Staurolite-bearing parageneses are formed in metapelites of favourable chemical composition at a temperature of ~500–650°C mainly due to Chl + Ms (Hoschek, 1969).

In the metamorphic complex of the Northern Ladoga region, the staurolite zone is clearly distinguished between the staurolite isograd, separating it from zones of lower metamorphism, and the sillimanite isograd, separating it from zones of higher metamorphism (Velikoslavinsky, 1972). The distribution zone of staurolite occupies a significant territory, the width of the zone varies from 25 km west of the lake Yanisjarvi up to 3 km in the east, in the area of the western contact of the Salma rapakivi massif. According to the results of this study, within the zone, three blocks of development of staurolite-containing rocks can be distinguished: Western (from the village of Vyartsilya to the village of Ruskeala and along the western coast of Lake Yanisjarvi), Central (from the village of Kharlu to Myakisalo Island) and Eastern (south of the village of Suistamo) (Figure I-2-1). These blocks are clearly separated by large faults of meridional strike. The differences between the identified blocks can also be traced in the chemical compositions of the rocks and their constituent minerals. The staurolite-bearing rocks of the entire zone are represented by staurolite-biotite, garnet-staurolite-biotite, and staurolite-andalusite-biotite varieties. When moving to a higher temperature zone, staurolite parageneses are replaced by sillimanite ones.

1.3. Geochemical characteristics of rocks

The chemical compositions of the Ladoga series rocks characterize the sedimentary nature of the protolith, while the ratios of the contents of major elements are different, in contrast to igneous rocks. Ladoga series rock have SiO_2 57–76 wt. % and increased contents of Fe_2O_3t (3.2–13.9 wt.%), MgO (0.5-6.9 wt.%), TiO_2 (0.26-2.07 wt.%), decreased CaO (0.45-4.35 wt.%) and Na_2O (0.44–5.59 wt.%) and are characterized by a predominance of MgO over CaO (MgO/CaO=1–4) (Ladoga Proterozoic…, 2020). This work considers only calcium-poor high-alumina metapelitic rocks with a low Ca/(Al+Mg+Fe) ratio, due to which they do not form epidotes, calcium hornblende, basic and intermediate plagioclases, grossular-rich garnets, clinopyroxene and wollastonite (Korikovsky, 1979).

As a result of field research, a number of staurolite-bearing and staurolite-free rocks were selected from the mid-temperature staurolite (staurolite-andalusite) zone (Fig. I-2-1). The chemical compositions of the rock samples used in the work are given in Table 1.

The ratios of the content of the main major oxides to silica are characterized by negative correlations, except for the ratios CaO/SiO_2 and Na_2O/SiO_2 (Fig. I-3-1), which is characteristic of immature sediments. The ratio of petrogenic oxides to alumina content clearly shows positive correlations with TiO_2, Fe_2O_3, MgO and K_2O (Fig. I-3-2), which is a reflection of the granulometric differentiation of the material and an indicator of low chemical weathering of rocks (Ladozhskaya Proterozoic..., 2020).

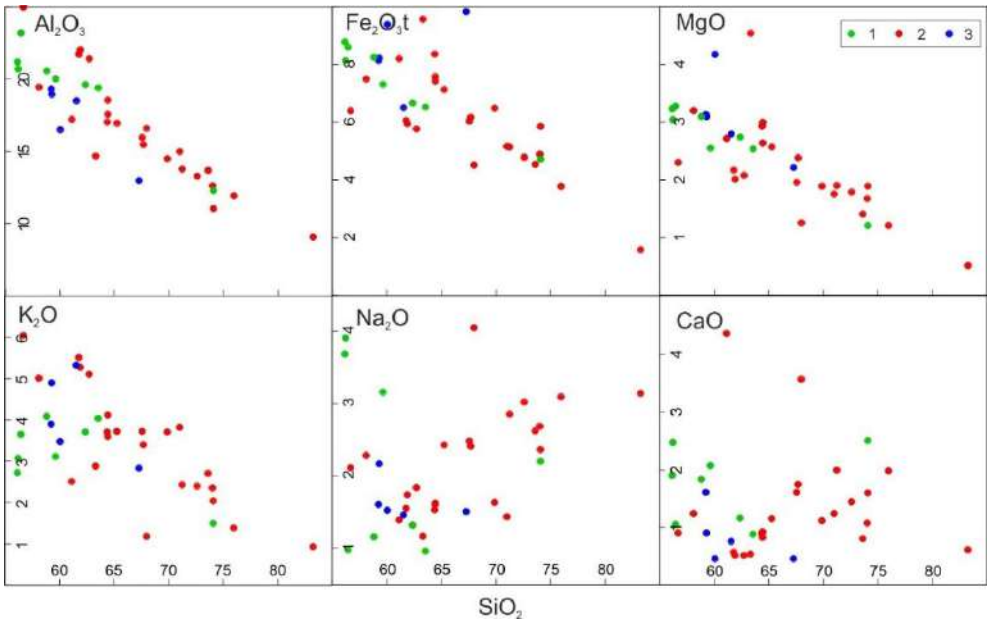

Figure I-3-1. Binary variation diagrams (SiO_2, wt.% – main petrogenic oxides, wt.%) for metasediments of the Ladoga series of the staurolite zone: 1 – Western block, 2 – Central block, 3 – Eastern block.

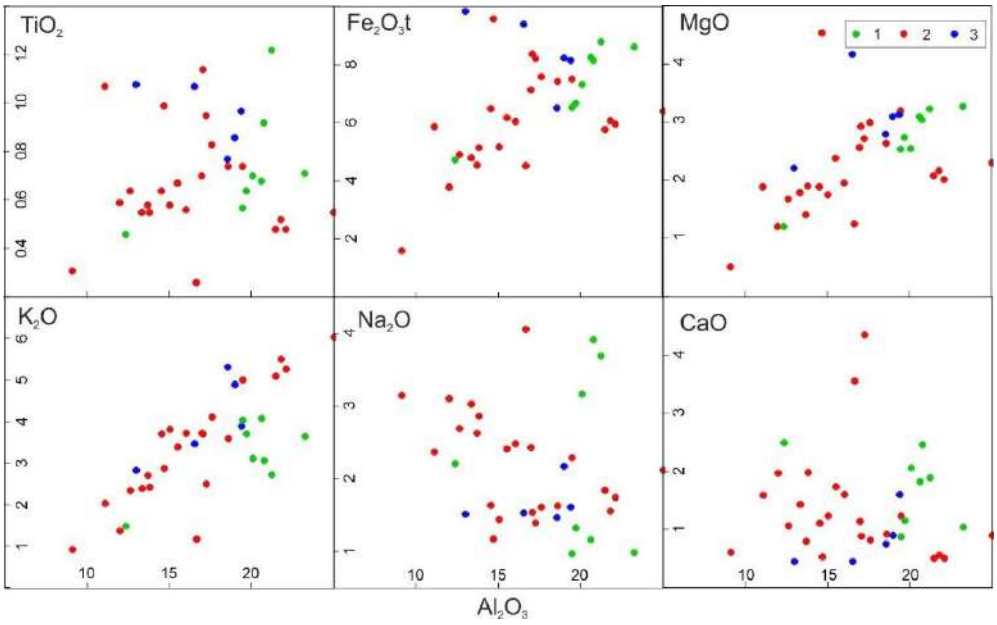

Figure I-3-2. Binary variation diagrams (Al_2O_3, wt.% – main petrogenic oxides, wt.%) for metasediments of the Ladoga series of the staurolite zone: 1 – Western block, 2 – Central block, 3 – Eastern block.

To classify the Ladoga metapelites and establish the possible primary nature of the protolith, the compositions of the Ladoga series rocks are plotted on a triangular diagram by N.P. Semenenko (Efremova, Stafeev, 1985) (Fig. I-3-3). Although the coordinates of this triangle were initially proposed by the author as the ratio of major elements to the sum: CaO / (FeO + Fe_2O_3 + MgO + Al_2O_3 + K_2O + Na_2O), Al_2O_3 / (FeO + Fe_2O_3 + MgO + Al_2O_3 + K_2O + Na_2O), (FeO + MgO) / (FeO + Fe_2O_3 + MgO + Al_2O_3 + K_2O + Na_2O), it should be noted that the operation of dividing all numerators by the same

denominator is redundant. However, this does not prevent the use of this classification diagram for a general analysis of rock compositions

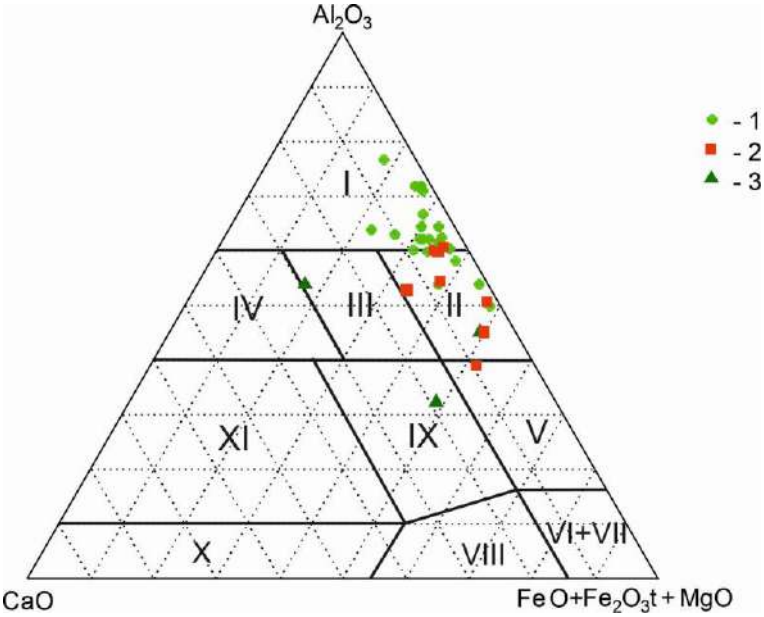

Figure I-3-3. A-C-FM diagram for rocks of the mid-temperature metamorphic zone of the Northern Ladoga region. 1 – Bt and Grt-Bt, Bt-Ms schist, 2 – St, St-Grt schist, 3 – Amph gneiss. Name of fields according to N.P. Semenenko (Efremova, Stafeev, 1985): I – aluminosilicate, II – ferrous-magnesian-aluminosilicate, III – alkaline earth-aluminosilicate ortho-series, IV – calc-aluminosilicate, V – aluminous-magnesian-ferrous-silicon, VI – ferrous-siliceous, VII – magnesian ultrabasic, VIII – alkaline-earth-low-alumina ultrabasic ortho-series, IX – alkaline-earth-alumina of the main ortho-series, X – calc-carbonate, XI – aluminous-calcareous rocks.

We have identified 2 groups of compositions, reflecting the varieties of rocks of the Ladoga series. Metamorphic rocks belong to the fields of aluminosilicate and ferruginous-magnesian-aluminosilicate rocks (Fig. I-3-3), while concentrating at the boundary of these two fields. Staurolite schists, which have a more ferruginous-magnesian composition, noticeably stand out from the general distribution.

The diagram also shows several samples of amphibole schists of the Sortavala series, which are sharply distinguished by their increased CaO content. The compositions of these rocks fall into the regions of the alkaline earth-aluminosilicate and alkaline earth-alumina basic ortho-series. The protolith of these rocks contained a large amount of volcanogenic material of basic composition, which characterizes mafic volcanics of the Sortavala series, overlying Archean rocks (Ladozhskaya Proterozoic..., 2020). These schists were selected directly from the contact areas of the Ladoga and Sortavala series rocks; sometimes the rocks of these two series are difficult to distinguish during field observation, but after petrographic and petrochemical analysis, the metapelitic or metavolcanic nature of the studied rocks becomes clear. The compositions of the Sortavala series rocks do not meet the conditions for the formation of staurolite, so they are not considered further in the work.

Due to the heterogeneity of the staurolite zone, the compositions of the Ladoga series rocks were considered within three groups, according to their belonging to one or another block of the zone (Fig. I-3-4).

The binary and ternary composition diagrams show that the chemical compositions of the rocks of each of the three blocks have their own distinctive features. The group of rocks of the Eastern block is characterized by the most ferruginous compositions, stretching along the Al_2O_3-Fe_2O_3t side. The group of rocks of the Central block has the widest ranges in the content of the main petrogenic components and is characterized by the highest contents of Al_2O_3 and Na_2O. The group of rocks of the Western block occupies an intermediate position and forms a compact area between the groups of the Central and Eastern blocks. Thus, the rocks of the three blocks of the staurolite zone differ in chemical composition.

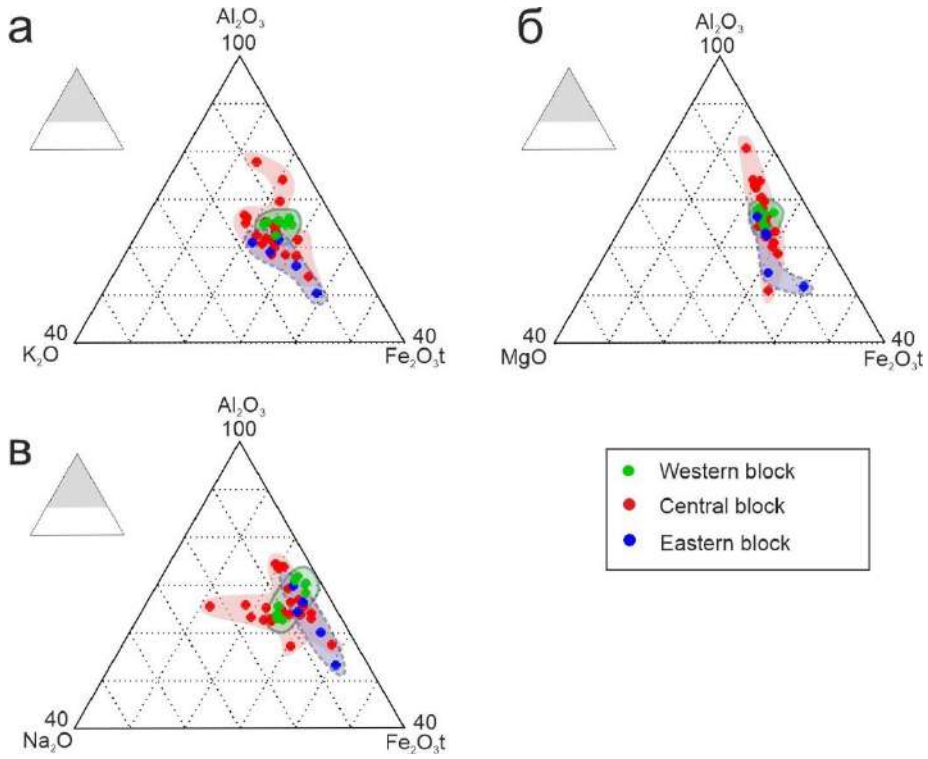

Figure I-3-4. Trernary diagrams of the composition of rocks in the mid-temperature metamorphic zone of the Northern Ladoga region: a) Al_2O_3-K_2O-Fe_2O_3t, b) Al_2O_3-MgO-Fe_2O_3t, c) Al_2O_3-Na_2O-Fe_2O_3t.

Based on the complex of geochemical characteristics, the metasediments of the Ladoga series are classified as immature, based on which it can be assumed that the concentrations of chemical elements in the rocks were not affected by significant changes during lithogenesis and, thus, the contents of elements in the sediments reflect their weighted average contents in the parent rocks (Ladoga Proterozoic ..., 2020).

Based on the content of the least mobile rare and rare earth elements, one can estimate the approximate contribution of various source rocks in the demolition area. Based on the Cr/Ti – Hf/Yb ratio, the assessment of the contribution of acidic rocks is 50-90%, basic – 10-50% and ultrabasic – up

to 10% (Ladoga Proterozoic…, 2020). Thus, the source of demolition for the formation of Ladoga sediments was not only acidic rocks of the Archean granite-gneiss basement, but also Proterozoic rocks represented by more mature continental crust, including various intrusions from ultrabasic to acidic composition.

1.4. Petrographic characteristics of rocks

Staurolite-biotite schists

(*Bt* – 30-35%, *Qtz* – 25-30%, *St* – 5-30%, *Pl* – 10-15%, *Ms* – 5-10%, *Chl* – 1-5%, accessory: *Ilm*, *Mz*).

Staurolite-biotite schists have a porphyroblastic structure: large staurolite crystals are located in a plagioclase-biotite-quartz groundmass. The colour of staurolite is usually brown to brown-black, yellow in thin sections (Fig. I-4-1). Staurolite porphyroblasts vary greatly in size from a few millimeters up to 5 cm (sometimes more) and in shape; both euhedral pseudohexagonal-prismatic crystals and xenomorphic grains are found. Staurolite is usually represented by poikiloblasts filled with numerous inclusions of small quartz grains and ilmenite needles. Along weakened or marginal zones, staurolite is replaced by aggregates of muscovite, chlorite and plagioclase. Sometimes staurolite is partially or completely replaced by andalusite or sillimanite. Staurolite is characterized by cruciform twinning.

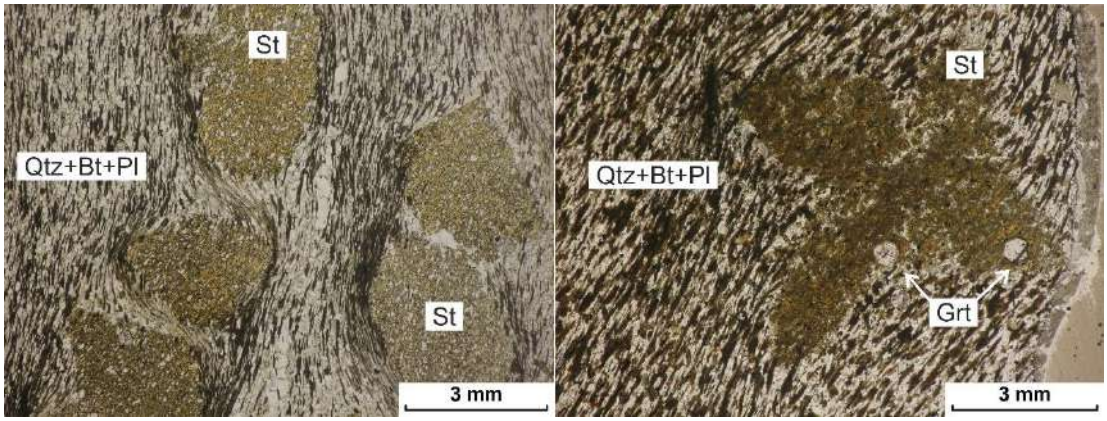

Figure I-4-1. Staurolite-biotite schist.

Staurolite often forms pseudomorphs, it can be partially or completely replaced by minerals such as muscovite, chlorite, biotite, andalusite and sillimanite (Fig. I-4-2). The replacement process occurs along cracks in staurolite, or along the edge zones of grains.

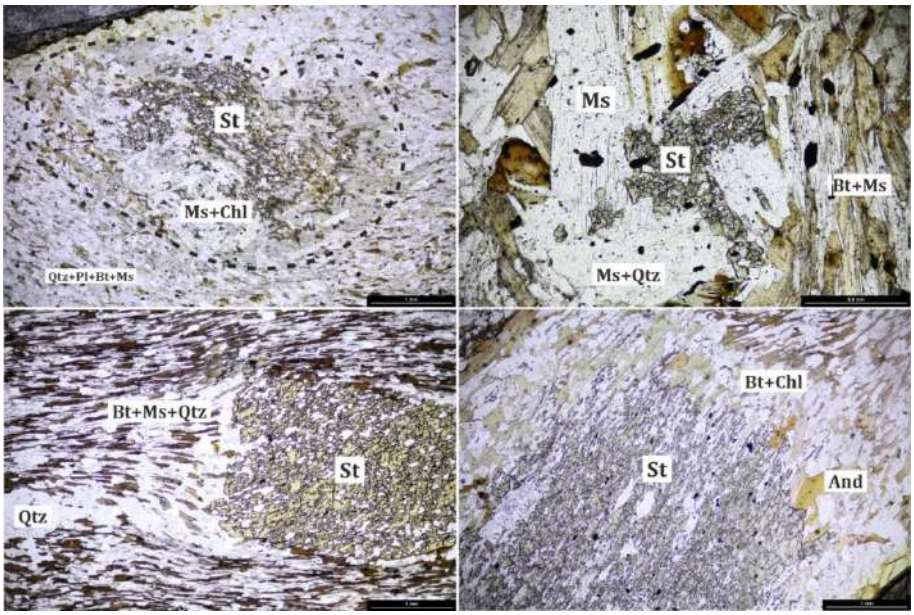

Figure I-4-2. Pseudomorphoses and replacements on staurolite.

Garnet-staurolite-biotite schists

Bt – 30-35%, *Qtz* – 25-30%, *St* – 5-30%, *Grt* – 5-10%, *Pl* – 10-15%, *Ms* – 5-10%, *Chl* – 1-5%, accessory: *Ilm, Mz, Ru*.

They are characterized by a lepidoblastic and porphyroblastic structure with a fine-grained matrix and a linear-schistose texture (Fig. I-4-3). Porphyroblasts are represented by large euhedral crystals of staurolite and garnet. The foliation is caused by the unidirectional orientation of biotite, quartz, plagioclase and muscovite grains in the groundmass. Often garnet crystals are found both directly in the matrix and in the form of inclusions in staurolite. Staurolite usually forms large porphyroblasts (up to 5 cm) of an euhedral prismatic or xenomorphic appearance, while garnet crystals are usually smaller in size (up to 1 cm) and mostly have an isomorphic appearance.

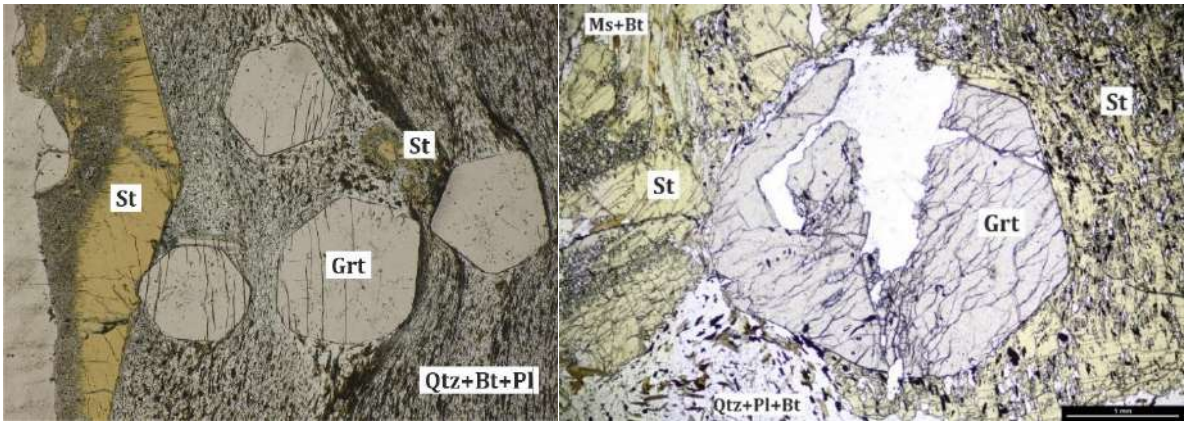

Figure I-4-3. Staurolite-garnet-biotite schist.

Staurolite-andalusite-biotite schists

Bt – 20-30%, *Qtz* – 20-30%, *And* – 10-15%, *St* – 10-15%, *Pl* – 10-15%, *Ms* – 5-10%.

They are characterized by a porphyrolepidoblastic texture; together with staurolite and garnet they form large porphyroblasts in a quartz-mica mass (Figure I-4-4). Andalusite often occurs in the form

of colorless euhedral prismatic crystals with pronounced cleavage. Andalusite also forms pseudomorphs on staurolite, replacing it partially or completely; in such cases, andalusite retains the appearance of staurolite porphyroblasts, usually of an isometric shape with numerous quartz inclusions (Fig. I-4-5).

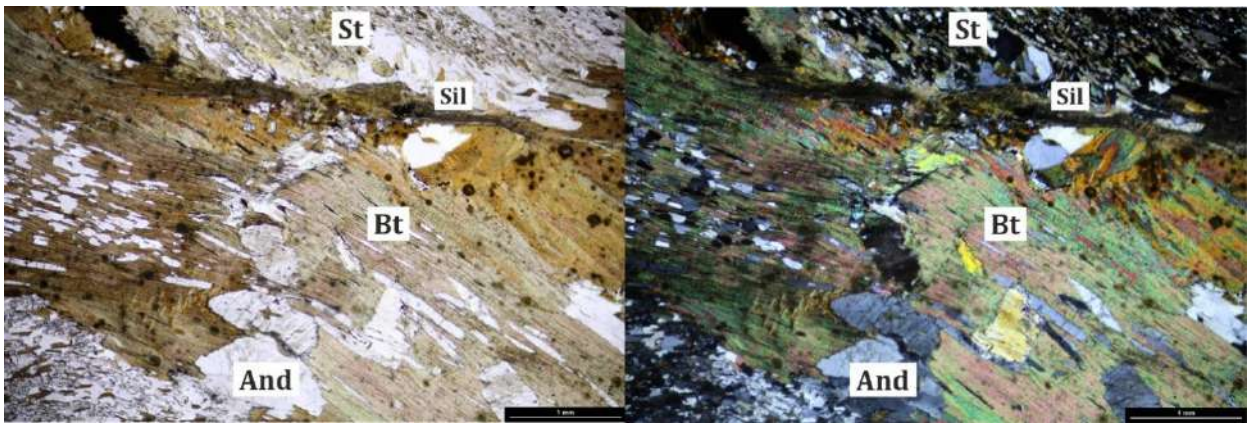

Figure I-4-4. Staurolite-andalusite-biotite schist.

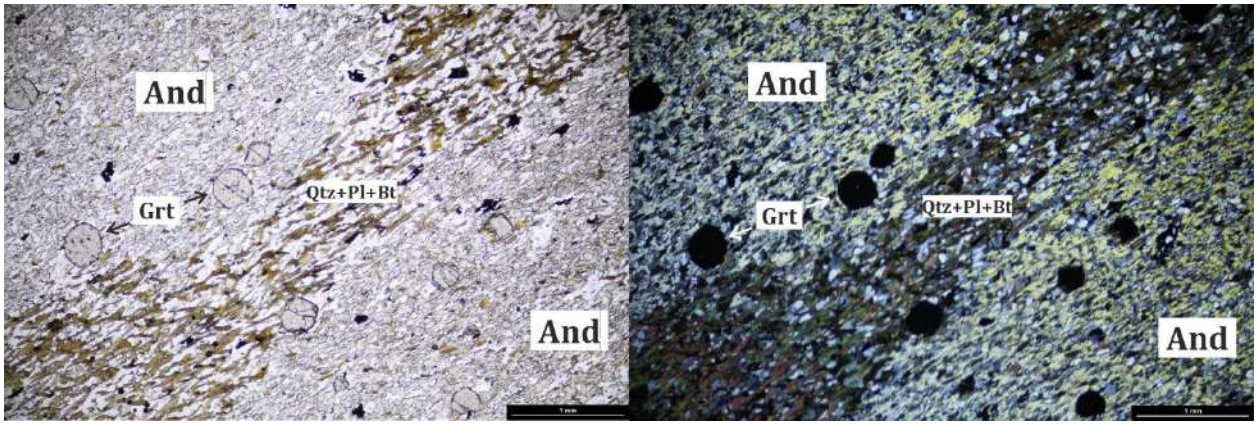

Figure I-4-5. Andalusite-biotite schist. Large porphyroblasts of andalusite – pseudomorphs after staurolite with inclusions of garnet crystals.

1.5. Features of mineral compositions

Staurolite. Staurolite crystals have a prismatic, flattened appearance, up to 2 cm in size (sometimes up to 10 cm). When examined microscopically, it is distinguished by a sponge-like structure, due to the abundance of inclusions of quartz, monazite, ilmenite; secondary minerals develop along cracks and weak zones – muscovite, biotite, chlorite, plagioclase (Fig. I-4-6). The iron content of staurolite varies from 0.75 to 0.90, with the most ferruginous compositions characteristic of staurolite from rocks of the Eastern block of the staurolite zone. In staurolite crystals, titanium content noticeably decreases from centre to edge (0.64-0.27 wt.% TiO_2), zinc content increases unevenly (0.09-0.9 wt.% ZnO), manganese content varies greatly (0.00-0.65 wt.% MnO) (Fig. I-4-7, I-4-8). In general, the staurolites from the three blocks differ in the content of main elements. Staurolites from the Western block are characterized by the highest content of Al, increased contents of Mg, Mn with relatively low iron content; staurolites from the Central block are characterized by high contents of Zn, Mn, Mg, Ti; staurolites from the Eastern block, on the contrary, have lower contents of Al, Mn, Zn , but the highest

contents of Fe and Mg are characteristic in one sample (Fig. I-4-9). The binary diagrams show that Al and Si form a strong negative correlation, pairs of elements Fe and Mg, Fe and Zn form a weak negative correlation (Fig. I-4-9). Mn and Fe do not correlate with each other, and the low concentration of Mn in staurolite must also be taken into account.

For staurolites from different parts of the staurolite zone, general crystallochemical formulas were calculated (according to Fedkin, 1975):

- The Western block: $[Fe^{2+}_{1.31\text{-}1.69}Mg^{2+}_{0.20\text{-}0.35}Ti^{4+}_{0.04\text{-}0.09}Zn^{2+}_{0.0\text{-}0.1}Mn^{2+}_{0.0\text{-}0.08}]_2^{IV\text{-}VI}[Fe^{2+}_{0.0\text{-}0.03}Fe^{3+}_{0.07\text{-}0.42}Cr^{3+}_{0.0\text{-}0.04}Al^{3+}_{8.82\text{-}9.0}]_9^{VI}[Al^{3+}_{0.09\text{-}0.35}Si^{4+}_{3.65\text{-}3.91}]_4^{IV}O_{24}(OH)_2$.
- The Central block: $[Fe^{2+}_{1.21\text{-}1.60}Mg^{2+}_{0.19\text{-}0.36}Ti^{4+}_{0.04\text{-}0.08}Zn^{2+}_{0.0\text{-}0.17}Mn^{2+}_{0.02\text{-}0.07}Ca^{2+}_{0.0\text{-}0.04}]_2^{IV\text{-}VI}[Fe^{3+}_{0.0\text{-}0.39}Cr^{3+}_{0.0\text{-}0.02}Al^{3+}_{8.76\text{-}9.23}]_9^{VI}[Al^{3+}_{0.06\text{-}0.33}Si^{4+}_{3.67\text{-}4.03}]_4^{IV}O_{24}(OH)_2$.
- The Eastern block: $[Fe^{2+}_{1.38\text{-}1.72}Mg^{2+}_{0.18\text{-}0.38}Ti^{4+}_{0.03\text{-}0.08}Zn^{2+}_{0.0\text{-}0.08}Mn^{2+}_{0.0\text{-}0.08}]_2^{IV\text{-}VI}[Fe^{2+}_{0.0\text{-}0.06}Fe^{3+}_{0.0\text{-}0.29}Cr^{3+}_{0.0\text{-}0.02}Al^{3+}_{8.97\text{-}9.16}]_9^{VI}[Al^{3+}_{0.05\text{-}0.28}Si^{4+}_{3.72\text{-}3.95}]_4^{IV}O_{24}(OH)_2$.

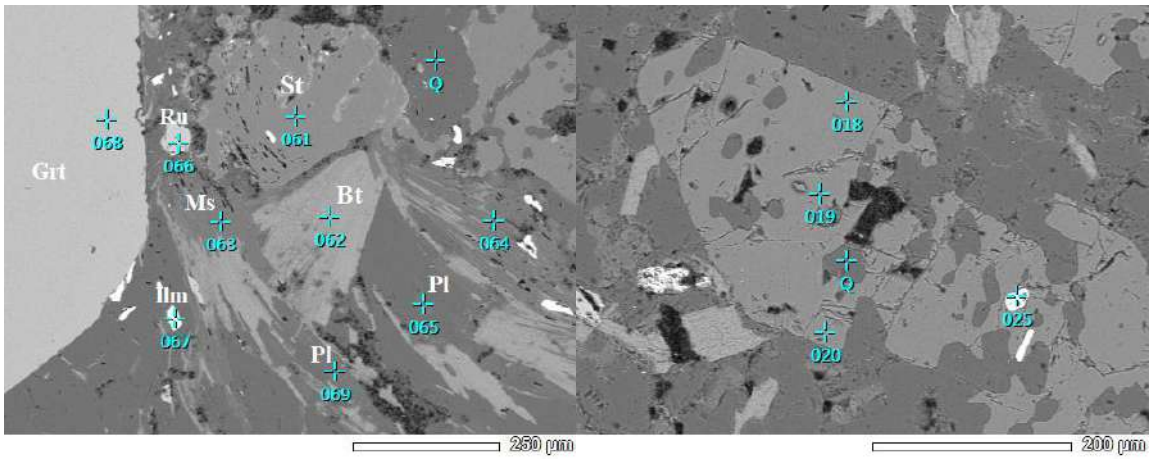

Figure I-4-6. a) Replacement of staurolite with muscovite, biotite with the release of quartz and plagioclase (sample B-05-177) (BSE); b) Euhedral prismatic crystal of staurolite with inclusions of quartz and ilmenite. Subject to replacement by mica with precipitation of quartz. (sample B-11-239-2) (BSE).

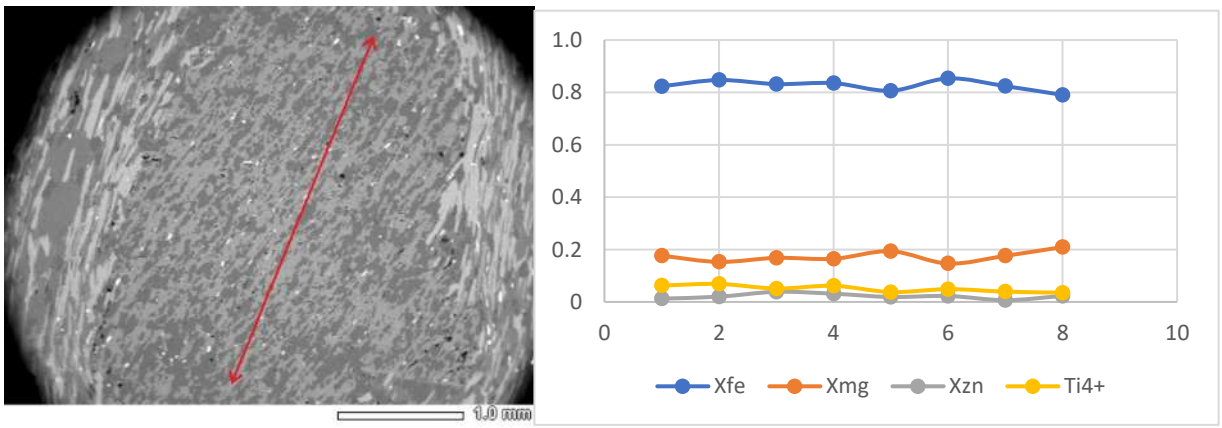

Figure I-4-7. Composition profile of staurolite (sample B-05-175).

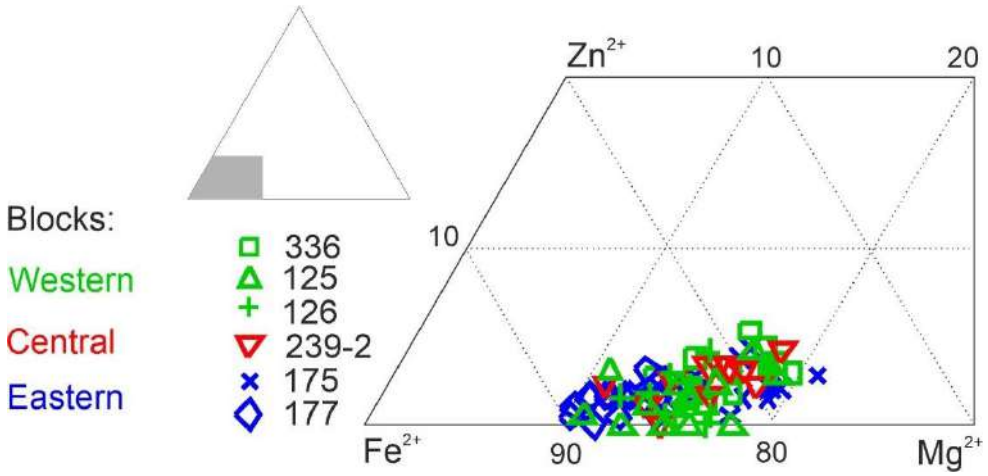

Figure I-4-8. Triple diagram of the composition of staurolite from rocks of the Ladoga series of the staurolite zone.

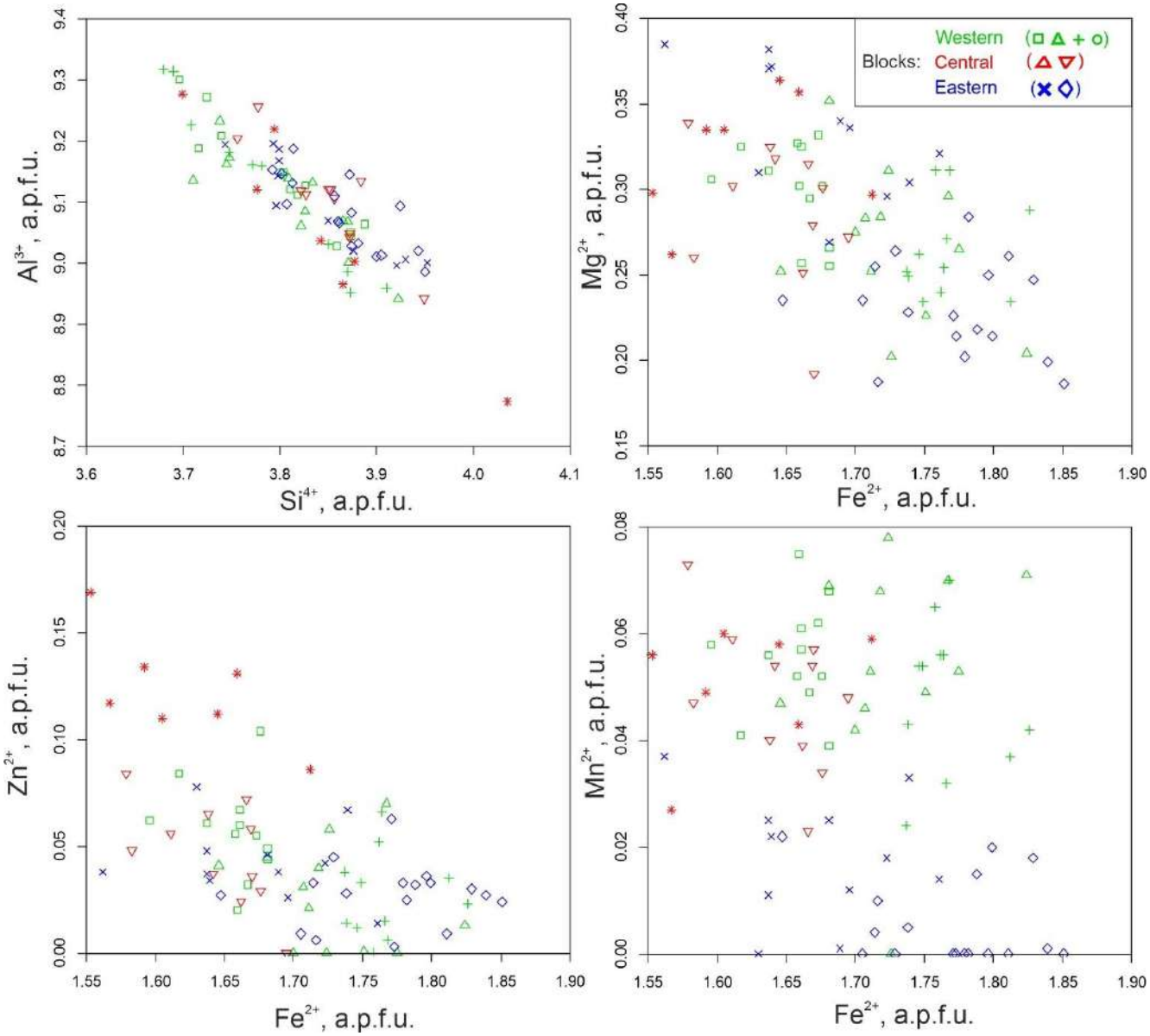

Figure I-4-9. Binary diagrams of staurolite composition, staurolites from different parts of the staurolite zone are shown in different colors.

Garnet. Garnet porphyroblasts are most often represented by rather large crystals of rhombic dodecahedral habit, sometimes xenomorphic grains (from 0.2 to 1-2 cm). Garnet contains a large number of small inclusions of quartz, ilmenite and monazite. Garnet is characterized by S-shaped growth structures. In some rocks, the composition of garnet is homogeneous, zoning is extremely weak: for garnet from the Eastern block - Alm (0.86-0.89), Sps (0.00-0.2), Prp (0.04-0.09), Grs (0.03-0.05) (Fig. I- 4-10 a), for garnet from the Western block - Alm (0.75-0.76), Sps (0.09-0.12), Prp (0.09-0.11), Grs (0.03-0.05) (Fig. I-4-11 a, b). However, in adjacent rocks with identical mineral composition, garnet often displays zoning with a pronounced “progressive” character - from the centre to the edge of the grains, the content of almandine and pyrope components noticeably increases with a decrease in spessartine and grossular. In the zoned garnet from the Eastern block, the content of end-members of solid solution varies within the following limits: Alm (0.62-0.77), Sps (0.07-0.20), Prp (0.05-0.10), Grs (0.07-0.12) (Fig. I-4-10 b) , from Western: Alm (0.61-0.70), Sps (0.14-0.21), Prp (0.05-0.08), Grs (0.08-0.15) (Fig. I-4-11 c), zoning is most clearly manifested in garnet from Central block: Alm (0.54-0.80), Sps (0.05-0.29), Prp (0.03-0.08), Grs (0.07-0.14) (Fig. I-4-12).

In general, garnets from the Eastern Bloc are more ferruginous; garnet from sample. Garnets from the sample B-05-177 is represented by almost pure almandine. A similar trend is observed for the composition of staurolite associated with garnet. Garnet from the Central Block is characterized by a high content of spessartine component with relatively high iron content (Fig. I-4-13).

Garnet is subject to secondary replacement by the association of plagioclase, biotite, quartz, as well as muscovite and chlorite. Sometimes garnets completely replaced by pseudomorphs are found. In a sample from the Central block (sample B-19-315), rather wide leucocratic plagioclase-quartz rims (1-1.5 mm wide) are observed around large xenomorphic garnet grains. At the contact between staurolite and garnet, a thin (~50 nm) quartz rim with small acicular ilmenite precipitates is sometimes observed (Fig. I-4-14). The relationship between staurolite and garnet is apparently only mechanical, there are no signs of reactionary substitution/exchange of components.

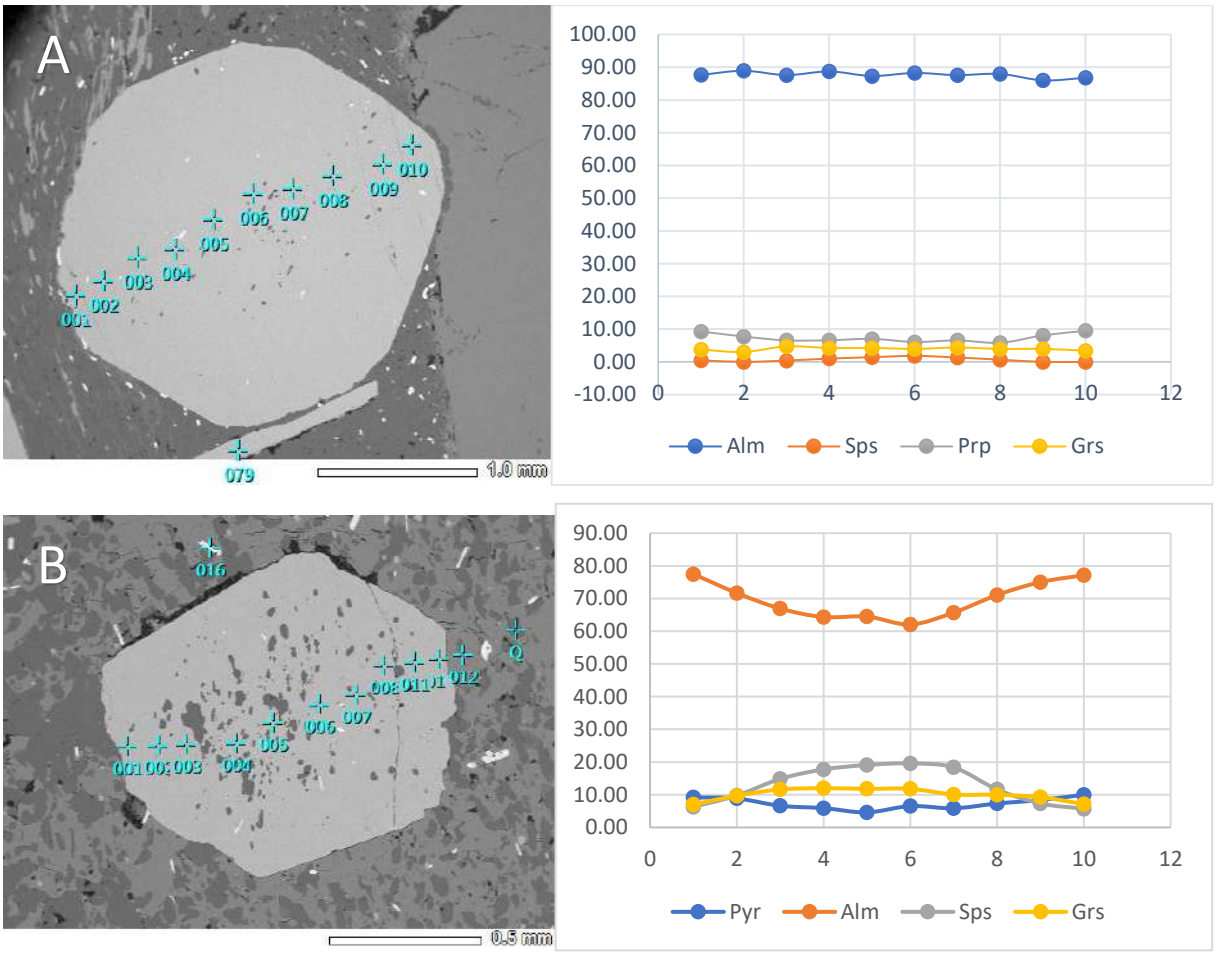

Figure I-4-10. Garnet crystals from the Eastern Block in BSE and concentration profiles for them. a) B-05-177; b) B-05-175.

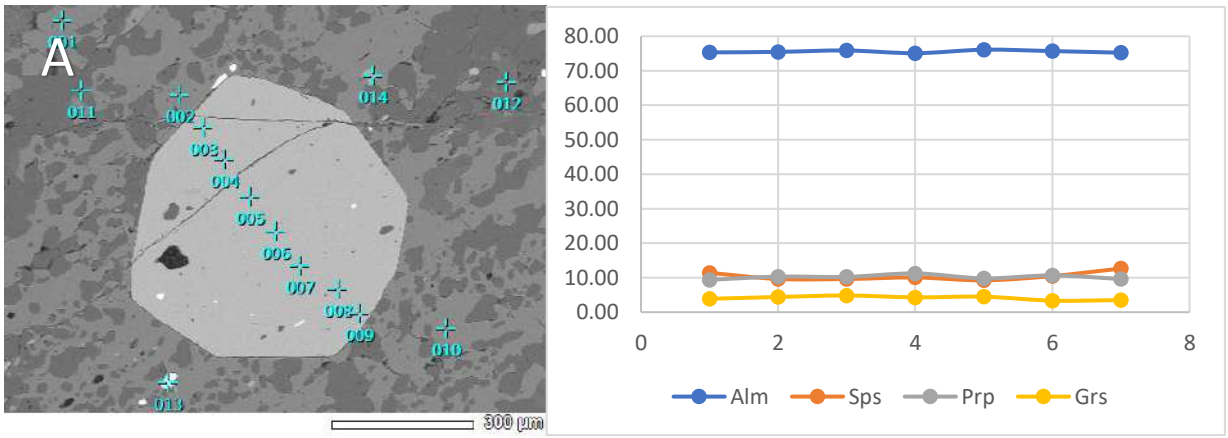

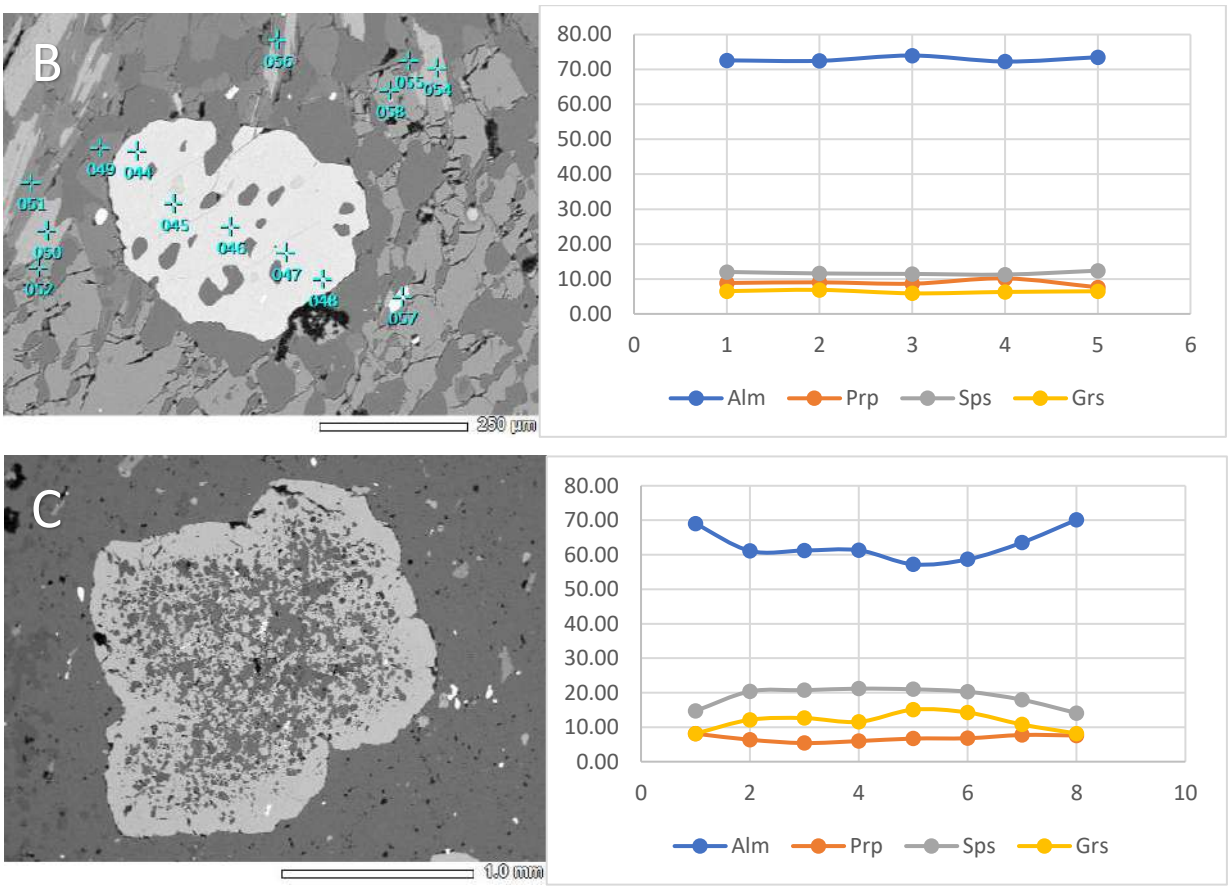

Figure I-4-11. Garnet crystals from the Western Block in BSE and their concentration profiles. a) B-19-336, b) B-03-125, c) B-03-120-2.

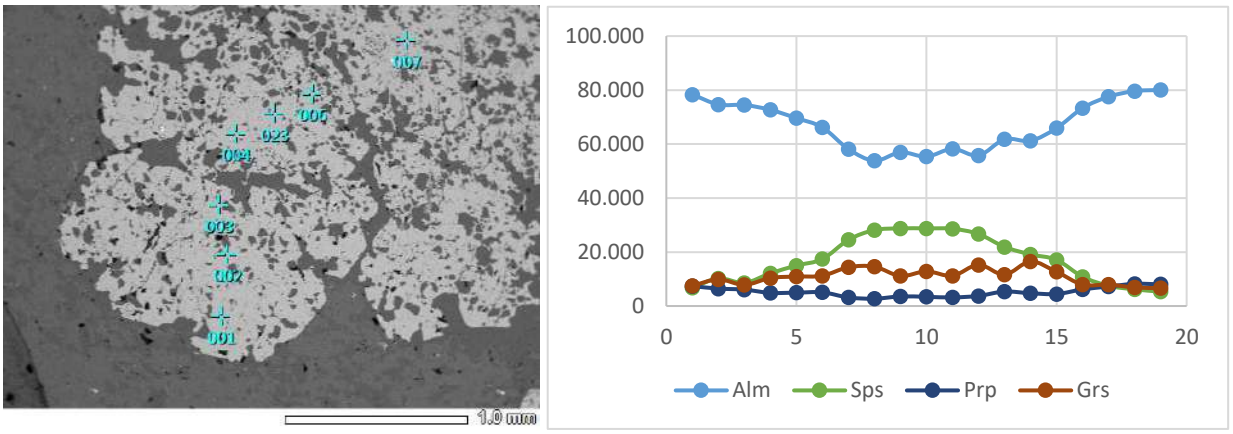

Figure I-4-12. Garnet crystal from the Central block in BSE and its concentration profile (sample B-19-315).

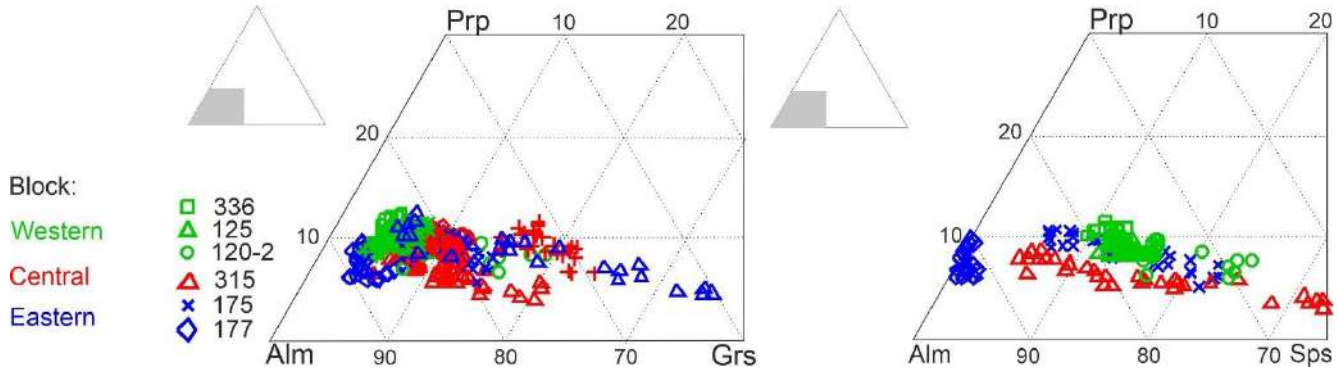

Figure I-4-13. Triple diagrams of the composition of garnets from Grt-Bt (B-19-315, B-03-120-2) and Grt-St-Bt (B-19-336, B-05-177, B-05-175, B-03-125) schists.

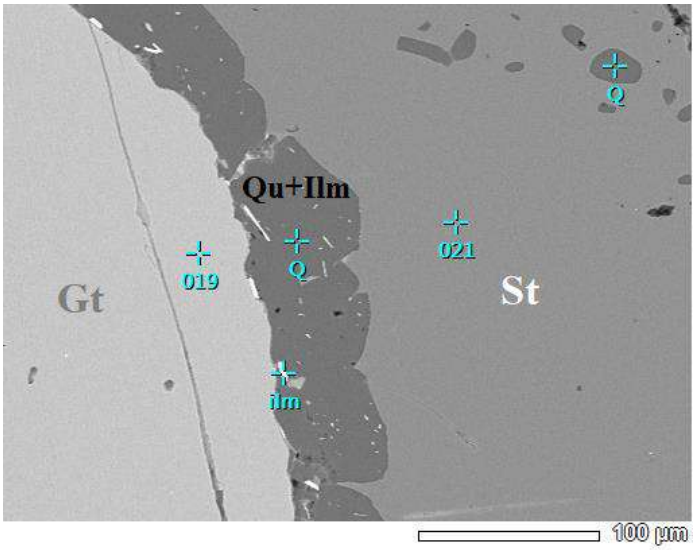

Figure I-4-14. Quartz rim with ilmenite needles between garnet and staurolite porphyroblasts (sample B-05-177) (BSE).

Plagioclase. Present in the matrix together with quartz and biotite, as well as in leucocratic zones around garnet porphyroblasts. It is represented by oligoclase-andesine (An_{20-26}) and andesine (An_{30-40}), in one sample of staurolite-biotite schist from the Central block (sample B-19-315) plagioclase is the most basic - the content of the anorthite component reaches An_{70} (Fig. I -4-15).

Biotite represented by lamellar crystals of brown, brown colors, sometimes replaced by chlorite. It is the main matrix mineral in schists and often envelops garnet and staurolite porphyroblasts. In terms of iron content, biotite at the contact with garnet and biotite from the matrix do not differ (X_{Fe} 0.58-0.62), while the former is characterized by a lower content of TiO_2 (0.87-1.48 wt.%) relative to the latter (1.50-1.72 wt.% TiO_2). Biotite from the Western and Central blocks of staurolite zone are distinguished by increased titanium content compared to biotite from the Eastern block (Fig. I-4-16 a).

According to the classification diagram (Deer, 1982) (Fig. I-4-16 b), biotites from the schists of the Ladoga series are represented predominantly by siderophyllite, which is the most aluminous and ferruginous representative of the biotite group. Biotite from one sample of the Eastern Block (sample B-05-175) is located at the istonite-siderophyllite boundary.

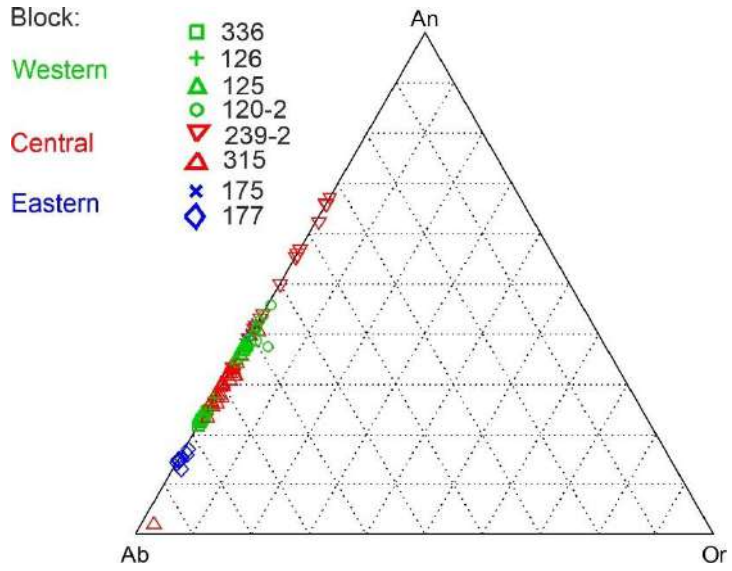

Figure I-4-15. Triple diagram of the composition of plagioclase from metapelitic schists of the staurolite zone.

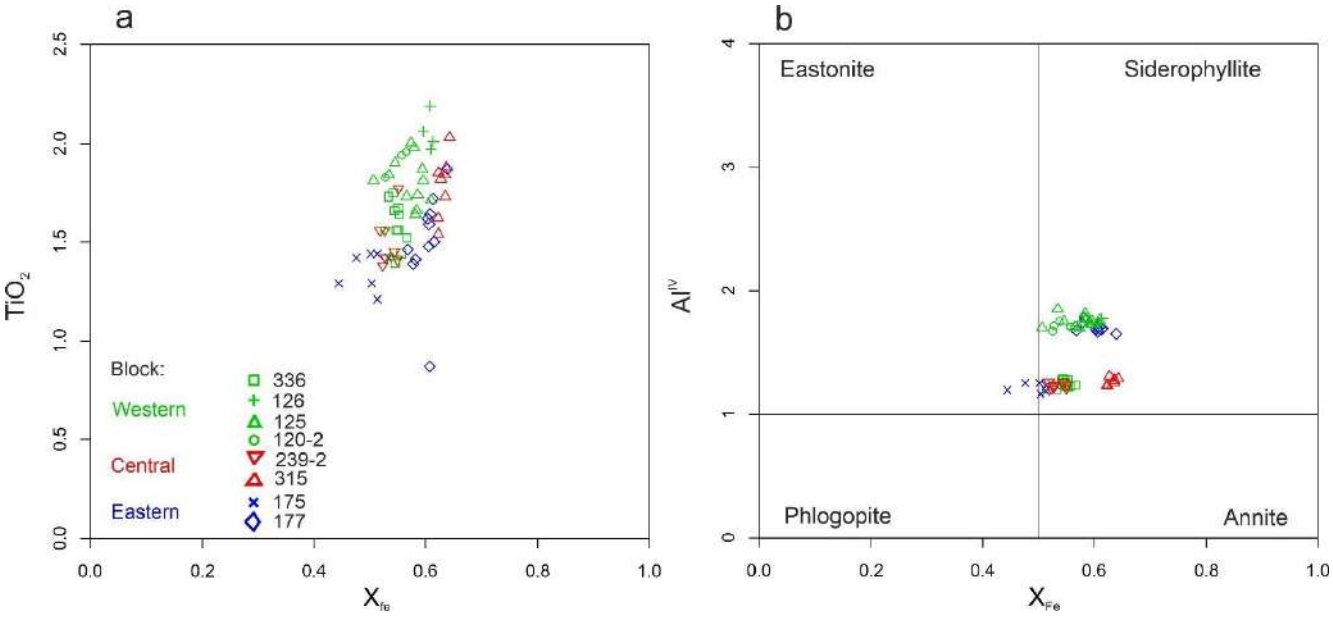

Figure I-4-16. A - Binary diagram of biotite composition. The abscissa axis shows iron content (XFe = (FeO+MgO)/FeO), and the ordinate axis shows the TiO_2 content in mass%. B - Classification diagram of biotite according to (Deer, 1982).

Summary of the chapter

In the medium-temperature zone of the metamorphic complex of the Northern Ladoga region, various schists and gneisses of predominantly metapelite composition are developed, among which staurolite-containing varieties are represented by staurolite-biotite, garnet-staurolite-biotite, staurolite-andalusite-biotite schists. Within the staurolite zone, three blocks of development of staurolite-containing rocks are distinguished: Western, Central and Eastern, separated by large faults of meridional strike. The differences between the identified blocks can also be traced in the chemical compositions of

the rocks and their constituent minerals. The reasons for the difference in the composition of rocks in the blocks we identify may be: 1) different erosional cuts and folding, as a result of which layers of metaturbidites from different places in the sequence emerge on the surface (the estimated thickness of the Ladoga series is up to 3 km); 2) perhaps mineral formation was determined by different crystallization regimes, as well as the specific composition of fluids within these three blocks. The collective monograph on the geology of the Ladoga region (Ladozhskaya Proterozoic..., 2020) notes the difference in grain size composition between the northern, central and southern sections of the Ladoga series. The northern sections are composed of more sorted sediments (from sandstones to pelites), while the central and southern sections are composed of less differentiated varieties (from sandstones to siltstones).

The chemical compositions of the rocks of each of the three blocks have their own distinctive features. The group of rocks of the Eastern block is characterized by the most ferruginous compositions, the group of rocks of the Central block has the widest ranges in the content of the main petrogenic components and is characterized by the highest contents of Al_2O_3 and Na_2O, the group of rocks of the Western block occupies a middle position and forms a compact area between the groups of the Central and Eastern blocks. The compositions of the main minerals in staurolite-bearing schists also differ in different parts of the staurolite zone: staurolites of the Western block are characterized by increased contents of Al_2O_3, TiO_2, MnO, ZnO with relatively low iron content, while staurolite and garnet from the Eastern block of the region are the most ferruginous. Garnet from the Central Block is characterized by a high content of spessartine component and relatively high iron content. Biotites from the Western and Central blocks are characterized by increased titanium content compared to biotite from the Eastern block.

CHAPTER 2. P-T CONDITIONS AND FLUIDS REGIME OF ROCKS FORMATION IN THE STAUROLITE ZONE OF THE NORTHERN LADOGA REGION

This chapter examines the features of staurolite-containing rocks of the Northern Ladoga region: the results of empirical and model data on the prograde and retrograde transformations of staurolite from the stage of formation, expansion of stability and subsequent replacement of this mineral by newly formed mineral aggregates are presented. The characteristics of the fluid regime of metamorphism in the medium-temperature zone of the complex are also considered.

2.1. Mineral thermobarometry

To determine the P-T conditions of metamorphism of Ladoga rocks from the staurolite zone, the TWEEQU multi-equilibrium thermobarometry method (Berman, 1991) was used using a combination approach (Dolivo-Dobrovolsky, 2006a). Most calculations were performed for the paragenesis Qtz + Pl + Bt + Grt + Ilm ± Ru, where garnet has 4 terminals (Alm, Prp, Sps, Grs), and biotite has 4 terminals (Phl, Ann, Eas, Sid). The calculations involve 3 independent reactions (IR), describing the relationships between the components of minerals – solid solutions and minerals of constant composition:

1. *Alm + Phl = Prp + Ann*
2. *Ms + Grs + Alm = Ann +An*
3. *Sid + Qtz + Prp + Grs = Alm + An + Phl*

The first of these reactions is an exchange (Fe-Mg) reaction between garnet and biotite, widely used as a geothermometer, while the second and third are shifted equilibrium reactions. The criterion for equilibrium in multi-equilibrium thermobarometry is the convergence of reactions at one point on the TWQ diagrams (Berman, 1991). Accordingly, those with the greatest convergence were selected as the results from all calculations. The results are presented in Table 3, Figure II-2-1 shows the results for samples from each block of the staurolite zone.

Based on the results of multi-equilibrium thermobarometry, P-T conditions for the formation of staurolite-containing and staurolite-free schists of the staurolite zone were established: for the Western block T = 550–615°C, P = 3.7-5.2 kbar, for the Central block T = 570-650°C, P = 4.1–4.8 kbar, for the Eastern block T=510-550°C, P = 3.7-5.5 kbar. In general, all estimates of the P-T conditions of metamorphism of rocks of the staurolite zone are determined in the intervals T = 510-650°C, P = 3-6 kbar, which corresponds to the estimates of other authors for the medium-temperature staurolite zone of the Northern Ladoga region (Baltybaev et al., 2000, etc.).

It is worth noting that for some samples (for example, sample B-19-315) the presence of muscovite was not noted in the paragenesis, which limits the number of independent reactions to two. The exchange reaction between garnet and biotite serves as a geothermometer - the line on the P-T diagram is subvertical, the second reaction has a subhorizontal slope and is taken as a geobarometer.

However, it is worth considering that a reliable assessment using the multi-equilibrium thermobarometry method comes from the intersections of at least three independent reactions.

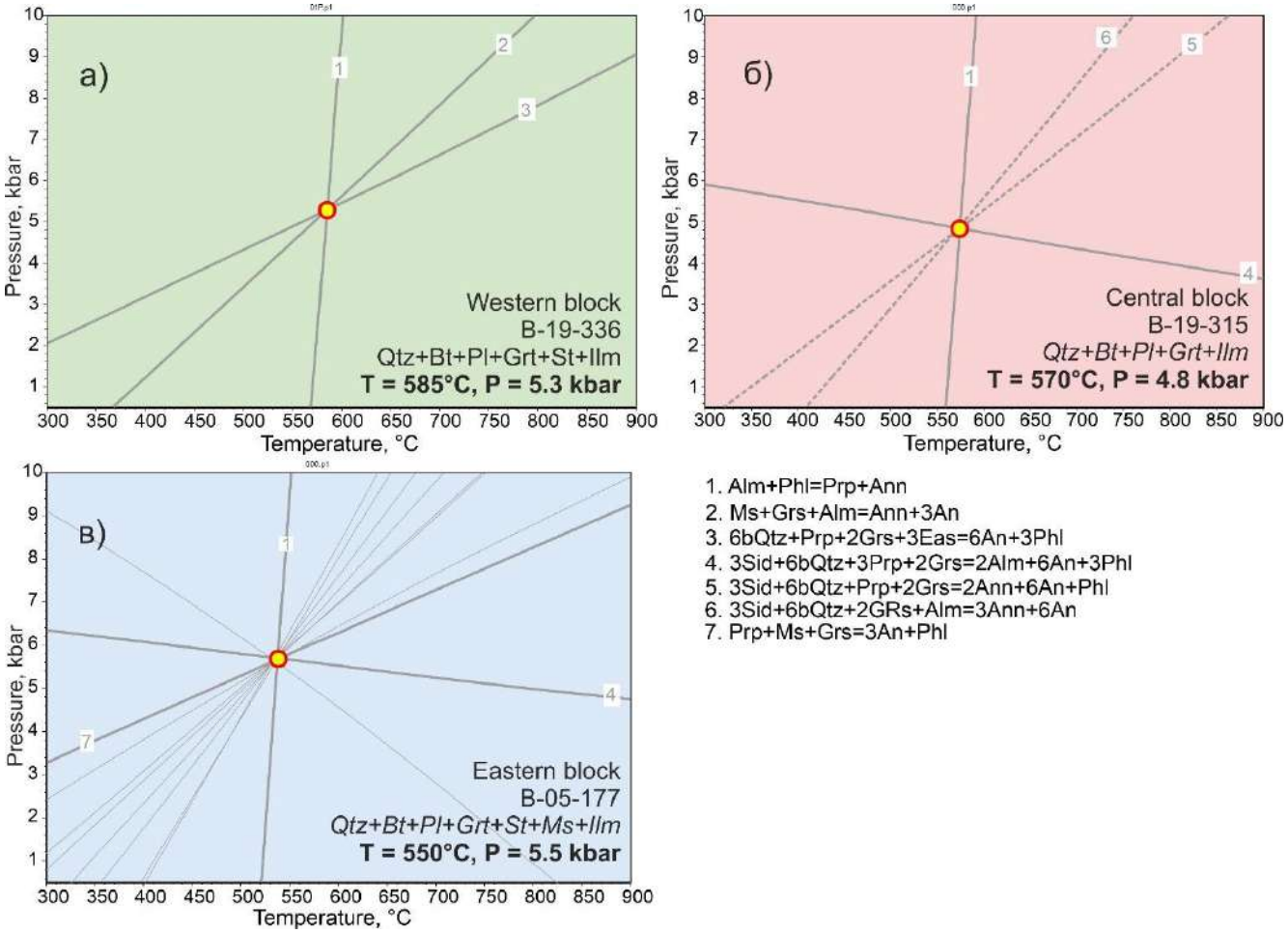

Figure II-2-1. TWQ diagrams with converging lines of mineral reactions for the assemblage Pl + Bt + Grt + Qtz + Ilm ± Rt from garnet-staurolite-biotite schists of the staurolite zone. a) B-19-336 (Western block); b) B-19-315 (Central block); c) B-05-177 (Eastern block).

2.2. Thermodynamic modeling

Applicability of modeling to natural samples

This part of the chapter provides examples of several mineral equilibrium calculations based on samples of metapelites of the Ladoga series. Using modeling, we can reconstruct the sequence of mineral formation that changes during the metamorphism of the parent rocks. A number of samples of Ladoga metapelites selected during field research were tested, the result showed excellent reproducibility of medium-temperature mineral parageneses observed in nature.

Sample B-05-177 is a garnet-staurolite-biotite schist from the western frame of the Kokkaselsky granite-gneiss dome (Eastern block of the staurolite zone). On the P-T diagram, the low-temperature (<500°C) region is represented by the association Qtz ± Bt + Pl + Ms + Chl ± Ilm ± Tit ± Ru, and the high-temperature (500–700°C) region is characterized by the appearance of Crd, St, Grt. The highest

temperature parageneses contain Opx, Sil, hydrous minerals disappear in them, and melt appears due to the anatexis of pelites (Fig. II-2-1).

Staurolite appears in the region: T = 510−635°C, P > 2 kbar (Fig. II-2-1 a, b). As T and P increase, a Qtz + Bt + St + Pl + Ilm + Grt paragenesis appears, stable in the region: T = 550–630°C, P > 3.5 kbar. In Qtz + Bt + St + Pl + Crd + Chl + Ilm paragenesis, with increasing P and T, Chl first disappears, Grt appears (at 540–550°C), and then Crd disappears. With an increase in P in the paragenesis Qtz + Bt + St + Pl + Ilm + Chl + And, And first disappears, Grt appears, and then Chl disappears (Borisova et al., 2024).

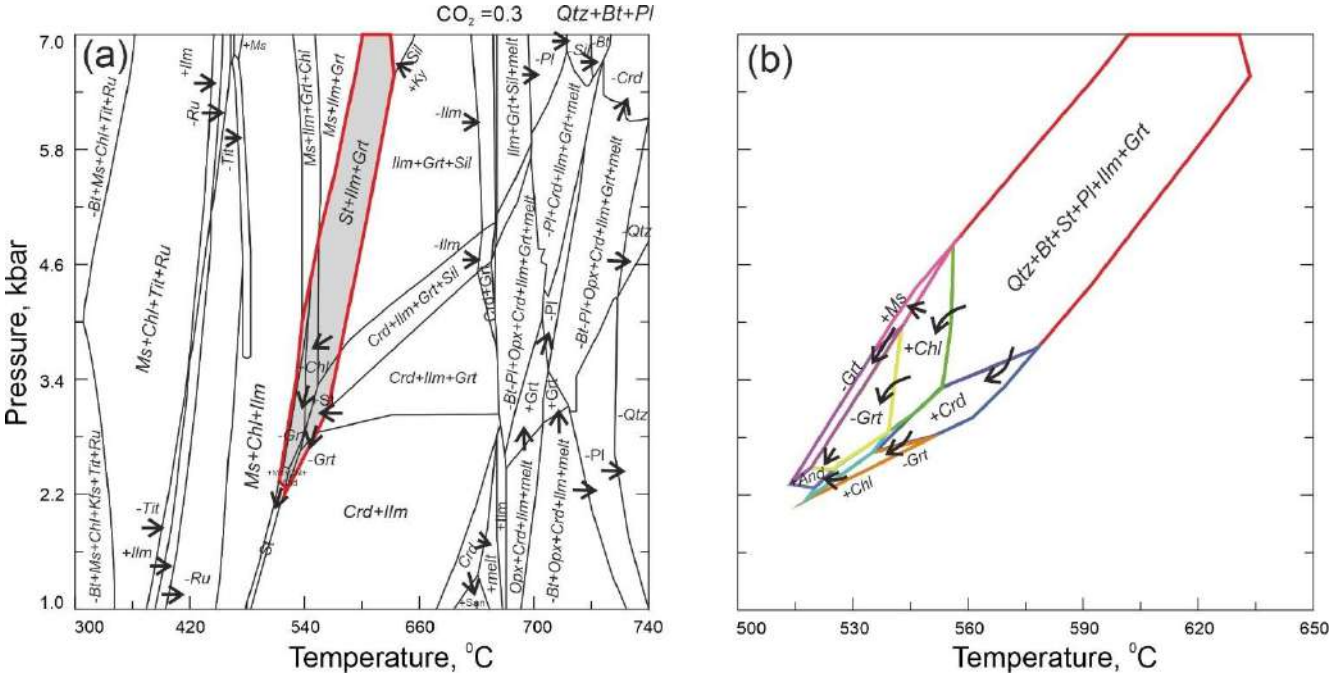

Figure II-2-1. Results of computer modeling of the mineral compositions of metapelites: a – P-T diagram of the stability fields of minerals (for the composition of sample B-05-177). The red line marks the area where staurolite is present; b – detailing of the area of existence of staurolite-containing parageneses. The "+" and "–" signs indicate the presence or absence of the mineral phase indicated by the arrow in a given area.

Next, consider modeling mineral formation using the example of a staurolite-free sample from the same Eastern block. Despite the fact that the sample of double-mica (Qtz + Bt + Ms + Pl) schists B-05-176 is located in close proximity to the above (within the staurolite zone), the development of staurolite is not observed in it either in the rock itself or during modeling (Fig. II-2-2). In the mid-temperature zone, where staurolite could develop, the Qtz + Bt + Ms + Pl paragenesis is reproduced in this rock.

For all tested samples of the Ladoga series, thermodynamic modeling well reproduced the observed mineral parageneses in the mid-temperature region: staurolite appears in the region: T = 510−635°C, P > 2 kbar. If metamorphism had occurred at higher temperatures, then instead of staurolite

rocks, cordierite- or sillimanite-containing ones would have appeared, and at lower temperatures, mica schists with chlorite would have appeared.

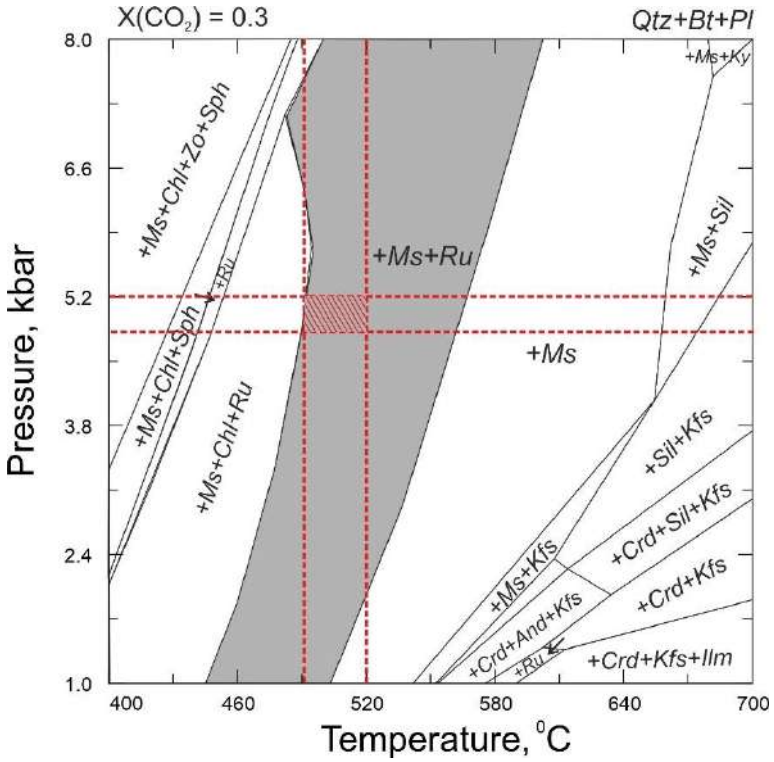

Figure II-2-2. P-T diagram of stability fields of minerals (for the composition of sample B-05-176).

In lithological units containing staurolite-free rocks (biotite, two-mica, garnet-biotite gneisses and schists, etc.), modeling of the sequence of metamorphic mineral formation showed good reproducibility of real parageneses: under the same P-T conditions in these rocks (with different bulk composition) staurolite is not formed.

Mineral formation modeling results

When modeling phase mineral equilibria using the PERPLE_X program (Connolly, 1990), the input data were the results of chemical analyses of metapelites (Tables 1, 2). For a detailed analysis of the processes of mineral formation, the most contrasting compositions of staurolite-bearing schists from three blocks of the staurolite zone were selected in order to assess the influence of rock composition on the formation of staurolite (Western block - sample B-19-336, Central - B-2011-239-2, Eastern - B-05-177). The selected compositions differ in the content of petrogenic oxides and reflect variations in the composition of metapelites within the entire staurolite zone of the Northern Ladoga region (Fig. II-2-3). In this part of the section, prograde and retrograde processes of transformation of staurolite parageneses in metapelites are considered. When solving a direct modeling problem, i.e. in the search for mineral parageneses observed in nature for given rock composition and P-T parameters, it was assumed that the system contains aqueous-carbon dioxide fluid, the mole fraction of carbon dioxide in which was taken

to be 0.3, according to the study of fluid inclusions in synmetamorphic quartz veins from metapelites (Baltybaev et al.., 2000).

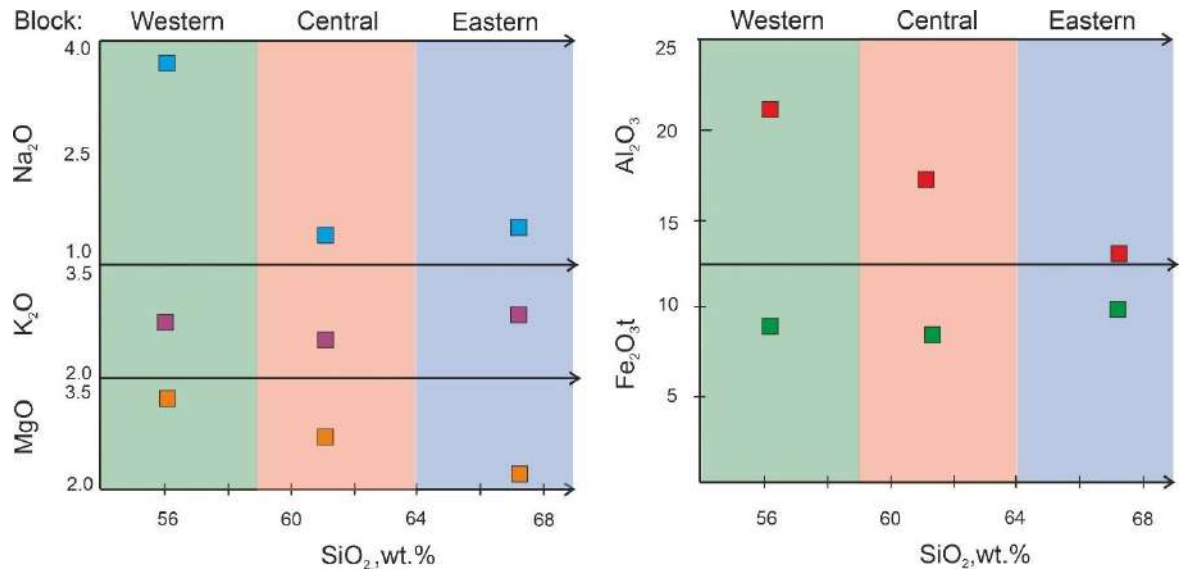

Figure II-2-3. Contents of petrogenic oxides (wt. %) in staurolite-containing schists with contrasting chemical composition from three blocks of the staurolite zone (B-19-336, B-2011-239-2, B-05-177).

Prograde transformations

The formation of staurolite in metapelites can occur either due to chloritoid (in the association Cld + Qtz + Ms + Chl) or due to chlorite and muscovite (Qtz + Ms + Bt + Chl) (Hoschek, 1969). In the Northern Ladoga region, in the metapelites of the biotite zone, where the development of chloritoid would be expected, there is a complete absence of associations with this mineral, despite the widespread development of staurolite in higher temperature zones (Velikoslavinsky, 1972). Previously, it was believed that the formation of staurolite in zoned metamorphic complexes occurs only due to chloritoid, but Hoschek (1969) showed that chloritoid rocks have an even narrower field of chemical compositions than staurolite rocks, and staurolite does not arise only due to the Cld + Qtz association + Ms + Chl, but also due to the association Qtz + Ms + Bt + Chl.

Thermodynamic modeling in the PERPLE_X program (Connolly, 1990) in the low- and medium-temperature range (<520°C) for all compositions of the Ladoga series rocks confirms the absence of chloritoid. Although for the most ferruginous and aluminous compositions of metapelites from other regions, the chloritoid is reproduced (Baltatzis, 1979; Keller et al., 2005; Moynihan, 2012, etc.). Computer modeling using a wide range of theoretical compositions has established that more aluminous and less magnesian compositions of the protolith with ratios (wt.%) of oxides $Al_2O_3/MgO > 10$ and $FeOt/MgO > 5$ are favorable for the appearance of chloritoid.

Thus, the modeling results confirm empirical observations about the absence of chloritoid in the metapelites of the Northern Ladoga region. As can be seen in the P-T diagrams (Fig. II-2-4) for the basic

composition of metapelites of the Ladoga region, the areas of development of staurolite-containing parageneses are preceded by the paragenesis Qtz + Bt + Pl + Ms + Chl + Ilm ± Grt.

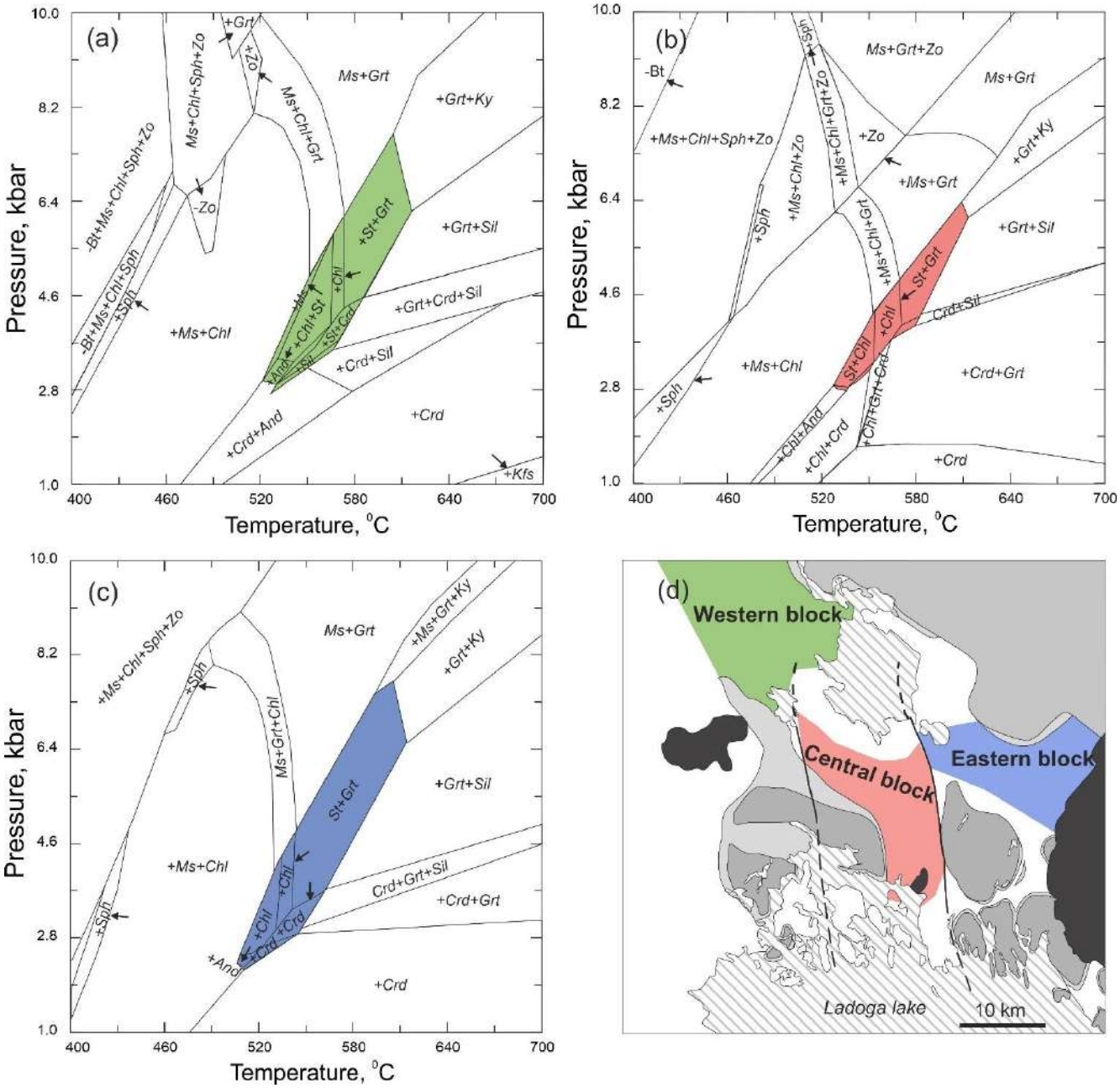

Figure II-2-4. P-T diagrams of mineral parageneses of metapelites: (a) for sample. B-19-336 from the Western block, (b) for sample. B-2011-239-2 from the Central block, (c) for sample. B-05-177 from the Eastern block, (d) blocks of the staurolite zone on the diagram of the Northern Ladoga region. In addition to the indicated minerals, Qtz, Bt, and Pl are present in all fields; for simplicity, the accessory minerals Ilm, Tit, and Ru are not shown.

Staurolite appears at T ≈ 510–620°C, P = 2-8 kbar (Fig. II-2-4). With increasing temperature, instead of staurolite, either sillimanite, at P > 4 kbar, or cordierite, at P < 4 kbar, is formed as an aluminosilicate phase. For example, with an increase in P-T parameters: in the staurolite-containing paragenesis Qtz + Bt + St + Pl + Crd + Chl + Ilm, chlorite first disappears, then garnet appears, followed

by the disappearance of cordierite. When the temperature of metamorphism increases to 670–700°C, the first melts of substance appear in the rock.

Andalusite coexists with staurolite in a small P-T window at P = 2.2-3 kbar, T = 510-530°C. If the pressure during metamorphism reached >6 kbar, then instead of staurolite, kyanite would form in the rock. Ilmenite is modelled as a titanium-containing phase, which is ubiquitous in real samples of metapelites in the matrix and as inclusions in rock-forming minerals.

It is worth noting that the configuration of the P-T regions of staurolite-bearing parageneses depends on the bulk composition of the rock, for example, for a sample from the Central block (Fig. II-2-4b) with increased calcareous content, the narrowest region of staurolite stability is modelled. For this metapelite composition, the staurolite region is at the same temperatures T = 510–620°C, but is limited in pressure P = 2.5–6.2 kbar. An increased CaO content in the metapelite protolith leads to an increase in the stability regions of garnet and zoisite, accompanied by a decrease in the stability region of staurolite. Another difference is the absence of muscovite and sillimanite in the paragenesis with staurolite. However, the P-T networks of staurolite-bearing Ladoga rocks are almost the same in principle.

Influence of rock magnesium content

One of the critical parameters determining the appearance of St is the magnesium content of the protolith: X_{Mg} = Mg/(Fe + Mg). Considering that the contents of MgO and FeO in the Ladoga metapelites vary widely (Tables 1, 2), binary diagrams were analysed that demonstrate mineral parageneses depending on the X_{Mg} of the rock (Fig. II-2-5). The diagram given as an example shows staurolite-bearing parageneses in T-X_{Mg} coordinates at P = 4 kbar, assumed for these rocks (Baltybaev et al., 2000).

In the binary plot, the position of sample B-05-177 with X_{Mg} = 0.18 is marked on the X_{Mg} axis with an arrow. The mineral assemblages corresponding to this bulk-rock composition evolve with increasing temperature as follows: Qtz + Bt + Pl + Ms + Chl + Ilm ± Ru ± Tit → + St (560°C) → - Ms (565°C) → + Grt (550–570°C) → - Chl (580°C) → + Crd, - St, + Sil (620°C) → partial melting (> 670°C).

Had the protolith composition corresponded to another rock with, for example, XMg = 0.3, then the staurolite stability field would have significantly shrunk, the disappearance of Chl and subsequent appearance of Grt would have taken place at a higher temperature, and no Als would have been formed with increasing temperature.

For a Fe richer protolith (for example, with X_{Mg} = 0.1), a temperature increase leads to the following sequence of mineral assemblages: *Qtz + Bt + Pl + Ms + Chl + Ilm → + Grt, - Chl (550–555°C) → + St, - Ms (560–565°C) → - St, + Sil (600–605°C)* → partial melting (> 660°C). The staurolite stability field for this composition is the broadest, although X_{Mg} of the rock is still not high enough for Crd to be stable.

In protoliths whose composition corresponds to various X_{Mg} values, staurolite is stable in P–T space within an almost rectangular field ($0 < X_{Mg} < \sim 0.3$) within a narrow temperature range of ~550 to ~605°C (Fig.II-2-5). An increase in XMg of the rock to >0.3 leads to that the staurolite stability field narrows and wedges out rather quickly.

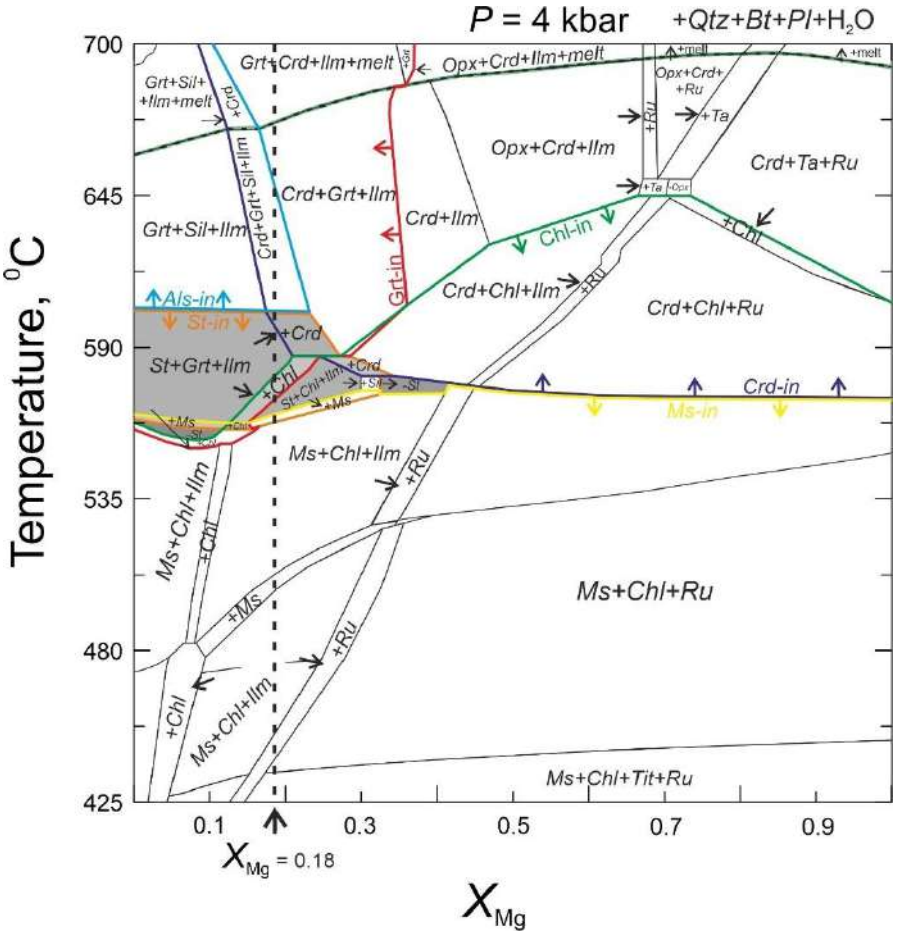

Figure II-2-5. Binary diagram T(°C)-X_{Mg}, modeling mineral parageneses depending on the magnesium content of the rock and changing temperature at P = 4 kbar. Orange line – appearance of St, red – Grt, yellow – Ms, green – Chl, blue – Crd, blue – Als (Sil). The position of sample B-05-177 with X_{Mg} = 0.18 is shown on the X_{Mg} axis by an arrow.

Retrograde transformations

Staurolite is subject to changes at the post-crystallization stage. The replacement of staurolite, for example, by muscovite is described in some works (eg, Grew and Sandiford, 1984). This process is recorded at the regressive stage of metamorphism at T = 300−370°C, P = 3−5 kbar, when clinozoisite, margarite, and pumpelite appear together with muscovite in the staurolite-talc-chlorite-corundum rock (Grew, Sandiford, 1984). In the Northern Ladoga region, for example, staurolite is in places replaced by quartz-muscovite or muscovite-chlorite mineral associations, as well as andalusite until almost complete pseudomorphs are formed. It is usually not difficult to recognize the replacement of staurolite by superimposed minerals by characteristic structural and textural features.

Influence of water activity in fluid

To assess the influence of fluid composition on the stability fields of staurolite, recalculations were made at a fraction of H_2O in the carbon dioxide-water fluid equal to 0.2-1.0 (Fig. II-2-6). For the rocks of the medium-temperature zone of the metamorphic complex of the Northern Ladoga region, the carbon dioxide-water composition of the metamorphic fluid was established, while the H_2O:CO_2 ratio was taken as 0.3-0.4: 0.7-0.6 (colored areas in the diagram) according to the study of optically visible fluid inclusions (Baltybaev et al. , 2000).

It has been revealed that with an increase in the proportion of CO_2 in the fluid, the position of many metamorphic reactions, including staurolite-forming ones, shifts towards lower temperatures and pressures. Thus, with a purely aqueous fluid, the temperature range of stability of staurolite is T = 550–650°C, while when the proportion of H_2O is reduced to 0.2, it is equal to 450–530°C, which is ~ 100°C lower.

However, it is worth noting that the nature of the change in the configuration of the stability field of staurolite also depends on the bulk composition of the rock. For example, for low-calcium metapelites (sample B-19-336) with changes in X(H_2O), the size of the P-T field of stability of staurolite-containing parageneses is almost constant (Fig. II-2-6 a), and for higher calcium compositions (sample B-2011-239-2) with increasing X(H_2O) P-T, the stability region of staurolite greatly narrows (Fig. II-2-6 b).

Along with H_2O-CO_2, real fluid contains impurities of nitrogen, methane, dissolved salts, which should also be taken into account as components that reduce the activity of water in the fluid and, accordingly, affect the stability field of staurolite.

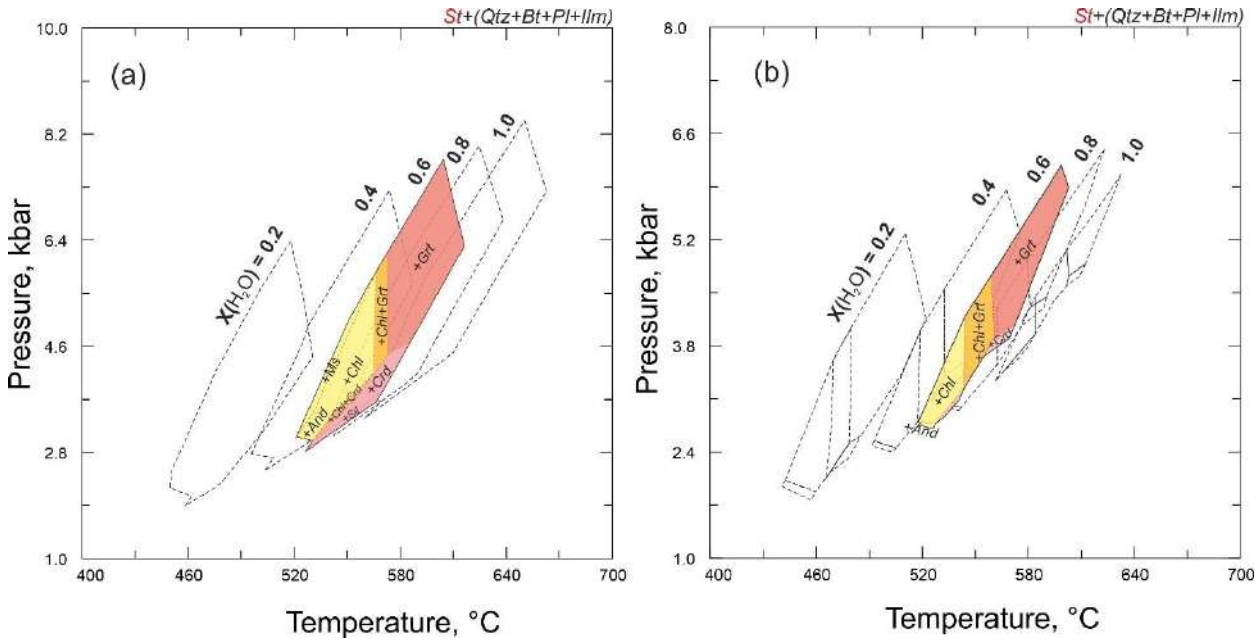

Figure II-2-6. Change in the position of the field of staurolite-containing parageneses depending on the X(H_2O) content in the carbon dioxide-aqueous fluid: (a) B-19-336 from the Western block; (b) B-2011-239-2 from Central Block. The areas corresponding to natural samples with a fraction of H_2O = 0.6 are highlighted in colour.

2.3. Fluid regime of metamorphism

To characterize the metamorphic fluid of the medium-temperature zone of the Northern Ladoga region, a study of fluid inclusions in quartz from synmetamorphic (syndeformational) veins of rocks of the Ladoga series was carried out. In addition to the composition of the fluid, which, according to the study of optically visible fluid inclusions, is taken to be carbon dioxide-aqueous (Baltybaev et al., 2000), the CO_2 density in the inclusions is important, which in turn is a dependent function of the P-T conditions of metamorphism. This makes CO_2 density determination an important independent method for assessing the P-T conditions of a fluid capture process.

Samples of quartz veins were collected from rocks of the Ladoga series of the staurolite zone, which presumably formed simultaneously with metamorphic and/or tectonic processes of rock transformation (Fig. II-3-1). Quartz is an ideal mineral for studying fluid inclusions because it is present in almost all metamorphic rocks and is stable over a wide range of metamorphic parameters, and it is transparent, which allows even microscopic inclusions to be observed. Quartz is chemically inert towards the trapped fluid, i.e. not capable of cation exchange with components dissolved in aqueous fluid inclusions.

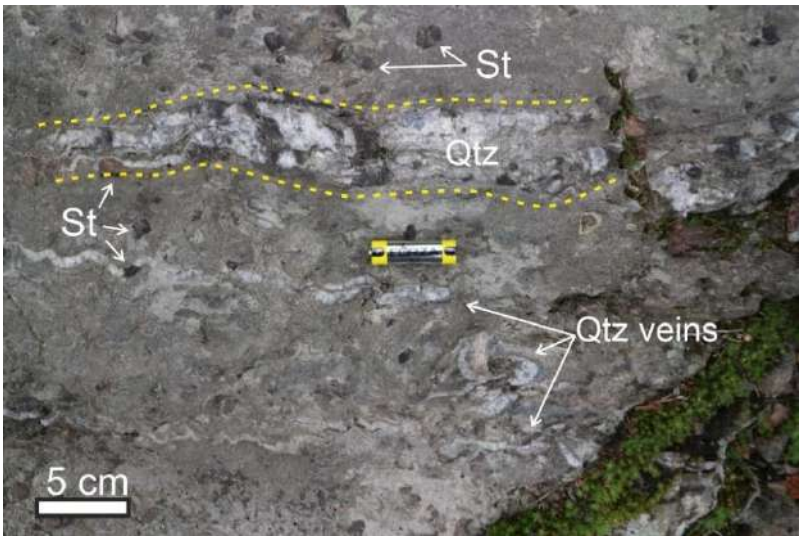

Figure II-3-1. Photo of quartz syndeformation veins in rocks of the staurolite zone..

Fluid inclusions in quartz plates were studied using a Raman spectrometer at the Geomodel Research Center of St. Petersburg State University. For analysis, primary inclusions that formed simultaneously with the host mineral substance were preferred, because of the interest in the fluid of the progressive stage of metamorphism. But it is worth considering that due to the very small sizes of inclusions and the ambiguity in determining the primacy of substance capture, both secondary (the formation of which occurred after the formation of the crystal as a result of superimposed processes, for example, at the regressive stage of metamorphism) and primary-secondary inclusions could be analysed.

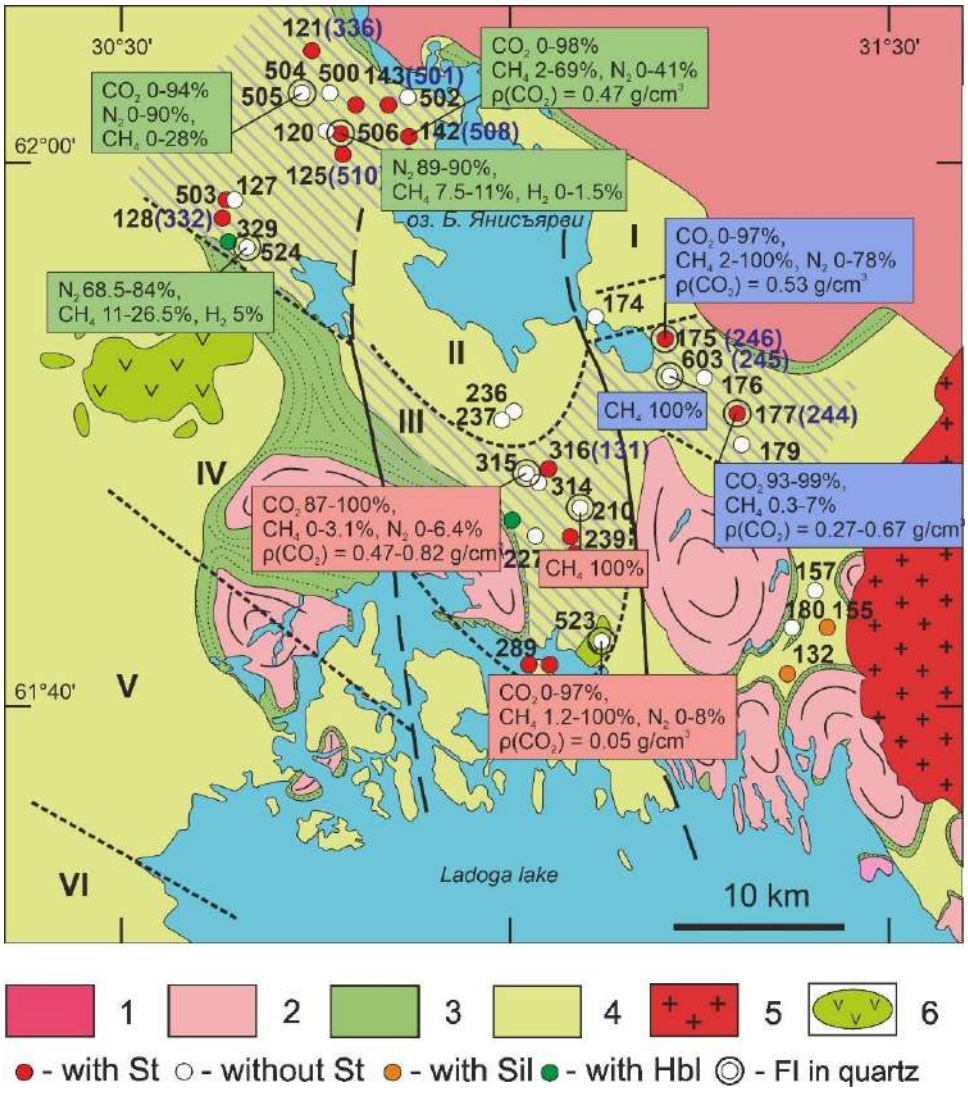

Figure II-3-2. Fact map. Crosses indicate sampling points for quartz veins. In the footnotes there is a generalized composition of inclusions and the carbon dioxide density range for each sample.

As a result, 9 quartz thin sections from different areas of the medium-temperature staurolite zone were analysed (Fig. II-3-2, Table 4). The following are micrographs of inclusions in different plates (Fig. II-3-3), Raman spectra (Fig. II-3-4–7), relative concentrations of gases in mixtures and density CO_2.

Sample B-19-315 from the Central block: In inclusions in the composition of gases, the predominant role is played by CO_2 92–94%; there are also impurities of nitrogen 5-6% and methane 1–1.5% (Fig. II-3-4 a). In some inclusions, only water was recorded (Fig. II-3-4 b). The CO_2 density was determined in the range 0.58–0.76 г/см^3.

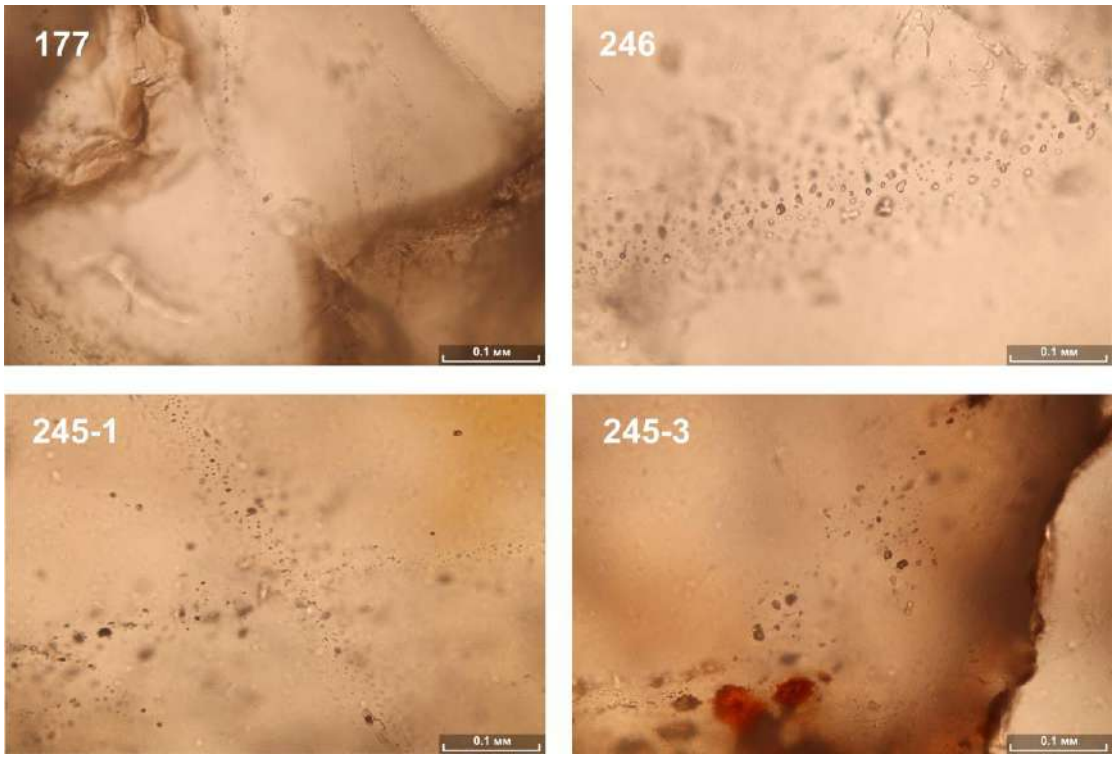

Figure II-3-3. Microphotographs of fluid inclusions.

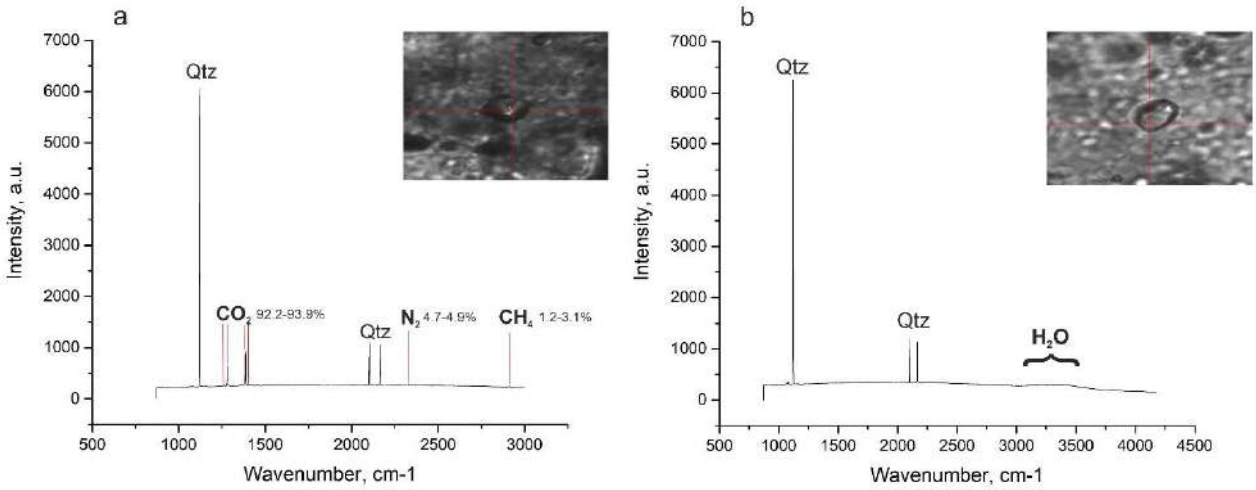

Figure II-3-4. Raman spectra of fluid inclusions in the sample B-19-315. A – in a gas mixture of CO_2, N_2, CH_4; B – water inclusion.

Sample B-04-177 from the Eastern block. The composition of gases in inclusions is almost entirely carbon dioxide CO_2 (98-100%) with a small admixture of methane (0.3–2%) (Fig. II-3-5). The density of CO_2 was determined to be 0.42 and 0.62 g/cm3. An interesting three-phase carbon dioxide inclusion was also recorded: an inner area (1) with a CO_2 density of 0.27 g/cm3, a central area (2) with a higher CO_2 density of 0.67 g/cm^3, and in the outer area (3) there are HCO_3 and CO_3^{2-} ions dissolved in water (Fig. II-3- 6). In addition to carbon dioxide, a number of pure methane inclusions were discovered.

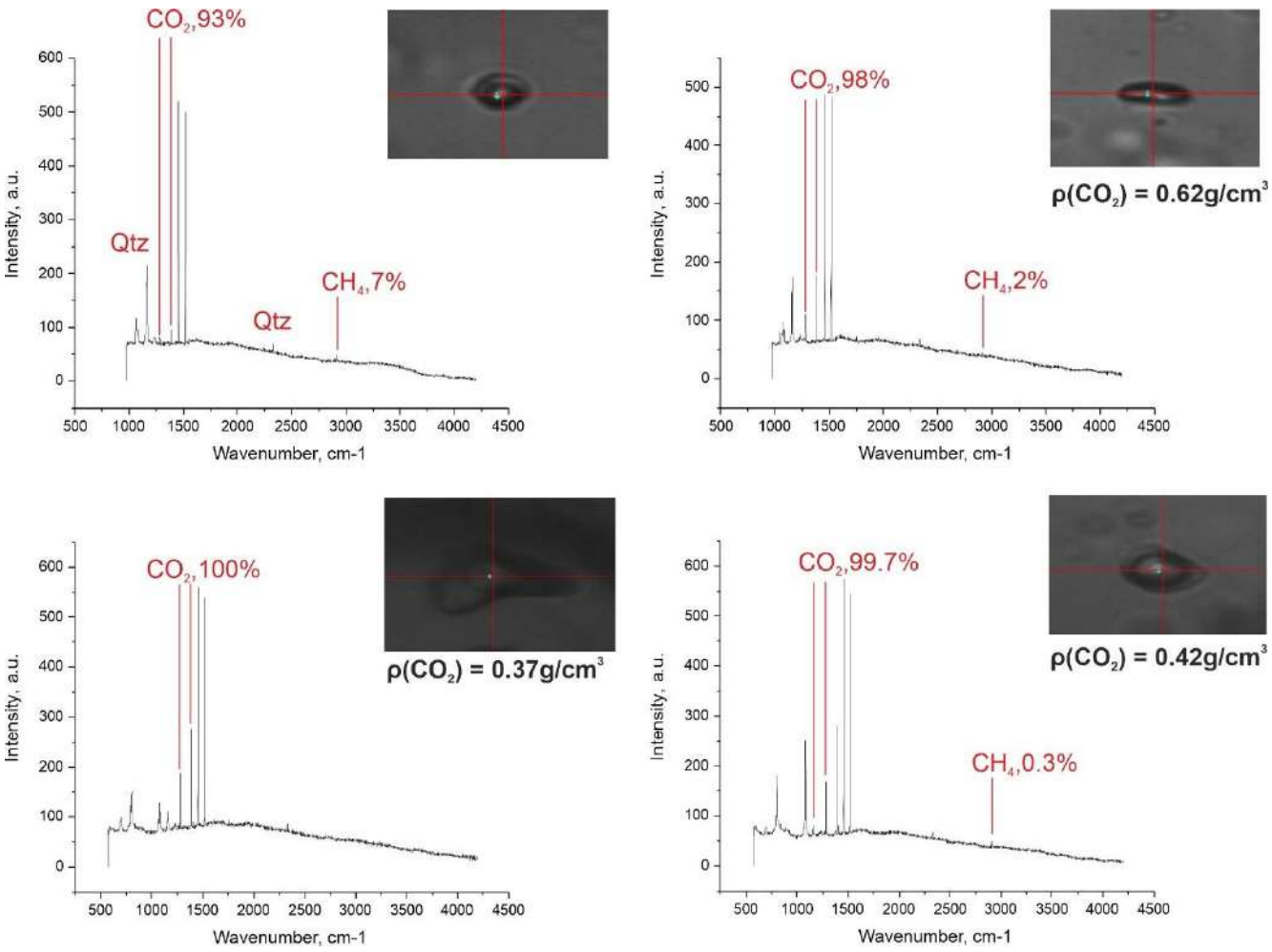

Figure II-3-5. Raman spectra of carbon dioxide inclusions from sample B-05-177.

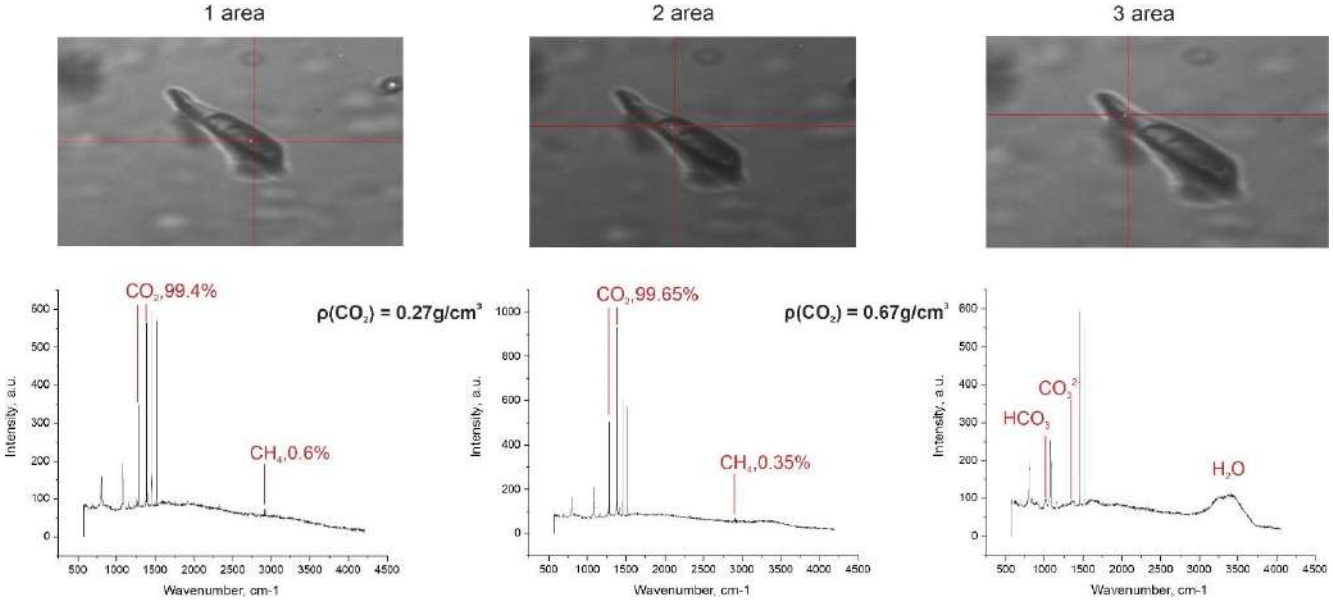

Figure II-3-6. Raman spectra of a three-phase inclusion from sample B-05-177. The outer area contains inclusions dissolved in water HCO_3 и CO_3^{2-}.

Sample of B-22-524 from the Western block. This sample contains predominantly nitrogen (68.5–84%) inclusions with methane (11–26.5%) and a small admixture of hydrogen (5%) (Fig. II-3-7).

In the samole B-20-501 inclusions with a gas phase composition predominantly consisting of CO_2 (85–94%) with N_2 impurities (6–15%) were analysed. In inclusions of this sample, the CO_2 density is lower relative to inclusions from other parts of the staurolite zone and is estimated at 0.29–0.44 g/cm^3.

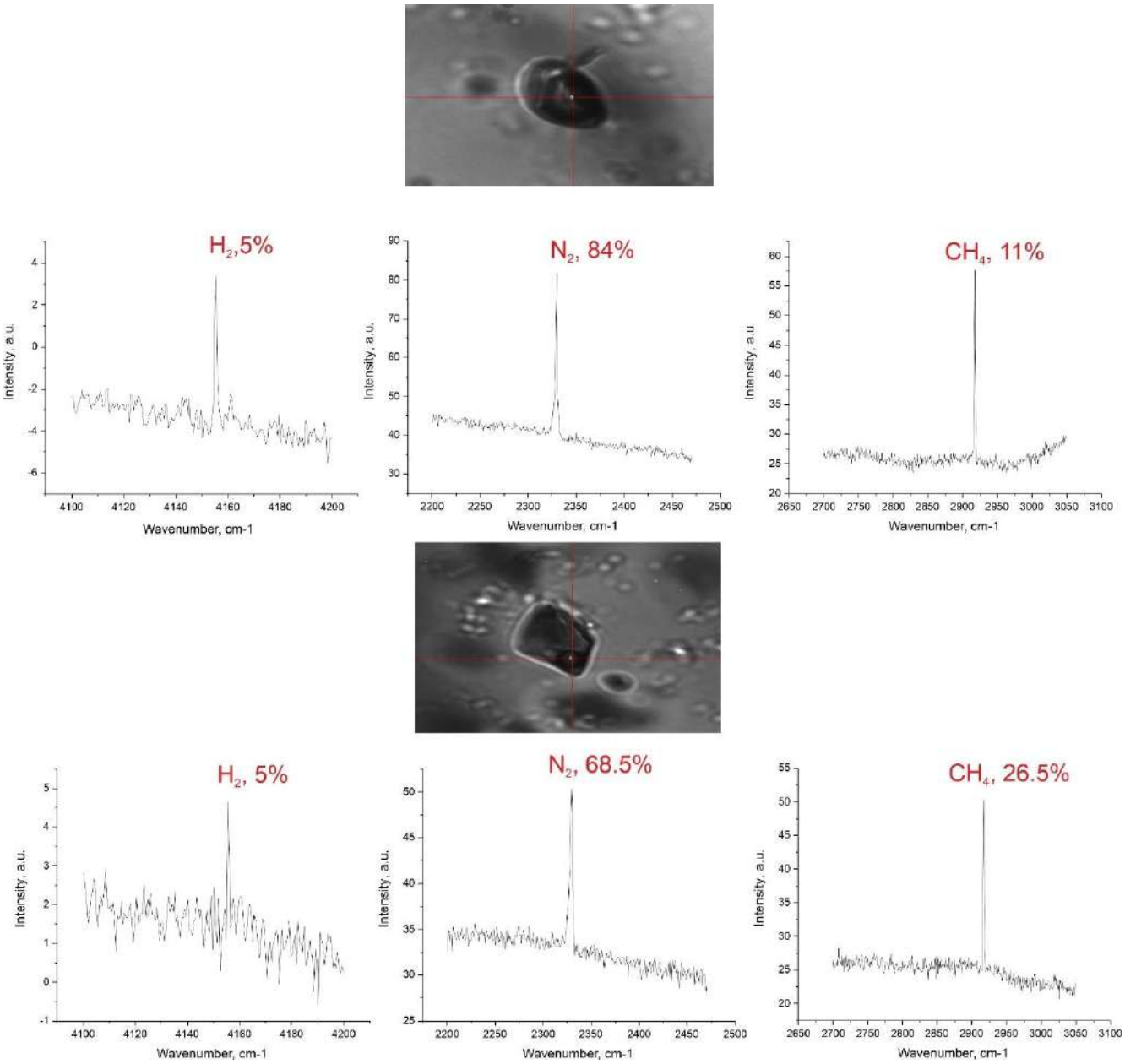

Figure II-3-7. Raman spectra (fragments) of inclusions in the sample B-22-524.

Pressure determination

The CO_2 density was determined from the distance between doublets of the Raman spectrum of carbon dioxide according to the methods given in the following articles (Frezzotti et al., 2012; Burke, 2001; Wanga et al., 2011). A detailed description of the methodology is presented in the section "Factual material, methods and methodology." Due to the fact that the CO_2 density in fluid inclusions is a function dependent on the P-T conditions of inclusion capture, one of the parameters can be calculated knowing the other two.

For inclusions from rocks throughout the staurolite zone, different values of CO_2 density are recorded, where the minimum value is 0.42 g/cm^3, and the maximum is 0.82 g/cm^3. Taking the metamorphism temperature of the average temperature zone of the zonally metamorphosed complex of the Northern Ladoga region equal to 500-600 °C, then at these values of CO_2 density the pressure corresponds to the range of 1–3 kbar (Fig. II-3-8). We accept the obtained values as underestimated, because according to the methods of classical mineral thermobarometry and literature data (Baltybaev et al., 2000, 2009), the metamorphic pressure in the studied complex should have been about 4–5 kbar. The reasons for the underestimation of pressure values could be: 1) water was not captured during the analysis; if it were present, the density of CO_2 would be higher, and, therefore, higher pressures would be obtained; 2) inclusions of the regressive stage of metamorphism, which is characterized by reduced P-T conditions, were analysed (Borisova et al., 2024).

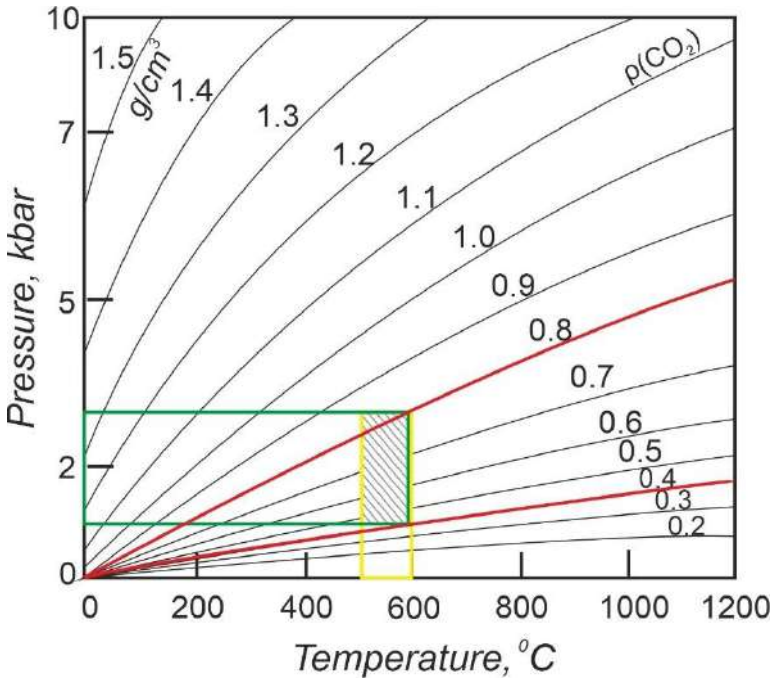

Figure II-3-8. Diagram of CO_2 density versus pressure and temperature. With a CO_2 density in the inclusion equal to 0.58-0.76 g/cm^3 and T = 500-600 °C (medium temperature zone), P = 1-3 kbar.

2.4. Verification of the conditions for the formation of staurolite and chloritoid in metapelites

Data on naturally occurring rocks (Korikovsky, 1979; Ballèvre et al., 1989; Chopin et al., 2003; and others) and experimental calibrations (Comodi et al., 2002; and others) indicate that staurolite-bearing mineral assemblages are stabile under pressures of 1–2 to ~32 kbar at temperatures of 450 to ~700°C. The temperature range in which staurolite and its assemblages are stabile at pressures of 3–8 kbar is wide, but it rapidly narrows as the pressures increases to 10–1 kbar, and the composition of the mineral shifts toward the more magnesian member of this solid solution. It is because staurolite is stable within a narrow P–T field that makes this mineral so convenient to apply in mapping metamorphic complexes and in constructing maps and schematic representations of metamorphic zoning. Because of

this, the concept of the staurolite zone of metamorphism was coined as long back as the mid-19th century (Barrow, 1893).

Metamorphic zonal complexes in which staurolite was found are widespread worldwide (Abu El-Enen et al., 2004; Baltatzis, 1979; Corrie and Kohn, 2008; Garcia-Casco and Torres-Roldan, 1999; Keller et al., 2005; Lal and Shukla, 1970; Liu et al., 2020; Moynihan, 2012; Pattison and Vogl, 2005; Pattison and Tinkham, 2009; Ugwuonah et al., 2017; Wang et al., 2018; and others). The broad variations in the composition the protoliths of these rocks puts forth the problem as to how the metamorphic zones distinguished in these complexes are related to the PT parameters (metamorphic grades). In this context, it is important to find criteria for determining whether some P–T parameters have been reached by a given rocks in spite of that the rock actually does not contain the indicator minerals (for example, staurolite). The fact that this mineral is stable within a fairly narrow temperature range opens, on the one hand, broad possibilities for modern thermodynamic simulations and, on the other hand, enables the researcher to successively apply criteria for estimating whether staurolite is or is not stable and thus constrain the boundaries of the metamorphic staurolite facies (subfacies).

Staurolite can be formed by decomposing chloritoid by the reaction Cld + Qtz = St + Grt + H_2O (Whitney et al., 1996). In the presence of chlorite, the reaction Grt + Chl + Ms = St + Bt + Qtz + H_2O can proceed, which continues until one of the three reactant minerals is completely exhausted (Yardley, 1989). If, for example, the first phase to be exhausted is garnet, then the reaction stops, and staurolite is further can be produced by a continuous reaction involving the remaining phases Chl + Ms = St + Bt + Qtz + H_2O at a higher temperature than that of the aforementioned discontinuous reaction (Yardley, 1989). However, chloritoid can sometimes not to be produced at all if the Grt–Chl assemblage is stable at lower temperatures. This can take place, for example, if the rock contains an elevated Mn concentration, which widens the stability field of garnet at relatively low temperatures (Karabinos, 1985).

Chloritoid was documented in numerous metamorphic complexes, in which it is stable in low- and medium-pressure metapelites, both enriched in depleted in Al. High-pressure metapelites are often also characterized by elevated Mg concentrations.

The P–T parameters under which chloritoid-bearing metapelites are stable range from those of the greenschist to the mid-amphibolite facies, staurolite–kyanite zone. In greenschist-facies rocks, staurolite is a common mineral, which occurs, together with chlorite and muscovite, in rocks that contain more Fe and Al than is necessary to form the Chl–Ms assemblage (Turner and Verhoogen, 1960; Albee, 1983; Johnson et al., 2003).

Chloritoid is typical of metapelites affected by HP–HT metamorphism. This mineral is formed, together with chlorite, talc, and/or kyanite, in the course of early subduction by the decomposition of carpholite under parameters of the lower blueschist facies at 12–16 kbar and 450–550°C (Bucher, 2005;

Palin and Dyck, 2021). As the metamorphic grade increases to the eclogite facies (>20 kbar and >600°C), chloritoid decomposes into magnesian garnet (pyrope) and kyanite, and magnesian staurolite can also be formed in lithologies richest in Al (Palin and Dyck, 2021).

Most researchers believe that the protoliths of chloritoid-bearing rocks consisted of the redeposited and metamorphosed material of ancient weathering crusts of the laterite (or kaolinite) type (e.g., Franceschelli et al., 2003). Such metamorphism produces pyrophyllite from kaolinite at a temperature close to 300oC, and pyrophyllite can, in turn, be replaced by chloritoid in associations rich in chlorite, and the complete decomposition of pyrophyllite to kyanite occurs at 400oC. At approximately 500oC, chloritoid decomposition results in staurolite and garnet, which marks the transition to the amphibolite facies (Bucher and Grapes, 2011).

The KFMASH system is characterized by prograde sequences of mineral assemblages depending on the chemical composition of the protoliths. The Fe-rich series is characterized by the following sequence of mineral assemblages: Chl + Cld, Grt + Cld, Grt + St, Grt + Ky, and Grt + Sil, without Bt. In magnesian rocks, the sequence is Chl + Prl, Chl + Ky, Bt + Ky, Bt + Sil, and neither garnet nor staurolite or hedenbergite are formed. The Fe richest association with Bt is Grt + St + Bt, with X_{Fe}(max) = 0.88. The low-temperature boundary of the stability field of these phases (560°C) occurs at a temperature 10°C higher than the maximum temperature of chloritoid stability (Richardson, 1968; Bucher and Grapes, 2011). In P–T diagrams, mineral assemblages with chloritoid (chloritoid zone) can be regarded, under some conditions, as in a zone analogous to the biotite zone (Spear, 1993). In the KFMASH system, chloritoid + biotite are stable within a narrow temperature range under relatively low pressures (Harte and Hudson, 1979), although some researchers (Spear and Cheney, 1989; Wang and Spear, 1991) are prone to think that the P–T field in which this association is stable is much larger.

The effect of oxygen partial pressure on staurolite origin by the reaction Cld + O_2 ↔ St + Mgt + Qtz is as follows: an increase in the oxygen pressure from that at the NNO to that at the QFM buffers decreases the staurolite crystallization temperature from 635 ± 15°C to 580 ± 10°C at Ptot = P_{H2O} = 10 kbar (Ganguly, 1968; Ganguly and Newton, 1968).

The staurolite stability field in the Fe–Al–Si–O–H at hydrothermal synthesis in the presence of the quartz–fayalite–magnetite (QFM) buffer lies at P > 1.5–3.0 kbar and 530–700°C (Richardson, 1967, 1968). Similar parameters (540°C at 4 kbar and 565°C at 7 kbar) were obtained for staurolite origin by the reaction Chl_{40} + Ms ↔ St + Bt + Qtz + H_2O in the presence of QFM buffer at $P_{tot} = P_{H2O}$ (Hoschek, 1969). The upper temperature limit for staurolite stability in the presence of muscovite and quartz in the reaction St + Ms + Qtz ↔ Als + Bt + H_2O was evaluated at 575°C at 2 kbar and 675°C at 5.5 kbar (Hoschek, 1969). Of course, if $P_{tot} > P_{H2O}$ the temperature at which staurolite is formed and decomposes (because water is released in this reaction) shall be lower. According to calculations in (Hoschek, 1969),

the temperature at which staurolite is formed at Ptot > P_{H2O} = 5 kbar shall be approximately 100°C lower, i.e., close to 450°C (Nagaitsev, 1974).

In the northern Ladoga area, metapelites of the pre-staurolite (biotite) zone do not contain chloritoid (Velikoslavinskii, 1972). It was previously thought that staurolite is formed in zonal metamorphic complexes only via chloritoid decomposition, but it was demonstrated (Hoschek, 1969) that chloritoid-bearing rocks are characterized by narrower variations in chemical composition than those of staurolite-bearing rocks, and staurolite can be formed not only by the decomposition of the assemblage Cld + Qtz + Ms + Chl but also at the expense of the assemblage Qtz + Ms + Bt + Chl. In G. Hoschek's AKF, ACF, and AFM triangular plots of mineral assemblages with the fields of chloritoid- and staurolite-bearing rocks, the composition point of staurolite rocks in the northern Ladoga area do not plot within the composition field of chloritoid. This provides grounds to think that the reason for the absence of chloritoid from the rocks in the area is their unsuitable composition, with their difference from chloritoid-bearing rocks being their elevated Mg and Ca concentrations (Velikoslavinsky, 1972).

Thermodynamic simulations with the PERPLEX software (Connolly, 1990) in the low- and medium-temperature region (<520°C) with the compositions of rocks of the Ladoga Group confirm the absence of chloritoid. However, chloritoid was obtained in the simulations with Fe- and Al-richer metapelites from elsewhere. Numerical simulations with a broader range of theoretical compositions led us to establish that chloritoid is stable in more aluminous and less magnesian compositions of the protoliths with the ratios (in wt. %) $Al_2O_3/MgO > 10$ and $FeO_t/MgO > 5$.

2.5. Influence of Zn^{2+} in staurolite on its stability

Although most natural staurolites contain more iron than other metals, they almost always contain small amounts of Ti, Mn, Cr, and V (Smith, 1968; Griffen and Ribbe, 1973). It is believed that these metals have virtually no effect on the crystal chemistry of the mineral. More often, relatively high concentrations of Mg and Zn are found in staurolite. Zn-rich staurolites have been found in metapelites metamorphosed at fairly high temperatures (e.g., Guidotti, 1970) and unusually high pressures (Ashworth, 1975), in intermediate-temperature metabasites of igneous origin (Gibson, 1978), in high-pressure, intermediate-temperature metagreywacke (Hollister, 1969), in pegmatites and hydrothermal veins (Tarnovskii, 1973; von Knorring et al., !979) and in low-temperature and high-pressure metabauxites (Feenstra et al., 2009). The ZnO content in staurolite can vary from zero to ~ 7 wt. %, but usually the content varies between 0.1-2.0 wt. % (Griffen, 1981).

Data from Guidotti (1970) and Ashworth (1975) suggest that the inclusion of Zn in the structure of staurolite extends its stability (relative to zinc-free staurolite) towards higher temperatures. Experiments on the synthesis of Zn-staurolite and iron-magnesium staurolite at P = 30 kbar and T = 750°C (Griffen, 1981) showed that the crystal chemistry of staurolite does not limit the incorporation of

zinc into the crystal lattice. Thus, the Zn content in natural staurolites is a result of the availability of zinc in various geological environments, or thermodynamic limitations on the stability of Zn-bearing staurolites.

In the staurolites we studied, the zinc content varies between 0-1.6 wt. % ZnO. Although it is believed that the inclusion of zinc in the structure of staurolite increases its stability, at the moment there are no thermodynamic models of the zinc component of staurolite, thanks to which it would be possible to evaluate its influence when calculating P-T networks. This also applies to other small components such as Ti, Cr, V, which can be included in the structure of staurolite. Taking into account the generally low ZnO contents in the staurolite of the Ladoga metapelites, as well as the moderate parameters of rock metamorphism, consistent with the results of classical thermobarometry and model calculations, we accept that the influence of the zinc component in the Ladoga staurolites is insignificant.

Summary of the chapter

Thermodynamic modeling of the mineral formation of staurolite-containing and staurolite-free rocks of the Ladoga series has established excellent reproducibility of real (natural) mineral parageneses.

Mineral formation modeling confirms the absence of chloritoid in the metamorphic complex of the Northern Ladoga region for the conditions of the pre-staurolite zone. It has been established that more aluminous and less magnesian compositions of the protolith with oxide ratios $Al_2O_3/MgO > 10$ and $FeO/MgO > 5$ are favorable for the appearance of chloritoid. The principal diagram of the prograde mineral formation of Ladoga rocks is the sequence: (Qtz + Bt + Pl ±Ilm) **+ Chl + Ms → St ± Grt → Sill/Crd + Grt**.

Based on the results of multi-equilibrium thermobarometry, P-T conditions for the formation of staurolite-bearing schists were established: for the Western block T = 550–615°C, P = 3.7–5.2 kbar, for the Central block T = 645–650°C, P = 4.1–4.9 kbar, for the Eastern block T = 510–550°C, P = 3.7–5.5 kbar.

The composition of the gas part of fluid inclusions in synmetamorphic quartz veins from rocks of the staurolite zone is predominantly carbon dioxide and methane; in the Eastern block the composition often contains nitrogen with admixtures of methane and hydrogen. In inclusions from rocks of the staurolite zone, all CO_2 density values and estimates of metamorphic pressure (P = 1–3 kbar) of rocks from them turned out to be underestimated compared to classical thermobarometry data (P = 4–5 kbar). It is assumed that quartz veins (or inclusions in them) arose at the late regressive stages of metamorphism of rocks of the staurolite zone.

An increase in the proportion of CO_2 in the fluid leads to a shift towards lower temperatures and pressures the position of many metamorphic reactions, including staurolite-forming ones.

CHAPTER 3. ISOTOPE DATING OF THE TIME OF METAMORPHIC EVENTS

This chapter presents the results of isotopic dating of the formation time of staurolite-containing parageneses in rocks of the Ladoga series. The Ladoga series represents metaturbidites of the pericratonic part of the Karelian craton; accordingly, the lower limit on the time of formation of the series – the beginning of the accumulation of turbidite deposits, is the minimum age of detrital zircon, estimated at 1898 ± 8 million years (Ladoga Proterozoic..., 2020). Sediments similar to the Ladoga ones are widespread in Finland; for the lower volcanic-sedimentary strata of the Tampere belt, there are dates of 1904 ± 4 and 1889 ± 5 Ma (Kähkönen et al., 1989). The age of 1892 ± 5 Ma of zircons from the monzodiorites of the Velimyak intrusion, cutting through the Ladoga series, is taken as the upper age limit for the formation of the Ladoga series (Ladoga Proterozoic…, 2020).

3.1. U-Pb dating of monazite

To establish the time of formation of staurolite-containing mineral parageneses, U-Pb (ID-TIMS, IGGD RAS) dating of monazite from aluminous gneisses and schist, including the staurolite-bearing ones we studied, was performed.

Monazite in metamorphic rocks is widely used as a chronometer mineral for dating metamorphic processes. The main advantages of this mineral for dating are, firstly, the high content of Th and U and the low rate of diffusion of cations (Cherniak et al. 2004), secondly, the formation and disappearance of monazite in the system occurs through solid-phase reactions, and thirdly, the temperature The closure of the U-Pb system in monazite is quite high and is generally estimated to be above 700°C and up to 800–850°C, which means that in granulite-facies rocks and below, monazite records an age close to the peak temperature of metamorphism (Hölttä, 2019). However, monazite is sensitive to changes in P-T parameters and fluid regime, with the result that grains in one sample may represent either a progressive or a retrograde stage, or both stages simultaneously (Hölttä, 2019).

U-Pb dating of metamorphogenic monazites from metamorphic rocks of the Northern Domain revealed an age of 1.80–1.79 Ga (Fig. III-2-1, Table 5).

The concordant (with a probability of 0.58 at a 95% significance level) age of monazite in garnet-andalusite-staurolite gneiss (sample B-03-125) is 1787 ± 5 Ma. For the garnet-staurolite gneiss (B-03-126), a concordant age of monazite was obtained at 1787 ± 5 Ma (with a probability of 0.18 at a 95% significance level). Monazite from garnet-biotite-sillimanite gneiss (sample B-03-132) has a concordant (with a probability of 0.81 at a 95% significance level) age of 1794 ± 5 Ma.

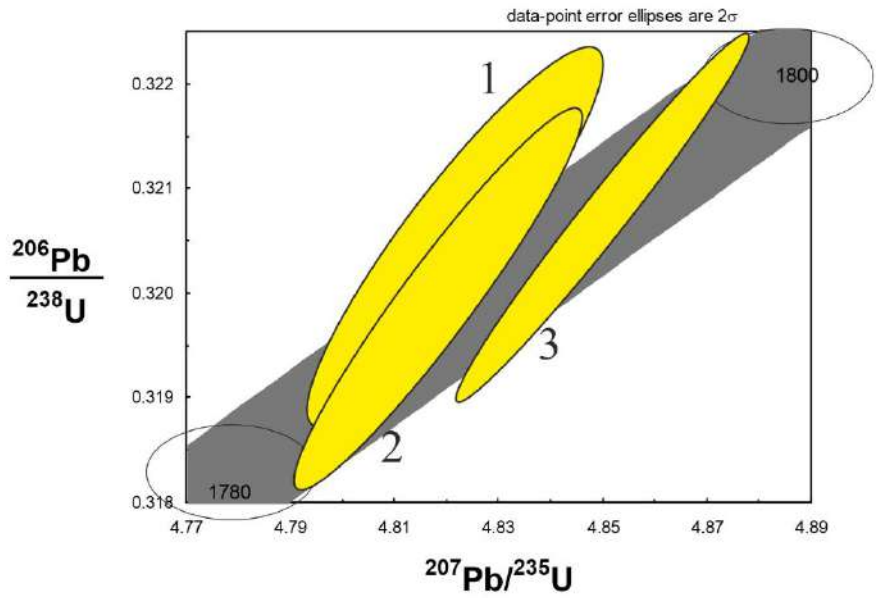

Figure III-2-1. Concordia diagram for monazites from the Northern Domain metamorphic rocks. Ellipse numbers (1-3) correspond to the serial numbers of samples in Table 5.

3.2. Sm-Nd dating

It is believed that rare earth elements, which include Sm and Nd, remain inactive during regional metamorphism, hydrothermal alteration and chemical weathering, so the metamorphic rocks we studied can be reliably dated by the Sm–Nd method. It has also been established that the results of Sm–Nd dating are satisfactory for relatively ancient rocks, since the low Sm/Nd ratio in rocks and minerals does not contribute to the effective accumulation of radiogenic ^{143}Nd (Radioisotope methods..., 2012). To estimate the age of a rock by the Sm–Nd method, one or several isochrones are constructed according to the Sm–Nd ratio in the bulk composition of the rock, in minerals, in our case in garnet, plagioclase and staurolite (Fig. III-2-1).

Garnet is one of the most common minerals of metamorphic rocks, it is not only successfully used in thermobarometry, but is also one of the chronometer minerals of metamorphic processes (Griffin, Brueckner, 1985, etc.). The high incorporation of HREE into the crystal lattice of garnet compared to LREE promotes the use of this mineral for Sm-Nd dating (Thöni, 2003). This isotope dating method is based on the decay of the radioactive isotope ^{147}Sm to form ^{143}Nd. However, interpretation of Sm-Nd data on the age of garnet is not always simple and is accompanied by a number of problems, such as 1) the influence of inclusions containing high amounts of LREE; 2) isotopic disequilibrium both between garnet and matrix minerals, and between the garnet matrix and inclusions in it; 3) uncertainty regarding the closing temperature of the isotope system (Tc) (Thöni, 2003). Empirical estimates of the closure temperature for neodymium diffusion vary widely from 480-900°C, such estimates may be the result of garnet crystallization over a long period of time (Smit et al., 2013).

Sm-Nd dating of garnet and other minerals from staurolite-bearing Ladoga rocks revealed an age of 1793 Ma (Fig. III-2-1, Table 6), which, within the limits of method error, coincided with the U-Pb

age estimate for monazite. Sm-Nd ages were obtained by constructing a mineral Sm-Nd isochron of garnet for gneisses located in the vicinity of the sampling points of the above monazites.

Thus, we can assume that the formation of metamorphic mineral parageneses in the rocks we studied took place about 1790-1800 million years ago. Similar geochronological data are known for other rocks of the Northern Ladoga region (Ladoga Proterozoic..., 2020 and references therein).

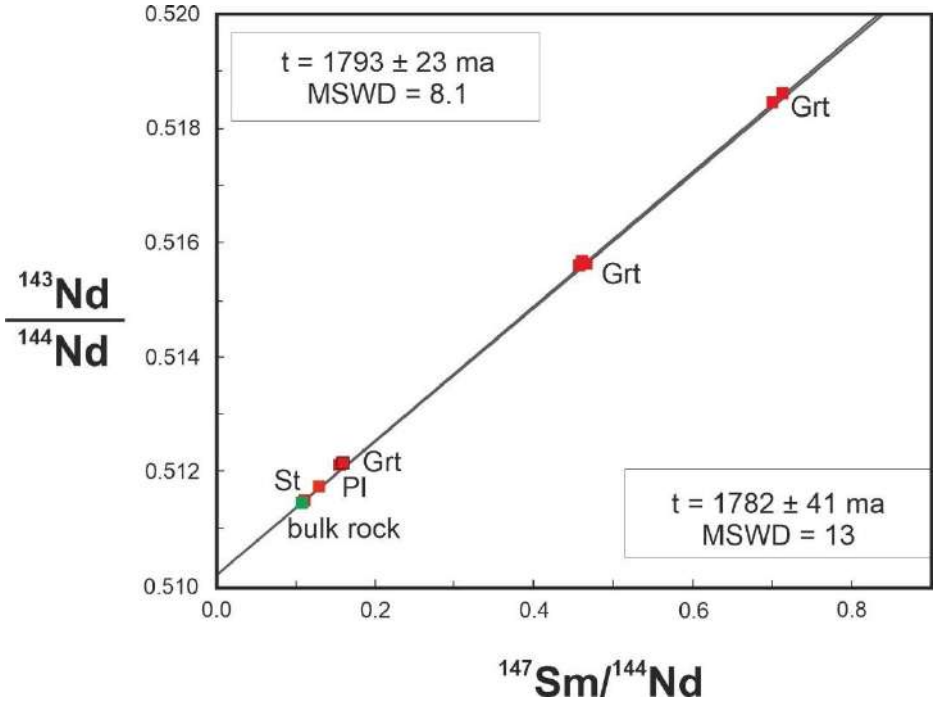

Figure III-2-1. Sm-Nd isochron using the isotopic composition of garnet grains, plagioclase, staurolite and bulk-rock composition.

Summary of the chapter

Both dating methods U-Pb dating of metamorphogenic monazites and Sm-Nd dating of garnets and other minerals from metamorphic rocks of the Northern Domain, revealed a metamorphic age of 1.80–1.79 billion years. The data obtained are consistent with other geochronological data for the region (Ladoga Proterozoic..., 2020, etc.).

CHAPTER 4. PETROCHEMICAL CRITERIA AND THERMODYNAMIC REGIME OF STAUROLITE FORMATION IN METAPELITES

This chapter presents the definition and justification of the ranges of ratios of key petrogenic components in metapelites, which help in resolving the issue of identifying the staurolite zone and metamorphic facies both in the Northern Ladoga region and other regions where medium-temperature metamorphic complexes are developed. The data from this chapter is represented in the publication of the author of the dissertation (Borisova, Baltybaev, 2021).

4.1. The problem of determining the staurolite isograd

A lot of work has been devoted to the study of the zonal-metamorphosed complex of the Northern Ladoga region, starting from the middle of the last century (Sudovikov, 1954; Nagaitsev, 1965, 1974; Kitsul, 1963; Predovsky et al., 1967; Sudovikov et al., 1970; Velikoslavinsky, 1972; Baltybaev et al., 2000, 2009) and, even despite the comprehensive study of the region with detailed areal geological mapping, the identification of a staurolite isograd in the northern part of the metamorphic complex turned out to be ambiguous. Almost simultaneously, in the 70s of the 20th century, various variants of the metamorphic zoning scheme were proposed (Fig. IV-1-1 a, b), their differences are especially clearly visible when determining the low-temperature boundary of the staurolite zone – staurolite isograd (and, accordingly, the facies of the rocks) on this area.

When mapping the metamorphic zoning of S.V. Nagaitsev (1965, 1974) and D.A. Velikoslavinsky (1972) metamorphic mineral isogrades were determined based on petrographic data - the appearance of critical mineral associations when muscovite parageneses replaced higher-temperature biotite-staurolite ones:

$Ms + Chl \rightarrow Bt + And \pm St + Qtz + H_2O$;

$Ms + Chl \pm Mgt \rightarrow Bt + St + Qtz + H_2O$.

A.A. Predovsky and colleagues (1967) drew the boundary of the first appearance of staurolite to the north – in a lower temperature zone, based on their observations of the geological structure and material composition of strata in this region (Fig. IV-1-1b).

Later geological work, when carrying out work on geological further study of the areas, accompanied by the compilation of a map of metamorphism (Geological structure..., 1989f) also did not clarify this issue, leading to the emergence of another scheme of metamorphic zoning, in which the position of the staurolite subfacies rocks differs from those indicated above (Fig. IV-1-1c).

The ambiguous interpretation of the position of the staurolite isograd is explained, from our point of view, by the peculiarity of the appearance of staurolite: in addition to the necessary P-T conditions for its formation, a suitable chemical composition of the original rocks is also required. In the absence of staurolite in the rock, it was classified as a zone of lower temperature metamorphism, considering that

the temperatures here did not reach the level of appearance of staurolite, although a proper analysis of the composition of the protolith was not carried out.

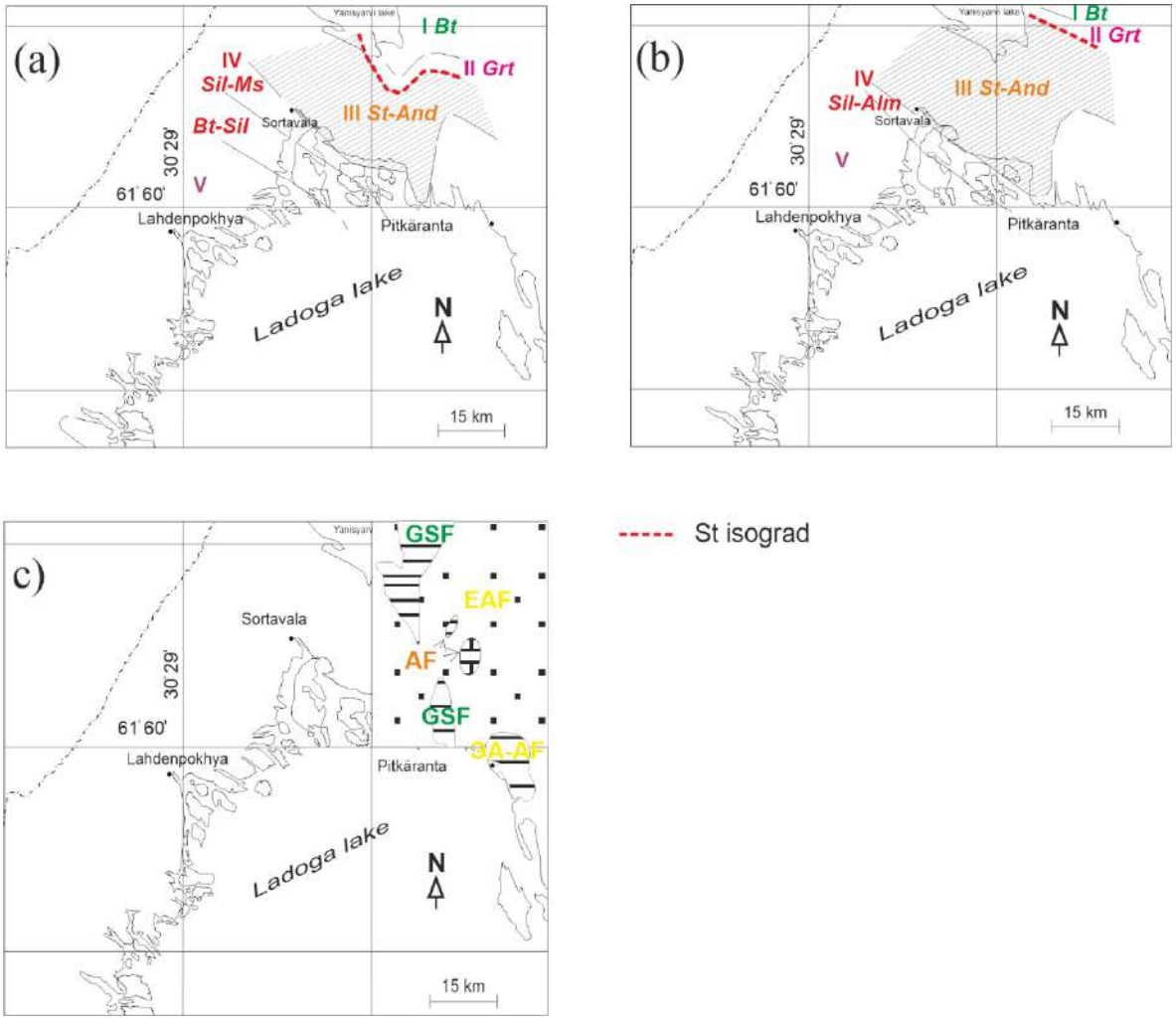

Figure IV-1-1. Schemes of metamorphic zoning of the Northern Ladoga region: a – according to Yu.V. Nagaitsev (1965, 1974), b – according to A.A. Predovsky et al. (1967), in – according to (Geological structure..., 1989). Name of metamorphic zones: I – biotite, II – garnet, III – staurolite-andalusite, IV – sillimanite-muscovite (-almandine) and biotite-sillimanite, V – ultrametamorphism. Metamorphism facies: GSF – greenschist, EAF – epidote-amphibolite (staurolite zone), AF – amphibolite. In diagram (c), when identifying metamorphic facies, the facies scheme according to N.L. Dobretsov (1969) was used, the epidote-amphibolite facies in which, according to P-T parameters, corresponds to the staurolite facies according to S.P. Korikovsky (1979). The ambiguity in drawing the low-temperature boundary of the staurolite zone is clearly visible when comparing figures (a) and (b).

Due to the fact that the appearance of staurolite-containing parageneses depends not only on the temperature of metamorphism (~500–650°C in Fe-Mg metapelite systems), but also on the chemical composition of the protolith (high-alumina protoliths, which have a number of features, are favorable), we propose a method for identifying potentially staurolite-containing rocks using calculated "petrochemical modules". The values of these modules are calculated in such a way as to predict the presence of staurolite in medium-temperature metamorphic strata containing rocks of a wide chemical composition (Borisova, Baltybaev, 2021).

Petrochemical modules can serve as objective and quantitatively unambiguous parameters of metamorphosed rocks in the form of the ratio of the main rock-forming chemical components, based on which one can determine the possibility of staurolite formation upon reaching a certain threshold of temperature and pressure (Borisova, Baltybaev, 2021). It is important that the presence of metamorphic staurolite is possible only in a very narrow temperature range, although in this case the areas of distribution of staurolite-containing rocks in zonal complexes occupy tens or a few hundred km^2. The proposed method, in addition to clarifying the boundaries of the zone, should also help in determining the level of metamorphism of the staurolite facies (subfacies), even if this mineral is not observed. It is obvious that the erroneous assignment of rocks that do not contain staurolite to the pre-staurolite zone has a strong influence on the reflection of boundaries on metamorphic maps or diagrams, which is what happened in the examples of metamorphism schemes in the Northern Ladoga region discussed above (Nagaitsev, 1965, 1974; Predovsky et al., 1967; Velikoslavinsky, 1972, Geological structure..., 1989).

4.2. Thermodynamic modeling

When modeling phase mineral equilibria using the PERPLE_X program (Connolly, 1990), the input data were the results of chemical analyses of metapelites (Table 1). In solving the direct problem of the simulations, i.e., conducting searches for mineral assemblages corresponding to those found in nature, the rock composition and P–T parameters were specified under the assumption that the system contains H_2O–CO_2 fluid, with its X_{CO2} assumed to be 0.2 based on data derived from studying fluid inclusions hosted in synmetamorphic quartz veins in the metapelites (Baltybaev et al., 2000). Computations made for comparison for some parts of the phase diagrams at X_{CO2} = 0.1 and 0.6 did not show any significant differences in the simulated phase relations in the medium-temperature parts of the diagrams.

Thermodynamic modeling made it possible to determine the exact boundaries of the protolith compositions for the formation of staurolite along them. First, a sample of all existing metapelite compositions was tested. Then the compositions of the Ladoga metapelites, which we called “basic compositions,” were modified by alternating changes in the contents and ratios of elements in them. When modifying the “basic compositions” of metapelites, the limits of the modified petrogenic components were determined using uneven grids with a step of 0.1−0.5 wt.% on the corresponding rectangular and triangular diagrams in order to more accurately delineate the boundaries of staurolite and non-staurolite rocks. For all such compositions, various pseudosections were simulated in the average temperature region of 500−650°C, at 2−10 kbar. Processing of real and theoretical chemical compositions of samples made it possible to clarify the threshold values of petrogenic components that determine the probability of the formation of staurolite and staurolite-free mineral parageneses in a given P-T area (Borisova, Baltybaev, 2021).

4.3. Verification of simulation results on other objects

Staurolite-bearing rocks from some regions of the world have been tested for consistency of the staurolite parageneses described in them with the results of computer modeling. The figurative points of the compositions of these rocks are plotted in Fig. IV-4-1 (Borisova, Baltybaev, 2021).

Staurolite-bearing schists of the Tabo Belt. This belt is one of the four pan-African metamorphic belts of the Sinai Peninsula, which make up the northern continuation of the East African Orogen. The critical mineral assemblages of the metapelites indicate that the regional metamorphism occurred at parameters of the amphibolite facies and define the following zoning: (Qtz + Pl + Ilm) + Grt + Bt ± Ms → St + Grt + Bt ± Ms → Sil/And + St + Grt + Bt → Crd + St + Grt + Bt ± Ms ± And. The peak metamorphic parameters were T ≈ 590–640°C and P = 5–6 kbar, and the retrograde metamorphism proceeded at T = 560–590°C and P = 4.5–5 kbar (Abu El-Enen et al., 2004).

Staurolite-bearing metapelites in Eastern Dalradian, Scotland. These schists are classic, meaning that they were the first rocks in which types of metamorphic zoning were distinguished (Barrow, 1893). The staurolite-zone rocks typically contain the mineral assemblage St + Grt + Bt + Ms + Pl + Qtz and occur in metamorphic rocks of both the Barrovian and the Buchan type. The metamorphic parameters were estimated at T = 540–580°C, P = 8–11 kbar (Baltatzis, 1979).

Staurolite-bearing schists of the southern Appalachian metamorphic belt. The metapelite of the Great Smoky Mountains Group, which were metamorphosed during the Taconian orogeny (at 450 Ma), are now part of the West Blue Range Thrust, the westernmost metamorphic belt of the southern Appalachians. The metamorphic grades increase starting with the chlorite zone in the northwest through the biotite, garnet, and staurolite zones to the kyanite one in the southeast. The peak metamorphic parameters were evaluated at 600°C, 6–8 kbar (Corrie and Kohn, 2008).

Metapelites of the Torrox unit in the Betic Reaf Belt, southern Spain. These metapelites contain the following mineral assemblages: (1) St + Bt + Grt + And ± Crd for the andalusite schists; (2) St + Bt + Grt + Fib + And ± Crd for the fibrolite schists; (3) and St + Bt + Grt + Ky + Fib + And ± Crd for the kyanite schists. The metamorphism occurred in an extensional environment in the Late Paleogene–Early Neogene and gave way to rapid isothermal decompression. As a result, the high-pressure mineral assemblages were replaced by low-pressure ones. The peak metamorphic parameters were 600°C, 6–8 kbar (Garcia-Casco and Torres-Roldan, 1999).

Monte Rosa paragneisses. The gneisses make up one of the upper nappes in the western Alps. The nappes consist of high-grade metapelite gneisses, whose protolith was sedimentary rocks and which were metamorphosed to the amphibolite facies during the late Alpine episode at 9–12 kbar and 595–755oC (Keller et al., 2005).

Precambrian staurolite schists in the Kishangarh area, India. The rocks were metamorphosed to P–T parameters of the staurolite–kyanite zone, make up an individual lithologic unit, and occur in

association with micaceous quartzites, calcicates, graphite schists with marble beds, amphibolites, and some other rocks (Lal and Shukla, 1970). The staurolite was reportedly formed at medium pressures and a temperature of 500–675°C.

Metapelites of the Wutai complex. The complex is located in the central part of the Trans-North China Orogen and is dominated by metamorphosed volcano-sedimentary rocks and Late Archean gneisses of the tonalite–trondhjemite series. The metamorphism (at 1.97–1.80 Ga) of this complex was characterized by a clockwise P–T path, from 3–7 kbar and T = 570–630°C through 9–10 kbar and 615–660°C to 6–9 kbar and 655–680°C. The metapelites consist mostly of Grt, St, Bt, Fib, Pl, and Qtz (Liu et al., 2020).

Metapelites in the southeastern Yukon area. Metapelites in the Hyland River area make up rocks units consisting of an extensive group of schists and gneisses overlying the Logan Batholith and the eastern part of the Mount Billings Batholith. The metapelites of the group contain Qtz + Pl + Bt + Ilm+ St + Als (Sil and/or And) ± Ms ± Grt ± Sp assemblages. The metamorphic parameters were T ≈ 550–575°C, P = 3–4 kbar (Moynihan, 2012).

Staurolite-bearing metapelites in the aureole of the Nelson Batholith. The batholith is a large Jurassic intrusive body in southeastern British Columbia, which is surrounded by a contact aureole 0.7–1.8 km thick in graphite-bearing clay host rocks. The contrasting prograde sequences of mineral assemblages around the aureole reflect the pressure variations. The staurolite metapelites occur within a broad zone, and their P–T metamorphic parameters are 3.5–4 kbar and 500–650°C (Pattison and Vogl, 2005; Pattison and Tinkham, 2009).

Metapelites in the Keffi area, Nigeria. The metamorphic complexes including these metapelites are part of the Pan-African Trans-Saharan Belt and belong to the so-called Great Schist Belt of Nigeria. The metamorphic parameters of the staurolite-bearing schists (Grt + Bt + St + Ms + Pl + Qtz + Ilm) were evaluated at 6.4–7.7 kbar and 570–615°C, which is close to the peak parameters (Ugwuonah et al., 2017).

Metapelites in the Archean Yanpo Group. These metapelites belong to the recently distinguished Zhōngxiáng Complex in southern China, and their material was provided by the erosion of the Yangtze Craton. The metapelites consists of amphibolite-facies mineral assemblages of unvarying mineralogical composition, including Qtz, Bt, Pl, Kfs and lower amounts of Sil, Grt, St, and Ms. No exact parameters of the metamorphism are reported, but the mineral assemblages indicate that these parameters should have corresponded to the lower amphibolite facies of the andalusite–sillimanite facies series (Wang et al., 2018).

Simulations of mineral assemblages of the aforementioned rocks with the PERPLEX software yielded P–T parameters of 500–650°C and <9 kbar and are obviously in good agreement with the mineral assemblages found in the rocks, with staurolite-bearing mineral assemblages reproduced for all of the mineral assemblages.

4.4. Petrochemical modules for metapelites

Analysis of the stability fields of staurolite parageneses for a wide range of metapelite compositions showed that the most informative when describing the characteristics of chemical compositions are the ratios of oxides of the main major components:Al_2O_3 / SiO_2, CaO / FM (где FM = FeO + Fe_2O_3 + MgO), K_2O / FM, Na_2O / FM (рис. IV-4-1) (Borisova, Baltybaev, 2021).

To more accurately constrain the ranges of these ratios, all available chemical compositions of staurolite-bearing rocks were regarded as reference compositions, which were then modified by adding to them up to 10 wt. % of each major oxide in some of the analysed projections of the compositions. Thus we artificially expanded the ranges of the possible metapelite compositions to determine by simulations whether staurolite can be stable in any of them. If no staurolite was simulated in a given composition, then the composition of the protolith was modified in such a way as to determine the extreme concentration of the component that controlled the stability of this mineral. The increments in the concentrations of each major oxide did not exceed 10 wt. % in order for the newly simulated bulk compositions not to extend outside the range typical of the metapelite group.

Analysis of the simulation results shows that staurolite can be stable only in metamorphic rocks of pelitic composition whose ratios (in wt. %) of major oxides lie within the following ranges (Fig. IV-4-2):

1. Al_2O_3 / SiO_2 = 0.19–0.92, with FeO + Fe_2O_3 + MgO (FM) within the range of 7–17 wt. %;
2. CaO / FM = 0.01–0.44;
3. K_2O / FM = 0.07–0.83;
4. Na_2O / FM = 0.02–0.34.

The total of alkalis shall therewith not exceed 6–6.5 wt. %, as is typical of metapelites.

The list of the applicable modules can be extended by using, for example, the ratios CaO / K_2O, CaO / Na_2O or Al_2O_3 / FM etc., but these ratios are linearly dependent on one another and thus cannot yield principally new results.

Thus, staurolite is a very informative mineral for solving a wide range of problems. Knowledge of the patterns of its formation increases the reliability of determining the facies of rocks and helps to reasonably draw boundaries between zones with different levels of metamorphism. The variety of possible compositions of protoliths from which staurolite is formed can be characterized by fairly narrow ranges (Fig. IV-4-1, IV-4-2) (Borisova, Baltybaev, 2021).

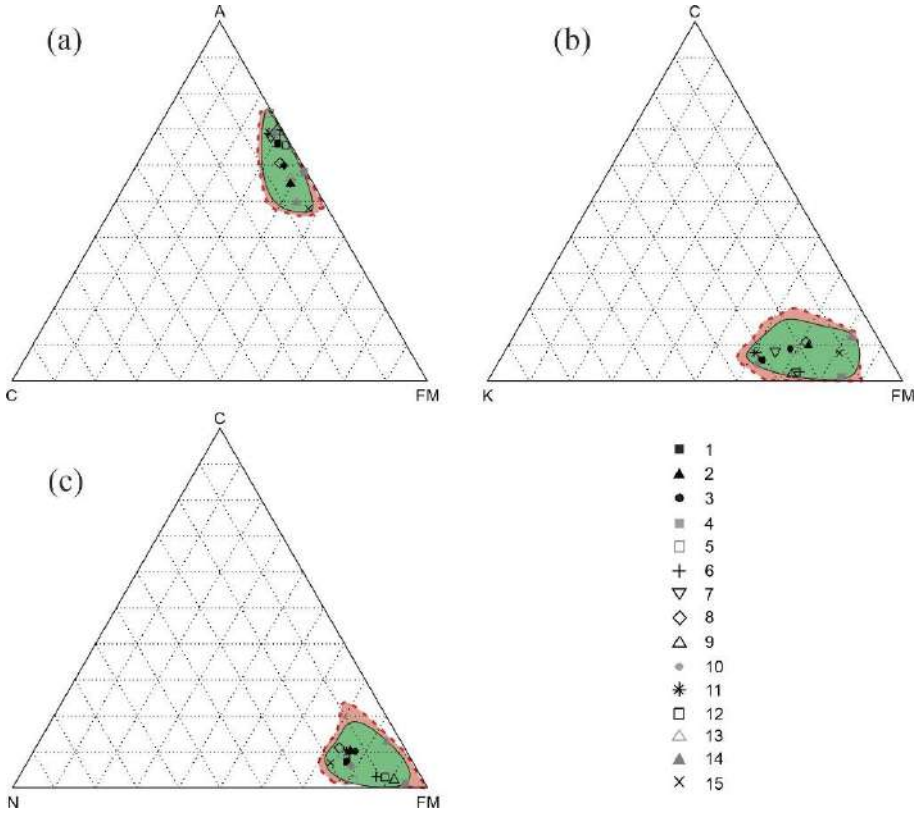

Figure IV-4-1. CAFM [CaO–Al_2O_3–(FeOt + MgO)], KAFM [K_2O–CaO–(FeOt + MgO)], and NCFM [Na_2O–CaO–(FeOt + MgO)] diagrams for staurolite-bearing rocks in the northern Ladoga area and metamorphic complexes elsewhere worldwide. Average composition of the Ladoga-Group metapelites: (1) our data, (2) (Material…, 1964), (3) (Predovskii, 1967). Composition of metapelites in other complexes elsewhere: (4) (Lal, 1970) India; (5, 6) (Baltatzis, 1979) Scotland, (7) (Garcia-Casco, 1999) Spain, (8) (Abu El-Enen, 2004) Egypt, (9) (Keller, 2005) western Alps, (10) (Corrie, 2008) North Caroline, United States, (11) (Pattison, 2009) British Columbia, (12) (Moynihan, 2012) Yukon, United States,(13) (Ugwuonah, 2017) Nigeria, (14) (Wang, 2018) southern China, (15) (Liu, 2020) northern China. The pale pink field is theoretical rock compositions (514 samples) in which staurolite can be formed upon the rocks reach the P–T parameters of its stability, and the dark green field comprises the composition points of naturally occurring staurolite-bearing rocks in the northern Ladoga area and other metamorphic complexes worldwide (74 samples).

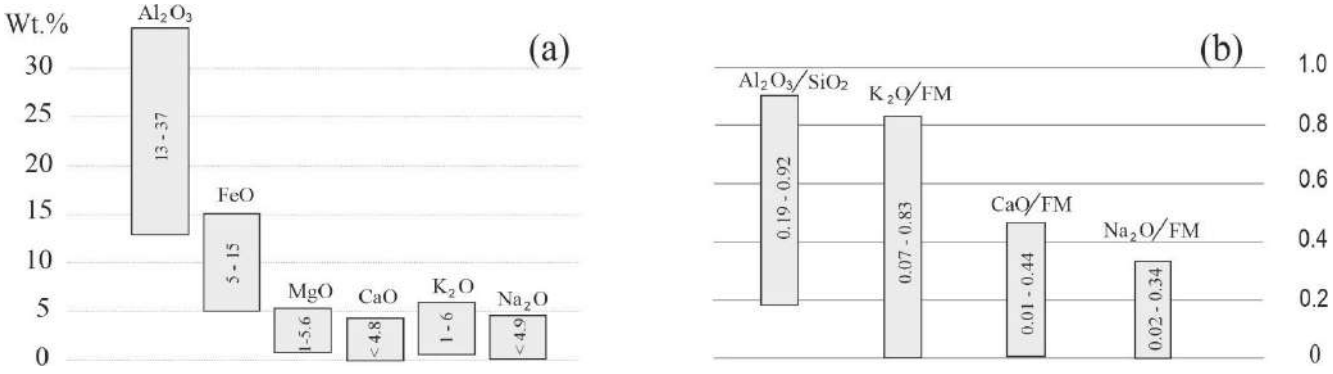

Figure IV-4-2. Composition of the protoliths in which staurolite can be formed by metamorphism at 500–650°C under low and medium pressures. (a) Possible ranges of major oxide concentrations; (b) ranges of the values of the petrochemistry modules.

4.5. Position of staurolite-containing rocks in the scheme of metamorphic facies

The staurolite facies of metamorphism is distinguished based on a combination of critical mineral assemblages of the staurolite zone, which is bounded by reactions involving other index minerals or their

assemblages. Each metamorphic facies can be spatially compared with a certain zone or zones in a metamorphic zoning. Metamorphic facies commonly comprise a number of mineral subfacies, as was proposed, for example, by S.P. Korikovsky (1979), who distinguished the staurolite metamorphic facies as an individual rank. The authors of this publication adhere to this system of metamorphic facies.

The position of staurolite-bearing rocks in the system of metamorphic facies was extensively discussed in the literature. For example, the assemblage St + Qtz was ascribed to the epidote-amphibolite facies (Ramberg, 1952; Francis, 1956), with its replacement by andalusite and kyanite assemblages with increasing metamorphic grade. N.G. Sudovikov (1964), A.A. Predovskii (1967), and Yu.V. Nagaitsev (1974) attributed the staurolite–andalusite subfacies, together with the sillimanite–almandine one, to the amphibolite facies. According to V.S. Sobolev (Facies…, 1970), staurolite rocks are stable within the epidote-amphibolite under relatively low pressures and amphibolite facies and within the facies of kyanite schists (an analogues of epidote amphibolites) under high pressures.

One of the latest petrogenetic grids for Fe–Al metapelites in the KFMASH system was proposed by I.I. Likhanov and his colleagues (Likhanov et al., 2005). The medium and high-temperature parts of most currently used diagrams were determined to be practically exactly identical, with differences between them occurring only at low and intermediate metamorphic grades at T < 570°C. The reasons for the origin of some mineral assemblages is, first of all, the effect of the chemical composition of the metapelites (e.g., Hoschek, 1969), with the main role played by the X_{Fe} and X_{Al} of the coexisting minerals. According to the petrogenetic grid in (Likhanov et al., 2005), the stability field of the assemblage St + Bt и Bt + Als lies within a narrow temperature range, with the St + Bt assemblage giving way to the Bt + Als one with increasing temperature, and with the latter assemblages replaced by the Grt + Bt + Als association, which is stable within a broad pressure range.

In the northern Ladoga area, staurolite-bearing schists are spatially associated with diopside marbles and andalusite schists of the amphibolite facies (Kitsul, 1963; Nagaitsev, 1974). This provides evidence in support of the conclusion (Sudovikov, 1964) that staurolite is formed at prograde metamorphism near the high-temperature boundary of the epidote-amphibolite facies, although most of its stability field occurs in the low-temperature portion of the amphibolite facies (Predovskii, 1967). It is worth mentioning that, in spite of some differences in their approaches, all researchers point out that the distinguished metamorphic zones are directly related to the corresponding facies and subfacies of metamorphism (Borisova, Baltybaev, 2021).

Summary of the chapter

Zoned-metamorphosed complexes, where metapelites with different levels of metamorphism are represented, are found throughout the world, one of such complexes is the Northern Ladoga region. One of the unresolved problems here was the ambiguity of the position of the staurolite isograd, which was

interpreted differently by different authors. Due to the fact that the appearance of staurolite-containing parageneses depends not only on the temperature of metamorphism, but also on the chemical composition of the protolith, we propose a method for identifying potentially staurolite-containing rocks using calculated “petrochemical modules”.

Based on the natural and theoretical compositions of metapelite protoliths, the ranges of contents of major elements indicating the appearance of staurolite in a given temperature and pressure range were quantitatively characterized. The proposed four petrochemical modules Al_2O_3 / SiO_2, CaO / (FeOt + MgO), K_2O / (FeOt + MgO), Na_2O / (FeOt + MgO) represent the ratios of the main rock-forming chemical components in metapelites, the values of which determine the potential for the formation of staurolite. A new methodological approach is applicable when compiling maps and diagrams of metamorphism

CHAPTER 5. PETROCHEMICAL CRITERIA AND THERMODYNAMIC REGIME OF STAUROLITE FORMATION IN METABASITES

Considering the multiplicity of factors controlling the appearance of staurolite, the purpose of this chapter is to highlight the most significant petrogenic components of the rock that determine the formation of magnesian staurolite, as well as to clarify the P-T-X conditions for the crystallization of this mineral in metamorphic rocks of basic composition. The undertaken thermodynamic modeling of staurolite mineral formation and the derivation of petrochemical modules are based on natural objects that are quite comprehensively and fully characterized in the geological literature (Borisova et al., 2022).

Along with the widespread ferruginous staurolite, characteristic of medium-temperature high-alumina metapelites, there are a number of finds of magnesian staurolite in metamorphosed rocks of basic composition - metabasites (Ríos et al., 2014 and references therein). Metabasites of the amphibolite facies metamorphism consist primarily of hornblende, plagioclase and ±quartz, but they may also contain chlorite, garnet, epidote group minerals and, more unusually, staurolite. Iron-rich amphibolites are typically dominated by staurolite-garnet mineral assemblages, while their more magnesium-rich counterparts contain chlorite and cordierite. Sometimes staurolite in the form of an accessory mineral is present together with kyanite in corundum amphibolites.

The application of the petrochemical modules Al_2O_3/SiO_2, CaO/FM , K_2O/FM, and Na_2O/FM in the form of ratios of certain major components of rocks makes it possible to identify the principal possibility of the stable crystallization of Fe-staurolite in metapelites within given temperature and pressure ranges (Borisova and Baltybaev, 2021). Since petrochemical modules in metapelites have shown their promise in predicting staurolite mineral parageneses, the question naturally arose about using similar modules to predict staurolite in mafic rocks. In this work, thermodynamic modeling is used to analyse the appearance of staurolite in metabasites with changes in the composition of the metamorphic fluid and variations in the content of major oxides in the protolith. Based on an analysis of the P-T-X conditions of staurolite mineral formation, quantitative ratios of major elements in the rock (petrochemical modules) are proposed that are necessary for the appearance of predominantly magnesian staurolite in metabasites (Borisova et al., 2022).

The main method we applied to analyse the mineral assemblages of staurolite was numerical simulations of the mineral-forming processes by means of minimizing the Gibbs free energy with the PERPLEX v. 6.91 software (Connolly, 1990, with updates at 2021, www.perplex.ethz.ch). The simulations were carried out using the hp62ver.dat (Holland and Powell, 2011) thermodynamic database for minerals and solid solutions, which includes actual thermodynamic parameters for plagioclase, amphiboles, biotite, garnet, spinel, olivine, orthopyroxene, omphacite, talc, chlorites, white micas, chloritoid, staurolite, cordierite, and ilmenite in the system MnNCKFMASH ($MnO–Na_2O–CaO–K_2O–FeO–MgO–Al_2O_3–SiO_2–H_2O–CO_2$).

To constrain the ranges of metabasite compositions potentially suitable for staurolite stability in them, we used amphibolites (six samples) in which staurolite has been unambiguously identified (Purttscheller and Mogessie, 1984; Enami and Zang, 1988; Gil Ibarguchi et al., 1991; Tsujimori and Liou, 2004; Faryad and Hoinkes, 2006) and approximately 150 additional analyses to expand the ranges of the real amphibolite compositions (Fig. V-1). These additional compositions allowed us to much more accurately determine the threshold values of concentrations of various major components that are critical for staurolite stability in the tested rocks. The applicability and validity of this approach has been tested in (Borisova and Baltybaev, 2021).

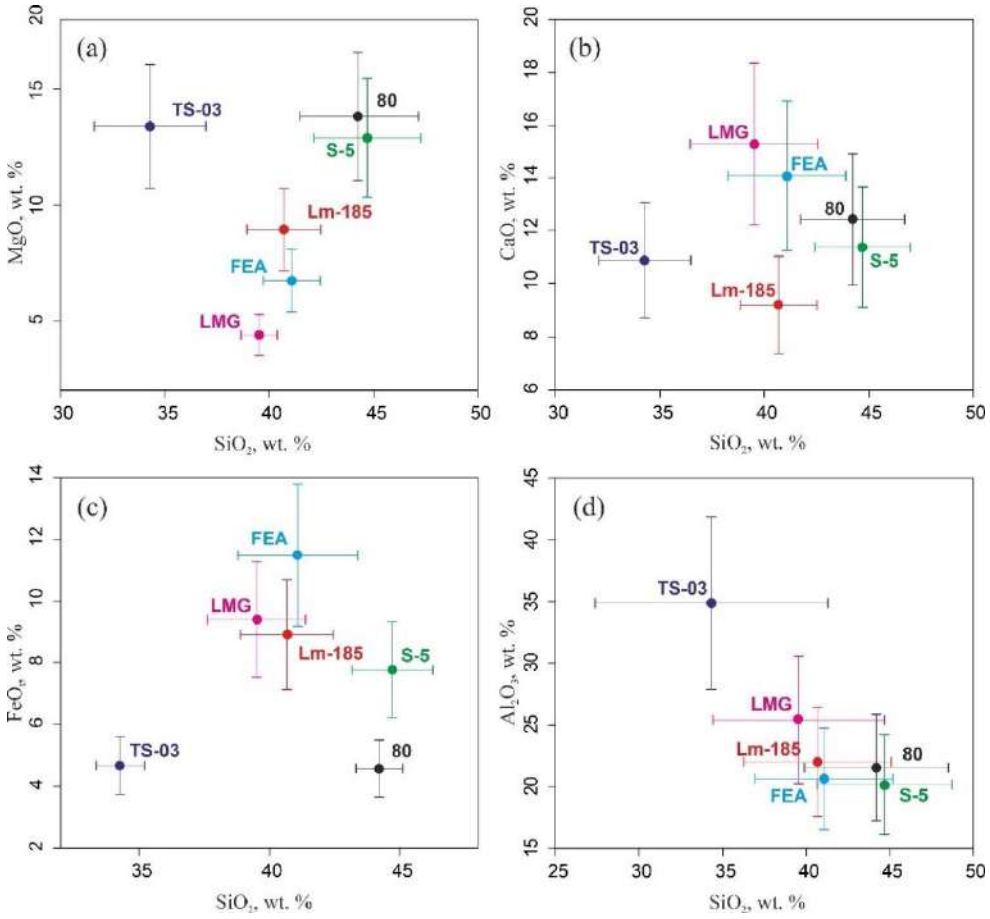

Figure V-1. (a) $MgO–SiO_2$, (b) $CaO–SiO_2$, (c) $FeOt–SiO_2$, (d) $Al_2O_3–SiO_2$ diagrams for staurolite-bearing metabasites. Data points correspond to the composition of natural rocks from which the theoretical compositions were calculated, and the ranges are shown with horizontal and vertical bars.

When modeling phase mineral equilibria, the input data were the results of chemical analyses of metabasites (Table 7). When solving the direct modeling problem to reproduce naturally occurring mineral assemblages based on a specified composition of a rock and P-T parameters, we assumed that the system contains either pure H_2O or H_2O-CO_2 fluid. For the latter, we recalculated the phase diagrams by stepwise adding (with increments of 0.2) CO_2 to the fluid to a maximum CO_2 mole fraction of 0.8, a value above which ($X_{CO2} > 0.8$) staurolite ceases to remain stable in any rocks in the whole spectrum of the studied compositions.

The modeling results are presented for 3 groups of mafic protoliths with different magnesium contents: 1) FeO/MgO << 1 (the composition of sample 80 from Gil Ibarguchi et al., 1991 was taken as the standard for this group), 2) FeO/MgO ~ 1 (the composition of sample LMG from Tsujimori, Liou, 2004 was chosen as the standard for the group), 3) FeO/MgO >> 1 (the composition of sample Lm-185 from Faryad, Hoinkes, 2006 was chosen as the standard). As shown by the results of modeling mineral formation, the identification of such groups of metabasites is very promising for identifying the patterns of formation of staurolite and its parageneses (Borisova et al., 2022).

5.1. Natural finds of staurolite in metabasites

Below is a description of metabasites, the compositions of which are accepted as basic. Note that the compositions of amphibolites in which the presence of staurolite was established by direct observations and confirmed by thermodynamic modeling of mineral formation were used from the literature data. The variety of tectonic settings in which staurolite metabasites were discovered determined the large P-T range of their formation (Borisova et al., 2022).

- *Sample Lm-185* (Faryad and Hoinkes, 2006) is an aluminous amphibolite from the Speik complex in the Eastern Alps, which contains coexisting kyanite, staurolite, garnet, and calcic amphibole. Textural features of the minerals, mineral thermobarometry, and thermodynamic simulations suggest that the rock was affected by prograde metamorphism to the high-pressure amphibolite facies (P = 11–12 kbar, T = 580°C) and was affected by subsequent decompression to 5 kbar. The sample was taken from the central part of the metabasite belt of the Speik complex, but it is uncertain whether its high alumina concentration is primary or resulted from overprinted hydrothermal alterations before the amphibolite-facies metamorphic event. If the protolith of the rock was of magmatic nature, it corresponded to gabbro. The rock is coarse-grained, with large garnet porphyroblasts, but without garnet where the rock is sheared. The rock consists of amphibole (close to 58 vol %), garnet (14 vol %), clinozoisite (6 vol %), plagioclase (5 vol %), margarite + muscovite (8 vol %), chlorite (5 vol %), kyanite (4 vol %) and accessory staurolite, with some other minerals found as inclusions in garnet. Texture relationships seen in this rock indicate that it has been formed by four pulses of mineral-forming processes: prograde metamorphism (Grt + Ky + St + Kfs? + Rt + Tur + Ap + Amp + Ep + Ms?) and three episodes of retrogression. The absence of cordierite from this rock indicates that the maximum temperature at decompression to 6.5 kbar was lower than 590°C (Faryad and Hoinkes, 2006).

The staurolite of this rock is Fe-rich: X_{Mg} = 0.21–24. The ZnO concentration of this mineral is very low, 0.13 to 0.47 wt. %, which corresponds to 0.013–0.046 Zn a.p.f.u. The mineral always contains minor concentrations of Mn and Ti (no more than 0.4 wt. %).

- *Sample S-5* (Purttscheller and Mogessie, 1984) is staurolite-bearing garnet amphibolite (St + Hbl + Grt + Ky) from the Ötztal Alps. The rock was affected by Hercynian metamorphism to P = 3–4 kbar,

T = 670°C. The protolith of the rock is of reportedly undoubted magmatic nature. The rock contains staurolite as small (2–10 nm) inclusions of acicular crystals in hornblende and garnet and, mostly, as such crystals at contacts of these minerals. The staurolite has XMg = 100 Mg/(Mg + Fe) = 0.32, which is higher than that of this mineral in metapelites (XMg = 0.21). All other compositional characteristics of the staurolite are the same as those of this mineral in metapelites. We are in doubt as to whether these authors have indeed reasonably accurately and realistically evaluated the metamorphic parameters of the rock, but nevertheless, we use the analysis of this sample to as much as possible cover all possible compositions of the protoliths whose metamorphism might have resulted in staurolite-bearing rocks.

- *Sample TS-03* (Enami and Zang, 1988) is a garnet–corundum rock that contains magnesian (X_{Mg} = 0.68–0.74) staurolite and was found as isolated blocks in an ultramafic complex emplaced into Precambrian pelitic gneisses in the Donghai district, Jiangsu province, east China. The rock is dominated by garnet and corundum and contains some amounts of zoisite and sodic phlogopite, along with secondary magnesian staurolite, chlorite, aluminous pargasite, clinozoisite, and magnesian allanite. The corundum hosts fine-crystalline inclusions of aggregates of diaspore, margarite, dolomite, and calcite (<0.03 mm). The equilibrium crystallization conditions of the primary assemblage were evaluated at T = 800–850°C, P = 11–30 kbar. The Mg-staurolite occurs as acicular and/or prismatic crystals and pseudomorphs after garnet and corundum with chlorite, which were formed according to the reaction Grt + Crd + H_2O = Mg-St + Chl. The equilibrium crystallization pressure of the staurolite was evaluated at >11 kbar, whereas the equilibrium temperature was slightly lower than that of the primary assemblage.

The rock has a very high Al_2O_3/SiO_2 ratio and a low FeOt (4.7 wt. %), which makes this chemical composition close to that of diaspore bauxite. The rock is also relatively rich in MgO and CaO, whose concentrations are explained by the authors as related to dolomite and limestone in association with the bauxite. Similar to the composition of the previous sample, we used the composition of this one to as widely as possible cover of protolith compositions in which staurolite can be formed at metamorphism.

- *Sample LMG, FEA* (Tsujimori and Liou, 2004) is kyanite-staurolite-epidote amphibolite from a metacumulus sequence of the Fuko Pass in the Oeyama belt, southwestern Japan. The rocks are leucocratic metagabbro that consists mostly of clinozoisite and kyanite with subordinate amounts of hornblende, margarite, paragonite, staurolite, rutile, chlorite, zoisite, and muscovite; the accessory minerals are ilmenite and apatite. Evidence of the following three metamorphic events was identified in the rocks: relics of granulite-facies metamorphism Cpx + Pl + Spl ± Opx (M1), of the high-pressure epidote-amphibolite facies Hbl + Czo + Ky + St + Pg + Rt ± Ab ± Crn (M2), and of retrogression when margarite, paragonite, muscovite, chlorite and sometimes plagioclase pseudomorphs were formed (M3). The metamorphic peak parameters were evaluated at P = 11–19 kbar, T = 550–800°C. The coarse-crystalline clinozoisite (up to 15 mm) hosts inclusions of all M2 minerals. The staurolite has X_{Mg} = 0.16–

0.29 and contains ZnO = 0.9–2.0 wt. %. Sample FEA differs from LMG in that the former is more intensely sheared.

- *Sample 80* (Gil Ibarguchi et al., 1991) is a kyanite-staurolite ultramafic rock that was found as lenses (10 × 1 m) in eclogites (whose composition is close to N-MORB) in the Cabo Ortegal complex in northwestern Spain. The parameters of metamorphism to the eclogite facies were evaluated at T = 800°C, P > 17 kbar. The kyanite-staurolite rock shows a mineral lineation accentuated by elongate amphibole, zoisite, and kyanite crystals, with this lineation coinciding with that in the eclogite (due to elongate omphacite crystals). The primary phases other than hornblende, zoisite, and kyanite are garnet, staurolite, and spinel. This rock is unusual in that its kyanite and staurolite are enriched in Cr to 4.35 wt. % and 6.4 wt. %, respectively. The staurolite has X_{Mg} = 0.58−0.74.

5.2. Influence of the content of petrogenic components in mafic protolith on the formation of staurolite

The modeling results showed a strong dependence of the mineral composition of metabasic rocks on the initial chemical composition of the protolith. Differences were revealed both in the number of simulated P-T regions of parageneses with staurolite, and in the configurations and sizes of these regions. In order to generalize the results and identify the main patterns of mineral formation, the compositions of metabasites were grouped according to the content of key petrogenic components that affect the stability of staurolite. Below is information about the features of mineral formation both for the original compositions of the above rocks and for various modifications of these compositions within 3 groups of metabasites (Borisova et al., 2022).

Protolith with high magnesium content (FeO/MgO << 1). For the initial composition of sample. 80 three areas of staurolite-containing mineral parageneses are modeled (Fig. V-2-1, gray fields): 1) the first, the most high-pressure (P = 26–29 kbar, T = 630–690°C) is characterized by the presence of high-pressure minerals such as omphacite and lawsonite, including accessory rutile: St + Grt + Amph + Cpx + Bt ± Tlc ± Chl ± Ky ± Lws ± Zo ± Rt; 2) the second region is medium-pressure, strongly elongated along the pressure axis (P = 11–20 kbar, T = 670–700°C), characterized by a predominance of talc in the composition and the absence of high-pressure minerals, but muscovite appears: St + Grt + Amph + Zo ± Bt ± Tlc ± Chl ± Ms ± Ky; 3) the third region is low-pressure, the smallest in area (~ P = 8–10 kbar, T = 690–730°C), characterized by the presence of plagioclase: St + Grt + Amph + Pl ± Chl ± Ms.

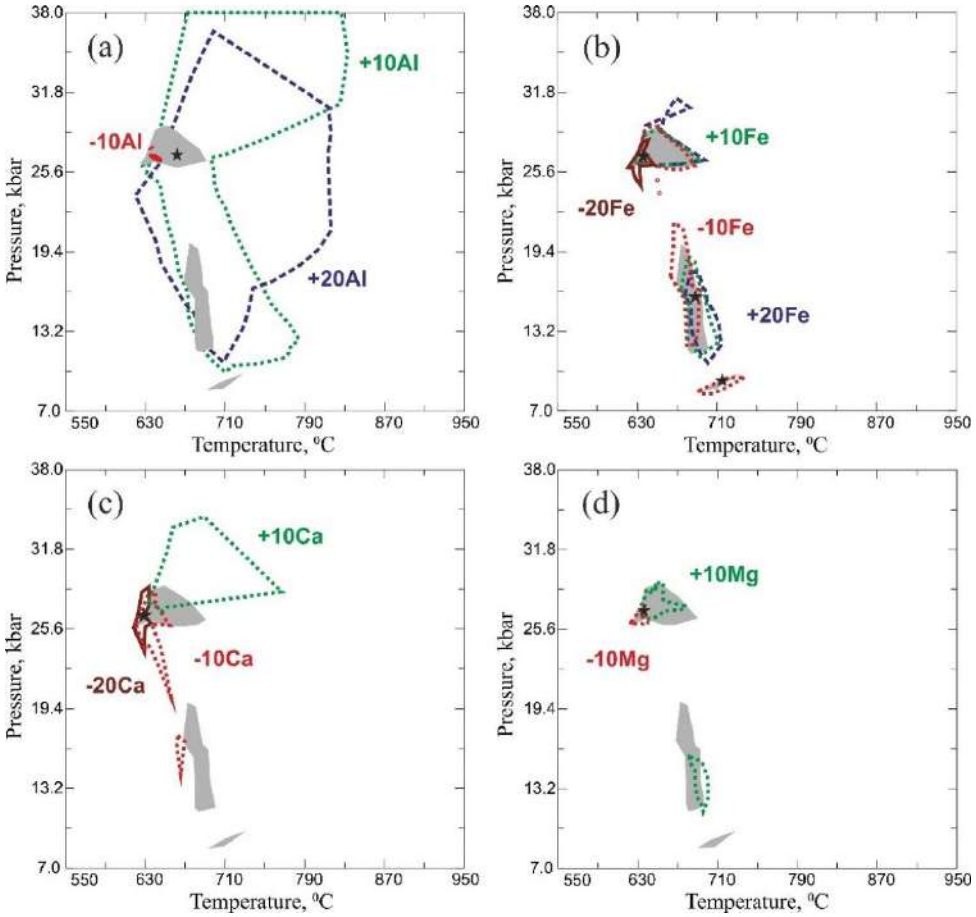

Figure V-2-1. Changes in the configurations of staurolite stability fields in P–T diagrams with variations in the concentrations of major components in the protolith. The basic composition of the metabasite was assumed to be that of sample 80. (a) Al_2O_3, (b) FeOt, (c) CaO, (d) MgO, where «+10», «+20», «−10», and «−20» mean the increase or decrease in the content of the respective component by 10 or 20% relative to the original (unmodified) composition of the rock. Gray fields are the fields with staurolite at the unmodified composition of the rock, green lines contour fields at the addition of 10% of the components, blue lines correspond to the addition of 20%, and red and brown ones pertain to a decrease by 10 and 20%, respectively.

A change in the **Al_2O_3** content sharply affects the configuration of the P-T field of stability of staurolite in a rock of mafic composition and is the most important criterion for the stability of staurolite. With increasing Al_2O_3 content (from -10Al to +20Al), the stability fields of staurolite greatly expand and combine into one. When the Al_2O_3 content decreases by 10% from the initial composition, the stability field of staurolite-containing parageneses greatly decreases and with a further decrease, staurolite is not formed.

With an increase in the **FeOt** content (from -10Fe to +20Fe), the high- and medium-pressure staurolite fields experience a slight shift relative to their initial positions, and the low-pressure field disappears at +10 Fe. In general, a change in the FeOt content on the position and size of the stability fields of staurolite in the P-T field does not have such a strong effect in comparison with a change in the alumina content.

A change in the **CaO** content in the rock noticeably affects the configuration of the stability fields of staurolite. With a slight increase in the calcium content, the field of staurolite stability expands in the

high-pressure region, but after a certain threshold of calcium content, staurolite ceases to form. A decrease in calcium content is less critical for changing the stability of staurolite, although there is a tendency for staurolite to disappear in the low-pressure part of the P-T diagram.

Both a decrease and an increase in the **MgO** content in the rock by 10% lead to a noticeable decrease in the areas of stability of staurolite and its quantitative content. At -20Mg, +20Mg, staurolite does not form in the rock.

Protolith with magnesium content FeO/MgO ≈ 1. For the composition of the LMG amphibolite sample (Tsujimori, Liou, 2004), the region of staurolite-containing mineral parageneses is observed at high pressures (P = 25–37 kbar, T = 610–720°C), it is characterized by the presence of such high-pressure minerals as omphacite, lawsonite and kyanite: St + Grt + Cpx + Ms + Rt ± Bt ± Lws ± Amph ± Crn ± Zo ± Ky (Fig. V-2-2 a-d).

An increase in the **Al_2O_3** content by 10% of the initial rock composition leads to an increase in the staurolite content in the rock from 4 to 7 vol. % and the appearance of corundum. In this case, no changes in the composition of minerals in the paragenesis are observed. With a further increase in Al_2O_3, staurolite does not form in the rock. A decrease in Al_2O_3 content by 10% leads to the disappearance of staurolite, while lawsonite and coesite appear in the rock.

An increase in the **FeOt** content by 10% leads to an increase in the amount of staurolite from 4 to 6.5 vol. %, while its magnesium content decreases. With a further increase in the FeOt content by 20%, the amount of staurolite decreases greatly to 0.12 vol. %, but the amount of pomegranate increases to 70 vol. %. There are no other critical qualitative and quantitative changes in paragenesis. When the FeOt content decreases by 10%, the amount of staurolite in the rock also decreases greatly from 4 to 0.6 vol. %, the amount of garnet also decreases, biotite disappears and lawsonite appears. The magnesium content of staurolite and garnet increases slightly. With a further decrease in the FeOt content in the rock, staurolite is not formed.

Both a decrease and an increase in the **CaO** content in the rock by 10% lead to the almost complete disappearance of areas of stability of staurolite.

An increase in **MgO** content by 10% leads to a slight increase in the amount of staurolite to 3.7 vol. %, a decrease in the amount of biotite and the disappearance of muscovite. There are practically no changes in the composition of minerals. With an increase in MgO by 20% of the initial value, the amount of staurolite also increases slightly, amphibole appears, and the jadeite component becomes larger in clinopyroxene.

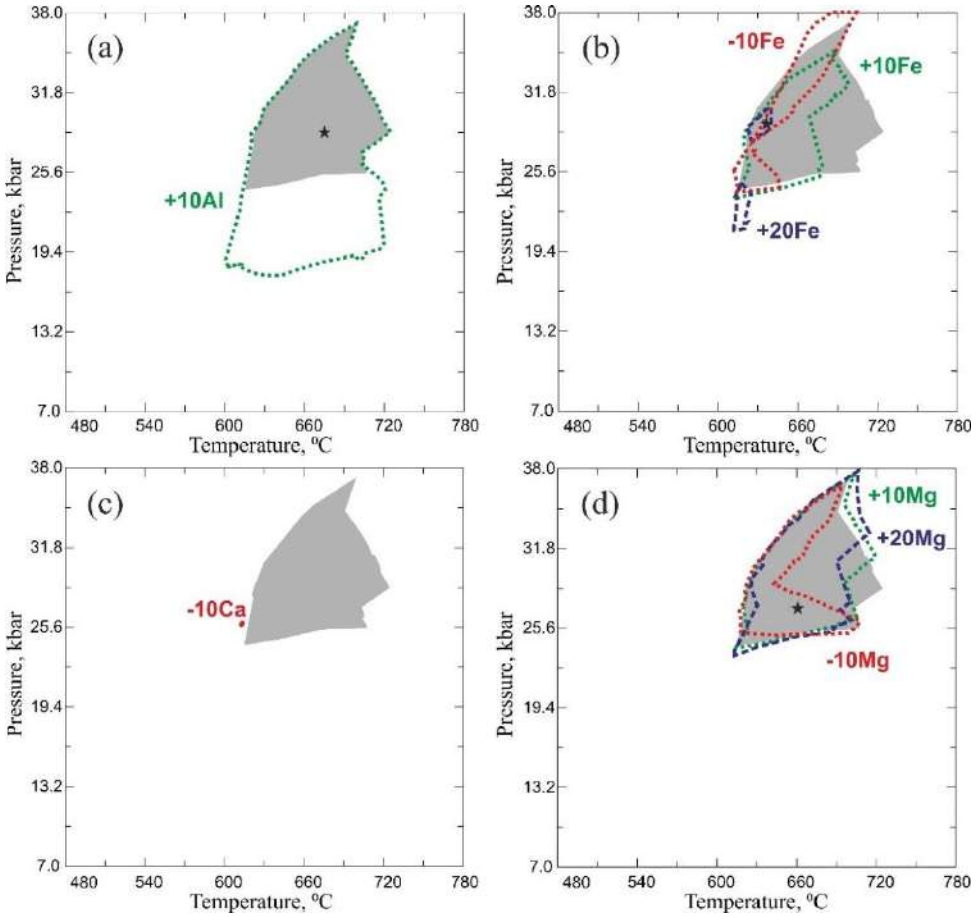

Figure V-2-2. Changes in the configurations of staurolite stability fields in P–T diagrams with variations in the concentrations of major components in the protolith. The basic composition of the metabasite was assumed to be that of sample LMG. (a) Al_2O_3, (b) FeOt, (c) CaO, (d) MgO. Other symbols are as in Fig. V-2-1 a-d.

Protolith with low magnesium content (FeO/MgO >> 1). For the composition of metabasite LM-185, the region of staurolite-containing parageneses is modeled at P = 25–32 kbar, T = 610–680°C. At the point P = 26 kbar and T = 630°C, approximately corresponding to the central part of the staurolite stability field, the following is observed: St (2.3 vol. %) + Grt (63.3 vol. %) + Cpx (18.5 vol. %) + Ms (12.2 vol. %) + Ky (2.5 vol. %) + Rt (< 1 vol. %) (Fig. V-2-3 a-d).

In general, with an increase in the **Al_2O_3** content in the rock, the content of staurolite greatly increases (from 1 to 17.4 vol.%), the content of garnet and clinopyroxene, on the contrary, decreases, kyanite disappears and biotite appears. With further growth of Al_2O_3, muscovite disappears in the rock, but amphibole is formed. The magnesium content of staurolite (from X_{Mg} = 0.76 to 0.72) and garnet (from Prp = 0.42 to 0.27) decreases. When the Al_2O_3 content in the rock decreases, staurolite does not form; quartz appears along with lawsonite and talc.

With an increase in the **FeOt** content in the rock, the amount of staurolite increases (from 1 to 7 vol.%) due to the disappearance of kyanite and a decrease in the proportion of muscovite. The magnesium content of garnet and staurolite also decreases slightly. With a significant increase in FeOt,

biotite develops in the rock. As FeOt decreases, the area of staurolite-containing parageneses greatly decreases, amphibole develops, and plagioclase and quartz appear.

With an increase in the **CaO** content, the stability field of staurolite parageneses increases and the amount of staurolite increases from 1 to 7.8 vol. %, kyanite and biotite disappear and zoisite appears. Staurolite becomes less magnesian, and the amount of pyrope in garnet decreases due to an increase in grossular. With a decrease in the CaO St content, parageneses are stable at low pressures, where parageneses with a predominant content of amphibole and plagioclase (anorthite) and a lower content of garnet are developed. Staurolite in the low-pressure region is noticeably more ferruginous: $X_{Mg} = 0.46$.

With an increase in the **MgO** content in the rock, the amount of staurolite increases (from 1 to 5–6 vol.%), kyanite disappears, biotite appears and, which is significant, magnesium chloritoid (up to 5.6 vol.%). The pyrope content in garnet decreases, and the composition of staurolite remains virtually unchanged. When the MgO content in the rock decreases, staurolite does not form.

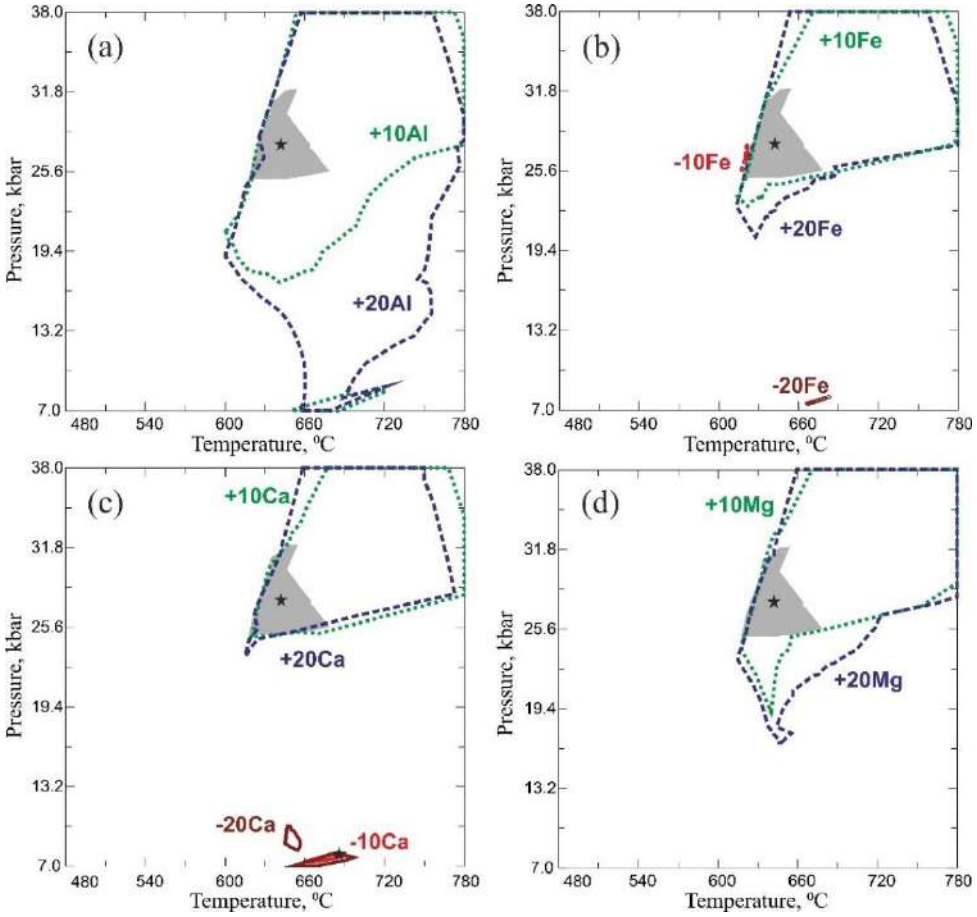

Figure V-2-3. Changes in the configurations of staurolite stability fields in P–T diagrams with variations in the concentrations of major components in the protolith. The basic composition of the metabasite was assumed to be that of sample Lm-185. (a) Al2O3, (b) FeOt, (c) CaO, (d) MgO. Other symbols are as in Fig. V-2-1 a-d.

The sequence of mineral formation and changes in the magnesium content of minerals

The general characteristics of mineral parageneses and their change with changes in temperature and pressure are given below using the example of the composition of an amphibolite in which the iron and magnesium contents are approximately equal (sample Lm-185, Fig. V-2-4).

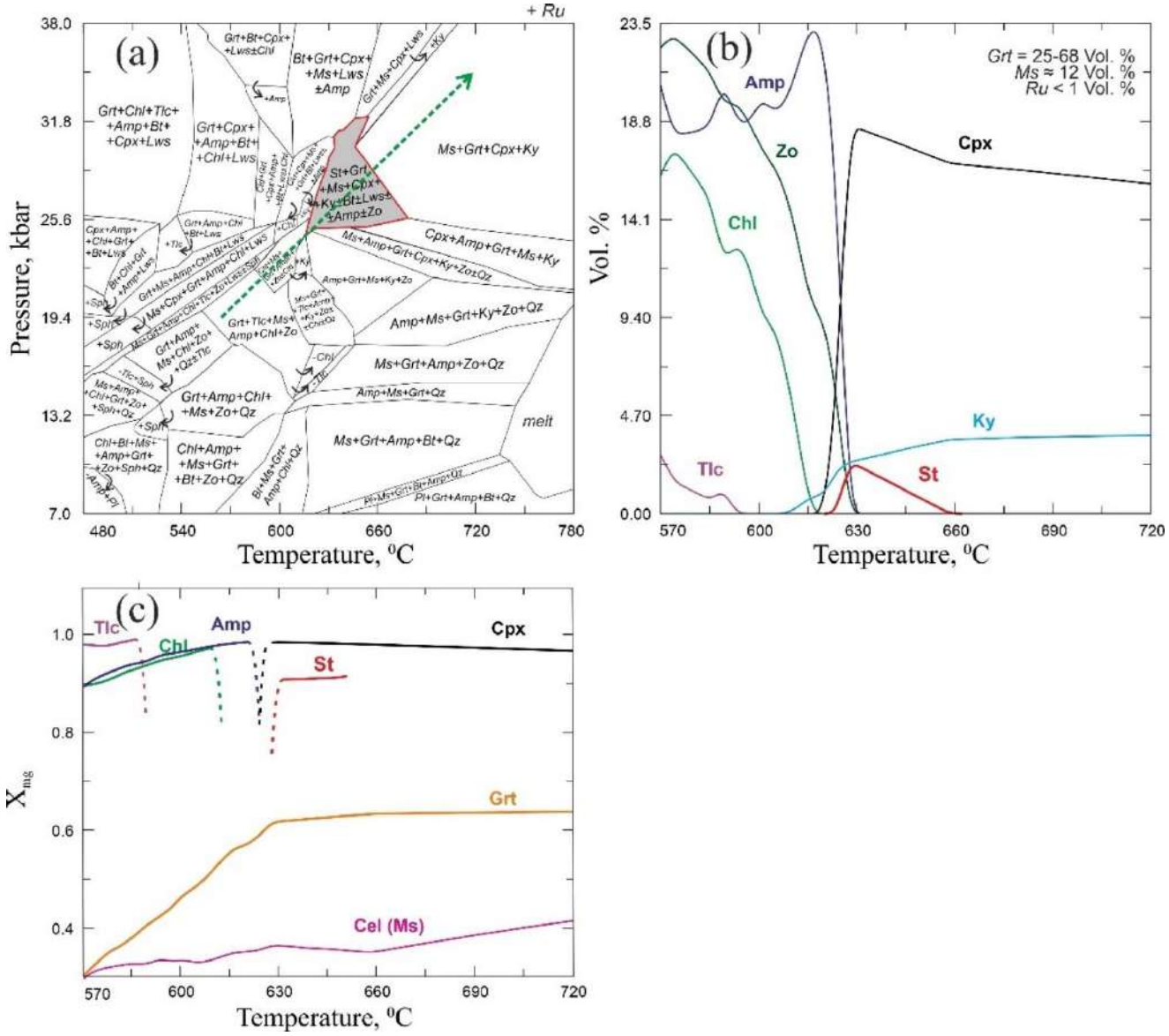

Figure V-2-4. Diagrams showing mineral assemblages, crystallization sequences, and variations in X_{Mg} of minerals for the specified P−T ranges and paths. (a) P−T diagram (pseudosection) of the stability fields of mineral assemblages for the composition of Lm-185. The red contour outlines the staurolite field. The signs "+" and "−" indicate that the specified mineral phase is present or absent, respectively, in the field indicated by an arrow. The green dashed line with an arrowhead is the P−T path along which the changes in the contents of minerals and their X_{Mg} are analysed (Figs. V-2-4b, c); (b) content (vol %) of minerals for the specified P−T path; (c) variations in the X_{Mg} of the Fe−Mg silicates along the P−T path.

The change in mineral parageneses is considered for the P-T range passing through the staurolite region (Fig. V-2-4 b). For this pseudo-section with increase of temperature and pressure, the appearance of the staurolite phase after the disappearance of such Fe-Mg minerals as chlorite and amphibole is modeled. Talc disappears somewhat earlier, which is then marked by the appearance of kyanite. At the same time, the staurolite paragenesis contains a significant amount of garnet and muscovite.

It is characteristic that the magnesium content of staurolite is higher than that of garnet (Fig. V-2-4 c), which corresponds to previously reported data on such a ratio at high pressures (Koch-Müller, 1997). There is a weak negative correlation between the magnesium content of staurolite and the magnesium content of clinopyroxene and garnet, as well as the content of the celadonite molecule in muscovite (Fig. V-2-4 c).

Thus, from the example considered, it follows that the increased magnesium content of staurolite in amphibolites is naturally inherited from high-magnesium minerals, mainly chlorite, the decomposition of which led to its appearance (Borisova et al., 2022).

5.3. Influence of metamorphic fluid composition on the formation of staurolite in metabasites

To estimate how the mineral assemblages depend on the fluid composition, we have simulated the mineral-forming processes at various H_2O and CO_2 proportions in the fluid. The composition of the fluid was varied from pure H_2O to pure CO_2 by adding CO_2 at X_{CO2} increments of 0.2 (X_{CO2} = 0−0.8). The changes were simulated for the compositions of metabasite samples 80 (Gil Ibarguchi et al., 1991), LMG (Tsujimori and Liou, 2004), and Lm-185 (Faryad and Hoinkes, 2006), all of which are rich in alumina but differ from one another in the Fe/Mg ratio, which turned out to be critical for staurolite stability. (fig. V-3-1) (Borisova et al., 2022).

For the amphibolite with ***FeO/MgO << 1*** (sample 80), mineral assemblages involving pure aqueous fluid were characterized above (Fig. V-2-1). With an increase in the proportion of carbon dioxide in the fluid to 0.8, the stability fields of staurolite-containing parageneses greatly expand and shift towards low temperatures and pressures (Fig. V-3-1 a). For example, with an increase in $X(CO_2)$ by 0.2, the boundaries of the St fields shift by 20–30°C and ~1 kbar. It is worth noting that at $X(CO_2)$ = 0.6, the high-pressure and medium-pressure fields merge into one, which expands maximum at $X(CO_2)$ = 0.8 in the region P = 7.6–30 kbar, T = 530–630°C. No qualitative mineral changes are observed.

For the amphibolite with ***FeO/MgO ~ 1*** (sample LMG), in which a rather wide P-T region of staurolite-containing mineral parageneses is modeled with aqueous fluid (Fig. V-3-1 b), with an increase in the proportion of $X(CO_2)$ St, the field shifts towards lower temperatures, expanding along the axis pressure. At $X(CO_2)$ = 0.8, staurolite is stable in the range P = 20–41 kbar, T = 520–610°C, but at P = 23–26 kbar the field greatly narrows along the temperature axis: T = 540–560°C. No qualitative mineral changes observed.

For the amphibolite with ***FeO/MgO >> 1*** (sample LM-185), there is a strong difference between the position of the stability fields of staurolite-containing parageneses with pure aqueous fluid and aqueous-carbon dioxide (Fig. V-3-1 c). At $X(CO_2)$ = 0.2, the stability field of staurolite-containing parageneses shifts by ~1.5 kbar towards higher pressures and by ~20°C towards low temperatures. At $X(CO_2)$ = 0.4, the area of the high-pressure field decreases and shifts towards higher pressures and lower

temperatures. A small low-pressure field also appears at P = 6–6.5 kbar, T = 620–635°C, where parageneses of staurolite with amphibole, plagioclase and quartz are developed. At X(CO_2) = 0.6, the high-pressure St field greatly decreases and shifts toward high pressures P = 32–34 kbar and low temperatures T = 580–600°C. The low-pressure field, on the contrary, expands and shifts towards lower P and T. At X(CO2) = 0.8, only the low-pressure field remains, which expands and shifts towards low temperatures: P = 4.5–8 kbar, T = 500–530° C.

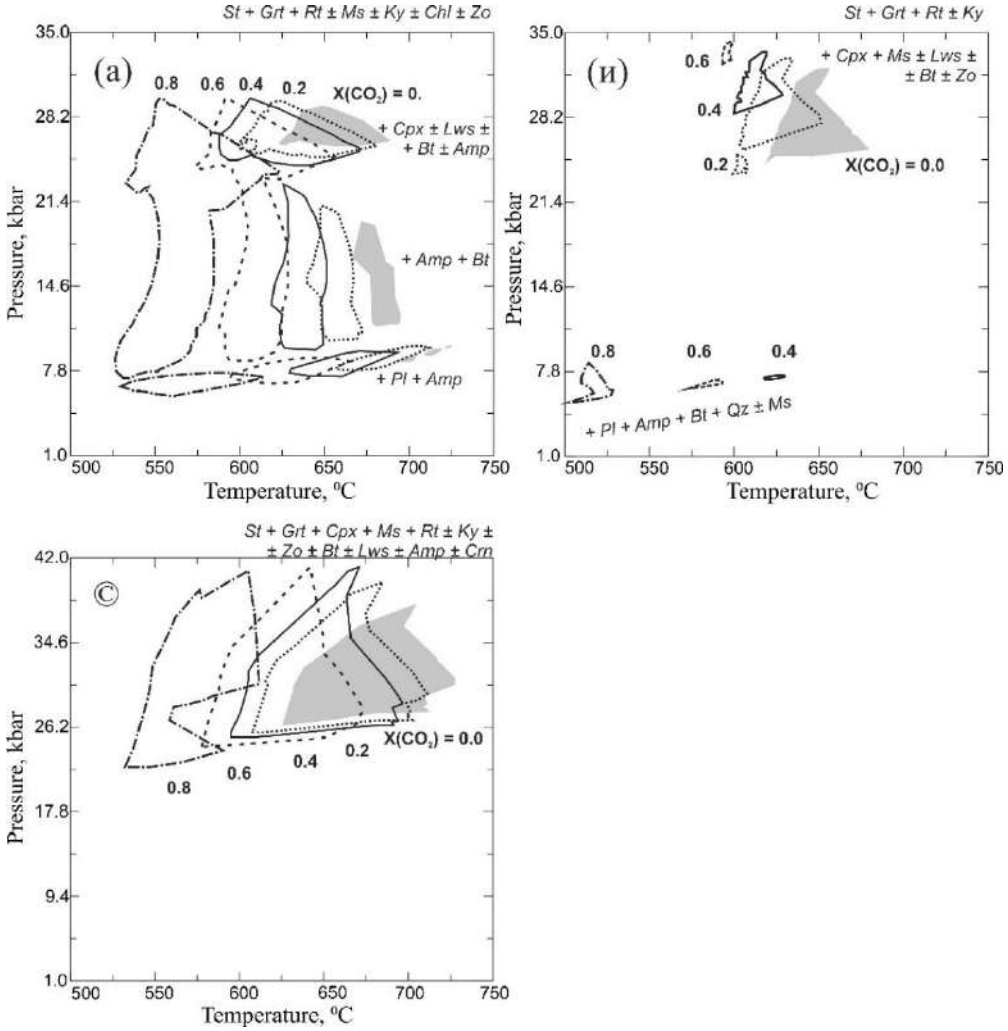

Figure V-3-1. Changes in the configurations of the stability fields of staurolite-bearing mineral assemblages depending on the fraction of CO_2 in the H_2O–CO_2 fluid. Gray fields are the stability fields of staurolite in the presence of pure H_2O fluid. Various lines show variations in of the fluid, from 0.2 to 0.8. (a) Modeling for the composition of sample 80, (b) same for sample Lm-185, (c) same for sample LMG.

Thus, with an increase in the proportion of carbon dioxide in the aqueous-carbon dioxide fluid, the stability fields of staurolite parageneses systematically shift towards lower temperatures. For some metabasites (samples 80 and LMG), with increasing X(CO_2), the stability fields of staurolite expand in both pressure and temperature, while in the case of sample LM-185, the high-pressure field, on the contrary, decreases, strongly shifting upward in pressure. The low-pressure field, where staurolite parageneses with Amph, Pl, Qtz are developed, appears only at X(CO_2) = 0.4 and with a further increase in the proportion of carbon dioxide in the fluid, it expands. (Borisova et al., 2022).

The noted features of changes in the configuration of staurolite fields at different CO_2 contents in the fluid can be explained by changes in the activity of water in the fluid, the decrease of which with increasing $X(CO_2)$ leads to a reduction in the temperature stability of water-containing minerals, including staurolite, instead of which "dry" mineral species are formed (Borisova and al., 2023).

5.4. Assessment of the influence of Fe^{2+}/Fe^{3+} in rock on the stability of staurolite in metabasites

Previously, modeling of mineral formation revealed (White et al., 2000) that when analyzing the stability of staurolite, it is necessary to take into account the content of ferric iron Fe^{3+} in the rock. Although it is often difficult to reliably judge the value of the Fe^{2+}/Fe^{3+} ratio in the rock at the considered stage of mineral formation, if we assume that FeO/Fe_2O_3 in mafic rocks was equal to 0.15 (Brooks, 1976) or 0.20–0.25 (Hughes and Hussey, 1979), then it is revealed some slight increase in the region of stable existence of staurolite compared to the composition where FeOt = FeO. When taking into account iron in the form of Fe^{3+} (Fig. V-4-1 b), the area of coexistence of staurolite with amphibole and corundum expands quite significantly towards lower pressures, in the upper part of the diagram, the stability field of staurolite with lawsonite and corundum also increases. However, no qualitative changes are observed in the mineral parageneses.

Given the poor knowledge of the thermodynamic properties of silicates containing ferric iron, the results of such calculations should be treated with caution. For this reason, we adhered to the calculation scheme without taking Fe^{3+} into account.

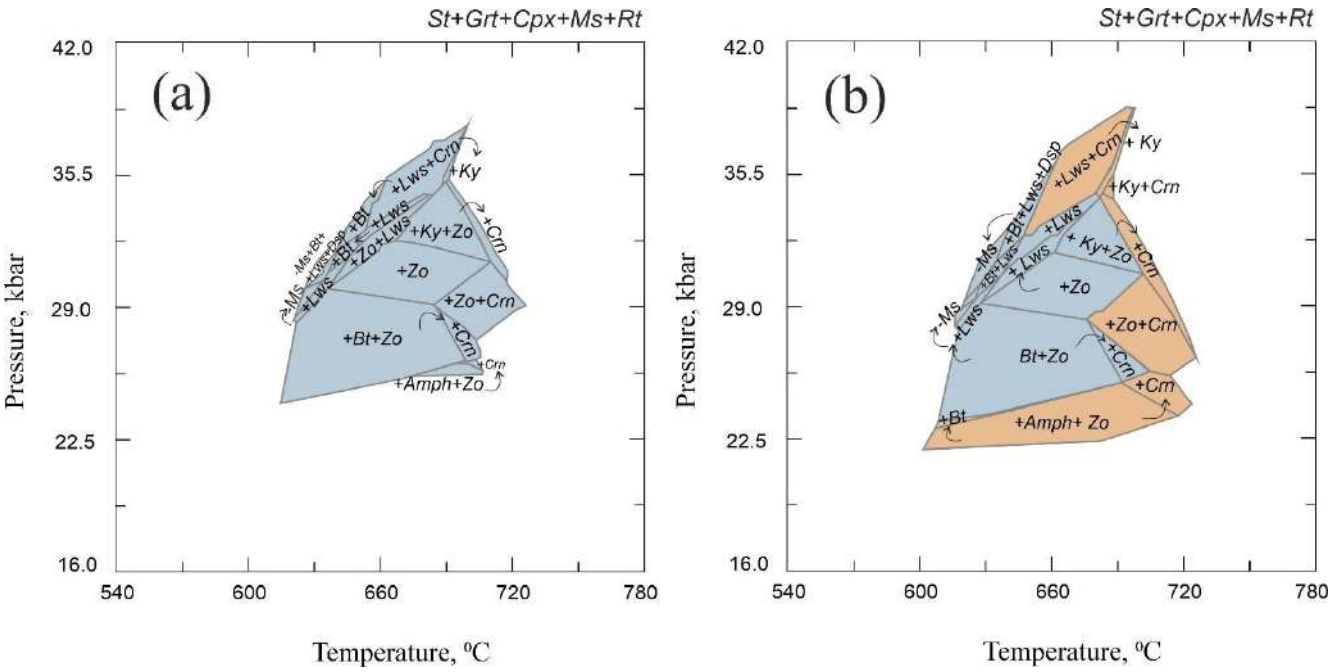

Figure V-4-1. Changes in the configuration of stability fields of staurolite parageneses depending on the Fe_{3+} content in the rock for the composition of the LMG sample. a – modeling with FeOt = FeO, b – with FeOt = FeO + Fe_2O_3.

5.5. Verification of the conditions for the formation of mineral phases of staurolite-containing parageneses in metabasites

High-pressure metabasites are characterized by a set of rock-forming minerals, consisting of garnet, clinopyroxene, amphiboles, talc with a small amount of mica and chlorites. The accessory part can be represented by minerals such as kyanite, zoisite, lawsonite, rutile and staurolite. In order to verify the adequacy of our results on modeling mineral phases in metabasites, we examined the conditions for the formation of some minerals presented in the literature.

Staurolite. The broad diversity of naturally occurring mineral assemblages of metabasites suggests that the number of the phases and their relationships strongly depend on the P−T parameters, bulk-rock compositions, and the composition of the fluids. Alumina content in the rocks is crucial for the stability of hornblende and staurolite. This conclusion is consistent with data in (Arnold et al., 2000) that staurolite and hornblende are formed in rocks with $Al_2O_3/(Al_2O_3 + FeO + MgO + CaO + Na_2O)$ = 35 wt. % at temperatures above 550°C and 595°C, respectively. The XMg of the staurolite lies within the range of 0.2 to 0.7. Thermodynamic simulations with the THERMOCALC software (Powell and Holland, 1988) indicate that staurolite- and hornblende-bearing mineral assemblages can be formed at pressures of 4–10 kbar and temperatures of 560–650°C. In such rocks (except Al- and Fe-richer lithologies), staurolite assemblages are stable within a narrow P-T field (Arnold et al., 2000). Analogously, according to (Tsujimori and Liou, 2004), the assemblage Hbl + Czo + Ky ± St + Pg + Ab ± Crn in Al-rich metabasites is typical of metamorphic parameters of the high-pressure epidote-amphibolite facies.

Although the occurrence of staurolite in "typical" amphibolites may be indicative of metamorphism under a relatively high pressure, interpretations of these assemblages in more aluminous lithologies are more ambiguous. Because of the high variability of staurolite-bearing mineral assemblages, the crystallization sequences of the minerals during metamorphism are uncertain (Arnold et al., 2000; Faryad and Hoinkes, 2006).

It is fairly hard to reasonably realistically specify the setting of staurolite in the mineral assemblages of metabasites because this mineral is documented in such rocks much more rarely than in metapelites. One of the reasons for this is (Purttscheller and Mogessie, 1984) that it is difficult to identify staurolite phases in metabasites because their grains are small.

Although staurolite and kyanite are found in amphibolite-facies rocks and usually occur in association with paragonite and garnet, amphibole may be absent from some Al-rich metabasites (Faryad and Hoinkes, 2006). Staurolite was also documented in metabasites containing gedrite (Spear, 1977, 1978, 1980).

The aforementioned facts and considerations imply that staurolite-forming reactions in metabasites are controlled by several factors but not only alumina content of the rocks. Staurolite and

kyanite stability in rocks strongly depends on their Fe and Mg concentrations (Arnold et al., 2000; Faryad and Hoinkes, 2006). Sometimes an important role is played by K_2O. Low K_2O concentrations hamper the formation of potassic feldspar, and hence, excess Al (if present), is accommodated to some extent in plagioclase and is favorable for staurolite stability in the presence of relatively high Fe concentrations.

Data in (Faryad and Hoinkes, 2006) show that staurolite can be formed in high-Al metabasites at T = 570°C, P > 10 kbar, together with clinozoisite, or at T = 540–450°C, P = 7–8 kbar, with plagioclase. The absence of chloritoid from the studied rock samples suggests either that this mineral has been completely replaced or that the prograde P–T path did not cross the stability field of chloritoid (Faryad and Hoinkes, 2006).

Metabasites typically contain more magnesian staurolite than this mineral in metapelites. Staurolite in which much Fe^{2+} is substituted for Mg was first found in high-pressure metamorphic rocks in the 1980s (Schreyer et al., 1984). Later on, magnesian staurolite has been found in other metabasites (e.g., Enami and Zang 1988; Gil Ibarguchi et al., 1991). One of the first studied magnesian staurolite (X_{Mg} = 0.965) samples originated from the Dora-Maira massif in the western Alps (Simon et al., 1997; Simon and Chopin, 2001) and contained much H^+. This staurolite was reportedly formed under ultrahigh-pressure metamorphism at T = 700°C and P = 30 kbar (Simon et al., 1997; Simon and Chopin 2001).

Staurolite samples with X_{Mg} up to ~ 0.4–0.6 were found in various rocks metamorphosed under high pressures (Schreyer et al., 1984; Ward, 1984, Grew and Sandiford, 1984; Nicollet, 1986). Magnesian staurolite is often found in equilibrium coexistence with corundum. This indicates that an environment undersaturated with silica is favorable for the origin of highly magnesian staurolite (e.g., Schreyer, 1967; Grew and Sandiford, 1985).

It has been hypothesized (Schreyer, 1967) that the absence of natural magnesian staurolite from the upper mantle, in which P–T parameters are reached that are necessary for the stability of magnesian staurolite (>11 kbar), is explained by the absence of highly aluminous rocks. W. Shreyer has also suggested that magnesian staurolite and quartz cannot be stable with each other because of the alternative stability of kyanite or other magnesian silicates. Indeed, kyanite and other aluminous minerals are typical of high-pressure eclogites (e.g., Dawson, 1980), and the breakdown of these minerals at a temperature decrease may result in Mg-rich staurolite.

When the possible sources of highly aluminous rocks at mantle depths were discussed, it was suggested that staurolite can be produced by high-pressure metamorphism in mafic rocks with minor amounts of crustal material, which is characterized by high alumina contents (Hellman and Green, 1979).

It has been experimentally proved (Hellman and Green, 1979) that staurolite can be formed in a mafic rock under a high pressure, in the presence of water. Experiments aimed at constraining the stability field of staurolite in the $MgO–Al_2O_3–SiO_2–H_2O$ system (Fockenberg, 1995) under various

water pressure have demonstrated that the mineral is stable at P = 12–66 kbar and T = 608–918°C. Hydrogen concentration in magnesian staurolite usually increases with increasing pressure (Holdaway et al., 1995; Fockenberg, 1995).

Scarce data are currently available that magnesian staurolite can be formed at very high temperatures (> 900–1000°C), as in the Central Zone of the Limpopo complex in South Africa (Schreyer et al., 1984; Tsunogae and Van Reenen, 2010), where magnesian (X_{Mg} = 0.44–0.58) staurolite was found in an equilibrium assemblage with sapphirine and quartz. Another find was made in southern India (Tsunogae and Santosh, 2003; Santosh et al., 2004; Shimpo et al., 2006), where magnesian (X_{Mg} ~ 0.58) accessory staurolite was found out to coexist with garnet, gedrite, sapphirine, corundum, spinel, and rutile.

Staurolite can have X_{Mg} < 0.3, which is lower than this parameter of other silicates coexisting with it (e.g., Deer et al., 1982; Enami, 1988). However, it is well known that of staurolite with, for example, garnet shows an inversion with increasing pressure (Koch-Müller, 1997). Staurolite-bearing Ca-poor rocks (without muscovite and potassic feldspar) sometimes contain unusual mineral assemblages with gedrite and cordierite, and the staurolite and garnet have the highest X_{Mg}, much higher than these parameters of the minerals in the surrounding muscovite-bearing metapelites metamorphosed to the same temperature and pressure. It is also known (from data on natural rocks) that the reactions forming and decomposing staurolite at prograde metamorphism are principally different: cordierite rims around staurolite have been found and documented in (Mezger and Passchier, 2003).

Magnesian staurolite has been synthesized at T = 700–950°C and P > 11 kbar (Schreyer, 1967; Schreyer and Seifert, 1969). Staurolite rich in Mg (X_{Mg} = 0.53–0.57) was experimentally synthesized from olivine tholeiite at T = 740–760°C and P = 24–26 kbar (Hellman and Green, 1979).

These and other experimental data suggest that Mg-rich staurolite can be stable in Mg- and Al-rich metamorphic rocks produced at high temperatures and pressures, which is consistent with or simulation results.

Lawsonite. Among the high-pressure minerals, which are often modeled together with staurolite in metabasites, there is lawsonite $CaAl_2(Si_2O_7)(OH)_2 \cdot H_2O$. Lawsonite is a typical mineral of metabasalts and calcium-rich metagreywackes and is considered an indicator mineral of high-pressure, low-temperature metamorphism. In the blueschist facies, lawsonite crystallizes at conditions ranging from 0.3 to 1.0 GPa and 150 to 400°C (Diessel et al. 1978). In metabasites it is usually found in association with glaucophane, chlorite, albite and mica, similar in composition to phengite. Lawsonite has a significant amount of water bound in its crystal structure, which is only released during its breakdown into denser minerals through progressive metamorphism.

The results of experiments in the CASH system (Schmidt, Poli 1994; Pawley 1994) showed that lawsonite is stable up to 1040–1080°C and 92–94 kbar, and the stability conditions for pure lawsonite

reach 120 kbar (equivalent to 350 km depth) and 960° C (Schmidt 1995). These conditions correspond to the conditions defined for subduction slabs. Thus, lawsonite may remain stable during subduction in descending oceanic crust to pressures exceeding 120 kbar, and its destruction may promote water recirculation in the mantle above subducting plates to depths greater than 200 km (Poli and Schmidt 1995).

In nature, lawsonite typically occurs in rocks of blueschist terranes metamorphosed under high-pressure, low-temperature conditions (mostly 3–15 kbar, see Evans and Brown, 1986 and references therein), and can also occur in basaltic xenoliths in kimberlites (Watson, Morton, 1969), originating from deep rocks (> 25 kbar) (Helmstedt and Schulze, 1988). Pauly and Schmidt (1995) experimentally showed that lawsonite occurs in basaltic and andesitic compositions: up to 780°C at 60 kbar in basalt and up to 900°C at 77 kbar in andesite. Relatively cold thermal regimes in subduction zones allow lawsonite, formed under blueschist facies conditions, to be preserved in subducted crust to a depth of more than 240 km.

The high water content in lawsonite, both in the form of H_2O molecules and in the form of OH-groups (11.5 wt.%), as well as the conditions of its stability indicate that this mineral is capable of transporting significant amounts of water to depth during the subsidence of the oceanic lithosphere (Kerrick , Connolly, 2001; Scambelluri, Phillipot, 2001; Hacker et al., 2003) along with other OH^- containing phases, such as antigorite, magnesiochloritoid, talc, phengite, staurolite and epidote. However, lawsonite is a carrier not only of H_2O, but also of the geochemically important trace element Sr (among others) in high- and ultrahigh-pressure rocks, where it controls the chemical balance of Sr in the rock as a whole (Tribuzio et al. 1996; Zack et al. 2002; Spandler et al. 2002). al. 2003).

Despite the close chemical similarity to anorthite, lawsonite has a higher density (3.09 instead of 2.76 g/cm^3) and a different Al coordination: octahedral in lawsonite and tetrahedral in anorthite. The results of studying the change in the structure of lawsonite at high P and T indicate that although lawsonite can be stable even at great depths under P-T regimes characteristic of subduction plates, it can become unstable during the process of exhumation. For these reasons, lawsonite is rarely preserved and is usually found as a relic in clinozoisite (Comodi and Zanazzi, 1996).

An example of lawsonite-containing rocks are the metamorphic rocks of the Pensantine sequence of the Pensantine ridge (Dobretsov, 1974; Rusin, 2020, etc.). The age of metamorphism is no later than 40 million years and no earlier than 94 ± 2 million years. For these rocks, there is a problem of local distribution of lawsonite in the context of metamorphic formations. Here the association of lawsonite-bearing rocks is represented by albite, lawsonite, muscovite, chlorite and quartz. Lawsonite is not found in association with epidote and alkaline amphibole and is confined to the lower part of the Pensantine sequence, occupying a certain horizon (Rusin, 2020), which requires explanation in the light of the problem of the lawsonite paradox discussed in the geological literature (Clark et al., 2006).

The lawsonite paradox lies in the fact that lawsonite equilibrium is theoretically and experimentally determined for a wide range of P-T (Newton and Kennedy, 1963; Liou, 1971, etc.) developing during subduction, but associations containing lawsonite are rare in nature. For example, lawsonite eclogites are found only in a few high-pressure, low-T terranes (Zack et al., 2004; Tsujimori et al., 2006). In the work of Clark et al. (2006), the lawsonite paradox is considered in two problems: 1) why are rocks containing lawsonite rare? 2) and what contributes to the preservation of lawsonite? The authors believe that at elevated pressure, the participation of high water-content, necessary for the formation of mineral parageneses containing lawsonite, is difficult. Also, the preservation of lawsonite blueschists and lawsonite eclogites requires exhumation with significant cooling, which greatly limits the formation of rocks according to the tectonic regime. The authors' modeling results indicate that eclogites are much more likely to be preserved than lawsonite-bearing blueschists due to the nature of the water content in mineral assemblages of natural blueschist facies and eclogite facies.

Thus, the P-T parameters of the formation of one of the “satellites” of the high-pressure mineral – lawsonite, are quite correctly reproduced during modeling mineral formation and the results obtained are in agreement with natural observations and experimental data on the conditions of formation of this mineral.

5.6. Petrochemical modules for metabasites

The compositions of metabasites favourable for the formation of staurolite most fully characterize the amount of Al_2O_3, MgO, FeOt, CaO in them, and since the contents of other petrogenic components are less or close to unity, their variations practically do not affect staurolite stability. With regard to this, the following ratios were assumed as the petrochemical modules that primarily control staurolite stability: MgO/CaO, CaO/FM, and Al_2O_3/FM. With regard to some features of the stability fields of staurolite in protoliths with various FeOt contents, these modules were calculated separately for three compositional groups of the metabasites with contrastingly different FeO/MgO ratios (Table 8, Fig. V-6-1) (Borisova et al., 2022).

Based on the value of the proposed petrochemical modules, one can roughly predict the possibility of the appearance of staurolite from mafic protolith during medium and high-pressure metamorphism. It is also possible to predict quantitative changes in the content of staurolite (vol. %) in metabasites depending on changes in the content of such petrogenic components as Al_2O_3, FeOt, MgO, CaO (Fig. V-6-2) (Borisova et al., 2022).

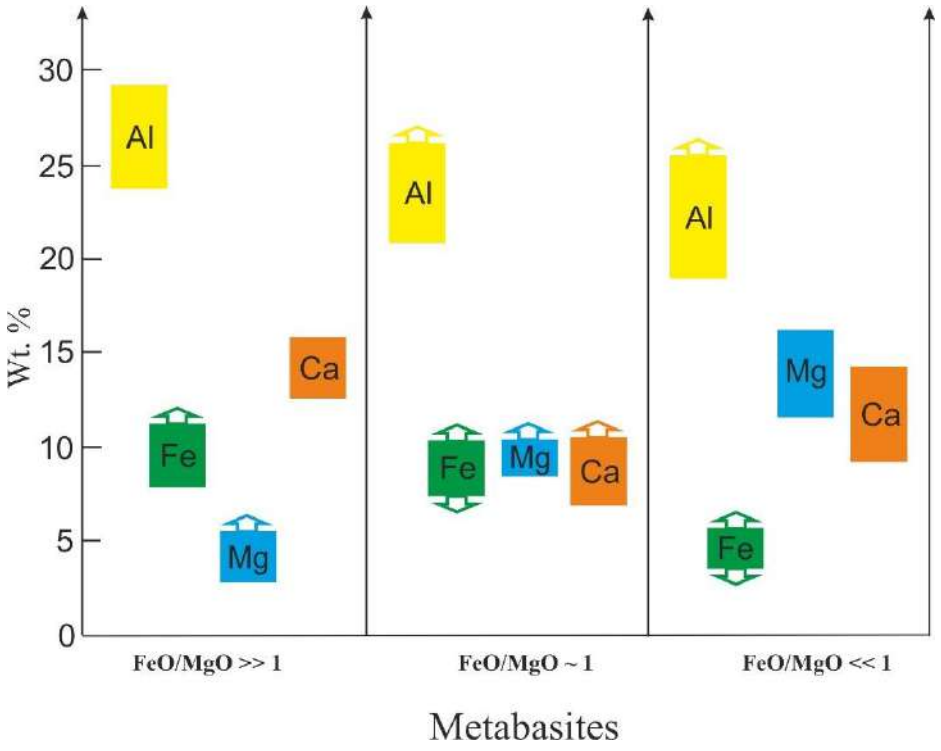

Figure V-6-1. Ranges of contents of components (Al_2O_3, FeOt, MgO, CaO) of mafic protoliths in which the formation of staurolite can be expected during metamorphism of medium and high pressures.

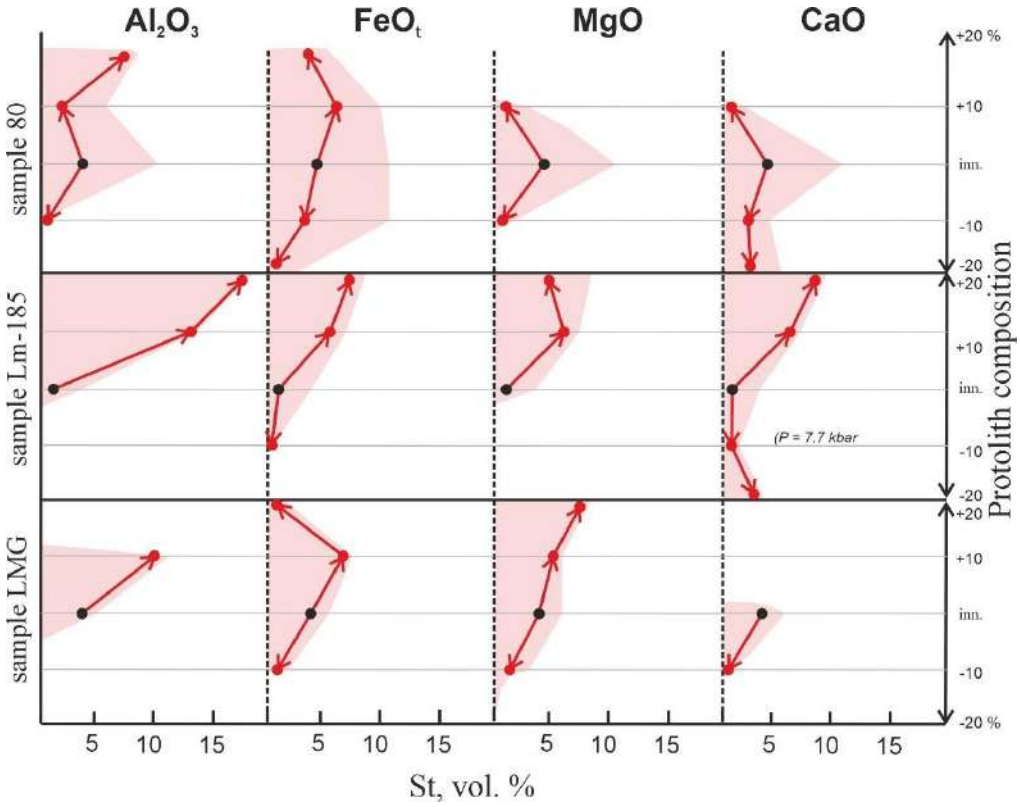

Figure V-6-2. Variations in the content (vol %) of staurolite depending on concentrations of major components (Al_2O_3, FeOt, MgO, and CaO) at their changes at increments of ±10 and ±20% for the various unmodified compositions of the protolith. Inn. – initial composition.

Summary of the chapter

Despite the fact that staurolite is a typical metamorphic mineral of metapelites, there are a number of finds of this mineral in rocks of metabasic composition, which are mainly amphibolites with high alumina content. The wide variety of mineral associations with staurolite in metabasites indicates that the formation of its parageneses is influenced by many factors: P-T conditions of metamorphism, bulk chemical composition of protoliths and fluid composition (Borisova et al., 2022).

To understand the general patterns of staurolite formation in the group of metabasites, it is necessary to distinguish subgroups of rocks with different magnesium content: FeOt/MgO << 1, FeOt/MgO ~ 1, FeOt/MgO >> 1, because the ratio of these components has different effects on the configuration and number of P-T regions in which staurolite is stable. This feature is characteristic of metabasites and is not characteristic of metapelites.

The key factors and conditions of staurolite stability are as follows:

1. Staurolite is most typical of metabasites metamorphosed under medium and high pressures.

2. Alumina content in metabasites is of paramount importance for the stability of staurolite-bearing mineral assemblages and directly controls the configuration of the stability field(s) in P–T space.

3. An increase in the FeOt content in the rocks decreases the X_{Mg} of the staurolite, and a significant decrease in the FeOt content results in that amphibole and/or biotite are formed instead of staurolite.

4. A change in the CaO content notably affects the configuration of the staurolite fields: an insignificant increase in the CaO content expands the staurolite-bearing region toward higher pressures. If the rock contains a significant highest CaO content, no staurolite is formed. An increase in the CaO content is associated with a decrease in the X_{Mg} of the staurolite, which is usually controlled by the dominance of amphibole and/or clinopyroxene or sometimes also biotite, which are more magnesian than staurolite. A decrease in the CaO content is less important for staurolite stability: assemblages of this mineral with amphibole and plagioclase with subordinate amounts of garnet are formed at low pressures.

5. The role of MgO content in metabasites is that a decrease in the content of this component drastically decreases the content of staurolite in the rock and a decrease in its X_{Mg}.

6. An increase in the CO_2 mole fraction in the H_2O–CO_2 fluid shifts the stability fields of staurolite assemblages toward lower temperatures and higher pressures in the P–T diagrams.

A review of experimental and natural data on minerals that can be considered “companions” of essentially magnesian “high-pressure” staurolites, in particular lawsonite, confirms the results of good reproducibility when modeling their joint parageneses, i.e. The results obtained are in agreement with natural observations and experimental data on the conditions of these minerals.

CONCLUSION

The complex petrographic, petrochemical, mineralogical, geochronological study of staurolite-containing rocks of the metamorphic complex of the Northern Ladoga region allows us to sufficiently fully characterize the staurolite zone and highlight the features of staurolite formation in metapelites.

Staurolite-bearing varieties of rocks of the Northern Ladoga region are represented by staurolite-biotite, garnet-staurolite-biotite, staurolite-andalusite-biotite schists. Based on a set of structural (regional faults and folding) and material (chemical composition of rocks and minerals) features within the staurolite zone, three blocks of development of staurolite-containing rocks are distinguished: Western, Central and Eastern. Based on the results of multi-equilibrium thermobarometry and thermodynamic modeling, P-T conditions for the formation of staurolite-containing and staurolite-free schists in these blocks were established.

The adequacy of thermodynamic modeling of mineral formation is confirmed by the unambiguous reproducibility of real mineral parageneses in staurolite-containing and staurolite-free rocks of the Ladoga series. In addition, modeling of mineral formation confirms the absence of chloritoid in the metamorphic complex of the Northern Ladoga region for the conditions of the pre-staurolite zone. It has been established that more aluminous and less magnesian protolith compositions with certain ratios of Al_2O_3/MgO and FeOt/MgO oxides are favorable for the appearance of chloritoid. The schematic diagram of the prograde mineral formation of Ladoga rocks is the sequence: (Qtz + Bt + Pl ±Ilm) + **Chl + Ms → St ± Grt → Sill/Crd + Grt**.

The composition of the gas phase of fluid inclusions in synmetamorphic quartz veins from rocks of the staurolite zone is predominantly carbon dioxide and methane; in the Western block nitrogen and methane predominate. Estimation of pressure based on CO_2 density in inclusions shows that quartz veins and/or inclusions in them arose at the late stages of the regressive stage of metamorphism of rocks of the staurolite zone. Modeling of mineral formation showed that an increase in the proportion of CO_2 in the fluid leads to a shift towards lower temperatures and pressures in the position of many metamorphic reactions, including staurolite-forming ones.

U-Pb and Sm-Nd dating of metamorphogenic minerals from metamorphic rocks of the staurolite zone revealed a metamorphic time of 1.80–1.79 Ga, which is consistent with other dating results in the region where rocks of the Ladoga series are developed.

To solve the problem of the ambiguity of the position of the staurolite isograd in the zonal-metamorphosed complex of the Northern Ladoga region, a method for identifying potentially staurolite-containing rocks is proposed using calculated “petrochemical modules” in the form of the ratio of the main rock-forming chemical components in metapelites. Petrochemical modules are objective parameters of protoliths of metamorphic rocks, based on which it is possible to predict staurolite-containing parageneses for a certain threshold of temperatures and pressures and thereby more accurately

delineate the boundaries of low- and medium-temperature metamorphic zones (facies and subfacies) when compiling metamorphic maps or diagrams.

The formation of staurolite parageneses in metabasites is influenced by many factors: medium- and high-pressure conditions of metamorphism, the chemical composition of protoliths with a high alumina content, and fluid composition. To understand the general patterns of staurolite formation in the group of mafic protoliths, it is necessary to distinguish subgroups of rocks with different magnesium content: FeOt/MgO << 1, FeOt/MgO ~ 1, FeOt/MgO >> 1, because the ratio of these components fundamentally affects the configuration and number of P-T regions in which staurolite is stable. This feature is characteristic of metabasites and is not characteristic of metapelites.

Thus, thermodynamic modeling of mineral formation together with the analysis of petrological material makes it possible to qualitatively and quantitatively establish a number of patterns of staurolite formation in rocks of both metapelitic and metabasic composition. Knowledge of the patterns of staurolite formation in protoliths of a wide range of compositions is a key element in solving various geological problems of theoretical and applied significance.

LIST OF ABBREVIATIONS

Ab – *albite*
Alm – almandine
Amp, Amph – amphibole
Als – minerals with the formula Al2SiO5
An – anorthitis
And – andalusite
Ann – annit
Bt – biotite
BSE – backscattered electrons
Cal – calcite
Cel – celadonite
Chl – chlorite
Cld – chloritoid
Crd – cordierite
Crn – corundum
Cpx – clinopyroxene
Di – diopside
Dol – dolomite
Eas – thinner
En – enstatite
Ep – epidote
Fib – fiberboard
Fo – forsterite
Fsp – feldspars
Grs – grossular
Grt – pomegranate
Hbl – hornblende
Hyp – hypersthene
Ilm – ilmenite
Kfs – potassium feldspar
Ky – kyanite
Lws – lawsonite
M – melt – melt
Mgt – magnetite
Ms – muscovite
Mt – magnetite
Opx – orthopyroxene
Or – orthoclase
Phl – phlogopite
Pl – plagioclase
Prp – pyrope
Qtz – quartz
REE – rare earth elements
Ru/Rt – rutile
Ser – sericite
Sid – siderophylite
Sil – sillimanite
Sp – spinel
Sph – sphalerin
St – staurolite
Ta, Tlc – talc
Tit – titanite
Toz – topaz
Trm – tremolite
X_{Fe} – iron content
X_{Mg} – magnesium content
Zo – zoisite

BIBLIOGRAPHY

1. Abu El-Enen M.M., Will T.M., Okrusch M. P-T evolution of the Pan-African Taba metamorphic belt, Sinai, Egypt: Constraints from metapelitic mineral assemblages // Journal of African Earth Sciences. 2004. V. 38. P. 59-78.

2. Albee A.L. Metamorphism of Pelitic Schists: Reaction relations of chloritoid and staurolite // Geolog. Soc. Amer. Bull. 1983. V. 11. P. 3249-3268.

3. Arnold J., Powell R., Sandiford M. Amphibolites with staurolite and other aluminous minerals: Calculated mineral equilibria in NCFMASH // Journal of Metamorphic Geology. 2000. V. 18. No. 1. P. 23-40.

4. Ashwonh J.R. Staurolite at anomalously high grade // Contributions to Mineralogy and Petrology. 1975. V. 53. P. 281-291.

5. Ballèvre M., Pinardon J.L., Kiénast J.R. Vuichard J.P. Reversal of Fe-Mg partitioning between garnet and Staurolite in eclogite-facies metapelites from the Champtoceaux nappe (Brittany, France) // J. Petrol. 1989. V. 30. P. 1321-1349.

6. Baltatzis E. Staurolite-Forming Reactions in the Eastern Dalradian Rocks of Scotland // Contributions to Mineralogy and Petrology. 1979. V. 69. P. 193-200.

7. Baltybaev Sh.K., Glebovitsky V.A., Kozyreva I.V. and others. Geology and petrology of svecofennids of the Ladoga region. St. Petersburg: St. Petersburg State University, 2000. 198 p. (In Russ.).

8. Baltybaev Sh.K., Levchenkov O.A., Levsky L.K. Svecofennian belt of Fennoscandia: spatiotemporal correlation of Early Proterozoic endogenous processes. St. Petersburg: Nauka, 2009. 328 p. (In Russ.).

9. Barrow G. On an intrusion of muscovite-biotite gneiss in the southeast Highlands of Scotland and its accompanying metamorphism // Quarterly Journal of the Geological Society of London. 1893. V. 19. P. 33-58.

10. Berman R.G. Thermobarometry using multiequilibrium calculations: a new technique with petrologic applications // Can. Mineral. 1991. V. 29. No. 4. P. 833-855.

11. Berman R.G. WinTWQ (version 2.3): A software package for performing internally-consistent thermobarometric calculations // Geol. Surv. Canada. Open File 5462 (revised). 2007.

12. Borisova E.B., Baltybaev Sh.K. Petrochemical Criteria of Staurolite Stability in Metapelites at Medium-Temperature Lowand Medium-Pressure Metamorphism // Petrology. 2021. V. 29, No. 4. P. 336-350. DOI: 10.1134/S0869591121040020

13. Borisova E.B., Baltybaev Sh. K., J. A. D. Connolly. Staurolite in metabasites: P-T-X conditions and the ratios of petrogenic components as a criterion of the appearance of staurolite // Petrology. 2022. V. 30. Suppl. 1. P. S53-S71. DOI: 0.1134/S0869591123010034

14. Borisova E.B., Baltybaev Sh.K., Bocharov V.N. P-T conditions, fluid regime and time of formation of staurolite-containing parageneses in the rocks of the metamorphic complex of the Northern Ladoga region // Proceedings of Voronezh State University. Series: Geology. 2024. No. 1. P. 74–88. (In Russ.).

15. Brooks C.K. The Fe_2O_3/FeO ratio of basaltic analyses: An appeal for a standardized procedure // Bulletin of the Geological Society of Denmark. 1976. 25. P. 117-120.

16. Bucher K. Metamorphic rocks. Facies and Zones/Encyclopedia of Geology. Amsterdam: Elsevier, 2005. P. 402-409.

17. Bucher K., Grapes R. Petrogenesis of Metamorphic Rocks. Springer-Verlag Berlin Heidelberg, 2011. 428 p.

18. Burke E. A.J. Raman microspectrometry of fluid inclusions // Lithos. 2001. V. 55. P. 139-158.

19. Cardoso G. M. Röntgenographische Feinbaustudien am Cyanit und Staurolith // Z. Kristallogr. 1928. V. 66. P. 485-487.

20. Cherniak D.J., Watson E.B., Grove M., Harrison T.M. Pb diffusion in monazite: A combined RBS/SIMS study // Geochimica et Cosmochimica Acta. 2004. V. 68. No. 4. P. 829-840.

21. Chopin C., Goffe B., Ungaretti L., Oberti R. Magnesio-staurolite and zinco-staurolite: mineral description with a petrogenetic and crystal-chemical update // Eur. J. Mineral. 2003. V. 15. P. 167-176.

22. Clarke G.L., Powell R., Fitzherbert. The lawsonite paradox: a comparison of field evidence and mineral equilibria modeling // J. metamorphic Geol. 2006. V. 24. P. 715-725.

23. Comodi P., Montagnoli M., Zanazzi P.F., Ballaran T.B. Isothermal compression of Staurolite: A single-crystal study // American Mineralogist. 2002. V. 87. P. 1164-1171.

24. Comodi P., Zanazzi P.F. Effects of temperature and pressure on the structure of lawsonite // American Mineralogist. 1996. V. 81. P. 833-841.

25. Connolly J.A. Multivariable phase-diagrams - an algorithm based on generalized thermodynamics // American Journal of Science. 1990. V. 290. P. 666-718.

26. Corrie S.L., Kohn M.J. Trace-element distributions in silicates during prograde metamorphic reactions: implications for monazite formation // J. metamorphic Geol. 2008. V. 26. P. 451-464.

27. Dawson J.B. Kimberlites and Their Xenoliths / Springer-Verlag. 1980. 252 p.

28. Deer W.A., Howie R.A., Zussman J. Rock-forming Minerals, Volume 1a, Orthosilicates / Halsted Press, New York. 1982. P. 1-936.

29. Diessel C.F.K., Brothers R., Black P.M. Coalification and graphitization in high-pressure schists in New Caledonia // Contributions to Mineralogy and Petrology. 1978. V. 68. P. 63-78.

30. Dobretsov N.L. Glaucophane schist and eclogite-glaucophane schist complexes of the USSR. Novosibirsk: Nauka. 1974. 412 p. (In Russ.).

31. Dolivo-Dobrovolsky D.V. Computer program TWQ_Comb. Version 1.2.0.4. 2006b. URL: http://www.dimadd.ru/ru/Programs/twqcomb

32. Dolivo-Dobrovolsky D.V. Computer program TWQ_View. Версия 1.2.0.22. 2006c. URL: http://www.dimadd.ru/ru/Programs/twqview

33. Dolivo-Dobrovolsky D.V. On the combination approach in geothermobarometry. 2006a. URL:http://www.dimadd.ru/ru/Programs/o-kombinacionnom-podhode-v-geotermobarometrii

34. Dutrow B.L., Holdaway M.J., Hinton R.W. Lithium in staurolite and its petrologic significance // Contributions to Mineralogy and Petrology. 1986. V. 94. P. 496-506.

35. Efremova S.V., Stafeev K.G. Petrochemical methods for studying rocks: A reference guide. Moscow: Nedra, 1985. 511 p. (In Russ.).

36. Enami M., Zang Q. Magnesian staurolite in garnet- Crntndum rocks and eclogite from the Donghoi district, Jiangsu Province, Eas China // American Mineralogist. 1988. V. 73. P. 48-58.

37. Eskola P. The problem of mantled gneiss domes // Quarterly Journal of the Geological Society of London. 1949. V. 104. P. 461-476.

38. Evans B.W., Brown E.H. Blueschists and eclogites // Geological Society of America Memoir. 1986. V. 164. 423 p.

39. Facies of metamorphism / Dobretsov N.L., Reverdatto V.V., Sobolev V.S., Sobolev N.V., Khlestov V.V. M.: Nedra, 1970. T. 1. 432 p. (In Russ.).

40. Faryad S.W., Hoinkes G. Reaction textures in Al-rich metabasite; implication for metamorphic evolution of the Easern border of the Middle // Lithos. 2006. V. 90. P. 145-157.

41. Fedkin V.V. Staurolite. M.: Nauka, 1975. 272 p. (In Russ.).

42. Feenstra A., Rhede D., Koch-Muller M., Wiedenbeck M., Heinrich W. Hydrogen zoning in zinc-bearing staurolite from a high-P, low-T diasporite (Samos, Greece): A combined EMP-SIMS-FIB-FTIR study // American Mineralogist. 2009. V. 94. No. 5-6. P. 737–745.

43. Fockenberg T. Synthesis and chemical variability of Mg-staurolite in the system MgO-Al_2O_3-SiO_2-H_2O as a function of water pressure // European Journal of Mineralogy. 1995. V. 7. P. 1373-1380.

44. Fockenberg T. Synthesis and chemical variability of Mg-staurolite in the system MgO-Al_2O_3-SiO_2-H_2O as a function of water pressure // European Journal of Mineralogy. 1995. V. 7. P. 1373-1380.

45. Franceschelli M., Puxeddu M., Gattiglio M. Geochemistry and origin of chloritoid schists from the Alpi Apuane, Italy: Evidence of a prevailing lateritic signature // Eur. J. Mineral. 2003. V. 15. P. 575-588.

46. Francis G.H. Facies boundaries in pelites at the middle grades of regional metamorphism // Geol. Mag. 1956. V. 93. No. 5. P. 353-368.

47. Frezzotti M.L., Tecce F., Casagli A. Raman spectroscopy for fluid inclusion analysis // Journal of Geochemical Exploration. 2012. V. 112. P. 1-20.

48. Ganguly J. Analysis of the stabilities of chloritoid and staurolite and some equilibria in the system FeO-Al_2O_3-SiO_2-H_2O-O_2 // J. African Earth Sci. 1968. V. 266. № 4. P. 277-298.

49. Ganguly J., Newton R.S. Thermal stability of chloritoid at high pressure and relatively high oxygen fugasity // J. Petrol. 1968. V. 9. № 3. P. 444-166.

50. Garcia-Casco A., Torres-Roldan R.L. Natural metastable reactions involving garnet, staurolite and cordierite: implications for petrogenetic grids and the extensional collapse of the Betic-Rif Belt // Contributions to Mineralogy and Petrology. 1999. V. 136. P. 131-153.

51. Geological development of deep zones of mobile belts (Northern Ladoga region), ed. N.G. Sudovikov. L.: Nauka. 1970. 227 p. (In Russ.).

52. Geological structure and minerals of the North-Eastern Ladoga region. / Combined report on the Impilakhtinsky object of the “Sevzapgeologiya for 1984-89, resp. N.A. Artamonova, A.A. Dukhovsky. Leningrad, 1989. (funds). (In Russ.).

53. Gibson G.M. Staurolite in amphibolite and hornblendite sheets from the Upper Seaforth River, central Fiordland, New Zealand // Mineralogical Magazine. 1978. V. 42. V. 153-154.

54. Gil Ibarguchi J.I., Mendia M. Mg- and Cr-rich staurolite and Cr-rich kyanite in high-pressure ultrabasic rocks (Cabo Ortegal, northwestern Spain) // American Mineralogist. 1991. V. 76. P. 501-511.

55. Grew E.S., Sandiford M. A staurolite- talc assemblage in tourmaline- phlogopite- chlorite schist from northern Victoria Land, Antarctica, and its petrogenetic significance // Contributions to Mineralogy and Petrology. 1984. V. 87 P. .337-350.

56. Griffen D.T. Synthetic Fe/Zn staurolites and the ionic radius of $^{IV}Zn^{2+}$ // American Mineralogist. 1981.V. 66. P. 932-937.

57. Griffen D.T., Ribbe P. H. The crystal chemistry of staurolite // American Journal of Science. 1973. V. 273-A. P. 479-495.

58. Griffin W.L., Brueckner H.K. REE, Rb-Sr and Sm-Nd studies of Norwegian eclogites // Chem. Geol., Isot. Geosci. Sect. 1985. V. 52. P. 249-271.

59. Guidotti C.V. The mineralogy and petrology of the transition from the lower to upper sillimanite zone in the Oquossoc area, Maine // Journal of Petrology. 1970. V. 11. P. 277-336.

60. Gulbin Yu.L. P-T trends and modeling of the evolution of the mineral composition of metapelites of the Northern Ladoga region in the MnNCKFMASH system // Notes of the Russian Mineralogical Society. 2014. V. 143. Issue. 6. P. 34-53. (In Russ.).

61. Hacker B.R., Peacock S.M., Abers G.A., Holloway S.D. Subduction factory 2. Are intermediate-depth earthquakes in subducting slabs linked to metamorphic dehydration reactions? // Journal of Geophysical Research. 2003. V. 108(B1), P. 2030. DOI: 10.1029/2001JB001129.

62. Harte B., Hudson N. Pelite facies series and the temperatures and pressures of Dalradian metamorphism in E. Scotland // Geol. Soc. London. Spec. Publ. 1979. V. 8. P. 323-337.

63. Hawthorne F.C., Ungaretti L., Oberti R., Caucia F., Callegari A. The crystal chemistry of staurolite. I. Crystal structure and site populations // The Canadian Mineralogist. 1993a. V. 31. P. 551-582.

64. Hawthorne F.C., Ungaretti L., Oberti R., Caucia F., Callegari A. The crystal chemistry of staurolite. II. Order – disorder and the monoclinic → orthorhombic phase transition. // The Canadian Mineralogist. 1993b. V. 31. P. 583-595.

65. Hawthorne F.C., Ungaretti L., Oberti R., Caucia F., Callegari A. The crystal chemistry of staurolite. III. Local order and chemical composition // The Canadian Mineralogist. 1993c. V. 31. P. 597-616.

66. Hellman P.L., Green T.H. The high-pressure experimental crystallization of staurolite in hydrous marie compositions // Contr. Min. Petrol. 1979. V. 68. P. 369-372.

67. Helmstedt H., Schulze D.J. Eclogite-facies ultramafic xenoliths from Colorado Plateau diatreme breccias: Comparison with eclogites in crustal environments, evaluation of the subduction hypothesis, and implications for eclogite xenoliths from diamondiferous kimberlites. In D.C. Smith, Ed., Eclogites and eclogite facies rocks, 1988. P. 387-450. Elsevier Science, Amsterdarn.

68. Henry D.J. Tourmaline as a petrogenetic indicator mineral: an example from the staurolite-grade metapelites of NW Maine // American Mineralogist. 1985. V. 70. P. 1-15.

69. Hensen, B. J. Theoretical phase relations involving cordierite and garnet in the system MgO-FeO-Al_2O_3-SiO_2 // Contributions to Mineralogy and Petrology. 1971. V. 33. P. 191-214.

70. Holdaway M.J., Dutrow B.L., Shore P. A model for the crystal chemistry of staurolite // American Mineralogist. 1986. V. 71. P. 1142-1159.

71. Holdaway M.J., Mukhopadhyay B. Thermodynamic properties of stoichiometric staurolite $H_2Fe_4Al_{18}Si_8O_{48}$ and $H_6Fe_2Al_{18}Si_8O_{48}$ // American Mineralogist. 1995. V. 80.P. 520-533.

72. Holland T.J.B., Baker J., Powell, R. Mixing properties and activity-composition relationships of chlorites in the system MgO-FeO-Al_2O_3-SiO_2-H_2O // European Journal of Mineralogy. 1998. V. 10. P. 395-406.

73. Holland T.J.B., Powell R. An improved and extended internally consistent thermodynamic dataset for phases of petrological interest, involving a new equation of state for solids // J. metamorphic Geol. 2011. V. 29. P. 333-383.

74. Hölttä P., Huhma H., Lahaye Y., Mänttäri I., Lukkari S., O'Brien H. Paleoproterozoic metamorphism in the northern Fennoscandian Shield: age constraints revealed by monazite // International Geology Review. 2019. P. 1-28. DOI: 10.1080/00206814.2019.1611488

75. Hoschek G. The stability of staurolite and chloritoid and their significance in metamorphism of pelitic rocks // Contrib. Mineral. Petrol. 1969. V. 22. № 3. P. 208-232.

76. Hughes C. J., Hussey E. M. Standardized procedure for presenting Crnrected FejOj/ FeO ratios in analyses of fine-grained mafic rocks // Neues Jahrbuch fiir Mineralogie-Monatshefte, 1979. 12, P. 570-572.

77. Huhma H., Claesson S., Kinny P.D., Williams I.S. The growth of the Early Proterozoic crust: new evidence from Svecofennian detrital zircons // Terra Nova. 1991. V. 3. No. 2. P. 175-179.

78. Hurst V., Donnay J. D. H., Donnay, G. Staurolite twinning // Mineral. Mag. 1956. V. 31. P. 145-163.

79. Janoušek V., Farrow C. M., Erban V. Interpretation of whole-rock geochemical data in igneous geochemistry: introducing Geochemical Data Toolkit (GCDkit) // Journal of Petrology. 2006. V. 47(6). P. 1255-1259.

80. Johnson T.M., Brown M., Solar G.S. Low-pressure subsolidus and suprasolidus phase equilibria in the MnNCKFMASH system: Constraints on conditions of regional metamorphism in western Maine, northern Appalachians // Amer. Mineral. 2003. V. 88. P. 624-638.

81. Juurinen A. Composition and Properties of Staurolite // Ann. Acad. Sci. Fenn. Ser. A, III GeoI. 1956.V. 47. P. 1-53.

82. Kähkönen Y., Huhma H., Aro K. U-Pb zircon ages and Rb-Sr whole-rock isotope studies of early Proterozoic volcanic and plutonic rocks near Tampere, southern Finland // Precambrian Research. 1989. Vol. 45. Iss. 1–3. PP. 27-43.

83. Karabinos P. Garnet and staurolite producing reactions in a chlorite-chloritoid schist // Contrib. Mineral. Petrol. 1985. V. 90. P. 262-275.

84. Kazakov A.N. Deformations and superimposed folding in metamorphic complexes. Leningrad: Nauka, 1976. 237 p. (In Russ.).

85. Keller L.M., Abart R., Schmid S.M., De Capitani C. Phase relations and chemical composition of phengite and paragonite in pelitic schists during decompression: a case study from the Monte Rosa Nappe and Camughera- Moncucco Unit, Western Alps // Journal of Petrology. 2005. P. 1-22.

86. Kerrick D.M., Connolly J.A.D. Metamorphic devolatilization of subducted oceanic metabasalts: implications for seismicity, arc magmatism and volatile recycling // Earth and Planetary Science Letters. 2001. V. 189. P. 19-29.

87. Kitsul V.I. Petrology of carbonate rocks of the Ladoga formation. Moscow: Publishing House of the USSR Academy of Sciences, 1963. 171 p. (In Russ.).

88. Koch-Müller M. Experimentally determined Fe-Mg exchange between synthetic staurolite and garnet in the system MgO-FeO-Al_2O_3-SiO_2-H_2O // Lithos.1997/ V. 41. P. 185-212.

89. Korikovsky S.P. Facies of metapelite metamorphism. Moscow: Nauka, 1979. 264 p. (In Russ.).

90. Krogh T.E. Improved accuracy of U-Pb zircon ages by the creation of more concordant systems using an air abrasion technique // Geochem. Cosmochem. Acta. 1982. V. 46. P. 637-649.

91. Ladoga Proterozoic structure (geology, deep structure and minerageny) / Ed. N.V. Sharov. Petrozavodsk: Karelian Research Center RAS, 2020. 435 p. (In Russ.).

92. Lal R.K., Shukla R.S. Paragenesis of staurolite in pelitic schists of Kishangarh, District Ajmer, India // Mineralogical magazine. 1970. V. 37, No. 289. P. 561-567

93. Likhanov I.I., Reverdatto V.V., Selyatitsky A.Yu. Mineral equilibria and P-T diagram for ferrous-alumina metapelites in the KFMASH system // Petrology. 2005. V. 13. No. 1. P. 81-92. (In Russ.).

94. Liou J. G. P-T stabilities of laumontite, wairakite, lawsonite and related minerals in system $CaAl_2$-Si_2O_8-SiO_2-H_2O. Journal of Petrology. 1971. V. 12. P. 378-411.

95. Liu J.-H., Zhang Q.W.L., Lia Zhen M.G., Zhang Hui C.G., Chen Y-C., Wu Ch.-M. Metamorphic evolution and U-Pb geochronology of metapelite, northeastern Wutai Complex: Implications for Paleoproterozoic tectonic evolution of the Trans-North China Orogen // Precambrian Research. 2020. V. 350. P. 1-13.

96. Lobach-Zhuchenko S.B., Chekulaev V.P., Afanasyeva L.I. Chemical composition of the Ladoga formation of the Baltic shield and the question of the balance of matter during metamorphism and ultrametamorphism // Geochemistry. 1972. No. 3. P. 355-362. (In Russ.).

97. Lonker S.W. The Hydroxyl Content of Staurolite // Contrib. Mineral Petrol. 1983. V. 84. P. 36-42.

98. Ludwig K.R. Isoplot/Ex : A geochronological Toolkit for Microsoft Excel. Version 2.05. Vol. 1a. Berkeley Geochronology Center Special Publication. 1999. 49 p.

99. Ludwig K.R. PbDat for MS-DO S. Vers. 1.21 // U. S. Geol. Surv. Open-File Rep. 1991. No. 88-542.

100. Materials for the study of the mineralogy of metamorphic rocks of the northwestern Ladoga region. / In the book: Mineralogy and Geochemistry, V. 1. Leningrad: Leningrad University Publishing house, 1964. P. 131-156. Author: V.I. Lebedev, Yu.V. Nagaitsev, V.E. Pototskaya, E.D. Prudnikov, Yu.S. Shapkina, G.M. Yurova. (In Russ.).

101. Mezger J.E., Passchier C.W. Polymetamorphism and ductile deformation of staurolite-Crndierite schist of the Bossost Dome: indication for Variscan extension in the Axial Zone of the central Pyrenees // Geol. Mag. 2003.V. 140 (5). P. 595-612.

102. Morozov Yu.A. The structure-forming role of transpression and transtension // Geotectonics. 2002. No. 6. P. 3-28. (In Russ.).

103. Moynihan D. P. A preliminary assessment of low pressure, amphibolite-facies metamorphism in the upper Hyland River area (NTS 105H), southeast Yukon // Yukon exploration and geology. 2012. P. 99-114.

104. Nagaitsev Yu.V. Petrology of metamorphic rocks of the Ladoga and White Sea complexes. Leningrad: Leningrad State University Publishing House, 1974. 160 p. (In Russ.).

105. Nagaitsev Yu.V. To characterize the zonality of metamorphism of the Ladoga formation. Leningrad: Proceedings of Leningrad State University, vol. 3, No. 18. 1965. (In Russ.).

106. Nárary-Szabó I. The structure of staurolite // Z. Kristallogr., 1929. V. 71. P. 109-116.

107. Nárary-Szabó I., Sasvári K. On the structure of staurolite $HFe_2Al_9Si_4O_{24}$ // Acta Crystallographica. 1958. V. 11. P. 862-865.

108. Newton R.C., Kennedy G.C. Some equilibrium reactions in the join $CaAl_2Si_2O_6$-H_2O // Journal of Geophysical Research. 1963. V. 68. P. 2967-2983.

109. Nicollet C. Saphirine et staurotide riche en magnesium et chromedans les amphibolites et anorthosites i Crnindon du Vohibory Sud,Madagascar // Bulletin de Min6ralogie. 1986. V. 109. P. 599-612.

110. Palin R.M., Dyck B. Metamorphism of pelitic (Al-rich) rocks // Encyclopedia Geol. (Second Edition). Oxford: Academic Press, 2021. P. 445-456.

111. Pattison D. R. M., Tinkham D. K. Interplay between equilibrium and kinetics in prograde metamorphism of pelites: an example from the Nelson aureole, British Columbia // J. metamorphic Geol. 2009. V. 27. P. 249-279.

112. Pattison D.R.M., Vogl J.J. Contrasting sequences of metapelitic mineral-assemblages in the aureole of the tilted Nelson batholith, British Columbia: implications for phase equilibria and pressure determination in andalusite-sillimanite-type settings // Canadian Mineralogist. 2005. V. 43. P. 51-88.

113. Pattison, D.R.M., Tracy, R.J. Phase equilibria and thermobarometry of metapelites. In: D.M. Kerrick, Ed., Contact metamorphism // Mineralogical Society of America Reviews in Mineralogy. 1991. V. 26. P. 105-206.

114. Pawley A.R. The pressure and temperature stability limits of lawsonite: Implications for H_2O recycling in subduction zones // Contributions to Mineralogy and Petrology. 1994. V. 118. P. 99-108.

115. Perchuk A.L., Plechov P.Yu., Sazonova L.V., Safonov O.G., Tikhomirov P.L., Shur M.Yu. Fundamentals of petrology of igneous and metamorphic processes. Tutorial. Moscow: KDU, 2015. 472 p. (In Russ.).

116. Poli S., Schmidt M.W. H_2O transport and releasei n subduction zones: Experimental constraints on basaltic and andesitic systems // Journal of Geophysical Research. 1995. V. 100. P. 22299-22314.

117. Poty B., Leroy J., Jachimowicz L. Fluid inclusions studies in quartz from fissures of western and central Alps // Schweizer Mineralogische und Petrographische Mitteilungen.1976. V. 54. P. 717-752.

118. Powell R., Holland T.J.B., Worley B. Calculating phase diagrams involving solid solutions via non-linear equations, with examples using THERMOCALC // Journal of Metamorphic Geology. 1998. V. 16. P. 577-588.

119. Predovsky A.A., Petrov V.P., Belyaev O.A. Geochemistry of ore elements of Precambrian metamorphic series (on the example of the Northern Ladoga region). Leningrad: Nauka, 1967. 139 p. (In Russ.).

120. Purttscheller F., Mogessie A. Staurolite in gamet amphibolite from Sölden, Ötztal Old Crystalline Basement, Austria // Tschermaks Mineralogische und Petrographische Mitteilungen. 1984. V. 32. P. 223-233.

121. Radioisotope methods for the chronology of geological processes: textbook. allowance / S. V. Rasskazov, I. S. Chuvashova. Irkutsk: ISU Publishing House, 2012. 300 p. (In Russ.).

122. Raman C.V., Krishnan K.S. The optical analog of the Compton effect // Nature. 1928. V. 121. P. 711.

123. Ramberg H. The origin of metamorphic and metasomatic rocks / Univ. Chicago press, 1952. 317 p.

124. Richardson S.W. Staurolite stability in a part of the system Fe-Al-Si-O-H // J. Petrol. 1968. V. 9. P. 467-488.

125. Richardson S.W. The stability of Fe-staurolite + quartz. Washington: Carnegie Institution of Washington Yearbook, 1967. V. 66. P. 398-402.

126. Ríos C.A., Castellanos O.M. First report and significance of the staurolite metabasites associated to a sequence of calc-silicate rocks from the Silgará Formation at the central Santander Massif, Colombia // Revista de la Academia Colombiana de Ciencias Exactas, Físicas y Naturales. 2014. V. 38. No. 149. P. 418-429.

127. Ronov A.B., Migdisov A.A., Lobach-Zhuchenko S.B. Problems of evolution of the chemical composition of sedimentary rocks and regional metamorphism // Geochemistry. 1977. No. 2. P. 163-186. (In Russ.).

128. Rusin A.I., Zvorygina A.A., Valizer P.M. Lawsonite eclogites and metasomatites of the Utarbaevsky association of the Maksyutovsky complex // Lithosphere. 2021. T. 21. No. 6. P. 867-883. (In Russ.).

129. Santosh M., Tsunogae T., Koshimoto S. First report of sapphirine-bearing rocks from the Palghat-Cauvery Shear Zone System, Southern India // Gondwana Research. 2004. V. 7. P. 620-626.

130. Saranchina G.M. Granitoid magmatism, metamorphism and metasomatism of the Precambrian (on the example of the Ladoga region and other areas). Leningrad, 1972. 128 p. (In Russ.).

131. Scambelluri M., Phillipot P. Deep fluids in subduction zones // Lithos. 2001. V. 55. P. 213-227.

132. Schmidt M.W. Lawsonite: Upper pressure stability and formation of higher density hydrous phases // American Mineralogist. 1995. V.80. P. 1286-1292.

133. Schmidt M.W., Poli S. The stability of lawsonite and zoisite at high pressure: Experiments in CASH to 92 kbar and implications for the presence of hydrous phases in subducted lithosphere // Earth and Planetary Science Letters. 1994. V. 124. P. 105-118.

134. Schreyer W. A reconnaissance study of the system MgO-Al_2O_3-SiO_2-H_2O at pressures between l0 and 25 kb // Carnegie Institution of Washington Year Book. 1967. V. 6. P. 380-392.

135. Schreyer W., Horrocks P.C., Abraham K. High-magnesium staurolite in a sapphirine-garnet rock from the Limpopo Belt, Southern Africa // Contributions to Mineralogy and Petrology. 1984. V. 86. P. 200-207.

136. Schreyer W., Seifert F. High-pressure phases in the system MgO-Al_2O_3-SiO_2-H_2O // Amer. J. Science. 1969. V. 267- A. P. 407-443.

137. Shimpo M., Tsunogae T., Santosh M. First report of garnet-Crntndum rocks from Southern India: implications for prograde high-pressure (eclogite-facies?) metamorphism // Earth and Planetary Science Letters. 2006. V. 242. P. 111-129.

138. Shuldiner V.I., Baltybaev Sh.K., Kozyreva I.V. Tectono-metamorphic zoning of the Ladoga region // Proceedings of St. Petersburg University. 1997. V. 7. Issue 3. P.63-70. (In Russ.).

139. Simon G., Chopin C. Enstatite-sapphirine crack-related assemblages in ultrahigh-pressure pyrope megablasts, Dora-Maira massif, western Alps // Contributions to Mineralogy and Petrology. 2001. V. 140. P. 422-440.

140. Simon G., Chopin C., Schenk V. Near-end-member magnesiochloritoid in prograde-zoned pyrope, Dora-Maira massif, western Alps // Lithos. 1997. V. 41. P. 37-57.

141. Skerl A.C., Bannister F.A. Lusakite, a cobalt-bearing silicate from Northern Rhodesia // Mineralogical Magazine and Journal of the Mineralogical Society. 1934. V. 23. No. 146. P. 598-606.

142. Smit M.A., Scherer E.E., Mezger K. Lu-Hf and Sm-Nd garnet geochronology: Chronometric closure and implications for dating petrological processes // Earth and Planetary Science Letters. 2013. V. 38. P. 222-233.

143. Smith J.V. The crystal structure of staurolite // American Mineralogist. 1968. V. 53. P. 1139-1155.

144. Spandler C., Hermann J., Arculus, R. Redistribution of trace elements during prograde metamorphism from lawsonite blueschist to eclogite facies; implications for deep subduction-zone processes // Contributions to Mineralogy and Petrology. 2003. V. 146. P. 205-222.

145. Spear F., Cheney J. A petrogenetic grid for pelitic schists in the system SiO_2-Al_2O_3-FeO-MgO-K_2O-H_2O // Contrib. Mineral. Petrol. 1989. V. 101. P. 149-164.

146. Spear F.S. Metamorphic Phase Equilibria and Pressure-Temperature-Time Paths: Monograph. Min. Soc. America, Washington, D.C. 1993. 799 p.

147. Spear F.S. Petrogenetic grid for amphibolites from the Post Pond and Ammonoosuc Volcanics // Carnegie Inst. Wash. Year Book. 1978. V. 77. P. 805-808.

148. Spear F.S. Phase equilibria of amphibolites from the Post Pond Volcanics, Vermont // Carnegie Inst. Wash. Year Book. 1977. V. 76. P. 613-619.

149. Spear F.S. The gedrite-anthophyllite solvus and the composition limits of orthoamphibole from the Post Pond Volcanics, Vermont // Amer. Mineral. 1980. V. 65. № 11-12. P. 1103-1118.

150. Stowell, H.H., Taylor, D.L., Tinkham, D.K., Goldberg, S.A., and Ouderkirk, K.A. Contact metamorphic P-T-t paths from Sm-Nd garnet ages, phase equilibria modeling, and thermobarometry // Journal of Metamorphic Geology. 2001. V. 19. P. 645-660.

151. Sudovikov N.G. Tectonics, metamorphism, migmatization and granitization of rocks of the Ladoga formation / LAGED AS USSR. 1954. Issue. 4. 198 p. (In Russ.).

152. Sudovikov N.G., Glebovitsky V.A., Sergeev A.S. and others. Geological development of deep zones of mobile belts (Northern Ladoga region). Moscow: Publishing House of the USSR Academy of Sciences, 1970. 228 p. (In Russ.).

153. Svetov A.P., Sviridenko L.P. Precambrian stratigraphy of Karelia. Sortavala series of svekokarelids of the Ladoga region. Petrozavodsk: KarRC RAS, 1992. 152 p. (In Russ.).

154. Tarnovskii G. Zinc-containing staurolite from pegmatites and hydrothermal formations of eastern Siberia // Voprosy Mineralogii i Geokhimii, Mestorozhdenii Vostocbnoi Sibiri. 1973. V. 70-76.

155. Thompson, A.B. Mineral reactions in pelitic rocks: I. Prediction of P-T-X(Fe-Mg) phase relations. II. Calculation of some P-T-X(Fe-Mg) phase relations // Americal Journal of Science. 1976. V. 276. P. 401-424, 425-454.

156. Thöni M. Sm-Nd isotope systematics in garnet from different lithologies (Eastern Alps): Age results, and an evaluation of potential problems for garnet Sm-Nd chronometry // [Chem. Geol. 185 (2002) 255-281]. Chemical Geology. 2003. V. 194. P. 353-379.

157. Tinkham D.K., Zuluaga C.A., Stowell H.H. Metapelite phase equilibria modeling in MnNCKFMASH: The effect of variable Al2O3 and MgO/(MgO+FeO) on mineral stability // Geological MateriAls Research. 2001. V. 3. No. 1. P. 1-42.

158. Tinkham, D.K., Stowell, H.H. Lack of evidence for loading during garnet growth: Southern Nason terrane, Cascades Crystalline Core, Washington // Geological Society of America, Cordilleran Section, 2000. V. 32. P. A-71.

159. Tribuzio R., Messiga B., Vannucci R., Bottazzi P. Rare earth element redistribution during high-pressure-low-temperature metamorphism in ophiolitic Fe-gabbros (Liguria, northwestern Italy): Implications for light REE mobility in subduction zones // Geology. 1996. V. 24. P. 711-714.

160. Tsujimori T., Liou J.G. Metamorphic evolution of kyanite-staurolite-bearing epidote-amphibolite from the Early Palaeozoic Oeyama belt, SW Japan // Journal of Metamorphic Geology. 2004. V. 22. P. 301-313.

161. Tsujimori T., Sisson V. B., Liou J. G., Harlow G. E., Sorenson S. S. Very low-temperature record in subduction process: a review of worldwide lawsonite eclogites // Lithos. 2006. DOI:10.1016/j.lithos.2006.03.054.

162. Tsunogae T., Santosh M. Sapphirine and Crntndum-bearing granulites from KaRtr, Madurai Block, Southern India // Gondwana Research. 2003. V. 6. P. 925-930.

163. Tsunogae T., van Reenen D.D. High-pressure and ultrahigh-temperature metamorphism in the Central Zone of the Limpopo Complex, southern Africa / Geological Society of America. 2010. Monograph.

164. Turner F.J., Verhoogen J. Igneous and Metamorphic Petrology. N.Y., USA: McGrawHill Book Co., 1960.

165. Ugwuonah E.N., Tsunogae T., Obiora S.Ch. Metamorphic P-T evolution of garnet-staurolite-biotite pelitic schist and amphibolite from Keffi, north-central Nigeria: Geothermobarometry, mineral equilibrium modeling and P-T path // Journal of African Earth Sciences. 2017. V. 129. P. 1-16.

166. Vance D., Mahar E. Pressure-temperature paths from P-T pseudosections and zoned garnets; potential, limitations and examples from the Zanskar Himalaya, NW India // Contributions to Mineralogy and Petrology. 1998. V. 132. P. 225-245.

167. Velikoslavinsky D.A. Comparative characteristics of regional metamorphism of moderate and low pressures. Leningrad: Nauka, 1972. 190 p. (In Russ.).

168. Velikoslavinsky D.A. Metamorphic zones in the Northern Ladoga region and assessment of the temperatures of metamorphism of kyanite and andalusite types of regional metamorphism // Metamorphic belts of the USSR. Leningrad: Nauka, 1971. P. 61-70. (In Russ.).

169. von Knorring O., Sahama Th.G., Siivola J. Zincian staurolite from Uganda // Mineralogical Magazine. 1979. V. 43. P. 4-16.

170. Wang K., Dong S., Li Z-X., Han B. Age and chemical composition of Archean metapelites in the Zhongxiang Complex and implications for early crustal evolution of the Yangtze Craton // Lithos. 2018. V. 320-321. P. 280-301.

171. Wang P., Spear F.S. A field and theoretical analysis of garnet + chlorite + chloritoid + biotite assemblages from the tristate MA, CT, NY area, U.S.A. // Contrib. Mineral. Petrol. 1991. V. 106. P. 217-235.

172. Wanga X., Choub I.-M., Hua W., Burrussc R.C., Sund Q., Songe Yu. Raman spectroscopic measurements of CO_2 density: Experimental calibration with high-pressure optical cell (HPOC) and fused silica capillary capsule (FSCC) with application to fluid inclusion observations // Geochimica et Cosmochimica Acta. 2011. V. 75. No. 14. P. 4080-4093.

173. Ward C.M. Magnesium staurolite and green chromian staurolite from Fiordland, New Zealand // American Mineralogist. 1984. V. 69. P. 531-540.

174. Watson K.D., Morton D.M. Eclogite inclusions in kimberlite pipes at Garnet Ridge, northeastem Arizona // American Mineralogist. 1969. V. 54. P. 267-285.

175. Wegmann C. E. Uber die Tektonik der jungeren Faltungin Ostfinnland // Geol. Surv. of Finland. Bull. 1928. Guide 37. P. 1-22.

176. White R.W., Powell R., Holland T.J.B., Worley B.A. The effect of TiO_2 and Fe_2O_3 on metapelitic assemblages at greenschist and amphibolite facies conditions: mineral equilibria calculations in the system K_2O-FeO-MgO-Al_2O_3-SiO_2-H_2O-TiO_2-Fe_2O_3 // J. metamorphic Geol. 2000. V. 18. P. 497-511.

177. Whitney D.L., Mechum T.A., Kuehner S.M., Dilek Y.R. Progressive metamorphism of pelitic rocks from protolith to granulite facies, Dutchess County, N.Y., USA: Constraints on the timing of fluid infiltration during regional metamorphism // J. Metamorph. Geol. 1996. V. 14. № 2. P. 163-181.

178. Yardley B.W.D. An Introduction to Metamorphic Petrology // Geological Magazine. 1989. V. 127. No. 1. P. 81-82.

179. Zack T., Foley S.F., Rivers T. Equilibrium and disequilibrium trace element partitioning in hydrous eclogites (Trescolmen, Central Alps) // Journal of Petrology. 2002. V. 43. P. 1947-1974.

180. Zack T., Rivers T., Brumm R., Kronz A. Cold subduction of oceanic crust: Implications for a lawsonite eclogite from Dominican Republic // European Journal of Mineralogy. 2004. V. 16. P. 909-916.

APPENDICES

Table 1. Content of major elements (wt. %) in metapelites of the Ladoga series.

Sample	Mineral	SiO_2	TiO_2	Al_2O_3	Fe_2O_3t	MnO	MgO	CaO	Na_2O	K_2O	H_2O	Sum
B-21-501	St	56.18	0.92	20.72	8.16	0.11	3.05	2.46	3.92	3.07	1.34	100.00
B-21-506	St	74.02	0.46	12.33	4.74	0.06	1.21	2.50	2.21	1.50	0.79	100.00
B-21-507	St	56.40	0.71	23.21	8.63	0.07	3.28	1.05	0.99	3.65	1.87	100.00
B-21-508	St	63.49	0.57	19.42	6.53	0.03	2.54	0.88	0.97	4.04	1.76	100.00
B-21-509	St	62.32	0.64	19.65	6.67	0.05	2.75	1.16	1.33	3.72	1.81	100.00
B-21-510	St	58.77	0.68	20.59	8.26	0.04	3.10	1.83	1.17	4.10	1.52	100.00
B-19-336	St-Grt	56.09	1.22	21.20	8.79	0.10	3.24	1.90	3.70	2.73	0.79	99.76
B-05-177	St-Grt	67.25	1.08	12.98	9.85	<0.01	2.22	0.45	1.52	2.84	1.75	99.93
B-05-175	St-Grt	59.20	0.97	19.34	8.15	0.20	3.14	1.60	1.61	3.91	1.61	99.72
B-05-174	Bt	60.03	1.07	16.53	9.41	0.04	4.18	0.45	1.53	3.48	3.08	99.81
B-05-176	Bt-Ms	61.48	0.77	18.52	6.51	0.05	2.80	0.75	1.47	5.33	2.08	99.76
B-05-179	Bt-Ms	59.22	0.86	18.96	8.24	0.05	3.10	0.90	2.18	4.90	1.48	99.89
B-2011-227	Bt-Ms	58.09	0.74	19.45	7.50	0.08	3.20	1.24	2.29	5.02	2.05	99.65
B-2011-239-2	St	61.11	0.95	17.22	8.21	0.04	2.72	4.35	1.40	2.51	1.47	99.99
10903/1	St	64.42	0.74	18.55	7.43	0.05	2.64	0.92	1.63	3.61	–	99.99
088/1b	Bt-Ms	56.62	0.55	25.00	6.40	0.05	2.31	0.90	2.12	6.05	–	100.00
088/1a	Bt-Ms	61.76	0.52	21.76	6.08	0.05	2.17	0.57	1.56	5.52	–	99.99
089/1a	Bt-Ms	61.87	0.48	22.06	5.95	0.07	2.02	0.51	1.75	5.28	–	99.99
089/1b	Bt-Ms	62.69	0.48	21.44	5.79	0.05	2.08	0.51	1.85	5.11	–	100.00
10803/1	Bt-Ms	64.34	1.14	17.04	8.37	0.05	2.93	0.89	1.54	3.71	–	100.01
091/3	Bt-Ms	64.37	0.83	17.57	7.60	0.06	3.00	0.82	1.61	4.13	–	99.99
092/1	Bt-Ms	65.25	0.70	16.95	7.14	0.05	2.58	1.15	2.44	3.74	–	100.00
090/1	Bt-Ms	67.55	0.56	16.00	6.05	0.07	1.96	1.60	2.49	3.73	–	100.01
087/1	Bt-Ms	69.86	0.64	14.50	6.49	0.14	1.90	1.11	1.64	3.72	–	100.00
083/1	Bt-Ms	73.57	0.58	13.68	4.56	0.05	1.42	0.80	2.63	2.71	–	100.00
091/2	Bt-Ms	74.00	0.64	12.62	4.90	0.04	1.68	1.07	2.70	2.36	–	100.01
086/1	Bt-Ms	74.04	1.07	11.07	5.86	0.06	1.90	1.59	2.37	2.04	–	100.00
091/1	Bt-Ms	75.92	0.59	11.97	3.80	0.05	1.21	1.97	3.11	1.39	–	100.01
10403/2	Bt-Ms	67.63	0.67	15.49	6.19	0.07	2.39	1.74	2.42	3.41	–	100.01
10303/1	Bt-Ms	70.94	0.58	15.00	5.17	0.05	1.76	1.24	1.44	3.82	–	100.00
10403/1	Bt-Ms	71.22	0.55	13.80	5.16	0.06	1.91	1.98	2.87	2.44	–	99.99
11003/1	Bt-Ms	72.58	0.55	13.31	4.80	0.07	1.79	1.44	3.04	2.41	–	99.99

Table 2. Content of major elements in rocks of the metapelite group.

Oxides, wt. %	**Real compositions of rocks from the staurolite (staurolite-andalusite) zone**				**Theoretical compositions**			
	Materials for study …, 1964	Predovsky et al., 1967	Authors' data on the Northern Ladoga region	Other regions	All	Max Min	Only *St*-containing	Max Min
SiO_2	56.65 6.87	58.94 3.58	58.96 4.21	57.14 7.51	57.92 4.69	*70.21* *40.15*	58.27 4.58	*70.21* *40.15*
Al_2O_3	18.39 2.81	19 2.03	16.89 1.93	21.25 3.91	20.55 3.34	*37.60* *9.95*	20.55 3.23	*37.60* *12.98*
FeOt	9.19 2.35	7.84 0.87	10.07 2.30	8.53 2.37	8.72 2.28	*23.50* *1.25*	8.72 1.93	*23.20* *2.42*
MnO	0.12 0.06	0.09 0.04	0.06 0.07	0.10 0.03	0.10 0.04	*0.32* *0.01*	0.10 0.04	*0.32* *0.01*
MgO	4.04 1.08	3.27 0.56	3.28 0.65	2.84 1.13	2.75 0.94	*5.63* *0.20*	2.85 0.91	*5.63* *0.41*
CaO	1.81 0.94	1.51 0.68	1.82 1.05	0.93 0.68	1.44 0.91	*6.28* *0.00*	1.31 0.77	*5.37* *0.00*
Na_2O	2.35 0.84	1.8 0.96	1.66 0.71	1.33 0.85	1.66 0.68	*7.53* *0.00*	1.63 0.66	*6.90* *0.00*
K_2O	3.25 0.62	3.67 0.46	3.03 0.39	3.39 1.28	3.52 0.81	*7.30* *0.00*	3.45 0.79	*5.99* *0.00*
P_2O_5	0.16 0.08	0.11 0.03	0.10 0.05	0.15 0.08	0.93 0.15	*3.00* *0.00*	0.94 0.15	*2.00* *0.00*
TiO_2	1.08 0.22	0.87 0.13	1.05 0.28	1.04 0.28	0.14 0.06	*0.46* *0.03*	0.14 0.06	*0.46* *0.03*
Number of samples	7	10	8	27	574		514	

Note. For samples, the arithmetic mean is given in the numerator, and the standard deviation is given in the denominator; for theoretical compositions, the maximum content of the component is given in italics in the numerator, and the minimum in the denominator.

Table 3. Results of multi-equilibrium thermobarometry for rocks from the staurolite zone.

Sample	**Block**	**P, kbar**	**T, °C**	**IR**	**Paregenesis**
B-03-125	Western	4.8	615	3	Qtz+Bt+Pl+Grt+St+Ms+Ilm+Ru
B-19-336	Western	3.7–5.2	550–587	3	Qtz+Bt+Pl+Grt+St+Ms+Ilm
B-03-120-2	Western	2.6-3.1	520	2	Qtz+Bt+Pl+Grt+Ilm
B-2019-315	Central	4.8	570	2	Qtz+Bt+Pl+Grt+Ilm
B-05-175	Western	3.9-4.8	520-550	3	Qtz+Bt+Pl+Grt+Ms+Ilm
B-05-177	Western	3.7-5.5	510–550	3	Qtz+Bt+Pl+Grt+St+Ms+Ilm

Table 4. Relative concentrations of gases in mixtures and density of carbon dioxide.

Block	Sample	n	CO_2, %	CH_4, %	N_2, %	H_2, %	ρ(CO_2), g/cm^3
Western	175	1	97	2	1	–	0.526
		1	30	70	–	–	–
		1	–	22	78	–	–
		4	–	100	–	–	–
	177	1	98	2	–	–	0.62
		1	99.7	0.3	–	–	0.42
		1	99.4	0.6	–	–	0.27
		1	99.65	0.35	–	–	0.67
		4	–	100	–	–	–
	603	5	–	100	–	–	–
Central	315	1	93	1.4	5.6	–	0.564
		1	93.2	1.2	5.6	–	0.656
		1	92.2	3.1	4.7	–	0.7
		1	93.9	1.2	4.9	–	0.656
		1	93.6	–	6.4	–	0.7
		1	100	–	–	–	0.825
		1	87	13	–	–	0.47
		1	95.4	–	4.6	–	0.47
	210	5	–	100	–	–	–
	523	1	83	9	8	–	–
		1	88	4	8	–	–
		1	97.1	1.2	1.7	–	0.046
		1	–	100	–	–	–
Western	505	1	–	28	72	–	–
		1	–	10	90	–	–
		1	94	–	6	–	0.44
		1	94	–	6	–	0.34
		1	85	–	15	–	–
	506	1	–	10	90	–	–
		1	–	7.5	91	1.5	–
		1	–	11	89	–	–
	524	1	–	11	84	5	–
		1	–	26.5	68.5	5	–

Table 5. Results of U-Pb isotope studies of monazite.

№	$^{206}Pb^a/^{204}Pb$	$^{207}Pb^a/^{204}Pb$	$^{208}Pb^a/^{204}Pb$	$^{207}Pb/^{235}U$	$^{206}Pb/^{238}U$	Rho	Th^b/U	Age, Ma			Concordant age. Ma	MSWD
								$^{206}Pb/^{238}U$	$^{207}Pb/^{235}U$	$^{207}Pb/^{206}Pb$		
Mnz, B-03-125												
1	14750	1624	51760	4.814	0.3198	0.96	9.7	1788.7	1787.4	1785.8	1786.9±4.6	0.31/0.58
Mnz, B-03-126												
2	2904	330.3	12690	4.818	0.3204	0.9	12	1791.6	1788.1	1784.1	1787.3±4.7	1.8/0.18
Mnz, B-03-132												
3	6820	761.3	8710	4.848	0.3206	0.96	3.5	1792.7	1793.2	1793.8	1793.5±4.6	0.059/0.81

Note: a – isotope ratios corrected for fractionation and Pb blank; b – Th/U ratio calculated from the Pb isotopic composition of the mineral and its age. Mnz - monazite. The decomposition of minerals and the release of Pb and U were carried out according to the Krogh method (Krogh, 1992). The level of laboratory contamination with Pb did not exceed 0.1 ng for monazite and 0.4 ng for sillimanite, and U – 0.01 ng. Isotopic measurements of

Pb and U were performed on a MAT-261 mass spectrometer. Errors in measuring Pb/U isotope ratios are 0.5% (2σ). All calculations were carried out using Ludwig programs (Ludwig, 1991, 1999).

Table 6. Results of Sm-Nd isotope studies of garnet-bearing gneiss.

Sample	**Analysed fraction**	**Sm**	**Nd**	**$^{147}Sm/^{144}Nd$**	**$^{143}Nd/^{144}Nd$**	**+/-2s**
B-03-120	Bulk-rock	7.2	41.1	0.1103	0.511468	15
	Grt single grain1	3.344	13.4	**0.1569**	0.512116	16
					0.512134	8
	Grt single grain2	4.08	15.85	0.1619	0.512144	19
					0.512149	8
	Grt single grain3	1.563	2.105	0.4669	0.515637	33
					0.515522	72
	Grt_4e, leaches	1.93	10.8	0.1286	0.511760	21
	Grt_4	1.50	2.1	0.4582	0.515649	9
	Grt_4	1.50	2.1	0.4565	0.515606	17
	Grt_4	1.50	2.1	0.4574	0.515633	21
	Grt_5	1.12	0.99	0.7129	0.518630	86
	Grt_5	1.12	1.00	0.7017	0.518461	30
	Pl	0.19	0.76	0.1513	0.511826	66
	St	5.69	29.50	0.1167	0.511553	45

Table 7. Content of major elements in rocks of the metabasic group.

Oxydes, wt. %	**Real compositions of staurolite-containing metabasites**			**Theoretical compositions**			
	1 group (Fe/Mg << 1)	2 group (Fe/Mg ~ 1)	3 group (Fe/Mg >> 1)	All	Max Min	Only *St*-containing	Max Min
SiO_2	42.55 4.13	40.88 0.20	43.80 4.29	40.73 3.09	*48.73* *27.31*	40.88 3.06	*48.73* *30.79*
Al_2O_3	22.67 6.10	21.31 0.68	23.84 1.63	24.11 4.17	*41.84* *16.14*	24.20 4.11	*38.36* *16.14*
FeOt	6.19 1.57	10.21 1.29	10.19 0.79	7.80 2.18	*13.80* *3.66*	7.60 2.16	*11.50* *3.66*
MnO	0.15 0.05	0.21 0.05	0.18 0.07	0.16 0.05	*0.25* *0.07*	0.16 0.05	*0.25* *0.07*
MgO	13.61 0.46	7.84 1.10	3.49 0.89	9.95 3.33	*16.60* *3.50*	10.05 3.29	*15.21* *3.50*
CaO	12.06 0.91	11.64 2.44	9.91 5.38	12.22 1.81	*18.35* *7.36*	12.14 1.83	*18.35* *7.36*
Na_2O	0.90 0.42	1.52 0.32	0.83 0.08	1.12 0.45	*2.21* *0.12*	1.08 0.43	*2.21* *0.12*
K_2O	0.19 0.15	0.68 0.32	0.61 0.03	0.46 0.24	*1.89* *0.00*	0.47 0.26	*1.89* *0.00*
P_2O_5	0.11 0.11	0.08 0.03	0.04 0.03	0.10 0.08	*0.33* *0.00*	0.11 0.08	*0.33* *0.00*

TiO_2	0.32 0.27	0.77 0.01	0.76 0.26	0.45 0.27	*0.78* *0.02*	0.44 0.28	*0.78* *0.02*
Number of samples	4	2	2	144		90	

Note. For samples, the arithmetic mean is given in the numerator, and the standard deviation is given in the denominator; for theoretical compositions, the maximum content of the component is given in italics in the numerator, and the minimum in the denominator.

Table 8. Petrochemical modules for three groups of metabasites, differing in ratio FeO/MgO.

Метабазиты	**FeO/MgO**	**MgO/CaO**	**CaO/FM***	**Al_2O_3/FM**	
1 group	<< 1	1.31	0.67	1.22	max
		1.11	0.58	1.21	min
2 group	~ 1	1.21	0.52	1.37	max
		0.97	0.45	1.23	min
3 group	>> 1	0.33	1.11	2.07	max
		0.29	0.97	1.77	min

Contents of major elements and crystal chemical formulas in rock-forming minerals of medium-temperature metapelites of the Ladoga series

Table 9. Microprobe analyses and crystal-chemical coefficients calculated from them for staurolites from metapelites of the staurolite zone.

Sample	B-03-125									B-03-126						
Point number	1	2	7	8	9	52	59	65	66	1	2	3	4	6	7	11
SiO_2	27.57	26.17	27.04	26.58	27.65	27.20	27.68	26.59	27.20	26.42	26.73	26.46	26.31	25.06	25.59	27.69
TiO_2	0.62	0.81	0.51	0.62	0.74	0.70	0.57	0.68	0.69	0.66	0.58	0.54	0.53	0.47	0.48	0.81
Al_2O_3	53.33	54.68	53.35	55.19	55.70	54.97	55.03	54.14	54.15	51.81	52.66	55.00	56.53	52.90	54.82	53.84
FeO	15.33	14.90	14.04	14.62	14.75	14.64	14.63	14.62	14.30	14.89	14.60	15.30	14.85	14.25	14.41	14.81
MnO	0.59	0.58	0.57	0.65	0.39	–	0.45	0.40	0.35	0.34	0.57	0.31	0.20	0.45	0.35	0.45
MgO	0.96	1.40	1.65	1.48	1.37	0.96	1.21	1.06	1.30	1.32	1.44	1.11	1.21	1.15	1.16	1.11
ZnO	0.12	0.67	0.43	–	0.30	0.56	0.20	0.01	–	0.21	0.06	0.33	0.37	0.60	0.13	0.32
Sum	98.52	99.21	97.59	99.14	100.90	99.03	99.77	97.50	97.99	95.65	96.64	99.05	100.00	94.88	96.94	99.03
Si^{4+}	3.91	3.68	3.85	3.72	3.81	3.83	3.86	3.80	3.86	3.85	3.85	3.72	3.65	3.68	3.67	3.90
Ti^{4+}	0.07	0.09	0.06	0.07	0.08	0.07	0.06	0.07	0.07	0.07	0.06	0.06	0.06	0.05	0.05	0.09
Al^{3+}	8.92	9.06	8.96	9.11	9.05	9.12	9.05	9.11	9.05	8.91	8.94	9.12	9.25	9.15	9.25	8.95
Fe^{2+}	0.13	0.42	0.23	0.31	0.17	0.08	0.11	0.15	0.08	0.24	0.23	0.33	0.33	0.39	0.31	0.08
Fe^{3+}	1.69	1.33	1.44	1.40	1.53	1.64	1.60	1.59	1.62	1.57	1.53	1.48	1.40	1.36	1.41	1.67
Mn^{2+}	0.07	0.07	0.07	0.08	0.05	–	0.05	0.05	0.04	0.04	0.07	0.04	0.02	0.06	0.04	0.05
Mg^{2+}	0.20	0.29	0.35	0.31	0.28	0.20	0.25	0.23	0.28	0.29	0.31	0.23	0.25	0.25	0.25	0.23
Zn^{2+}	0.01	0.07	0.05	–	0.03	0.06	0.02	–	–	0.02	0.01	0.03	0.04	0.07	0.01	0.03
Sum	15	15	15	15	15	15	15	15	15	15	15	15	15	15	15	15
XFe	0.85	0.75	0.76	0.78	0.81	0.86	0.83	0.85	0.84	0.82	0.80	0.83	0.82	0.78	0.82	0.84

Note – XFe = $Fe^{2+}/(Mg^{2+}+Fe^{2+}+Mn^{2+}+Zn^{2+})$. The contents of the main elements for all tables are presented in wt. %, end-member content – in molecular %.

Table continuation 9.

Sample	B-03-126				B-19-336											
Point number	12	13	23	24	1	2	10	15	16	18	19	23	24	32	33	34
SiO_2	27.06	27.22	26.90	27.54	25.95	25.78	25.49	25.90	26.23	25.41	26.20	26.62	25.99	26.29	25.03	26.87
TiO_2	0.54	0.47	0.51	0.57	0.50	0.72	0.36	0.47	0.64	0.48	0.48	0.56	0.77	0.48	0.52	0.50
Al_2O_3	55.62	55.53	55.45	54.81	52.53	51.08	53.85	52.45	53.28	53.10	53.48	52.77	54.53	52.18	53.45	53.16
FeO	15.11	14.94	15.03	15.04	13.47	13.38	13.40	13.45	13.84	13.50	13.32	13.63	13.99	13.65	13.50	13.19
MnO	0.27	0.46	0.47	0.55	0.49	0.31	0.45	0.42	0.55	0.46	0.33	0.61	0.51	0.42	0.39	0.47
MgO	1.30	1.26	1.15	1.49	1.17	1.14	1.43	1.49	1.23	1.48	1.50	1.39	1.56	1.38	1.34	1.42
ZnO	0.15	0.12	0.50	–	0.62	0.44	0.57	0.51	0.41	0.55	0.78	0.19	0.52	0.96	0.29	0.58
Sum	100.05	100.00	100.01	100.00	94.73	92.85	95.55	94.69	96.18	95.06	96.38	95.69	97.58	95.36	94.52	96.19
Si^{4+}	3.76	3.79	3.75	3.83	3.81	3.87	3.70	3.80	3.79	3.71	3.78	3.87	3.70	3.84	3.67	3.88
Ti^{4+}	0.06	0.05	0.05	0.06	0.06	0.08	0.04	0.05	0.07	0.06	0.08	0.05	0.05	0.05	0.06	0.05
Al^{3+}	9.11	9.10	9.10	8.99	9.09	9.03	9.21	9.07	9.08	9.14	9.09	9.03	9.14	8.98	9.24	9.05
Fe^{2+}	0.26	0.23	0.30	0.23	0.17	0.07	0.31	0.23	0.19	0.31	0.19	0.13	0.36	0.23	0.30	0.08
Fe^{3+}	1.50	1.51	1.46	1.52	1.48	1.61	1.31	1.42	1.49	1.33	1.42	1.52	1.30	1.44	1.36	1.51
Mn^{2+}	0.03	0.05	0.06	0.07	0.06	0.04	0.06	0.05	0.07	0.06	0.04	0.08	0.06	0.05	0.05	0.06
Mg^{2+}	0.27	0.26	0.24	0.31	0.26	0.25	0.31	0.33	0.27	0.32	0.32	0.30	0.33	0.30	0.29	0.31
Zn^{2+}	0.02	0.01	0.05	–	0.07	0.05	0.06	0.06	0.04	0.06	0.08	0.02	0.05	0.10	0.03	0.06
Sum	15	15	15	15	15	15	15	15	15	15	15	15	15	15	15	15
XFe	0.83	0.82	0.81	0.80	0.79	0.82	0.76	0.77	0.80	0.75	0.76	0.79	0.74	0.76	0.78	0.78

Table continuation 9.

Sample	B-2011-239-2											B-19-316				
Point number	1	2	3	17	15	9	10	13	12	18	19	1	2	3	4	6
SiO_2	26.75	27.41	27.47	27.91	26.83	26.73	27.37	27.93	27.50	26.44	26.53	25.51	26.57	26.58	25.89	27.25
TiO_2	0.50	0.43	0.77	0.67	0.53	0.62	0.56	0.56	0.53	0.42	0.40	0.34	0.49	0.65	0.52	0.52
Al_2O_3	55.62	54.69	55.49	56.06	53.21	55.58	55.41	55.34	52.84	53.15	53.16	52.28	53.03	52.31	55.1	56.19
FeO	14.14	13.36	14.55	14.40	13.57	13.97	14.29	13.62	13.87	13.23	13.79	13.4	14.16	13.53	13	13.46
MnO	0.48	0.39	0.41	0.33	0.33	0.45	0.46	0.62	0.19	0.48	0.28	0.34	0.48	0.47	0.46	0.23
MgO	0.91	1.23	1.31	1.22	1.51	1.52	1.34	1.64	1.47	1.39	1.39	1.62	1.38	1.68	1.4	1.26
ZnO	0.35	0.46	–	0.24	0.61	0.36	0.56	0.82	0.68	0.52	0.27	1.2	0.81	1.04	1.6	1.14
Sum	98.75	97.97	100.00	100.83	96.59	99.23	99.99	100.53	97.08	95.63	95.82	94.69	96.92	96.26	97.97	100.05
Si^{4+}	3.77	3.88	3.82	3.85	3.86	3.74	3.81	3.86	3.94	3.84	3.84	3.745	3.82	3.845	3.672	3.783
Ti^{4+}	0.05	0.05	0.08	0.07	0.06	0.07	0.06	0.06	0.06	0.05	0.04	0.038	0.053	0.071	0.055	0.054
Al^{3+}	9.23	9.13	9.09	9.11	9.02	9.16	9.08	9.01	8.93	9.09	9.08	9.045	8.985	8.917	9.211	9.195
Fe^{2+}	0.13	0.01	0.11	0.06	0.14	0.24	0.19	0.15	0.07	0.14	0.15	0.39	0.27	0.252	0.333	0.13
Fe^{3+}	1.54	1.57	1.58	1.60	1.49	1.39	1.48	1.42	1.59	1.47	1.52	1.256	1.432	1.384	1.209	1.433
Mn^{2+}	0.06	0.05	0.05	0.04	0.04	0.05	0.05	0.07	0.02	0.06	0.03	0.042	0.058	0.058	0.055	0.027
Mg^{2+}	0.19	0.26	0.27	0.25	0.32	0.32	0.28	0.34	0.31	0.30	0.30	0.355	0.296	0.362	0.296	0.261
Zn^{2+}	0.04	0.05	–	0.02	0.06	0.04	0.06	0.08	0.07	0.06	0.03	0.13	0.086	0.111	0.168	0.117
Sum	15	15	15	15	15	15	15	15	15	15	15	15	15	15	15	15
XFe	0.84	0.82	0.83	0.84	0.78	0.77	0.79	0.74	0.80	0.78	0.81	0.70	0.76	0.72	0.70	0.78

Table continuation 9.

Sample	B-05-177															
Point number	11	13	14	15	16	17	21	24	25	48	49	50	51	52	53	59
SiO_2	25.19	25.29	25.45	26.37	27.02	28.01	26.82	27.47	27.66	26.69	26.64	26.67	26.17	26.19	26.87	27.06
TiO_2	0.27	0.43	0.45	0.49	0.55	0.64	0.55	0.53	0.38	0.54	0.52	0.53	0.58	0.53	0.54	0.64
Al_2O_3	50.49	51.39	52.02	52.07	53.43	54.37	53.75	53.02	54.39	52.27	53.00	53.13	53.59	53.11	52.68	53.94
FeO	13.83	14.36	14.15	14.59	14.86	14.48	14.21	14.25	13.88	14.61	14.63	14.86	15.27	15.05	15.15	14.49
MnO	–	–	–	–	–	–	0.08	0.03	0.18	0.12	–	0.16	–	0.15	0.01	–
MgO	0.99	1.16	0.96	1.14	1.33	1.12	0.87	1.19	1.11	1.00	0.93	0.99	0.86	1.14	0.92	1.24
ZnO	0.56	0.08	0.03	0.33	0.24	0.09	0.06	0.31	0.26	0.30	0.31	0.31	0.22	0.28	0.25	0.43
Sum	91.33	92.71	93.06	94.99	97.43	98.71	96.34	96.80	97.86	95.53	96.03	96.65	96.69	96.45	96.42	97.80
Si^{4+}	3.84	3.79	3.80	3.87	3.86	3.95	3.87	3.95	3.93	3.90	3.87	3.85	3.78	3.78	3.89	3.85
Ti^{4+}	0.03	0.05	0.05	0.05	0.06	0.07	0.06	0.06	0.04	0.06	0.06	0.06	0.06	0.06	0.06	0.07
Al^{3+}	9.08	9.09	9.16	9.00	9.00	9.03	9.15	8.99	9.10	8.99	9.07	9.04	9.11	9.05	8.99	9.05
Fe^{2+}	0.18	0.23	0.13	0.15	0.16	–	–	–	–	0.09	0.09	0.15	0.21	0.27	0.11	0.11
Fe^{3+}	1.58	1.57	1.64	1.64	1.61	1.71	1.72	1.71	1.65	1.69	1.69	1.64	1.63	1.55	1.72	1.61
Mn^{2+}	–	–	–	–	–	–	0.01	–	0.02	0.01	–	0.02	–	0.02	–	–
Mg^{2+}	0.23	0.26	0.21	0.25	0.28	0.24	0.19	0.26	0.23	0.22	0.20	0.21	0.18	0.25	0.20	0.26
Zn^{2+}	0.06	0.01	–	0.04	0.03	0.01	0.01	0.03	0.03	0.03	0.03	0.03	0.02	0.03	0.03	0.05
Sum	15	15	15	15	15	15	15	15	15	15	15	15	15	15	15	15
XFe	0.85	0.85	0.88	0.85	0.84	0.87	0.89	0.85	0.85	0.86	0.88	0.86	0.89	0.84	0.88	0.84

Table continuation 9.

Sample	B-05-175										
Point number	12	26	66	28	29	39	64	41	63	43	62
SiO_2	27.55	26.28	27.50	25.57	24.97	27.09	26.26	25.64	26.79	26.52	25.38
TiO_2	0.30	0.57	0.65	0.46	0.69	0.43	0.57	0.44	0.34	0.33	0.35
Al_2O_3	53.57	52.53	54.30	52.46	52.04	52.73	53.37	52.74	51.77	54.30	51.84
FeO	13.74	13.84	14.62	13.12	13.47	13.52	14.38	13.59	12.66	13.66	14.07
MnO	0.18	0.10	0.15	–	0.01	0.20	0.27	0.20	0.30	0.09	0.11
MgO	1.75	1.54	1.41	1.40	1.52	1.72	1.41	1.22	1.75	1.79	1.44
ZnO	0.32	0.24	0.40	0.71	0.34	0.35	0.63	0.42	0.35	0.45	0.13
Sum	97.41	95.10	99.03	93.72	93.04	96.04	96.89	94.25	93.96	97.14	93.32
Si^{4+}	3.92	3.84	3.86	3.79	3.72	3.91	3.77	3.78	3.95	3.78	3.78
Ti^{4+}	0.03	0.06	0.07	0.05	0.08	0.05	0.06	0.05	0.04	0.04	0.04
Al^{3+}	8.99	9.04	8.99	9.15	9.14	8.98	9.04	9.16	8.99	9.12	9.09
Fe^{2+}	0.11	0.16	0.14	0.17	0.26	0.11	0.30	0.19	0.03	0.25	0.28
Fe^{3+}	1.53	1.53	1.58	1.45	1.42	1.53	1.43	1.49	1.53	1.38	1.47
Mn^{2+}	0.02	0.01	0.02	–	–	0.02	0.03	0.02	0.04	0.01	0.01
Mg^{2+}	0.37	0.34	0.30	0.31	0.34	0.37	0.30	0.27	0.38	0.38	0.32
Zn^{2+}	0.03	0.03	0.04	0.08	0.04	0.04	0.07	0.05	0.04	0.05	0.01
Sum	15	15	15	15	15	15	15	15	15	15	15
XFe	0.78	0.80	0.82	0.79	0.79	0.78	0.78	0.81	0.77	0.76	0.81

Table 10. Microprobe analyses and crystal chemical coefficients calculated from them for garnets from metapelites of the staurolite zone.

Sample	B-03-125															
Point number	21	22	23	32	25	43	44	45	46	47	48	70	81	72	73	74
SiO_2	36.59	36.69	36.94	37.28	36.94	36.11	37.04	36.36	36.62	36.85	36.73	36.1	37.46	37.14	36.51	36.61
Al_2O_3	20.46	20.19	20.48	20.32	19.96	21	20.21	20.33	20.81	19.7	20	20.74	21.2	20.63	20.81	20.03
FeO	32.86	33.76	33.12	33.47	33.63	33.08	33.04	33.8	33.46	33.88	33.78	33.33	32.39	32.92	32.94	33.51
MgO	5.83	4.83	4.68	4.77	5.06	5.49	5.26	4.97	4.95	4.91	5.37	5.63	5	4.81	5.03	5.43
MnO	2.09	2.39	2.39	1.97	2.11	2.22	2.2	2.21	2.13	2.51	1.88	1.83	1.95	2.29	2.26	1.84
CaO	2.18	2.14	2.4	2.19	2.3	2.11	2.25	2.34	2.02	2.16	2.23	2.36	1.99	2.21	2.44	2.58
Sum	100.01	100	100.01	100	100	100.01	100	100.01	99.99	100.01	99.99	99.99	99.99	100	99.99	100
Si^{4+}	2.97	2.975	2.989	3.026	3.001	2.926	3.004	2.95	2.969	2.989	2.989	2.934	3.033	3.006	2.955	2.978
Al^{3+}	1.957	1.929	1.953	1.944	1.911	2.005	1.932	1.944	1.989	1.883	1.918	1.986	2.023	1.968	1.985	1.92
Fe^{2+}	2.126	2.168	2.172	2.27	2.197	2.097	2.181	2.138	2.196	2.161	2.197	2.119	2.193	2.208	2.126	2.156
Fe^{3+}	0.104	0.121	0.069	0.003	0.088	0.144	0.06	0.156	0.073	0.138	0.103	0.146	–	0.02	0.104	0.124
Mn^{2+}	0.401	0.332	0.321	0.328	0.348	0.377	0.361	0.342	0.34	0.337	0.37	0.388	0.343	0.33	0.345	0.374
Mg^{2+}	0.253	0.289	0.288	0.238	0.256	0.268	0.266	0.267	0.257	0.304	0.228	0.222	0.235	0.276	0.273	0.223
Ca^{2+}	0.19	0.186	0.208	0.19	0.2	0.183	0.196	0.203	0.175	0.188	0.194	0.205	0.173	0.192	0.212	0.225
Sum	8	8	8	8	8	8	8	8	8	8	8	8	8	8	8	8
Prp	9	10	10	8	9	9	9	9	9	10	8	8	8	9	9	7
Alm	72	73	73	75	73	72	73	72	74	72	74	72	74	73	72	72
Sps	14	11	11	11	12	13	12	12	11	11	12	13	12	11	12	13
Grs	6	6	7	6	7	6	7	7	6	6	6	7	6	6	7	8

Table continuation 10.

Sample	B-03-120-2															
Point number	17	18	19	20	23	24	25	27	28	29	35	38	39	43	61	62
SiO_2	36.98	36.81	37.14	37.8	36.64	36.61	37.09	36.48	36.96	36.75	36.72	35.98	25.89	36.77	36.9	36.58
Al_2O_3	20.55	20.37	20.76	20.11	20.71	20.55	21.14	20.97	20.16	20.01	20.59	19.51	21.52	20.27	21.46	21.2
FeO	31.42	31.61	31.61	30.52	31.9	32.8	30.77	32.08	31.12	31.32	31.33	30.87	25.63	32.12	31.63	27.72
MgO	6.27	6.07	6.43	6.2	5.9	6.71	6.35	6.2	6.48	6.45	6.16	6.36	0.27	6.4	6.41	8.79
MnO	2.21	1.98	1.93	2	1.87	1.46	2.19	1.79	1.88	1.82	2.21	2.04	13.85	1.87	2.01	1.56
CaO	2.57	3.17	2.79	3.37	2.97	2.21	3.24	2.49	3.21	2.85	2.98	2.73	0.08	2.86	2.8	4.15
Sum	100	100.01	100.66	100	99.99	100.34	100.78	100.01	99.81	99.2	99.99	97.49	87.24	100.29	101.21	100
Si^{4+}	2.993	2.982	2.99	3.059	2.97	2.974	2.972	2.96	3.003	3.007	2.97	2.994	2.212	2.977	2.95	2.957
Al^{3+}	1.96	1.945	1.97	1.918	1.979	1.967	1.996	2.005	1.93	1.93	1.963	1.913	2.167	1.934	2.022	2.02
Fe^{2+}	2.074	2.051	2.08	2.065	2.081	2.143	2.001	2.101	2.05	2.088	2.024	2.049	0.421	2.065	2.037	1.808
Fe^{3+}	0.053	0.09	0.049	–	0.081	0.085	0.061	0.076	0.065	0.055	0.096	0.099	1.41	0.111	0.078	0.066
Mn^{2+}	0.43	0.417	0.439	0.425	0.405	0.462	0.431	0.426	0.446	0.447	0.422	0.448	0.02	0.439	0.434	0.602
Mg^{2+}	0.267	0.239	0.232	0.241	0.226	0.177	0.262	0.216	0.228	0.222	0.267	0.253	1.764	0.226	0.24	0.188
Ca^{2+}	0.223	0.275	0.241	0.292	0.258	0.192	0.278	0.216	0.279	0.25	0.258	0.243	0.007	0.248	0.24	0.359
Sum	8	8	8	8	8	8	8	8	8	8	8	8	8	8	8	8
Prp	9	8	8	8	8	6	9	7	8	7	9	8	80	8	8	6
Alm	69	69	70	68	70	72	67	71	68	69	68	68	19	69	69	61
Sps	14	14	15	14	14	16	15	14	15	15	14	15	1	15	15	20
Grs	7	9	8	10	9	6	9	7	9	8	9	8	0	8	8	12

Table continuation 10.

Sample	B-03-120-2						B-19-336									
Point number	64	65	67	73	68	69	3	4	5	6	7	8	9	25	27	28
SiO_2	36.44	36.57	36.6	36.25	37.04	36.55	38.35	38.28	37.67	37.47	37.87	38.02	38.02	37.34	38.58	37.44
Al_2O_3	21.06	20.55	20.45	20.02	20.29	20.72	20.3	20.93	20.49	20.75	20.56	21.25	20.36	20.68	20.73	20.86
FeO	28.27	28.51	27.65	26.68	29.16	32	33.03	33.42	33.15	32.88	33.21	33.66	33.05	33.24	32.85	33.1
MgO	8.92	9.14	8.76	8.98	7.85	6.09	4.94	4.21	4.15	4.35	3.98	4.6	5.49	5.69	4.79	5.12
MnO	1.32	1.47	1.67	1.63	1.92	1.86	2.31	2.56	2.51	2.76	2.4	2.66	2.37	2.29	2.52	1.98
CaO	4.3	3.94	4.87	5.11	3.73	2.79	1.33	1.52	1.65	1.47	1.53	1.16	1.2	1.27	1.43	1.43
Sum	100.31	100.18	100	98.67	99.99	100.01	100.26	100.92	99.62	99.68	99.55	101.35	100.49	100.51	100.9	99.93
Si^{4+}	2.944	2.962	2.959	2.969	2.998	2.964	3.101	3.065	3.057	3.034	3.077	3.032	3.068	3.014	3.092	3.04
Al^{3+}	2.005	1.961	1.949	1.933	1.935	1.98	1.934	1.975	1.96	1.98	1.969	1.997	1.937	1.967	1.958	1.996
Fe^{2+}	1.802	1.815	1.736	1.699	1.905	2.078	2.233	2.238	2.25	2.227	2.257	2.245	2.231	2.24	2.202	2.248
Fe^{3+}	0.108	0.116	0.133	0.129	0.069	0.092	–	–	–	–	–	–	–	0.004	–	–
Mn^{2+}	0.61	0.627	0.6	0.623	0.538	0.418	0.338	0.286	0.285	0.298	0.274	0.311	0.375	0.389	0.325	0.352
Mg^{2+}	0.159	0.177	0.201	0.199	0.232	0.225	0.278	0.306	0.304	0.333	0.291	0.316	0.285	0.276	0.301	0.24
Ca^{2+}	0.372	0.342	0.422	0.448	0.323	0.242	0.115	0.13	0.143	0.128	0.133	0.099	0.104	0.11	0.123	0.124
Sum	8	8	8	8	8	8	8	8	8	8	8	8	8	8	8	8
Prp	5	6	7	7	8	8	9	10	10	11	10	11	10	9	10	8
Alm	61	61	59	57	64	70	75	75	76	75	76	76	75	76	74	76
Sps	21	21	20	21	18	14	11	10	10	10	9	10	13	13	11	12
Grs	13	12	14	15	11	8	4	4	5	4	4	3	3	4	4	4

Table continuation 10.

Sample	B-19-336														
Point number	29	45	47	48	49	50	51	52	64	65	66	67	68	69	70
SiO_2	38.18	37.87	37.16	37.76	36.97	36.66	36.82	37.11	37.71	38.54	37.72	37.57	37.87	37.29	36.42
Al_2O_3	21.05	20.8	21.1	20.73	19.78	20.31	20.53	20.73	20.72	20.43	20.37	20.25	20.05	20.28	20.58
FeO	32.39	33.03	32.61	32.21	32.54	32.68	31.97	32.44	32.89	32.43	33.01	32.47	32.26	32.29	32.68
MgO	5.46	4.98	6.11	5.68	5.64	5.6	5.54	5.93	5.36	5.33	4.97	4.96	4.94	5.36	5.76
MnO	2.02	2.44	2.05	2.05	1.96	2.02	2.06	1.96	2.22	2.63	2.68	2.38	2.35	2.12	2.16
CaO	1.28	1.1	1.13	1.4	1.25	1.29	1.38	1.3	1.25	1.2	1.47	1.5	1.36	1.31	1.24
Sum	100.38	100.22	100.16	99.83	98.14	98.56	98.3	99.47	100.15	100.56	100.22	99.13	98.83	98.65	98.84
Si^{4+}	3.083	3.059	3.011	3.067	3.064	3.022	3.037	3.029	3.053	3.1	3.045	3.069	3.103	3.066	2.99
Al^{3+}	2.003	1.98	2.015	1.984	1.932	1.973	1.996	1.994	1.977	1.937	1.938	1.949	1.936	1.965	1.992
Fe^{2+}	2.187	2.231	2.21	2.188	2.255	2.253	2.205	2.214	2.227	2.181	2.228	2.218	2.211	2.22	2.216
Fe^{3+}	–	–	–	–	–	–	–	–	–	–	–	–	–	–	0.028
Mn^{2+}	0.373	0.341	0.419	0.391	0.396	0.391	0.387	0.41	0.368	0.363	0.34	0.343	0.343	0.373	0.401
Mg^{2+}	0.243	0.294	0.248	0.248	0.242	0.248	0.253	0.238	0.268	0.315	0.322	0.29	0.287	0.26	0.264
Ca^{2+}	0.111	0.095	0.098	0.122	0.111	0.114	0.122	0.114	0.108	0.103	0.127	0.131	0.119	0.115	0.109
Sum	8	8	8	8	8	8	8	8	8	8	8	8	8	8	8
Prp	8	10	8	8	8	8	9	8	9	11	11	10	10	9	9
Alm	74	75	75	74	76	76	74	75	75	74	75	75	75	75	75
Sps	13	11	14	13	13	13	13	14	12	12	11	12	12	13	14
Grs	4	3	3	4	4	4	4	4	4	3	4	4	4	4	4

Table continuation 10.

Sample	B-05-175															
Point number	1	2	3	4	5	6	7	8	10	11	30	31	32	33	34	46
SiO_2	38.06	37.7	37.42	37.5	37.69	37.78	37.71	38.24	38.29	38.18	38	38.04	37.53	38.49	38.99	38.01
Al_2O_3	20.09	20.38	20.41	20.34	20.79	20.83	20.97	20.6	20.89	20.72	20.77	21.34	21.02	20.89	20.22	20.8
FeO	34.36	32.02	29.92	28	28.15	27.25	28.58	30.97	33.51	32.72	34.28	32.53	31.75	32.86	33.72	32.86
MgO	2.76	4.3	6.55	7.62	8.23	8.49	7.88	4.99	2.45	3.16	2.51	3.32	3.32	3.17	2.55	3.54
MnO	2.29	2.22	1.66	1.44	1.13	1.61	1.43	1.79	2.44	2.05	2.47	2.37	2.22	2.42	2.4	2.08
CaO	2.43	3.38	4.05	4.08	4.02	4.05	3.42	3.4	2.42	3.15	2.43	3.36	3.58	3.19	2.47	2.71
Sum	99.99	100	100.01	98.98	100.01	100.01	99.99	99.99	100	99.98	100.46	100.96	99.42	101.02	100.35	100
Si^{4+}	3.081	3.044	3.028	3.066	3.055	3.051	3.054	3.091	3.087	3.083	3.053	3.033	3.038	3.07	3.138	3.071
Al^{3+}	1.917	1.94	1.947	1.96	1.986	1.983	2.001	1.963	1.985	1.972	1.967	2.005	2.006	1.964	1.918	1.981
Fe^{2+}	2.326	2.162	2.025	1.914	1.908	1.841	1.935	2.094	2.259	2.21	2.304	2.169	2.15	2.192	2.27	2.221
Mn^{2+}	0.189	0.294	0.449	0.528	0.565	0.581	0.54	0.342	0.167	0.216	0.171	0.224	0.228	0.214	0.174	0.242
Mg^{2+}	0.276	0.267	0.2	0.175	0.137	0.194	0.173	0.216	0.293	0.247	0.296	0.282	0.268	0.288	0.288	0.251
Ca^{2+}	0.211	0.292	0.351	0.357	0.349	0.35	0.297	0.295	0.209	0.273	0.209	0.287	0.311	0.273	0.213	0.235
Sum	8	8	8	8	8	8	8	8	8	8	8	8	8	8	8	8
Prp	9	9	7	6	5	7	6	7	10	8	10	10	9	10	10	8
Alm	77	72	67	64	64	62	66	71	77	75	77	73	73	74	77	75
Sps	6	10	15	18	19	20	18	12	6	7	6	8	8	7	6	8
Grs	7	10	12	12	12	12	10	10	7	9	7	10	11	9	7	8

Table continuation 10.

Sample	B-05-175												B-05-177			
Point number	47	48	49	50	51	70	71	72	73	74	81	82	1	2	3	4
SiO_2	37.88	37.46	38.18	37.24	37.63	37.82	37.24	37.92	38.3	38.77	37.38	37.1	37.3	37.23	37.49	37.02
Al_2O_3	20.43	20.32	20.78	19.63	20.68	20.15	20.48	21.13	20.52	20.84	20.5	20.78	19.84	20.64	20.5	20.4
FeO	29.67	28	27.39	28.25	34.04	29.81	29.99	28.81	31.64	34.23	31.58	34.32	39.06	39.19	38.58	39.04
MgO	6.69	8.71	8.67	7.55	2.91	6.74	7.03	6.83	4.14	2.64	4.96	2.76	0.2	–	0.18	0.44
MnO	1.59	1.36	1.36	1.73	2.07	1.97	1.86	1.61	2.15	2.29	1.85	2.5	2.3	1.91	1.62	1.63
CaO	3.75	4.16	3.63	3.73	2.68	3.52	3.4	3.7	3.35	2.57	3.73	2.55	1.29	1.04	1.63	1.47
Sum	100.01	100.01	100.01	98.13	100.01	100.01	100	100	100.1	101.34	100	100.01	99.99	100.01	100	100
Si^{4+}	3.066	3.037	3.09	3.072	3.044	3.059	3.015	3.062	3.087	3.09	3.023	2.995	3.035	3.03	3.053	3.019
Al^{3+}	1.949	1.941	1.982	1.909	1.972	1.921	1.954	2.011	1.949	1.958	1.954	1.977	1.902	1.98	1.968	1.961
Fe^{2+}	2.009	1.898	1.854	1.949	2.303	2.016	2.013	1.946	2.133	2.282	2.136	2.285	2.63	2.668	2.628	2.662
Fe^{3+}	–	–	–	–	–	–	0.017	–	–	–	–	0.032	0.028	–	–	0.001
Mn^{2+}	0.459	0.598	0.594	0.528	0.199	0.462	0.482	0.467	0.283	0.178	0.34	0.189	0.014	–	0.012	0.03
Mg^{2+}	0.192	0.164	0.164	0.213	0.25	0.238	0.224	0.194	0.258	0.272	0.223	0.301	0.279	0.232	0.197	0.198
Ca^{2+}	0.325	0.361	0.315	0.33	0.232	0.305	0.295	0.32	0.289	0.219	0.323	0.221	0.112	0.091	0.142	0.128
Sum	8	8	8	8	8	8	8	8	8	8	8	8	8	8	8	8
Prp	6	5	6	7	8	8	7	7	9	9	10	7	9	8	7	7
Alm	67	63	63	65	77	67	67	66	72	77	76	71	88	89	88	89
Sps	15	20	20	17	7	15	16	16	10	6	6	11	–	–	–	1
Grs	11	12	11	11	8	10	10	11	10	7	7	11	9	8	7	7

Table continuation 10.

Sample	B-05-177															
Point number	5	6	7	8	9	10	38	39	40	41	42	43	44	45	46	68
SiO_2	37.61	36.51	37.76	37.93	37.93	36.86	36.83	37.18	37.31	37.43	37.81	37.96	36.93	37.5	37.54	37.02
Al_2O_3	20.12	20.37	20.57	21.02	20.7	20.82	20.7	20.2	20.14	19.82	20.03	20.47	20.96	20.9	20.16	19.77
FeO	38.43	38.35	38.93	39.2	38	38.78	39.04	39.14	39.07	38.25	39.19	37.96	38.84	38.3	38.86	38.95
MgO	0.62	0.78	0.59	0.29	–	–	0.05	0.04	0.36	0.87	0.83	0.49	0.05	0.04	0.03	0
MnO	1.74	1.48	1.64	1.46	2	2.36	2.26	2.18	1.67	1.46	1.66	1.42	2.01	1.9	2.39	2.16
CaO	1.46	1.34	1.51	1.38	1.37	1.17	1.12	1.25	1.45	1.18	1.6	1.7	1.2	1.36	1	0.91
Sum	99.98	98.83	101	101.28	100	99.99	100	99.99	100	99.01	101.12	100	99.99	100	99.98	98.81
Si^{4+}	3.066	3.014	3.048	3.053	3.079	2.991	2.992	3.025	3.044	3.088	3.053	3.093	3.001	3.046	3.05	3.05
Al^{3+}	1.933	1.982	1.957	1.994	1.98	1.991	1.982	1.937	1.936	1.927	1.906	1.966	2.008	2.001	1.931	1.92
Fe^{2+}	2.62	2.648	2.628	2.639	2.58	2.603	2.617	2.648	2.665	2.639	2.646	2.587	2.64	2.602	2.641	2.684
Fe^{3+}	–	–	–	–	–	0.028	0.035	0.014	–	–	–	–	–	–	–	–
Mn^{2+}	0.043	0.055	0.04	0.02	0	0	0.003	0.003	0.025	0.061	0.057	0.034	0.003	0.003	0.002	0
Mg^{2+}	0.211	0.182	0.197	0.175	0.242	0.285	0.274	0.264	0.203	0.18	0.2	0.172	0.244	0.23	0.289	0.265
Ca^{2+}	0.128	0.119	0.131	0.119	0.119	0.102	0.097	0.109	0.127	0.104	0.138	0.148	0.104	0.118	0.087	0.08
Sum	8	8	8	8	8	8	8	8	8	8	8	8	8	8	8	8
Prp	7	6	7	6	8	10	9	9	7	6	7	6	8	8	10	9
Alm	87	88	88	88	86	87	87	88	89	88	88	86	88	87	88	89
Sps	1	2	1	1	–	–	–	–	1	2	2	1	–	–	–	–
Grs	7	6	7	6	8	10	3	4	4	3	5	5	3	4	3	9

Table continuation 10.

Sample	B-19-315															
Point number	1	2	3	4	23	6	7	8	24	10	28	27	11	12	13	14
SiO_2	37.18	37.15	38.50	36.95	37.41	37.63	37.41	38.40	37.59	37.63	37.51	37.26	36.98	37.43	37.63	37.93
Al_2O_3	21.02	20.27	20.86	21.12	20.58	20.64	20.71	20.11	20.34	20.39	20.06	20.12	20.60	20.38	20.64	20.90
FeO	34.46	33.17	32.77	31.91	30.56	29.08	25.54	23.64	24.94	24.29	25.46	24.36	27.61	27.02	29.01	32.24
MgO	2.93	4.43	3.73	5.25	6.50	7.55	10.64	12.19	12.44	12.46	12.36	11.50	9.50	8.32	7.43	4.70
MnO	1.82	1.59	1.50	1.20	1.22	1.25	0.78	0.67	0.87	0.84	0.78	0.92	1.32	1.17	1.10	1.52
CaO	2.58	3.38	2.70	3.56	3.74	3.85	4.93	4.99	3.81	4.40	3.83	5.20	3.99	5.67	4.35	2.72
Sum	99.99	99.99	100.06	99.99	100.01	100	100.01	100	99.99	100.01	100	99.36	100	99.99	100.16	100.01
Si^{4+}	3.013	3.017	3.118	2.999	3.037	3.051	3.034	3.117	3.058	3.056	3.056	3.041	2.999	3.027	3.047	3.075
Al^{3+}	2.007	1.94	1.991	2.02	1.969	1.973	1.98	1.924	1.95	1.952	1.926	1.935	1.969	1.943	1.969	1.997
Fe^{2+}	2.335	2.225	2.22	2.166	2.075	1.972	1.732	1.605	1.697	1.65	1.735	1.663	1.84	1.825	1.964	2.186
Fe^{3+}	–	0.027	–	–	–	–	–	–	–	–	–	–	0.032	0.003	–	–
Mn^{2+}	0.201	0.305	0.256	0.361	0.447	0.519	0.731	0.838	0.857	0.857	0.853	0.795	0.653	0.57	0.51	0.323
Mg^{2+}	0.22	0.192	0.181	0.145	0.148	0.151	0.094	0.081	0.106	0.102	0.095	0.112	0.16	0.141	0.133	0.184
Ca^{2+}	0.224	0.294	0.234	0.31	0.325	0.334	0.428	0.434	0.332	0.383	0.334	0.455	0.347	0.491	0.377	0.236
Sum	8	8	8	8	8	8	8	8	8	8	8	8	8	8	8	8
Prp	7	6	6	5	5	5	3	3	4	3	3	4	5	5	4	6
Alm	78	75	74	73	70	66	58	54	57	55	58	56	62	61	66	73
Sps	7	10	9	12	15	17	25	28	29	29	29	27	22	19	17	11
Grs	8	10	8	10	11	11	14	15	11	13	11	15	12	16	13	8

Table continuation 10.

Sample	B-19-315															
Point number	15	16	17	042	043	044	045	046	050	051	052	053	054	055	057	058
SiO_2	37.12	37.21	37.65	36.57	37.09	38.05	38.25	38.34	38.2	37.7	36.91	37.24	37.36	37.65	38.46	36.59
Al_2O_3	21.01	19.94	20.53	20.49	20.16	20.62	20.72	20.21	20.51	20.3	20.18	20.51	20.59	19.75	19.82	20.14
FeO	34.10	34.51	35.15	36.63	35.63	33.26	31.99	31.54	30.56	30.92	29.71	29.62	29.75	32.59	33.49	34.71
MgO	3.26	2.64	2.31	2.65	2.39	3.78	4.9	5.51	6.2	6.59	7.99	7.55	7.03	5.27	3.82	2.71
MnO	1.78	2.00	1.98	1.51	1.86	1.68	1.37	1.19	1.34	1.33	1.21	1.29	1.24	1.41	1.65	1.8
CaO	2.72	2.33	2.27	1.72	2.17	2.61	3.24	3.21	3.88	3.15	3.38	3.14	4.03	3.67	2.76	2.08
Sum	99.99	98.63	99.89	99.57	99.3	100	100.47	100	100.69	99.99	99.38	99.35	100	100.34	100	98.03
Si^{4+}	3.008	3.06	3.055	2.995	3.035	3.085	3.088	3.117	3.076	3.064	3.021	3.044	3.03	3.052	3.124	3.031
Al^{3+}	2.006	1.933	1.964	1.978	1.944	1.97	1.972	1.936	1.947	1.945	1.947	1.976	1.968	1.887	1.898	1.967
Fe^{2+}	2.311	2.373	2.386	2.476	2.438	2.255	2.16	2.144	2.058	2.102	2.023	2.025	2.018	2.201	2.275	2.405
Fe^{3+}	–	–	–	0.033	–	–	–	–	–	–	0.011	–	–	0.008	–	–
Mn^{2+}	0.224	0.184	0.159	0.184	0.166	0.26	0.335	0.379	0.423	0.454	0.554	0.523	0.483	0.362	0.263	0.19
Mg^{2+}	0.215	0.245	0.24	0.184	0.227	0.203	0.165	0.144	0.161	0.161	0.148	0.157	0.15	0.17	0.2	0.222
Ca^{2+}	0.236	0.205	0.197	0.151	0.19	0.227	0.28	0.28	0.335	0.274	0.296	0.275	0.35	0.319	0.24	0.185
Sum	8	8	8	8	8	8	8	8	8	8	8	8	8	8	8	8
Prp	7	8	8	6	8	7	6	5	5	5	5	5	5	6	7	7
Alm	78	80	80	83	82	76	72	72	69	71	68	68	68	74	76	81
Sps	8	6	5	6	6	9	11	13	14	15	19	18	16	12	9	6
Grs	8	7	7	5	6	8	9	9	11	9	10	9	12	11	8	6

Table 11. Microprobe analyses and crystal-chemical coefficients of plagioclases from metapelites of the staurolite zone.

Sample	B-03-125													B-05-126		
Point number	55	31	6	82	88	30	69	75	49	67	40	26	14	18	25	29
SiO_2	59.01	59.55	58.7	59.3	59.5	60.12	59.46	59.28	59.15	58.83	59.12	59	58.11	63.04	63.15	61.88
Al_2O_3	25.82	25.54	24.74	25.7	25.45	25.51	25.11	25.55	25.72	25.79	25.67	25.27	25.99	23.84	23.1	23.9
CaO	7.46	7.52	7.58	7.59	7.68	7.73	7.74	7.77	7.92	7.96	8.04	8.33	8.73	5.35	5	5.75
Na_2O	7.71	7.45	7.01	7.06	7.37	7.32	7.65	7.37	7.21	7.41	7.17	7.28	7.09	8.86	8.72	8.48
K_2O	0	0.03	0	0.04	0	0.02	0.05	0.04	0	0	0	0.12	0.08	0.08	0.03	0
Sum	100	100.15	98.03	100.01	100	100.7	100.01	100.01	100	99.99	100	100	100	101.23	100	100.01
Si^{4+}	2.63	2.65	2.68	2.65	2.66	2.67	2.65	2.65	2.64	2.62	2.64	2.64	2.60	2.76	2.80	2.75
Al^{3+}	1.35	1.34	1.33	1.36	1.34	1.33	1.32	1.34	1.35	1.36	1.35	1.33	1.37	1.23	1.21	1.25
Ca^{2+}	0.36	0.36	0.37	0.36	0.37	0.37	0.37	0.37	0.38	0.38	0.39	0.40	0.42	0.25	0.24	0.27
Na^{2+}	0.67	0.64	0.62	0.61	0.64	0.63	0.66	0.64	0.62	0.64	0.62	0.63	0.61	0.75	0.75	0.73
K^{2+}	0	0.002	0	0.002	0	0.001	0.003	0.002	0	0	0	0.007	0.005	0.004	0.002	0
Sum	5	5	5	5	5	5	5	5	5	5	5	5	5	5	5	5
An	35	36	37	37	37	37	36	37	38	37	38	39	40	25	24	27
Ab	65	64	63	63	63	63	64	63	62	63	62	61	59	75	76	73
Or	0	0	0	0	0	0	0	0	0	0	0	1	0	0	0	0

Table continuation 11.

Sample	B-19-336													
Point number	11	12	17	31	20	22	37	40	41	53	56	61	73	76
SiO_2	64.13	64.18	62.58	63.50	62.73	63.36	63.08	61.64	64.87	62.48	62.42	63.21	63.76	63.38
Al_2O_3	23.52	22.61	23.12	22.83	22.84	23.45	23.67	23.65	23.53	23.23	22.73	23.31	23.56	23.26
CaO	4.60	4.57	4.78	4.93	4.49	4.76	4.62	4.84	4.71	4.99	4.51	4.82	4.96	4.78
Na_2O	8.91	8.64	8.49	8.32	8.65	8.61	8.63	8.79	8.85	8.37	8.97	9.11	9.07	8.58
K_2O	0	0	0	0	0	0	0	0	0	0	0	0	0	0
Sum	101.16	100.00	98.97	99.58	98.71	100.18	100.00	98.92	101.96	99.07	98.63	100.45	101.35	100.00
Si^{4+}	2.81	2.85	2.81	2.84	2.82	2.81	2.80	2.76	2.83	2.80	2.80	2.78	2.79	2.82
Al^{3+}	1.22	1.18	1.22	1.20	1.21	1.23	1.24	1.25	1.21	1.23	1.20	1.21	1.21	1.22
Ca^{2+}	0.22	0.22	0.23	0.24	0.22	0.23	0.22	0.23	0.22	0.24	0.22	0.23	0.23	0.23
Na^{2+}	0.76	0.74	0.74	0.72	0.75	0.74	0.74	0.76	0.75	0.73	0.78	0.78	0.77	0.74
K^{2+}	0	0	0	0	0	0	0	0	0	0	0	0	0	0
Sum	5	5	5	5	5	5	5	5	5	5	5	5	5	5
An	22	23	24	25	22	23	23	23	23	25	22	23	23	24
Ab	78	77	76	75	78	77	77	77	77	75	78	77	77	76
Or	0	0	0	0	0	0	0	0	0	0	0	0	0	0

Table continuation 11.

Sample	B-2011-239-2														
Point number	29	30	31	32	40	41	42	43	46	47	52	53	54	55	61
SiO_2	59.58	54.49	58.90	52.46	52.56	59.27	58.66	54.86	51.53	59.30	58.48	51.68	55.57	54.72	58.02
Al_2O_3	26.56	29.10	26.06	29.79	30.70	26.36	26.74	29.23	30.44	24.97	26.27	31.20	27.33	29.14	26.44
CaO	8.33	11.57	8.34	12.17	13.03	8.00	8.57	11.09	12.71	6.78	8.67	13.48	10.23	11.17	9.25
Na_2O	6.62	4.83	7.16	4.01	3.72	6.15	6.04	4.82	3.64	7.43	6.73	3.64	5.66	4.97	6.71
K_2O	–	–	–	0.08	–	–	–	–	–	–	–	–	–	–	–
Sum	101.09	99.99	100.85	98.86	100.26	100.00	100.01	100.00	98.68	98.48	100.15	100.00	98.79	100.00	100.42
Si^{4+}	2.64	2.46	2.61	2.41	2.39	2.67	2.64	2.48	2.38	2.69	2.62	2.35	2.53	2.47	2.59
Al^{3+}	1.39	1.55	1.36	1.61	1.64	1.40	1.42	1.56	1.66	1.33	1.38	1.67	1.47	1.55	1.39
Ca^{2+}	0.40	0.56	0.40	0.60	0.63	0.39	0.41	0.54	0.63	0.33	0.42	0.66	0.50	0.54	0.44
Na^{2+}	0.57	0.42	0.62	0.36	0.33	0.54	0.53	0.42	0.33	0.65	0.58	0.32	0.50	0.44	0.58
K^{2+}	–	–	–	–	–	–	–	–	–	–	–	–	–	–	–
Sum	5	5	5	5	5	5	5	5	5	5	5	5	5	5	5
An	41	57	39	62	66	42	44	56	66	34	42	67	50	55	43
Ab	59	43	61	37	34	58	56	44	34	66	58	33	50	45	57
Or	–	–	–	–	–	–	–	–	–	–	–	–	–	–	–

Table continuation 11.

Sample	B-19-315															
Point number	18	19	25	26	30	31	33	34	35	36	38	61	62	63	65	68
SiO_2	61.06	61.23	60.99	61.66	62.22	59.85	60.32	62.15	60.07	58.87	62.45	60.92	62.48	61.32	69.48	61.99
Al_2O_3	24.54	24.72	24.76	24.21	24.20	25.67	24.69	24.12	24.61	26.41	24.01	24.42	24.85	25.01	18.95	23.86
CaO	6.78	6.41	6.13	5.44	5.83	7.97	6.66	5.65	6.85	7.99	5.46	6.46	5.92	6.11	0.40	5.25
Na_2O	7.57	7.64	8.00	7.97	7.70	6.36	7.28	8.09	7.55	6.72	7.86	7.01	7.68	7.17	10.45	8.04
K_2O	0.05	–	–	–	0.05	0.16	–	–	–	–	0.22	–	–	0.19	0.35	0.17
Sum	100.00	100.00	99.88	99.28	100.00	100.01	98.95	100.01	99.08	99.99	100.00	98.81	100.93	99.80	99.63	99.31
Si^{4+}	2.73	2.73	2.72	2.77	2.78	2.69	2.73	2.77	2.70	2.64	2.79	2.76	2.76	2.75	3.08	2.78
Al^{3+}	1.29	1.30	1.30	1.28	1.27	1.36	1.31	1.27	1.31	1.39	1.26	1.31	1.30	1.32	0.99	1.26
Ca^{2+}	0.32	0.31	0.29	0.26	0.28	0.38	0.32	0.27	0.33	0.38	0.26	0.31	0.28	0.29	0.02	0.25
Na^{2+}	0.66	0.66	0.69	0.69	0.67	0.55	0.64	0.70	0.66	0.58	0.68	0.62	0.66	0.62	0.90	0.70
K^{2+}	–	–	–	–	–	0.01	–	–	–	–	0.01	–	–	0.01	0.02	0.01
Sum	5	5	5	5	5	5	5	5	5	5	5	5	5	5	5	5
An	33	32	30	27	29	41	34	28	33	40	27	34	30	32	2	26
Ab	67	68	70	73	70	59	66	72	67	60	71	66	70	67	96	73
Or	–	–	–	–	–	1	–	–	–	–	1	–	–	1	2	1

Table continuation 11.

Sample	B-19-315													
Point number	69	70	71	72	73	74	82	83	84	85	86	87	100	101
SiO_2	59.76	62.87	62.96	63.20	59.52	59.99	63.02	62.09	60.96	59.58	63.35	61.66	62.73	59.47
Al_2O_3	25.43	24.05	23.70	23.56	24.31	24.34	24.08	24.74	23.57	24.61	23.34	25.02	23.25	25.33
CaO	7.37	5.29	6.28	5.15	6.58	6.86	5.39	6.96	5.67	6.26	5.35	5.91	4.96	7.94
Na_2O	7.33	8.43	8.08	7.99	7.66	7.64	8.59	7.33	8.13	7.35	7.86	7.26	8.91	7.26
K_2O	0.10	0.11	–	–	0.06	0.01	–	0.08	0.07	0.29	0.10	0.14	0.15	–
Sum	99.99	100.75	101.02	99.90	98.13	98.84	101.08	101.20	98.40	98.09	100.00	99.99	100.00	100.00
Si^{4+}	2.67	2.77	2.78	2.82	2.70	2.71	2.77	2.75	2.75	2.71	2.83	2.76	2.78	2.66
Al^{3+}	1.34	1.25	1.23	1.24	1.30	1.29	1.25	1.29	1.26	1.32	1.23	1.32	1.21	1.33
Ca^{2+}	0.35	0.25	0.30	0.25	0.32	0.33	0.25	0.33	0.27	0.31	0.26	0.28	0.24	0.38
Na^{2+}	0.63	0.72	0.69	0.69	0.67	0.67	0.73	0.63	0.71	0.65	0.68	0.63	0.76	0.63
K^{2+}	0.01	0.01	–	–	–	–	–	–	–	0.02	0.01	0.01	0.01	–
Sum	5.0	5.0	5.0	5.0	5.0	5.0	5.0	5.0	5.0	5.0	5.0	5.0	5.0	5.0
An	36	26	30	26	32	33	26	34	28	31	27	31	23	38
Ab	64	74	70	74	68	67	74	65	72	67	72	68	76	62
Or	1	1	–	–	–	–	–	–	–	2	1	1	1	–

Table continuation 11.

Sample	B-05-175							B-05-177							
Point number	17	21	36	45	57	79	83	32	55	58	65	69	74	91	92
SiO_2	59.17	58.18	59.34	59.26	59.31	58.45	58.67	65.4	65.3	65.18	65.01	65.04	66.26	66.07	63.77
Al_2O_3	26.01	26.15	25.89	26.23	25.92	26.26	26.64	21.88	22.13	22.07	21.92	22.46	21.99	22.14	22.49
CaO	7.65	8.29	7.94	7.70	7.91	8.21	8.03	3.05	2.69	3.38	3.14	3.09	2.9	3.02	3.19
Na_2O	6.92	6.34	6.57	6.65	6.82	6.87	6.47	9.28	9.67	9.03	9.92	9.62	9.58	9.66	9.16
K_2O	–	–	–	–	–	–	–	0.04	0.21	0.08	0.01	–	0.02	0.03	0.15
Sum	99.75	98.96	100.00	100.07	99.99	100.00	100.00	99.99	100	99.99	100	100.21	100.8	100.92	98.76
Si^{4+}	2.65	2.64	2.67	2.66	2.66	2.62	2.63	2.90	2.88	2.89	2.87	2.87	2.91	2.89	2.86
Al^{3+}	1.38	1.40	1.37	1.39	1.37	1.39	1.41	1.14	1.15	1.15	1.14	1.17	1.14	1.14	1.19
Ca^{2+}	0.37	0.40	0.38	0.37	0.38	0.39	0.39	0.15	0.13	0.16	0.15	0.15	0.14	0.14	0.15
Na^{2+}	0.60	0.56	0.57	0.58	0.59	0.60	0.56	0.80	0.83	0.78	0.85	0.82	0.82	0.82	0.80
K^{2+}	–	–	–	–	–	–	–	0.002	0.012	0.005	0.001	–	0.001	0.002	0.009
Sum	5	5	5	5	5	5	5	5	5	5	5	5	5	5	5
An	38	42	40	39	39	40	41	15	13	17	15	15	14	15	16
Ab	62	58	60	61	61	60	59	84	86	82	85	85	86	85	83
Or	–	–	–	–	–	–	–	–	1	1	–	–	–	–	1

Table 12. Microprobe analyses and calculated crystallochemical coefficients of biotites from metapelites of the staurolite zone.

Sample	B-03-126															
Point number	76	87	4	61	29	79	27	10	39	50	54	68	8	16	20	28
SiO_2	35.49	36.6	35.03	34.52	35.65	34.66	35.99	35.32	36.76	36.14	37.06	34.69	37.81	35.81	35.77	35.16
TiO_2	1.71	1.87	1.81	1.66	1.74	1.64	1.98	1.73	2	1.84	1.9	1.81	1.97	2.01	2.19	2.06
Al_2O_3	19.44	19.28	19.35	19.92	19.72	19.44	19.42	18.7	19.13	21.02	20.27	18.99	20.08	19.9	18.99	18.84
Cr_2O_3	–	–	0.39	–	–	–	–	0.18	–	–	–	–	–	–	–	–
FeO	21.79	21.37	21.71	22.21	21.42	21.12	21.48	20.33	21.54	18.78	20.54	22.69	22.77	22.4	21.76	21.07
MnO	0.14	0.05	0.04	0.11	0.22	0.16	0.22	0.21	0.08	0.18	0.22	0.18	0.1	0.27	0.22	0.14
MgO	7.86	8.18	8.27	8.49	8.53	8.55	8.71	8.74	8.99	9.2	9.62	9.74	8.2	7.91	7.87	8.02
Na_2O	0.39	–	0.25	0.22	0.05	0.04	0.1	0.29	0.26	0.33	0.14	–	0.18	0.23	0.53	0.19
K_2O	9.37	9.44	9.58	7.64	9.53	9.22	9.61	9.36	9.71	10.04	10.09	7.37	9.44	9.58	8.9	9.1
Sum	96.19	96.79	96.43	94.77	96.86	94.83	97.51	94.86	98.47	97.53	99.84	95.47	100.55	98.11	96.23	94.58
Si^{4+}	2.73	2.78	2.70	2.67	2.72	2.70	2.73	2.74	2.76	2.70	2.72	2.64	2.77	2.71	2.75	2.75
Ti^{4+}	0.10	0.11	0.11	0.10	0.10	0.10	0.11	0.10	0.11	0.10	0.11	0.10	0.11	0.11	0.13	0.12
Al^{3+}	1.76	1.73	1.76	1.82	1.77	1.78	1.73	1.71	1.69	1.85	1.76	1.70	1.73	1.77	1.72	1.73
Cr^{3+}	–	–	0.02	–	–	–	–	0.01	–	–	–	–	–	–	–	–
Fe^{3+}	–	–	–	0.06	–	–	–	–	–	–	–	0.31	–	–	–	–
Fe^{2+}	1.40	1.36	1.40	1.37	1.36	1.37	1.36	1.32	1.35	1.17	1.26	1.13	1.40	1.42	1.40	1.38
Mn^{2+}	0.01	–	–	0.01	0.01	0.01	0.01	0.01	0.01	0.01	0.01	0.01	0.01	0.02	0.01	0.01
Mg^{2+}	0.90	0.93	0.95	0.98	0.97	0.99	0.98	1.01	1.00	1.03	1.05	1.10	0.90	0.89	0.90	0.93
Na^{+}	0.06	–	0.04	0.03	0.01	0.01	0.02	0.04	0.04	0.05	0.02	–	0.03	0.03	0.08	0.03
K^{+}	0.92	0.92	0.94	0.75	0.93	0.92	0.93	0.93	0.93	0.96	0.95	0.72	0.88	0.93	0.87	0.91
Sum	7.88	7.81	7.90	7.79	7.87	7.87	7.88	7.88	7.88	7.87	7.88	7.72	7.82	7.88	7.87	7.86
XFe	0.61	0.59	0.60	0.58	0.58	0.58	0.58	0.57	0.57	0.53	0.55	0.51	0.61	0.61	0.61	0.60

Table continuation 12.

	B-19-336										B-03-120-2				
Point number	35	39	46	54	55	57	58	59	74	78	45	56	57	58	72
SiO_2	35.27	35.91	34.81	37.76	36.01	35.69	36.78	34.86	35.38	35.84	35.76	36.48	36.15	35.83	36.11
TiO_2	1.39	1.75	1.56	1.73	1.52	1.56	1.67	1.44	1.66	1.64	1.96	1.83	1.56	1.94	1.43
Al_2O_3	19.30	19.18	18.60	19.65	19.50	19.60	18.93	17.96	19.41	18.46	18.92	19.23	18.25	19.03	19.64
FeO	18.52	20.23	19.11	18.79	19.39	19.58	19.80	19.36	19.59	19.40	20.19	19.02	18.21	21.36	19.39
MnO	0.15	–	0.05	0.12	–	0.15	0.13	0.14	–	0.03	0.14	0.14	0.22	0.06	0.26
MgO	8.63	9.60	8.84	9.25	8.33	8.93	9.07	8.66	9.20	8.79	8.78	9.61	9.23	9.27	9.37
CaO	–	–	–	–	0.13	–	0.03	0.06	–	–	–	–	–	–	–
Na_2O	0.37	–	0.12	0.57	0.15	0.11	0.31	0.32	0.02	0.14	–	0.09	0.04	–	0.21
K_2O	8.89	8.59	8.68	8.64	8.63	9.04	9.00	7.98	8.98	8.79	9.23	9.76	9.22	7.68	9.45
Sum	92.52	95.26	91.77	96.51	93.66	94.66	95.72	90.78	94.24	93.09	94.98	96.16	92.88	95.17	95.86
Si^{4+}	2.75	2.72	2.74	2.80	2.77	2.73	2.77	2.77	2.71	2.78	2.76	2.77	2.82	2.74	2.75
Ti^{4+}	0.08	0.10	0.09	0.10	0.09	0.09	0.09	0.09	0.10	0.10	0.11	0.10	0.09	0.11	0.08
Al^{3+}	1.77	1.71	1.73	1.72	1.77	1.76	1.68	1.68	1.75	1.69	1.72	1.72	1.68	1.72	1.76
Fe^{3+}	–	–	–	–	–	–	–	–	–	–	–	–	–	0.05	–
Fe^{2+}	1.21	1.28	1.26	1.16	1.25	1.25	1.25	1.29	1.26	1.26	1.30	1.21	1.19	1.32	1.23
Mn^{2+}	0.01	–	–	0.01	–	0.01	0.01	0.01	–	–	0.01	0.01	0.02	–	0.02
Mg^{2+}	1.00	1.09	1.04	1.02	0.95	1.02	1.02	1.03	1.05	1.02	1.01	1.09	1.08	1.06	1.06
Ca^{2+}	–	–	–	–	0.01	–	–	0.01	–	–	–	–	–	–	–
Na^{+}	0.06	–	0.02	0.08	0.02	0.02	0.05	0.05	–	0.02	–	0.01	0.01	–	0.03
K^{+}	0.88	0.83	0.87	0.82	0.85	0.88	0.87	0.81	0.88	0.87	0.91	0.95	0.92	0.75	0.92
Sum	7.76	7.74	7.75	7.70	7.70	7.75	7.74	7.73	7.75	7.73	7.83	7.85	7.80	7.75	7.85
XFe	0.55	0.54	0.55	0.53	0.57	0.55	0.55	0.56	0.54	0.55	0.56	0.53	0.53	0.55	0.54

Table continuation 12.

Sample	B-2011-239-2							B-19-315							
Point number	6	33	34	44	45	56	57	76	77	80	81	93	94	97	98
SiO_2	36.82	36.90	38.39	35.58	35.62	35.25	36.69	35.00	36.93	35.10	34.66	33.97	33.78	34.07	34.11
TiO_2	1.56	1.56	1.38	1.77	1.42	1.45	1.41	1.73	1.85	1.54	1.62	1.82	2.03	1.84	1.88
Al_2O_3	20.95	19.18	20.49	18.60	18.59	19.07	18.89	19.17	19.30	18.28	18.20	18.18	17.98	17.22	17.72
FeO	17.83	19.00	19.03	18.87	18.52	18.79	19.59	22.04	22.17	21.70	20.85	22.27	22.02	22.11	22.28
MnO	0.09	–	–	0.26	0.03	–	–	–	0.14	–	0.16	0.26	0.12	0.18	0.28
MgO	9.29	9.55	9.72	8.63	9.28	8.84	9.02	7.12	7.53	7.40	7.11	7.43	6.89	7.13	7.15
Na_2O	0.08	–	0.05	0.19	0.05	–	0.11	0.24	0.34	0.04	0.17	0.25	0.23	0.28	0.09
K_2O	9.13	9.12	8.94	9.50	9.22	9.37	8.98	8.80	8.70	8.79	8.88	9.08	8.82	8.89	8.86
Sum	95.75	95.31	98.00	93.40	92.73	92.77	94.69	94.10	96.96	92.85	91.65	93.26	91.87	91.72	92.37
Si^{4+}	2.74	2.78	2.79	2.76	2.77	2.74	2.79	2.72	2.77	2.76	2.76	2.69	2.71	2.74	2.73
Ti^{4+}	0.09	0.09	0.08	0.10	0.08	0.08	0.08	0.10	0.10	0.09	0.10	0.11	0.12	0.11	0.11
Al^{3+}	1.84	1.70	1.76	1.70	1.70	1.75	1.69	1.76	1.71	1.70	1.71	1.70	1.70	1.63	1.67
Fe^{2+}	1.11	1.20	1.16	1.22	1.20	1.22	1.25	1.43	1.39	1.43	1.39	1.48	1.48	1.49	1.49
Mn^{2+}	0.01	–	–	0.02	0.00	–	–	–	0.01	–	0.01	0.02	0.01	0.01	0.02
Mg^{2+}	1.03	1.07	1.05	1.00	1.08	1.03	1.02	0.83	0.84	0.87	0.85	0.88	0.82	0.86	0.85
Na^{+}	0.01	–	0.01	0.03	0.01	–	0.02	0.04	0.05	0.01	0.03	0.04	0.04	0.04	0.01
K^{+}	0.87	0.88	0.83	0.94	0.91	0.93	0.87	0.87	0.83	0.88	0.90	0.92	0.90	0.91	0.90
Sum	7.69	7.72	7.67	7.77	7.76	7.76	7.72	7.75	7.71	7.74	7.75	7.83	7.78	7.81	7.79
XFe	0.52	0.53	0.52	0.55	0.53	0.54	0.55	0.63	0.62	0.62	0.62	0.63	0.64	0.63	0.64

Table continuation 12.

Sample	B-05-175							B-05-177							
Point number	19	60	35	44	67	76	78	35	62	73	76	77	80	82	85
SiO_2	35.25	36.58	37.38	37.58	35.53	38.53	35.46	38.5	36.32	36.35	35.13	37.34	35.78	33.83	35.81
TiO_2	1.44	1.440	1.29	1.42	1.42	1.29	1.21	1.41	1.87	1.59	1.48	1.39	0.87	1.46	1.64
Al_2O_3	18.21	20.38	18.52	19.93	18.69	19.40	18.71	20.82	17.67	18.38	18.18	19.81	18.72	18.41	18.67
Cr_2O_3	–	–	–	–	–	–	–	–	–	–	0.12	–	–	–	–
FeO	18.50	15.93	16.79	18.20	18.62	18.25	18.04	20.87	21.41	21.68	21	21.33	21.02	25.02	21.79
MnO	–	–	–	–	–	–	–	–	–	–	–	0.12	0.05	0.06	0
MgO	10.34	8.46	11.74	11.26	9.15	10.08	9.60	8.42	6.82	7.89	7.69	8.75	7.62	8.6	7.87
CaO	–	–	–	0.04	–	0.01	–	–	–	–	0.02	–	–	–	–
Na_2O	0.23	0.23	0.05	0.18	0.17	0.12	0.18	0.26	0.43	0.34	0.21	0.16	–	–	0.22
K_2O	8.40	8.49	8.67	8.82	8.38	8.93	8.55	9.69	8.28	9.25	9.15	9.06	8.92	7.71	9.11
Sum	92.37	91.51	94.44	97.43	91.96	96.61	91.75	99.99	92.8	95.48	92.98	97.96	92.98	95.09	95.11
Si^{4+}	2.74	2.82	2.81	2.75	2.77	2.84	2.77	2.80	2.87	2.81	2.79	2.78	2.81	2.62	2.78
Ti^{4+}	0.08	0.08	0.07	0.08	0.08	0.07	0.07	0.08	0.11	0.09	0.09	0.08	0.05	0.09	0.10
Al^{3+}	1.67	1.85	1.64	1.72	1.72	1.68	1.72	1.78	1.65	1.67	1.70	1.74	1.73	1.68	1.71
Cr^{3+}	–	–	–	–	–	–	–	–	–	–	0.01	–	–	–	–
Fe^{3+}	–	–	–	–	–	–	–	–	–	–	–	–	–	0.32	–
Fe^{2+}	1.20	1.03	1.05	1.11	1.22	1.12	1.18	1.27	1.42	1.40	1.39	1.33	1.38	1.30	1.41
Mn^{2+}	–	–	–	–	–	–	–	–	–	–	–	0.01	–	–	–
Mg^{2+}	1.20	0.97	1.31	1.23	1.06	1.11	1.12	0.91	0.80	0.91	0.91	0.97	0.89	0.99	0.91
Ca^{2+}	–	–	–	0.003	–	0.008	–	–	–	–	0.001	–	–	–	–
Na^{+}	0.03	0.03	0.01	0.03	0.03	0.02	0.03	0.04	0.07	0.05	0.03	0.02	–	–	0.03
K^{+}	0.83	0.83	0.83	0.82	0.83	0.84	0.85	0.90	0.84	0.91	0.93	0.86	0.89	0.76	0.90
Sum	7.77	7.61	7.72	7.74	7.71	7.68	7.74	7.78	7.75	7.84	7.84	7.79	7.77	7.76	7.84
XFe	0.50	0.51	0.45	0.48	0.53	0.50	0.51	0.58	0.64	0.61	0.60	0.58	0.61	0.57	0.61

Table 13. Microprobe analyses and crystal chemical coefficients calculated from them for muscovites from metapelites of the staurolite zone.

Sample	B-03-125									B-03-126				B-19-336	B-2011-239-2
Point number	5	11	28	38	51	56	78	80	86	17	19	21	30	36	35
SiO_2	44.65	47.07	47.67	48.59	46.29	48.15	45.64	47.32	47.01	47.81	45.1	44.56	47.17	44.50	47.06
TiO_2	0.5	0.64	0.83	0.6	0.8	0.52	0.48	0.54	0.54	0.6	0.53	0.39	0.63	0.65	0.21
Al_2O_3	34.11	36.65	36.59	35.91	36.42	35.73	35.67	35.33	36.74	37.16	36.41	35.26	37.15	35.04	35.99
FeO	2.08	1.38	1.02	1.04	0.94	1.05	1.16	1.38	1.06	0.88	0.63	0.74	0.72	0.87	2.19
MnO	0.02	–	–	–	–	–	0.15	–	–	0.13	0.23	0.03	–	0.04	0.07
MgO	0.61	0.42	0.46	0.49	0.32	0.69	0.33	0.56	0.27	0.27	0.05	0.49	0.33	0.30	0.82
Na_2O	1.03	1.21	0.97	1.01	0.78	1.17	1.03	0.91	0.85	1.22	1.59	0.91	1.26	1.24	0.73
K_2O	9.91	10.57	10.45	10.17	10.34	11.04	9.98	10.01	10.42	10.24	9.83	9.4	10.15	9.26	9.73
Sum	92.91	98.09	97.99	97.81	95.89	98.35	94.44	96.05	96.89	98.31	94.37	91.78	97.41	91.90	96.80
Si^{4+}	3.06	3.05	3.08	3.13	3.05	3.11	3.06	3.11	3.07	3.07	3.03	3.06	3.06	3.05	3.08
Ti^{4+}	0.03	0.03	0.04	0.03	0.04	0.03	0.02	0.03	0.03	0.03	0.03	0.02	0.03	0.03	0.01
Al^{3+}	2.76	2.80	2.78	2.73	2.83	2.72	2.82	2.74	2.83	2.81	2.88	2.85	2.84	2.83	2.78
Fe^{2+}	0.12	0.08	0.06	0.06	0.05	0.06	0.07	0.08	0.06	0.05	0.04	0.04	0.04	0.05	0.12
Mn^{2+}	–	–	–	–	–	–	0.01	0.00	0.00	0.01	0.01	–	–	–	–
Mg^{2+}	0.06	0.04	0.04	0.05	0.03	0.07	0.03	0.06	0.03	0.03	0.01	0.05	0.03	0.03	0.08
Na^{+}	0.14	0.15	0.12	0.13	0.10	0.15	0.13	0.12	0.11	0.15	0.21	0.12	0.16	0.17	0.09
K^{+}	0.87	0.87	0.86	0.84	0.87	0.91	0.85	0.84	0.87	0.84	0.84	0.82	0.84	0.81	0.81
Sum	7.03	7.03	6.98	6.96	6.98	7.03	7.00	6.97	6.98	6.99	7.03	6.97	6.99	6.98	6.97

Table continuation 13.

Sample	B-2011-239-2			B-05-175			B-05-177									
Point number	36	50	51	59	55	75	28	29	37	57	63	64	72	78	89	90
SiO_2	48.15	46.20	48.02	44.23	46.43	48.15	43.61	46.55	45.85	45.93	45.88	45.98	46.46	46.67	46.72	47.63
TiO_2	0.37	0.34	0.28	0.34	0.21	0.43	0.20	0.24	0.10	0.40	0.40	0.36	0.34	0.49	0.31	0.37
Al_2O_3	36.75	34.31	35.10	34.22	33.94	37.24	33.20	35.98	35.25	35.55	35.10	34.35	36.50	36.84	35.94	37.16
FeO	1.58	1.25	1.10	0.69	1.05	0.84	0.99	1.52	1.39	0.82	1.43	1.50	0.90	1.00	0.74	0.96
MnO	0.04	–	0.08	–	0.17	0.09	–	0.06	0.10	–	–	0.17	–	–	0.05	–
MgO	0.84	0.96	0.84	0.37	0.74	0.75	0.38	0.53	0.38	0.50	0.51	0.40	0.43	0.44	0.37	0.45
Na_2O	0.64	0.74	0.72	1.14	1.09	1.03	0.80	0.97	0.73	1.68	0.97	1.19	1.57	1.46	1.51	1.43
K_2O	10.13	10.08	9.96	9.08	9.27	9.23	9.80	10.07	10.16	9.02	9.63	9.85	9.08	9.06	8.92	9.36
Sum	98.50	93.88	96.10	90.07	92.90	97.76	88.98	95.92	93.96	93.90	93.92	93.80	95.28	95.96	94.56	97.36
Si^{4+}	3.09	3.11	3.15	3.09	3.15	3.09	3.10	3.07	3.09	3.08	3.09	3.11	3.07	3.06	3.10	3.08
Ti^{4+}	0.02	0.02	0.01	0.02	0.01	0.02	0.01	0.01	0.01	0.02	0.02	0.02	0.02	0.02	0.02	0.02
Al^{3+}	2.78	2.73	2.71	2.82	2.71	2.81	2.78	2.80	2.80	2.81	2.78	2.74	2.84	2.84	2.81	2.83
Fe^{2+}	0.08	0.07	0.06	0.04	0.06	0.05	0.06	0.08	0.08	0.05	0.08	0.08	0.05	0.05	0.04	0.05
Mn^{2+}	–	–	–	–	0.01	–	–	–	0.01	–	–	0.01	–	–	–	–
Mg^{2+}	0.08	0.10	0.08	0.04	0.07	0.07	0.04	0.05	0.04	0.05	0.05	0.04	0.04	0.04	0.04	0.04
Na^{+}	0.08	0.10	0.09	0.15	0.14	0.13	0.11	0.12	0.10	0.22	0.13	0.16	0.20	0.19	0.19	0.18
K^{+}	0.83	0.87	0.83	0.81	0.80	0.75	0.89	0.85	0.87	0.77	0.83	0.85	0.76	0.76	0.75	0.77
Sum	6.96	6.99	6.94	6.97	6.96	6.93	7.00	7.00	6.99	6.99	6.98	7.01	6.98	6.97	6.95	6.97